Chromatography Resin Characterisation to Analyse Lifetime and Performance During Biopharmaceutical Manufacture

by

Mauryn C. Nweke

Department of Biochemical Engineering
University College London
Gower Street
London
WC1E 6BT

A thesis submitted for the degree of
DOCTOR OF PHILOSOPHY

September 2017

DECLARATION

I confirm that the work presented in this thesis is my own unless indicated otherwise. The work presented was carried out under the supervision of Prof Daniel G Bracewell at the Department of Biochemical Engineering, University College London and Dr R. Graham McCartney, Eli Lilly & Co., Ireland, between October 2013 and September 2017. This thesis has not been submitted, either in whole or in part, for another degree or another qualification at any other university.

Mauryn C. Nweke

London, September 2017

ACKNOWLEDGMENTS

My acknowledgements extend as far back as when my time at UCL began in 2009. I would like to thank all the contributors to my academic career thus far, for without them, I would not have found myself here. I would especially like to thank my supervisor Prof Daniel G Bracewell, my industrial supervisor Dr Graham McCartney and my secondary supervisor Prof Nigel Titchener-Hooker for taking a chance on me and supporting me in my pursuit of this project. Your support has not been in vain! I also thank my Head of Department, Prof Gary J Lye and my mentor in many ways, Dr Sunny Bains, for helping me to develop my personal aspirations, I am grateful.

I could never thank my loved ones enough. I thank you for your ability to believe in me in my darkest moments and your ability to continue to support me when I could hardly support myself. A special thank you to Dr Pierre Affaticati for inspiring me to take the leap and to Yasmine Cherry, Rawan Al-Ramahi, Eliane Rozanes and Estefani Daravina-Alvear for encouraging me to believe that I can, in any aspect of life.

My mum and my brother are my world and everything I do and am is because of and thanks to their love. I love you, always and forever and words will never be enough to show my gratitude.

Finally and most importantly, I thank Him. For listening to me and for hearing my every cry, no matter how petty it is. You do not let me cry in vain and every day, for the rest of my days, belongs to you.

ABSTRACT

This thesis, completed in collaboration with Eli Lilly & Co., aims to understand and assess the structural and mechanical changes that occur as agarose-based chromatography resins are exposed to different bioprocessing conditions in an attempt to explore the mechanisms by which different resins age. By understanding this, there is significant potential for facilitating timely and improved decisions in large-scale chromatographic operations, maximising resin lifetime whist maintaining acceptable column performance.

Scanning electron microscopy (SEM) was used to image the structural properties of nine widely used agarose-based chromatography resins before use while pressure-flow analysis was used to characterise the mechanical properties of the same fresh resins. The results showed that the Capto family had the highest critical velocities (Capto Adhere- 492, Capto Q- 477 cm/hr), whilst Sepharose CL-6B, Sepharose 4 Fast Flow and Sepharose CL-4B had the lowest critical velocity values (283, 204, 149 cm/hr respectively).

There were practical limitations in using the pressure-flow technique alone to for mechanical characterisation, including the large quantity of chromatography resin and buffers and the stringent criteria required to pack a column. Dynamic mechanical analysis (DMA) was therefore developed as a novel technique in this field to address these limitations and allowed for further mechanical characterisation based on the viscoelastic properties using 1ml of resin.

The technique was applied to the nine studied resins and correlated with the results obtained using the pressure-flow technique. The same trends were observed – The Capto family showed the highest resistance to deformation (Capto Adhere- 2.7, Capto Q- 1.92 $1/\%min^{-1}$) through to Sepharose CL-6B, Sepharose 4 Fast Flow and Sepharose CL-4B which exhibited the lowest slurry resistances (0.59, 0.4, 0.3 $1/\%min^{-1}$ respectively). These results indicate that DMA can be used as a small volume, high-throughput technique, relative to pressure-flow analysis, for the mechanical characterisation of chromatography media.

The structural imaging and mechanical testing tools developed in this study were then applied to measure changes in resins that had undergone lifetime studies. These studies expose the resins to repeated cycles of use to understand how they age in a particular bioprocess, enabling decision making about their use. The first set of experiments exposed the resins to the cleaning cycle only, whilst in the second set of experiments, the resins had been used for lifetime studies in the production of monoclonal antibodies (termed ‘aged’ resins).

The results indicated that MabSelect (highly cross-linked protein A resin) and Q-Sepharose High Performance (anion exchange cross-linked resin) appeared to show similar mechanisms of aging. Their matrices showed agarose fibre breakage with increased exposure to process conditions. In the case of Capto Adhere (highly cross-linked multimodal anion exchange resin) and MabSelect Xtra (highly cross-linked protein A resin), the mechanism of aging appeared to be associated foulants coating the surface fibres. The results indicate that the interaction of CIP reagents and foulants (as opposed to CIP reagents alone) cause the greatest impact on the structural integrity of the resins.

Pressure-flow and DMA characterisation were used to examine the mechanical properties of the cycled resins to provide the first systematic study of these issues. The results showed that fresh resins were consistently more robust than either of the cycled resins but the greatest mechanical differences were observed between fresh resins and aged resins, which corroborated the structural analysis data. Statistical analysis was performed with one way ANOVA to determine whether DMA could be independently used to assess the impact of process conditions on the mechanical properties of chromatography media and the results show a >80% certainty that DMA can be employed for this purpose.

IMPACT STATEMENT

-

Research relevance and Eli Lilly & Co.'s interest

Large Scale chromatography is widely employed for the capture and purification of antibodies and other therapeutic proteins. Due to the high cost of most commercial use resins, there is a significant economic driving force to use these chromatographic materials for a large number of cycles. This however, needs to be balanced against the maintenance of acceptable column performance over the lifetime of the resin. Eli Lilly & Co. have observed that different matrices exhibit different limitations pertaining to column reuse. For example, sudden column collapse is particularly prevalent in hard bead support matrices, such as ceramic-based resins whereas agarose-based resins exhibit high back pressure symptoms. In both cases, the tools to understand the structural and mechanical implications are necessary and this research aims to provide advancements in this area (see figure 1 for Eli Lilly's areas of interest).

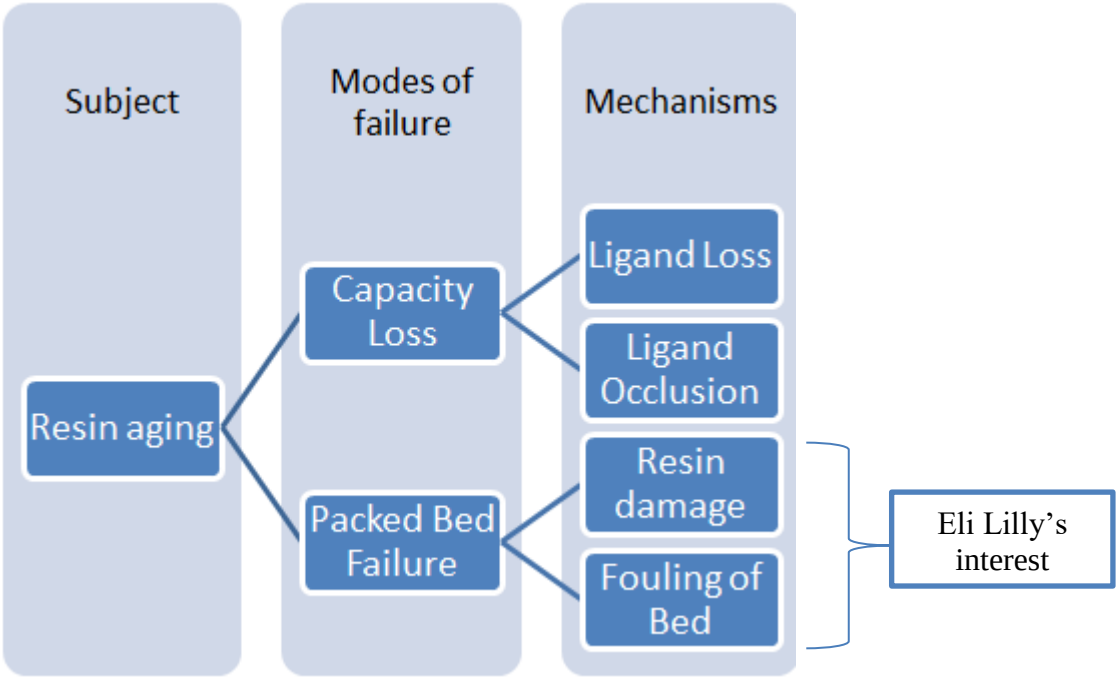

Figure 1 – Flow diagram showing possible mechanisms of aging of chromatography resins related to loss of capacity and failure of the packed bed system. The figure pinpoints Eli Lilly's interest for this research being associated with damage to the resins and the consequences of fouling.

Additionally, robust chromatographic performance is essential to meet regulatory expectations for biological products. It is a requirement to demonstrate the lifetime of the resin exceeds that of its intended use within the process and to establish procedures to monitor performance during operation. Hence there is a need to understand what the critical factors are in the aging process. Better process decisions can then be made to maximise resin usage by being able to better predict when mechanical column failure may occur. This project aims to address this by examining bead level events, which lead to mechanical failure of the column.

TABLE OF CONTENTS Page

List of figures Page

List of tables Page

List of abbreviations and notations

AEX – Anion exchange

AFM – Atomic force microscopy

A_s - Asymmetry

CA – Capto Adhere

CEX- Cation exchange

CHO – Chinese hamster ovary

CIP – Clean-in-place

CLSM – Confocal laser scanning microscopy

CPD – Critical point drying

CPP – critical process parameter

CQ – Capto Q

CQA – Critical quality attribute

CV – Column volume

DBC – Dynamic binding capacity

DMA – Dynamic mechanical analysis

DSP – Downstream processing

EM – Electron microscopy

FD – Freeze drying

HCP – Host cell protein

HETP – Height equivalent to a theoretical plate

HIC – Hydrophobic interaction chromatography

Hz – Hertz

IEX – Ion exchange

ISEC – Inverse size exclusion chromatography

kPa – Kilopascal

mAb – Monoclonal antibody

MPa – Mega pascal

MS – MabSelect

MSX – MabSelect Xtra

NaCl – Sodium chloride

NaOH – Sodium hydroxide

PAT – Process analytical technology

PF – pressure-flow

QbD – Quality by Design

Q-HP – Q-Sepharose High Performance

QTPP – Quality target product profile

S4FF – Sepharose 4 Fast Flow

SCL4B – Sepharose CL-4B

SCL6B – Sepharose CL-6B

SDR – Slurry deformation rate

SEM – Scanning electron microscopy

SMA – Steric mass action

TEM – Transmission electron microscopy

List of publications

Nweke, MC., Turmaine, M., McCartney, RG., Bracewell, DG., Drying techniques for the visualisation of agarose-based chromatography media by scanning electron microscopy, *Biotechnology Journal* (2016), 12, 1600583 (Relates to chapter 3)

Nweke, MC., McCartney, RG., Bracewell, DG., Mechanical characterisation of agarose-based chromatography resins for biopharmaceutical manufacture, *Journal of Chromatography A* (2017), v.1530, p.129-137 (Relates to chapter 4)

Conference presentations

European Synopsis on Biochemical Engineering Sciences (ESBES), Dublin 2016: Oral presentation - Techniques for chromatography resin characterisation to analyse lifetime and performance during biopharmaceutical manufacture.

The Engineering and Physical Sciences Research Council (EPSRC) Centre meeting, London 2016: Poster presentation - Techniques for chromatography resin characterisation to analyse lifetime and performance during biopharmaceutical manufacture.

INTRODUCTION
-
Research aims and objectives

This research aims to understand and characterise the structural and mechanical differences between a range of resins as a means of establishing a set of tools that can be used to assess changes that occur as agarose-based chromatography resins are exposed to different bioprocessing conditions to better understand the mechanisms by which different resins age. This will potentially facilitate timely and improved decisions in large-scale chromatographic operations, maximising resin lifetime whist maintaining acceptable column performance. The resins (outlined below) were selected as they are used frequently in the sponsoring company, Eli Lilly and readily available in-house. The expected output is a mechanistic understanding of the deterioration of the studied chromatography by studying a range of research objectives.

Objectives

- Ultrastructural visualisation and qualification of a range of commercially available agarose-based chromatography media
- Quantification of the observed ultrastructural properties

To fulfil these objectives, the use of scanning electron microscopy (SEM) will be employed as a high-resolution imaging technique to visualise the surface properties of nine commercially available agarose-based chromatography media with different % agarose content - Sepharose CL-4B, Sepharose CL-6B, Sepharose 4 Fast Flow, Sepharose 6 Fast Flow, Q-Sepharose High Performance, MabSelect Xtra, MabSelect, Capto Adhere and Capto Q. The four properties used for characterisation purposes are pore size, pore size distribution, apparent porosity and pore count. ImageJ software will be employed for quantitative analysis of these properties.

- Quantification of the mechanical properties of the resins

The traditionally used technique - pressure-flow – will be used to investigate how mechanical properties of the nine resins vary. In this procedure, an XK16 column at

15 cm bed height is used. The fluid flow rate is manually increased until a runaway rise in the pressure profile is observed. This is the point at which the column has 'failed' and is termed the critical velocity. This will provide an indication of the mechanical robustness of each resin. The quantity of resin and buffers used, as well as the stringent packing criteria necessary for pressure-flow characterisation mean that an additional mechanical characterisation tool that addresses these limitations will need to be investigated. The use of dynamic mechanical analysis (DMA) is employed for this purpose. It measures the mechanical properties of resins based on the viscoelasticity of a 1ml sample of slurry and will be correlated with pressure-flow results to ascertain whether it can be used as a small volume, high-throughput technique for the mechanical characterisation of chromatography media.

- The use of these tools to investigate structural and mechanical properties of a selection of these resins exposed to varying bioprocessing conditions.

SEM, pressure-flow characterisation and DMA will be used to assess the structural and mechanical changes observed in resins exposed to different bioprocessing conditions. A selection of 2 resins used at capture stage and 2 resins used post-capture (MabSelect, MabSelect Xtra, Q-Sepharose HP and Capto Adhere) will be exposed to repeated cycles of buffer only conditions (CIP-exposed) and aged conditions (resins used for lifetime studies in the production of monoclonal antibodies). They will then be structurally and mechanically analysed and the results will be compared to their non-processed (fresh) counterparts. Statistical analysis will also be employed to determine the significance of these results and to ascertain whether DMA can be used to mechanically characterise bioprocessed resins.

Thesis layout

Following this section, this thesis reviews literature to understand the role of chromatography and chromatography media. The importance of media characterisation is discussed and a range of techniques used for media characterisation is also discussed. Subsequently the materials and methods used in this research are outlined.

Chapter 3 – the first of 3 results chapters- discusses the use of scanning electron microscopy as a structural characterisation technique on 9 fresh agarose-based resins. Chapter 4 looks to explore whether any structural differences observed using SEM are indicative of mechanical differences. The pressure-flow technique is used to determine this. Also in this chapter, any limitations in using this technique for an enhanced understanding of resin mechanics are discussed.

The chapter subsequently discusses the ways in which the dynamic mechanical analysis technique addresses the limitations of the pressure-flow technique and its application to the 9 virgin/fresh agarose-based resins. Comparative studies are carried out between results from pressure-flow and DMA to determine whether a trend could be established.

Chapter 5 applies all aforementioned techniques to characterise resins that have been exposed to different bioprocess conditions. The objectives of this chapter are to investigate whether there are structural and mechanical differences between fresh resin, CIP-only exposed resin and aged resin. The results are then statistically corroborated.

Chapter 6 discusses whether these objectives were met and final conclusions, while chapter 7 discusses future work and developmental activities that could be undertaken based on the results obtained and the benefits to research and industry for improved process understanding.

CHAPTER 1
LITERATURE REVIEW

1. LITERATURE REVIEW

This literature review is structured to address the underlying principles that are covered in this research. The understanding of chromatography resin aging first requires comprehension of the column, its components and factors that affect performance before, during and post-operation.

In this literature review the history of chromatography in bioprocessing is briefly addressed, as well as its role, importance and various modes of operation. The components that constitute a column are also outlined and the role of chromatography resins is highlighted. A description of how agarose-based chromatography resins are manufactured is also provided as a basis for understanding the structural properties of the resins used in this study. The section on chromatographic operation is designed to take the reader through the different stages of purification, starting with packing. Subsequently, the structure-diffusion relationships and adsorption are discussed as a means of demonstrating the various stresses the column is exposed to during operation. This section concludes with resin lifetime and aging, which discusses the effects of repeated process conditions on the column and individual beads.

This leads on to highlight the importance of resin characterisation to meet both economic and regulatory needs, with particular emphasis on the need for established mechanical and structural characterisation techniques at industrial-scale. Currently used mechanical and structural characterisation techniques in research are subsequently discussed. This section is split into microscopy techniques (structural characterisation), chromatographic techniques and further techniques reported in literature for mechanical characterisation of chromatography media.

1.1.Chromatography in bioprocessing

Chromatography is a separation technique for biological molecules used to identify, quantify and/or remove impurities in substances. In 1900 the Russian scientist, Mikhail Tsvet, was the first to employ chromatography as a separation technique for the separation of plant pigments such as chlorophyll and carotenes, on the basis of colour disparity. During the 1940s and 1950s, the technique was developed further by Archer John Porter Martin and Richard Laurence Millington Synge, who established the techniques of partition chromatography and inspired the development of paper, gas and high performance liquid chromatography (Giddings and Keller, 2014).

It is now widely employed throughout the bioprocessing industry for the purification of biopharmaceuticals (Bahme, H. -J, P. Hedman, 2002). At large-scale, there are many modes of operation are employed (table 1). In the food industry, chromatography is used as a means of quality control by separating and analysing preservatives, additives, vitamins, amino acids and proteins (Rathore and Kapoor, 2016). It is used in environmental testing laboratories to separate trace quantities of contaminants such as DDT in groundwater PCBs in waste oil, the purification of drinking water and the testing of air quality. Mixed-mode chromatography is used widely as a polishing step and refers to a method that uses more than one form of interaction (e.g. ion exchange and hydrophobic) to achieve higher selectivity and thus better separation.

Table 1 Modes of chromatography

Type of chromatography	Separation principle
Ion exchange	Net charge
Hydrophobic interaction/ reverse phase	Hydrophobicity
Size exclusion	Size and shape
Affinity	Biological function
Chromatofocusing	Isoelectric point
Immunosorption	Antigenicity
Lectin affinity	Carbohydrate content
Immobilised metal affinity	Metal binding
Chemisorption	Chemical reactions
Hydroxyapatite, dye affinity	Miscellaneous

Of the main industries process-scale chromatography serves, (biotechnology and pharmaceuticals, food and nutraceuticals), the biotech and biopharma markets accounts for the largest share, with the biopharmaceuticals generating global revenues of $160 billion per year. The large-scale chromatography market is estimated to reach $8 billion by 2021 and approximately 70% of the cost of process-scale chromatography is accounted for by the amount of resins and solvents used (Tran, 2011). The importance of chromatography is noted by the key biological products used as therapeutic agents such as albumin, insulin, human growth hormone, platelet derived growth factors, monoclonal antibodies etc. However appropriate means must be found in order to force processing costs down.

1.2.Components of column chromatography

Column chromatography is comprised mainly of the following elements (figure 2):

- Column
- Stationary phase (section 1.3)
- Mobile phase

Other elements include:

- Fraction collection
- Pumping and detection system
- Solvent reservoirs

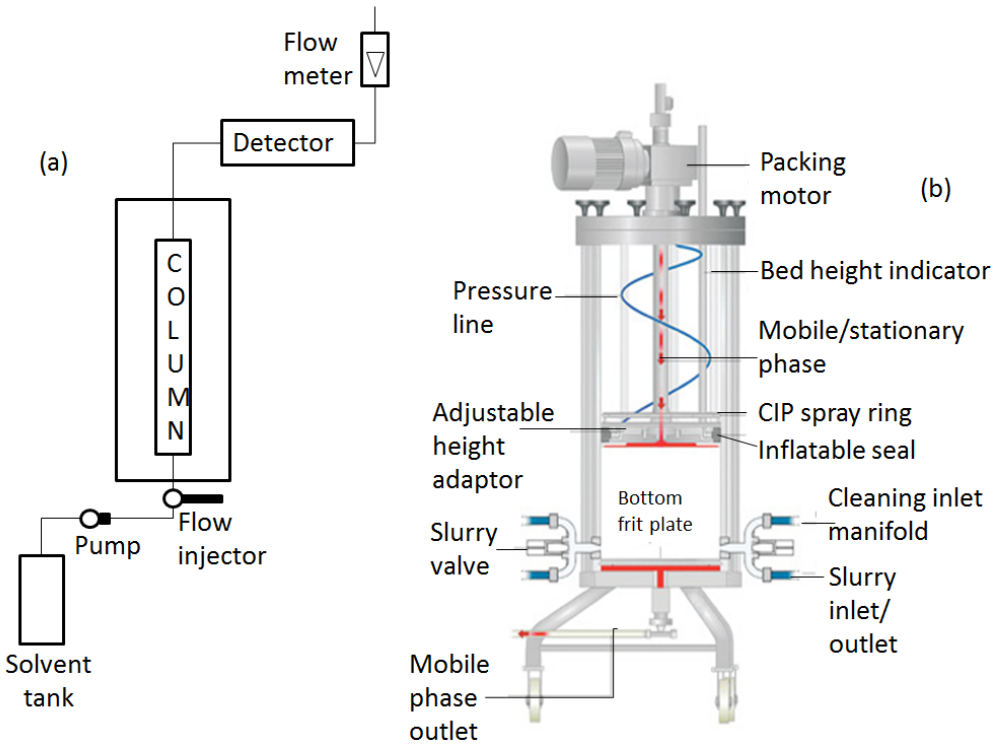

Figure 2 Industrial chromatography unit. (a) Schematic diagram (b) Chromatography column adapted from (Bio-Rad Laboratories, 2014)

Columns, as the name suggests, are cylindrical apparatuses. Smaller columns are usually made of borosilicate glass and larger columns are usually made of stainless steel (Clark, 2007). The physical column itself has a fixed length but attached is usually a variable end piece to adjust the bed length, so as to prevent dead spaces in the stationary phase, which could lead to back-mixing, reducing process performance.

Large-scale prepacked columns come readily available for use in manufacturing however are limited in packed bed height, resin type and column diameter. There is potential for growth in this area, however a number of limitations should be revised if it is to be as widely employed as non-prepacked options (Grier and Yakubu, 2016)

The mobile phase is also referred to as the eluent. It is chosen based on its ability to separate compounds effectively and provide the conditions under which separation can take place. In column chromatography, the mobile phase is largely the buffer system and this can vary depending on the mode of chromatographic operation. A buffer system is usually comprised of an equilibration buffer, an elution buffer, a wash buffer or regeneration buffer, a Clean-in-place (CIP) buffer and in some cases, deionised water.

1.3.The role of resins

Resins play the vital role in column chromatography. They can also be referred to as the stationary phase, the matrix, the column packing or the adsorbent. They are small bead particles that are provided in the form of slurry, approximately 100µm in size per bead, and prior to use are assumed spherical (figure 3). This slurry is poured into the column and allowed to settle to give a measured bed height. During operation resins are responsible for separating biological impurities such as host-cell proteins (HCPs), oligomers and nucleic acids from a target biologics, such as monoclonal antibodies, which must be purified to very high levels (often >99%) (Chochois *et al.*, 2011).

There are a number of properties that are considered ideal for base matrices (table 2). Furthermore, manufacturers must ensure that chromatography media meet a broad range of requirements before use for the separation/purification of biological products. These requirements include a number of safety considerations (leachables, toxicology), performance (capacity, specificity, throughput), cost (capital investment, longevity) and stability, among others (Ioannidis, 2009). Stability can be split broadly into two categories – chemical and mechanical. The chemical resistance of chromatography media is dependent on the coupling chemistry as well as the choice of spacer and ligand chemistry and stability. Whereas, the mechanical stability is dependent largely on the choice and composition of the base material, particle size distribution, particle porosity, and to a lesser extent, ligand and ligand deployment (Jagschies, Sofer and Hagel, 2008; Andersson, 2014).

The base material is chosen based on a number of factors such as cost, the properties of the material to be processed and surface area and mass transfer characteristics, giving rise to parameters such as dynamic binding capacity (DBC) maximum flow rates, maximum number of cycles etc. Based on this, different manufacturers use different composite materials for their chromatographic media (Jungbauer, 2005). There are a number of base materials that can be used in the formation of resin beads (table 3)

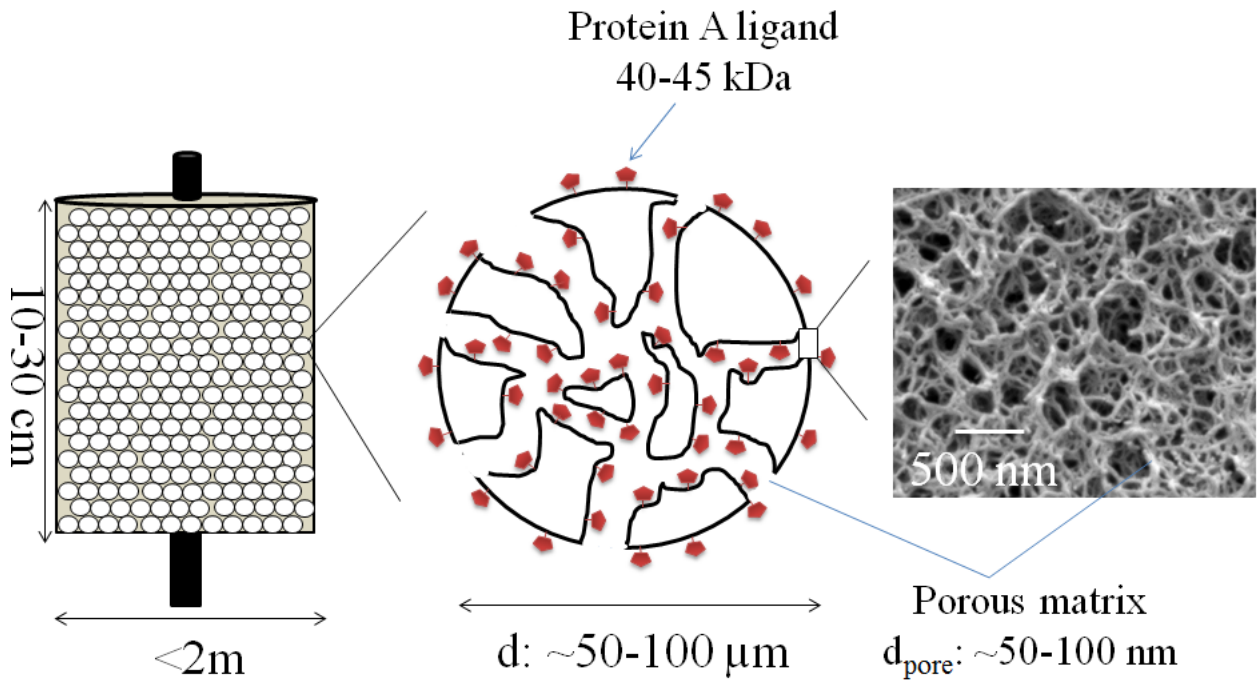

Figure 3 – showing size of typical large-scale column, schematic of resin structure and scanning electron microscopy (SEM) image of protein A resin prior to processing.

Table 2 Ideal base matrix compositional properties

Ideal base matrix compositional properties
Hydrophilic
Large pore size/ surface area
Spherical (mono-sized) particle
Low unspecific adsorption
Easy to functionalise
Reusability and low cost
Chemically stable
Mechanically stable

Table 3 Typical base materials used in the formation of chromatography media

Typical base materials for chromatography media
Agarose
Cellulose
Ceramics
Dextran
Polystyrene
Polyacrylamide
Silica
Synthetic/organic polymers

1.3.1. Agarose-based resins

Agarose is a commonly used base matrix material in biopharmaceutical purification as it relatively straightforward to manufacture and customise certain properties such as porosity and specific binding properties. Although resin manufacturing is not a study objective, it is important to understand these principles in relation to the mechanical properties of resins. Agarose is one of two main constituents of agar and is generally extracted from seaweed. It is composed of a polysaccharide polymer material formed of repeating units of 1-3-linked β-D galactose and 1,4-linked 3,6-anhydro-α-L-galactose (Gerstein, 2004). Once the agar has been processed, the agarose is in the form of a dry powder. It is then dissolved in an aqueous solution >85˚C, causing the chains to degrade (Mu, Lyddiatt and Pacek, 2005; Andersson, 2014). When the solution reaches a certain viscosity, it is cooled and poured, whilst simultaneously being stirred into a non-polar organic solvent which contains an emulsifier. These conditions induce the formation of spherical beads (emulsification). The stirring rate is a key parameter in determining certain structural characteristics such as porosity, pore size distribution and particle size distribution, which tends to range from 20-300 μm (Jungbauer, 2005) (figure 4).

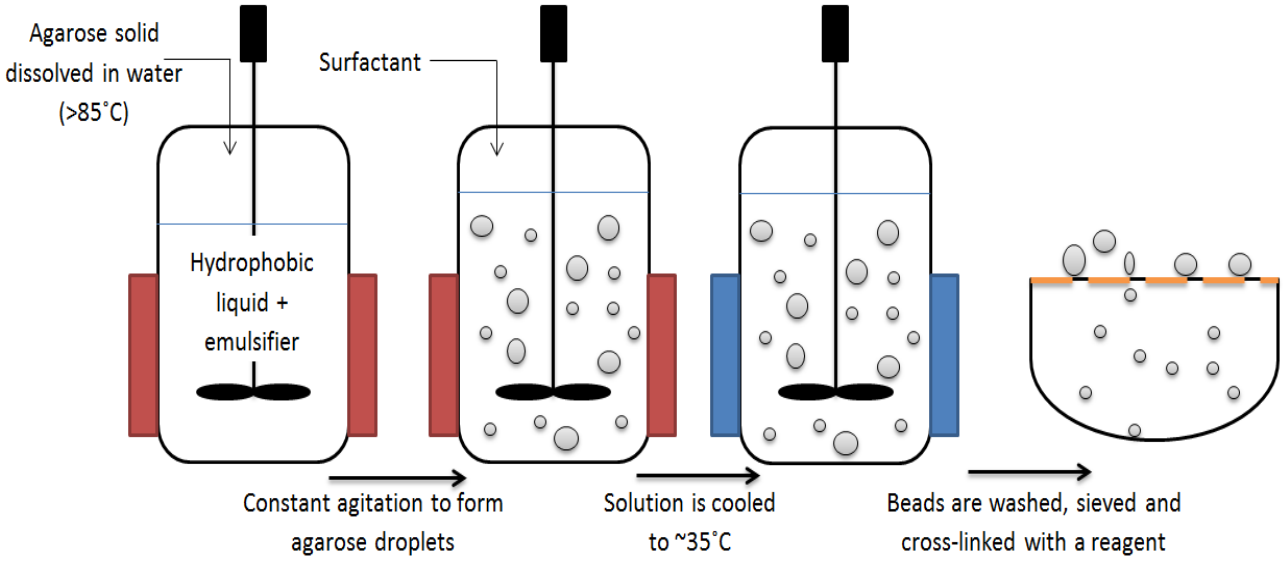

Figure 4 – General method for making porous agarose beads. The agarose solid is dissolved in water heated to about 90˚C. This is then added to a stirred vessel containing a hydrophobic solution (eg. Toluene or mineral oil) together with an emulsifier. The solutions are immiscible meaning that constant agitation causes the formation of agarose droplets. A surfactant is added to prevent droplet coalescing. The solution is then cooled to below the gelation point of agarose (~35˚C) and the beads are then washed, sieved to narrow the size distribution and cross-linked with a reagent.

Upon formation, the beads are insoluble and sediment into the higher density water phase, as opposed to the organic solvent phase. Any remaining solvent phase is then removed in a series of washing and sieving steps and the beads are subsequently cross-linked with a reagent such as epichlorohydrin. The extent to which this is done is one of the critical factors that determine the rigidity of the matrix. However, caution must be taken at this step as over-cross-linking may reduce porosity, ligand deployment and compressibility characteristics (Zhou *et al.*, 2008; Zhou, Ma and Su, 2009). When the process is completed, the resin can be used in various applications such as size exclusion and desalting. It may alternatively go on to be functionalised with different ligand chemistries, such as proteins, aromatic groups, non-polar, charged aliphatic groups etc. (Ioannidis, 2009; Yan *et al.*, 2009; Ioannidis *et al.*, 2012; Andersson, 2014). Now functionalised, they can be used as ion exchange, affinity chromatography, hydrophobic interaction chromatography (among others) and used in various biopharmaceutical applications such as the purification of monoclonal antibodies (Keller, Friedmann and Boxman, 2001).

1.4.Chromatographic operation: Packing

Efficient packing of a column is an important factor for the successful separation of biopharmaceutical products. The purpose of purification (e.g. capture stages, intermediate or polishing stages) and elution (whether it be gradient, step or isocratic) will have an impact on the requirements for column efficiency. Typically, the greater the bed height and the smaller the particle size, the more influential the effects of packing become. A well packed column will also provide a stable bed that will be slow to deteriorate over time (Jagschies, Sofer and Hagel, 2008).

Packing of homogenous chromatography media can be divided into two steps. The aim of the first step is to produce a homogenous consolidated bed. To achieve this, the beads are settled at a constant fluid velocity and are packed due to the viscous drag of the fluid. The selected velocity is dependent on the rigidity of the media and needs to be low enough in order to prevent particle deformation. Generally, the more rigid the particle, the higher the flow rate it can withstand. Research has gone into the stimulation of this consolidation phase by use of computational fluid models to track individual particles when packing smaller beds (Luo *et al.*, 2002; Hemph *et al.*, 2007). The studies capture the essential dynamics but are only modelled on very small-scale (~5mm) columns.

After bed consolidation, the second step is bed compression. The purpose of this step is to create a stable bed that will not deform if used within the set operation window. This operation window is chosen based on the elastic properties of the particles due to fluid stress and wall support (Bemberis, Noyes and Natarajan, 2003).
Compression of the column to its final bed height can be achieved by employing one (or a combination) of a number of packing methods. Such methods include:

- Constant flow
- Constant pressure
- Suction
- Pack-in-place
- Axial compression

In theory, all columns can be packed using constant flow or pressure methods. If no packing method is supplied by the manufacturer, the suggested mode of packing is by constant flow or constant pressure (Cheng, 2009).

Evaluating how well the bed has been packed is important in ensuring bed integrity during separation. Routinely repeating evaluation tests is recommended in order to ensure consistent column efficiency. Correlating the specifications of testing conditions to the required separation performance at certain stages of the purification process is crucial. For example, a column in capture mode using step elution does not require the same efficiency specifications as a column in the polishing stage using isocratic elution (Scharl *et al.*, 2016). It should be noted however, that if the measured efficiency, pressure drop or peak asymmetry is significantly reduced, this strongly indicates that the column needs to be repacked. The most commonly reported methods of column packing evaluation use the step and pulse method, both of which are measures of residence time distribution (Keener, Maneval and Fernandez, 2004).

The use of the step method is effective in manufacturing processes in which buffer salt concentration varies. The efficiency is measured by monitoring changes in conductivity as the concentration of the buffer is varied from high to low salt (or vice versa). The shape of the resulting curve is a step which can be likened to frontal analysis (Kennedy 2003). This analysis is generally performed in-process, and unlike pulse testing, does not require the input of an additional sample to the column. This evaluation can only be applied, however, if it has been verified that there is a linear relationship between changes in tracer concentration and the measured signal that has been subjected to evaluation.

The most commonly reported method of column evaluation involves adding a pulse. A pulse is a low molecular weight solute of a narrow sample zone (usually 1-2% v/v acetone or benzyl alcohol) (Rathore and Kumar, 2017). Subsequently, the values for zone broadening are then calculated in terms of *H* (or HETP – height equivalent to a theoretical plate) and/or peak symmetry (A_s – asymmetry factor) using the formulae below (Kennedy 2003) (figure 5):

$$N = 5.54 \left(\frac{t_r}{W_{1/2}}\right)^2 \quad (1.1)$$

Where N – number of plates

t_r – retention time of probe molecule

$W_{1/2}$ – width of peak at one half maximum height

$$HETP = \frac{L}{N} \quad (1.2)$$

Where L – total length of column

$$A_s = \frac{b}{a} \quad (1.3)$$

Where a – distance from leading edge of peak to midpoint of peak

b – distance from midpoint of peak to trailing edge of peak

A related method is the use of reduced HETP (HETP ÷ mean particle diameter). This normalizes HETP for particle diameter and is useful when comparing HETPs for columns with different particle sizes.

a

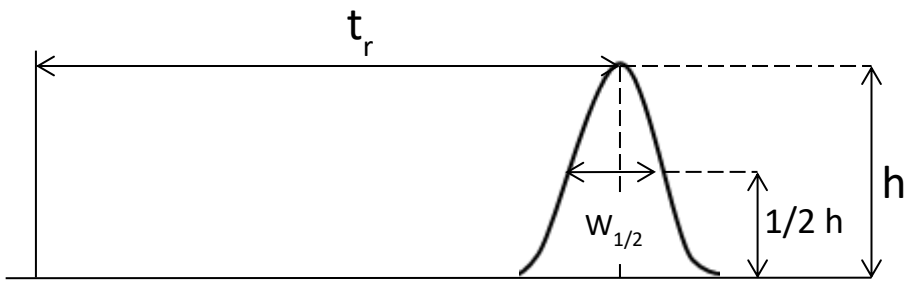

Injection

b

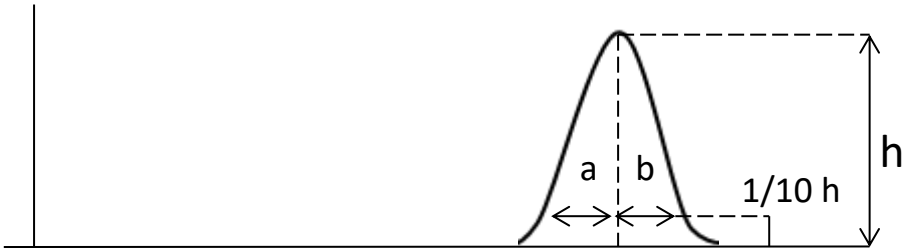

Injection

Figure 5 – pulse testing column evaluation method. (a) the HETP can be calculated by first calculating N (number of plates) using values from the width of the peak at half its maximum height ($W_{1/2}$) and the retention time of the probe molecule (t_r). (b) the asymmetry can be calculated by dividing b by a, where a is the distance from the leading edge of the peak to the midpoint and b is the distance from the midpoint to the trailing edge of the peak.

1.4.1. Structure-diffusion relationships

Post-packing, there are many in-process elements that contribute towards the gradual deterioration of resins and packed beds over time. In order to understand the factors that contribute towards performance reduction, it is first important to understand the interactions that occur between the different phases during column operation. There are two main areas to consider: the impact of process conditions on the individual beads and the impact of process conditions on the packed bed as a whole (Rathore and Kumar, 2017).

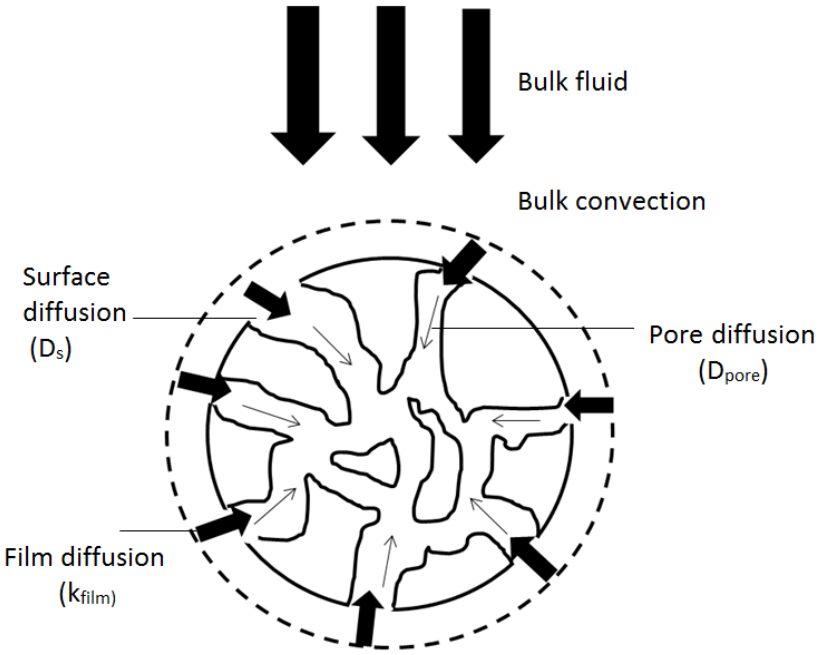

Figure 6 – Schematic of an individual chromatography bead showing mass transfer process of a solute. Binding of a solute to an immobilized ligand contributes to the rate of reaction at the binding site (not shown). Surface diffusion, pore diffusion and film diffusion also need to be accounted for at bead level.

Broadly, there are four factors influencing mass transfer at the bead level, namely, external mass transfer through the film layer around the bead particle (k_{film}), diffusion through the surface (D_s) and the pore (D_{pore}) of the bead, and reaction rate at the binding site of an immobilized ligand (figure 6) (Rathore and Kumar, 2017). Due to the complex nature of the movement of any given solute through a bead, the

partial differential equations vary greatly depending on how the movement is modelled. A complete description of mass transfer models is available in the form of the general rate model (GRM), which covers k_{film}, D_s, D_{pore}, and reaction rate (von Lieres and Andersson, 2010). Albeit, a numerical solution of the GRM is still computationally complex. The past decade has seen a rise in using readily available numerical solving tools such as chromX and CADET in the application of less complex models (von Lieres *et al.*, 2014). Such models include the transport dispersive model (TDM) and the lumped rate model (LRM). In TDM the external and internal mass transfer factors are combined to create one transfer coefficient (Hahn *et al.*, 2015) while in LMR reaction rate kinetics and mass transfer factors are combined into one parameter while pore and surface diffusion is assumed infinite. Whilst LMR is the simplest computational model used for ion-exchange chromatography, there still remains other, more simplistic approaches that describe the in-process interactions in a packed bed during column operation (figure 7).

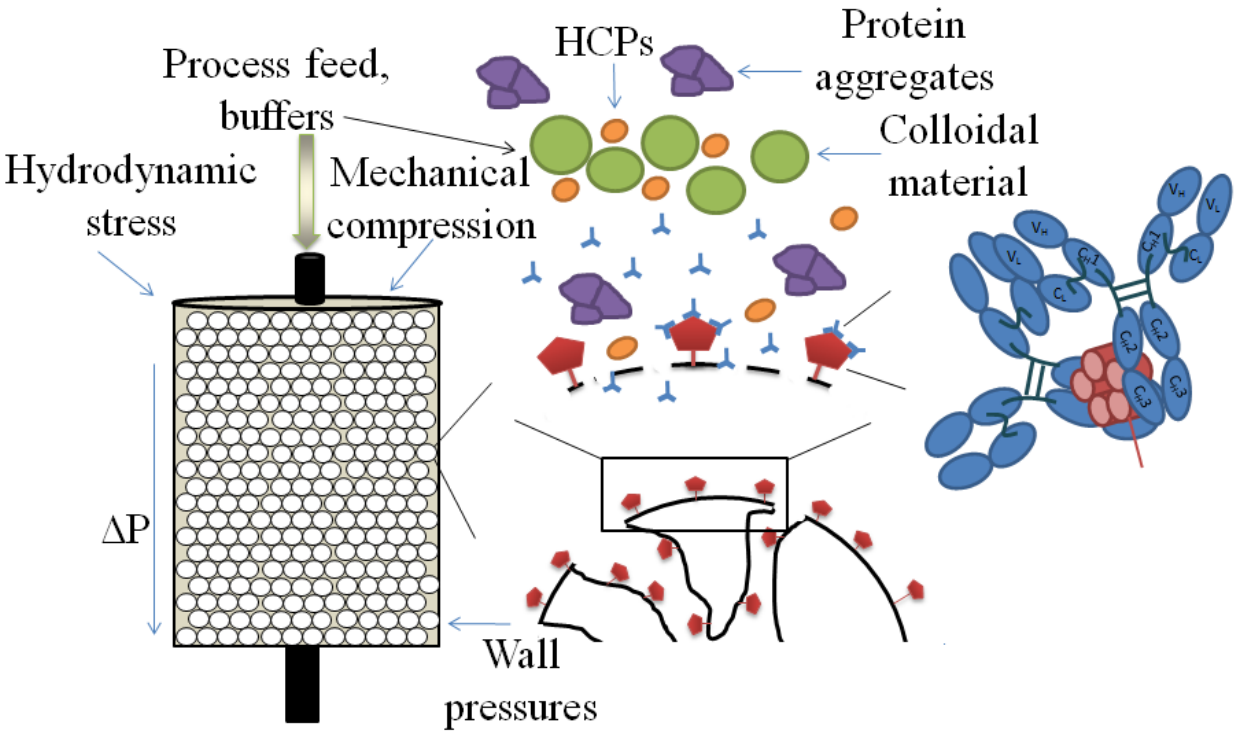

Figure 7– In-process factors that contribute to the movement of solute through the packed bed. The effects of flow rate, mobile phase viscosity, resistance to mass transfer due to pressure equilibriums should also be noted.

A more simplistic description of processes at work inside a column accounts for the time taken for the solute to equilibrate between the stationary and mobile phase (dissimilar to the plate model, which is based on the assumption that equilibration is infinitely fast). The resulting shape of a chromatographic peak is therefore affected by the rate at which elution occurs. It is also affected by the different paths a solute may travel between particles of stationary phase. If the various mechanisms which contribute to band broadening are considered, the result is the Van Deemter equation for plate height (figure 8);

$$\text{HETP} = A + B / u + C u \qquad (1.4)$$

where u is the average velocity of the mobile phase. A, B, and C are factors which contribute to band broadening (Ioannidis, 2009).

***A* - Eddy diffusion**

As the mobile phase moves through the column, solute molecules will take different paths through the stationary phase at random. This will bring about broadening of the solute band, as different paths are of different lengths.

***B* - Longitudinal diffusion**

Analyte concentration is reduced at the edges of the band than at the centre. Analyte diffuses out from the centre to the edges. This brings about band broadening. High mobile phase velocity means that the analyte spends less time on the column, which decreases the effects of longitudinal diffusion.

***C* - Resistance to mass transfer**

The analyte spends a certain amount of time equilibrating between the stationary and mobile phase. High mobile phase velocity will result in the analyte having a stronger affinity for the stationary phase. The result of this is that an analyte in the mobile phase will move ahead of an analyte in the stationary phase, resulting in broadening of the analyte band. The higher the velocity of mobile phase, the wider band broadening becomes.

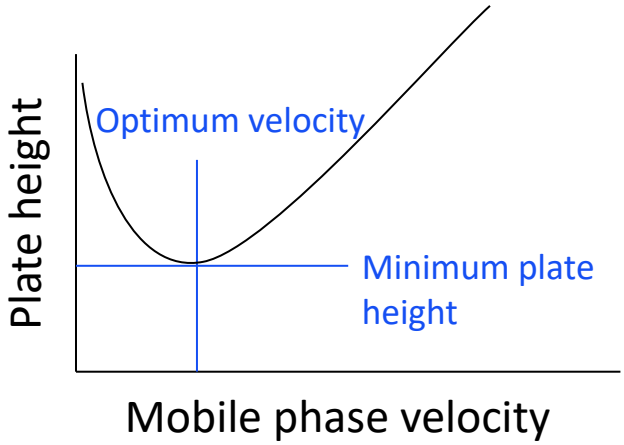

Figure 8 – Typical van Deemter plot of plate height vs. average linear velocity of mobile phase. The optimum mobile phase flow rate can be determined.

1.4.2. Adsorption

In chromatography, convective flow is what allows for the transport of the mobile phase through the stationary phase, whereas diffusion governs the transport of molecules through the porous adsorbent (Ioannidis, 2009). The adsorption of proteins refers to the reversible adhesion of molecules from the mobile phase to resin surface (Close, 2015). It is dictated by the thermodynamic interactions that occur when load material comes into contact with ligands covalently bound to the resin bead surface. At macroscopic level, components of the feed material distribute themselves between the stationary and mobile phases. Modelling the theory of adsorption is complicated for a number of reasons, as explained by Rabe et al. 2011 in table 4. However, there are experimentally- and empirically-derived adsorption isotherm models available that generically describe the interaction of components between the mobile phase and stationary phase. The most extensively studied models can be grouped as Equilibrium models (Mollerup, 2008).

Equilibrium isotherm models assume bound protein concentration at steady state. There are a number of commonly reported isotherms, including linear, Langmuir, steric mass action (SMA), preferential interaction quadratic, Freundlich, Brunauer, Emmet and Teller (BET) etc. The most simple equilibrium model is the linear isotherm which assumes that the stationary phase is under-challenged, meaning that there are a large number of free binding sites (Guichon, A and Shirazi, 2006). This is often seen in analytical chromatography where small amounts of protein are loaded onto the column. However this is not the case in industrial-scale bioseparations where the column is loaded to maximum capacity to achieve high productivity (Tugcu, Roush and Goklen, 2007). The most commonly used isotherm model is the Langmuir model as it can be extended to deal with more than one component/complexity (Close, 2015). It is based on four assumptions (Guichon, A and Shirazi, 2006):

1. The surface of the adsorbent is uniform, i.e. all the adsorption sites are equivalent
2. Adsorbed molecules do not interact
3. All adsorption occurs through the same mechanism
4. At the maximum adsorption, only a monolayer is formed i.e. molecules of adsorbate do not deposit on other

Generally, single component Langmuir isotherms are used to aid in the understanding of the impact of a single feature or aspect during chromatographic operation, as has been reported by Gu et al. 1990 and Sun & Yang 2008. Multicomponent Langmuir isotherms have been applied to understand competition between components (Lienqueo, Shene and Asenjo, 2009; Müller-Späth *et al.*, 2011; Guélat *et al.*, 2012). However, it is yet to be as widely applied as single component isotherms due to a lack of understanding (Close, 2015).

Table 4 The complexities associated with the accurate modelling of adsorption (Rabe, Verdes and Seeger, 2011)

Factors affecting the modelling of adsorption
Each molecule contains many electrostatic and hydrophobic groups heterogeneously distributed throughout the entire protein structure
Proteins are typically asymmetric and so representing them as a sphere is unrealistic. Proteins often simultaneously interact with multiple binding sites
Cooperative effects from proteins that are already adsorbed means that proteins are sometimes more likely to adsorb if there are pre-adsorbed proteins.
During adsorption and/or desorption proteins often unfold and change structure, potentially changing the groups exposed at the surface of the protein.
Due to the similar size of molecules to resin pore diameter, and the range of ionic strengths encountered, electrostatic force fields can interact causing the local conditions to vary.
Proteins can also self-associate (aggregate), both in solution and on the stationary phase, so interactions between components are very important.
Proteins often denature in extreme conditions or due to other components, e.g. proteases.

1.4.3. Resin lifetime and aging

Over repeated cycles of exposure to process conditions, the performance of the resin will experience a gradual decline over time. Most reports on resin aging tend to largely focus on quantifying the loss in performance characteristics by measuring certain parameters such as dynamic binding capacity (DBC), yield, throughput etc. (table 5) (Siu *et al.*, 2006; Jiang *et al.*, 2009; Gavara *et al.*, 2015; Scharl *et al.*, 2016). However the reports do not focus enough on the mechanisms by which the resins age, which lead to a decline in these performance characteristics.

Each report does allude to, however, the fact that selected process conditions largely determine the speed at which resins will begin to age. The packing process may cause the column to undergo mechanical compression (Cheng 2009; Bemberis et al. 2003; Keener 2004; Kennedy 2003). Further effects on the column include differences in pressure throughout the column, hydrodynamic stresses caused by changes in flow rate and column wall pressures (which are more prevalent with smaller-width columns) ((Hemph *et al.*, 2007). These issues lead to column compression and column plugging, all contributing to packed bed failure (figure 9). The impact of selected process conditions can also be observed at microscale. Deposits may become irreversibly bound to the matrix fibres leading to fouling of the bead surface (Siu *et al.*, 2007). Although the main contributor to the degradation of matrix fibres is not clear, exposure to strong CIP and regeneration conditions is highly likely to be the cause, potentially leading to the production of resin fines (Jiang *et al.*, 2009; Close, 2015).

Whilst reduced DBC and yield are often measured concurrently, it should be noted that reductions in DBC are related to ligand deterioration factors, whilst reductions in yield may also be related to previously mentioned factors. A decline in ligand performance may be occur for a number of reasons such as, leaching of the ligand off of the matrix, occlusion of the ligand by non-target molecules and inactivation of the ligand due to possible changes in ligand chemistry post-exposure to process conditions (Zhang, Xu, *et al.*, 2015).

Table 5 Parameters associated with the quantification of resin lifetime

Measurable parameters for determining chromatography resin lifetime	
Purity of product	Bed height
Impurities (e.g. DNA)	Dynamic/static binding capacity
Pressure/ flow rate	Packing integrity
Product yield	Leachables
Elution profile	Ionic capacity (IEX)
Regeneration profile	Appearance (microscopy)
Loading profile	Productivity
Voidage (inter/intra particle porosity)	Adsorption isotherms

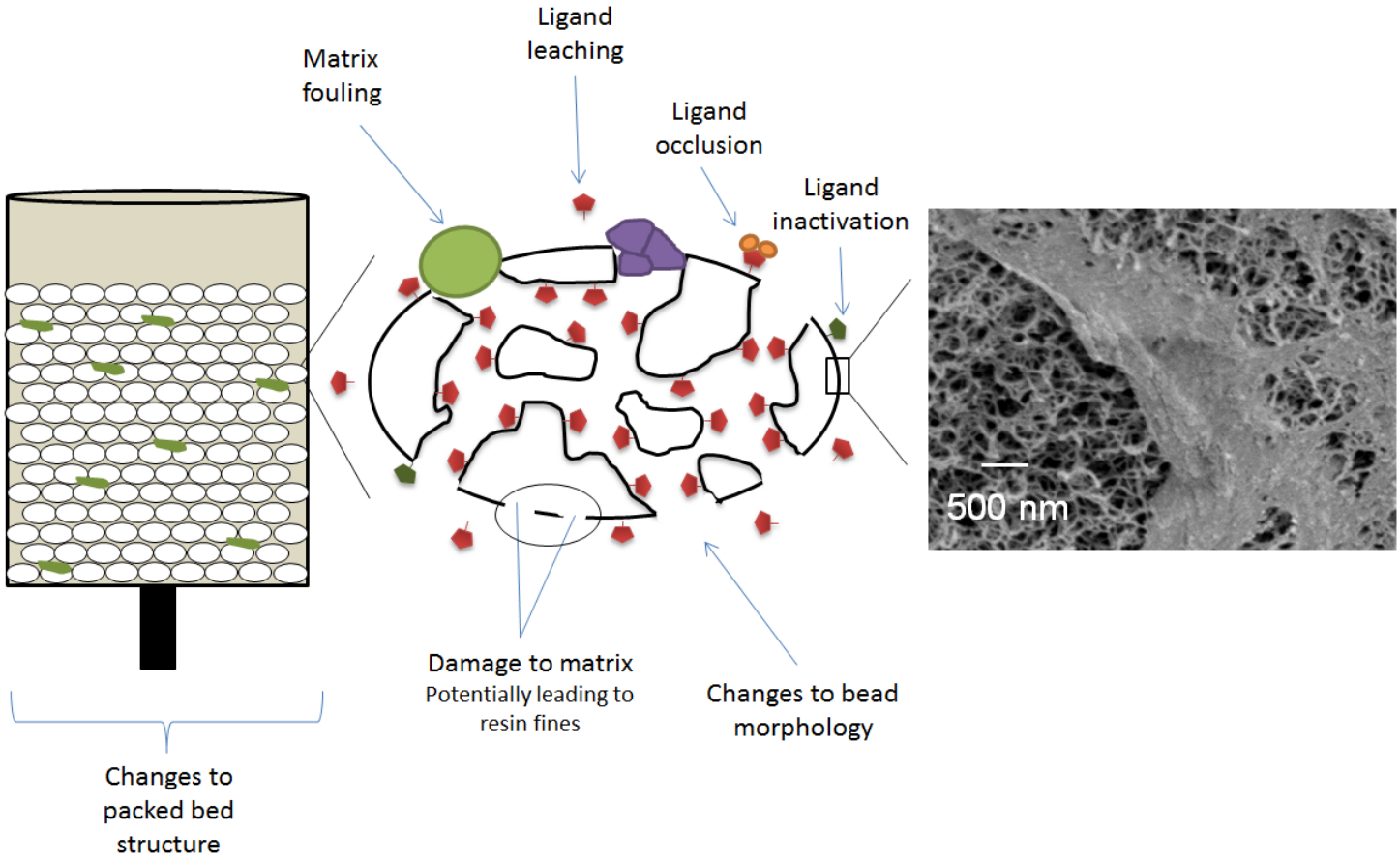

Figure 9 – Showing possible mechanisms of chromatography resin aging. Column-scale level changes include changes to packed bed structure. At bead level this could translate to changes to bead morphology, ligand leaching, ligand occlusion, ligand inactivation, matrix fouling and damage to matrix fibres, potentially leading to the production of resin fines

1.5.The importance of characterisation

Most Protein A resins are used for ≤100 cycles before a decline in performance parameters, such as DBC, yield, throughput etc., is observed (table 5). However, the expected use of these resins is estimated to be at least 3 times higher than its current usage (Rathore *et al.*, 2015; Hernandez, 2016). The lack of live/real-time tracking tools present during column operation makes it difficult to monitor column performance and the column aging process. Furthermore, increased product titres in recent years has led to heavier burdens on downstream purification, which has meant that regulatory authorities such as the FDA are requesting for better defined processes from manufacturers (Hentschel, 2013). The Quality by design approach (QbD) was introduced into the chemical manufacturing control (CMC) review process in 2004, followed by Process Analytical technology (PAT) initiatives, both with the objective of achieving a desired state for pharmaceutical manufacturing (Rathore, 2009). QbD has been defined in the International Conference on Harmonization (ICH) Q8 guideline as 'a systematic approach to development that begins with predefined objectives and emphasizes product and process understanding and process control, based on sound science and quality risk management' and there are a number of steps involved in the successful implementation of both QbD and PAT, which involve identifying quality target product profile (QTPP) and critical quality attributes (CQAs) (table 6a) as extensively outlined by Rathore & Kapoor 2016.

Table 6a Steps involved in the implementation of QbD/PAT

Steps involved in the implementation of QbD/PAT
Identify QTPP
Identify CQA
Define Product Design Space
Define Process Design Space
Redefine Product Design Space
Define Control Strategy
Process Validation
Process Monitoring

Whilst worthwhile and extensive research has been put into the validation and characterisation of chromatography media via measuring the changes in DBC, yield, throughput etc., not as much has gone into establishing mechanical and structural characterisation tools for these resins during and post-processing, as a means of fulfilling regulatory requirements. Whilst it has been noted that there are a lack of these tools at large-scale, a number of tools have been employed at research level that provide high-level structural and mechanical information of chromatography media during and post-bioprocessing and have shown good potential to be employed at larger-scales (table 6b).

Table 6b – showing techniques that can be used to meet certain QbD initiatives and their extent of use/maturity in research. Green indicates high usage, yellow- medium, blue- low (novel tools)

Technique/tool	**Maturity (references)**	**QbD applications**
Microscopy techniques (SEM, AFM, CLSM, TEM etc.)	(Linden *et al.*, 1999; Susanto *et al.*, 2006; Yang, Shi and Sun, 2006; Hubbuch and Kula, 2008; Ioannidis, 2009; Close *et al.*, 2013; Zhang, Daniels, *et al.*, 2015)	CQAs/CPPs associated with product yield and levels of impurities, product characterisation
Florescence real-time monitoring	(Pathak *et al.*, 2017)	PAT applications, IPC testing, process monitoring
Inter/intra particle porosity	(Yao and Lenhoff, 2004; Bacskay, Sepsey and Felinger, 2014; Sepsey, Bacskay and Felinger, 2014)	CPPs associated with voidage and changes to mass transfer properties
Pressure-flow	(Stickel and Fotopoulos, 2001; Tran *et al.*, 2007) (industry and resin manufacturers)	CPPs associated with pressure/ CQAs associated with mechanical integrity
Packing: Asymmetry/ HETP	(Bemberis, Noyes and Natarajan, 2003; Keener, Maneval and Fernandez, 2004; Dorn *et al.*, 2017; Kong *et al.*, 2017)	CPPs associated with packing integrity
X-ray topography	(Johnson *et al.*, 2017)	PAT applications, IPC testing, process monitoring
Mass spectrometry	(Thillaivinayagalingam *et al.*, 2007; Jin *et al.*, 2009; Laursen, Justesen and Rasmussen, 2011; Andersson, 2014; Lintern *et al.*, 2016)	CQAs associated with impurity levels, product characterisation
Micromanipulation	(Mu, Lyddiatt and Pacek, 2005; Yan *et al.*, 2009; Ioannidis *et al.*, 2012)	CQAs/ CPPs associated with yield and mechanical integrity

1.6.Mechanical and structural characterisation techniques

1.6.1. Microscopy techniques

Extensive research has gone into microscopy techniques that best characterise chromatography media. Examples include: Optical microscopy of agarose beads (Zhou *et al.*, 2008; Zhou, Ma and Su, 2009), transmission electron microscopy (TEM) of agarose beads (A Amsterdam, Er-El and Shaltiel, 1975; Attwood, Nelmes and Sellen, 1988), alongside freeze-fractured agarose gels (Waki, Harvey and Bellamy, 1982) gel slabs (Griess, Guiseley and Serwer, 1993), confocal laser scanning microscopy (CLSM) of lipid fouled protein A (Jin *et al.*, 2009) and protein uptake studies (Linden *et al.*, 2002). Atomic force microscopy (AFM) has also been employed in the investigation of agarose gel surfaces (Pernodet, Maaloum and Tinland, 1997; Maaloum, Pernodet and Tinland, 1998; Ioannidis, 2009) and finally scanning electron microscopy (SEM) has been used in to characterise agarose based resins (Medin, 1995; Zhou, Ma and Su, 2009; Close *et al.*, 2013) (figure 10). Other microscopically characterized (SEM) adsorbents include polyacrylamide and dextran based agarose composite beads (Grimaud *et al.*, 1978).

A commonly reported limitation of microscopy is sample preparation due to the sensitive nature of hydrogels. It is therefore crucial to choose the least invasive sample preparation technique to avoid damage to ultrastructural properties. However, it seems to be the case that the more invasive the sample preparation is, the better the quality of the images obtained, whether or not the extracted information is realistic. This is particularly prevalent in SEM and TEM. An example of this occurrence can be found in a number of pieces of research (A Amsterdam, Er-El and Shaltiel, 1975; Attwood, Nelmes and Sellen, 1988; Griess, Guiseley and Serwer, 1993) where sample staining, buffer exchange and sample embedment in epoxy resin resulted in average quality images whereas, freeze fracturing and freeze-drying improved the quality of the images (Waki, Harvey and Bellamy, 1982; Medin, 1995).

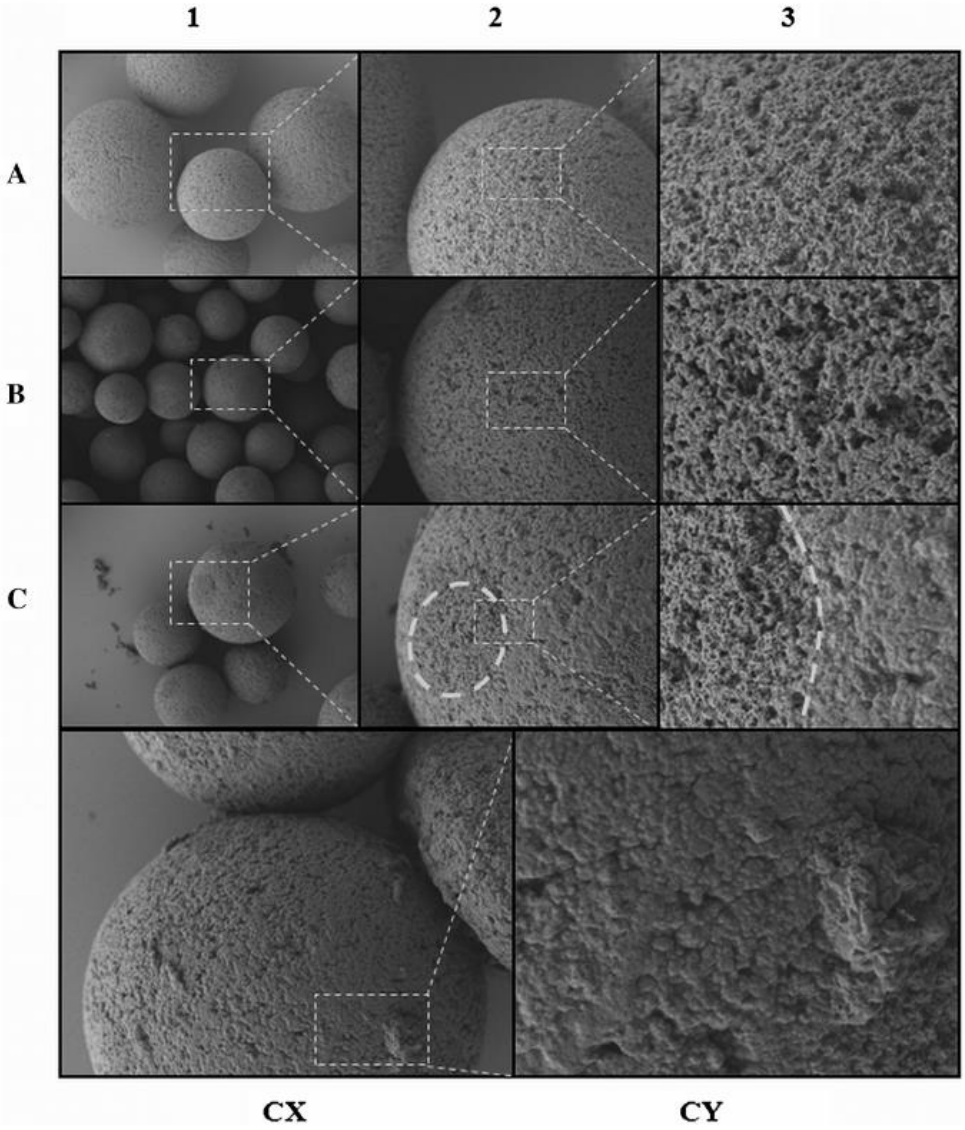

Figure 10 - Scanning electron microscopy images of A: clean, B: partially fouled. C: Extensively fouled resin particles. (Close *et al.*, 2013)

1.6.2. Chromatographic techniques

The inverse application of size exclusion chromatography (ISEC) also serves as a method for characterizing the porous structure of chromatographic adsorbents. In the initial stages of this technique, biomolecules are separated according to their size. Biomolecules ranging in size are introduced into the column. Molecules larger than the size exclusion limit of the adsorbent will not enter the pores of the gel and will quickly pass through the bed. Smaller molecules diffuse in and out of the porous network and therefore require more time to elute (Masters, 2012). As a result, the mixture separates in order of decreasing molecular size and the pore size and pore size distribution of the adsorbent can be determined. ISEC analysis of the adsorbent structure requires priori selection of a physical model that best describes the molecular probe properties alongside the structural characteristics of the adsorbent (Yao and Lenhoff, 2004). For this reason a limitation of this technique is that the obtained results will be heavily dependent on the selected probe and pore model (Hagel, Ostberg and Andersson, 1996).

A number of adsorbents have been structurally characterised using the ISEC technique. Such adsorbent composites include, dextran polyacrylamide, polyacrylamide-agarose (Grimaud *et al.*, 1978) alumina, silica (DePhillips and Lenhoff, 2000), controlled pore glass and polystyrene (Knox and Ritchie, 1987). Molecular probes used in ISEC include DNA, proteins, ficol and pullulan (Yao and Lenhoff, 2004) and dextrans (Hagel, Ostberg and Andersson, 1996).

More recently, Pathak et al. 2017 developed a real-time column monitoring tool using florescent markers to track the movement of process feed throughout the column. It was able to monitor foulant concentration build-up and deposition during chromatographic operation with an error of less than 1%. They were able to observe that fluorescence intensity consistently increased with resin reuse as more foulants were deposited over time, potentially signifying that this approach can be implemented as a means to monitor fouling and process control.

Pressure-flow characterisation is performed to obtain data that is representative of the pressure-flow relationship of the column during operation. This information is then used to predict the limit of the operating pressure drop and flow velocity. In contrast to open bed pressure-flow measurements, the top bed support is in contact with the bed, creating a compressed structure. Therefore, a compression factor (usually ranging from 1.15 to 1.20 for agarose-based resins) is applied during media packing. Packed bed pressure-flow information is mainly used to determine the pressure drop during column operation. The acquired data provides information regarding the flow velocity limit for the media in use. The limit denotes the point at which the bed will start to compress to such an extent that a gap is created between the top bed support and the bed (resin rigidity limit) (Jagschies, Sofer and Hagel, 2008).

In this technique, the flow rate is manually increased until a runaway rise in the pressure profile is observed. The flow rate at which this occurs is converted to linear velocity. This is the point at which the column has ‘failed’ and is termed the critical velocity. The more rigid the resin is, the higher the critical velocity. The degree to which any individual repeat may vary is reliant mainly on column packing and the resulting asymmetry. The probability that a column will pack in exactly the same way, despite using the same procedure is low. This is represented by the asymmetry value obtained.

1.6.3. Other techniques

Gel electrophoresis - This technique separates proteins according to their charge. When in a free solution (usually a gel medium), proteins separate at different speeds due to differences in their charge densities. The gel medium acts as an inert support for the electrophoresis buffer or may actively participate in the separation process via interaction with the proteins. The protein-gel interaction gives rise to separation and the electrical field promotes migration of proteins though the gel. Commonly used gels for electrophoresis include agarose and polyacrylamide (Laas, 1998). Structural properties and mass transport of solutes in agarose gels have been widely studied with this technique (Fatin-Rouge, Konstantin and Jacques, 2004). Similar to ISEC, when a mixture of biomolecules is applied, structural information of the gel can be obtained. Probes used to study the structure of agarose gels via electrophoresis include dextrans, proteins, DNA molecular weight ladders and polymer beads ranging between 10 and 140nm (Pluen *et al.*, 1999; Fatin-Rouge, Konstantin and Jacques, 2004).

Micromanipulation – Micromanipulation was first introduced as a theoretical concept by University College London in 1987 and the first practical rig was developed by the university of Birmingham in1990. It involves measuring mechanical properties of individual particulate matter. The technique was employed by Blewett 2000 to test the strength single particles of fungal hyphae under uniaxial extension. The technique had also been applied to mammalian cells, yeast cells and tomato cells (Zhang *et al.*, 1991; Srinorakutara, 1997; Mashmoushy, Zhang and Thomas, 1998; Wang, Wang and Thomas, 2003). More recently, it has also been applied to chromatography-based materials such as dextran beads, agarose beads, polymeric chromatographic adsorbents and gelatin-rich microparticles (Stenekes *et al.*, 2000; Mu, Lyddiatt and Pacek, 2005; Muller, Chung and Zhang, 2005; Ding *et al.*, 2007). More recently, advancements in the application of this technique had been made by Liu et al. 2005. The mechanical properties of single nanoparticles, 800 nm in size, were measured with an ESEM nanomanipulation rig, designed and constructed by this group of researchers.

Dynamic mechanical analysis (DMA) - This technique involves applying a small deformation to a sample in a cyclic manner and allows for the sample material to respond to changes in stress, temperature, strain, frequency, force as well as other parameters (figure 11). It is used widely in the bioengineering sector and the field of biosciences to characterise the viscoelastic properties of various biological tissue and other biomaterials. Traditionally, the stress and strain parameters are used to calculate Young's modulus to give an indication of changes in elastic properties. Moroni et al. 2006 used the technique to investigate the use of scaffolds to mimic human tissue. They found that the technique was particularly sensitive to pore size changes in scaffolds. With increasing porosity in the scaffolds, there was a decrease in elastic properties, which corresponded to an increase in strain. It has also been used to look at the mechanical properties of materials similar to agarose gels, such as hydrogels. Meyvis & Stubbe 2002 used DMA as a comparative technique to shear rheometry to investigate mechanical properties of pharmaceutical hydrogels. They found a strong correlation between the two techniques but observed that DMA can be used to investigate many more mechanical parameters than solely viscoelasticity. The technique has not yet been applied for the purposes of chromatography resin characterization. We apply this technique in this study in an attempt to address limitations associated with more established techniques.

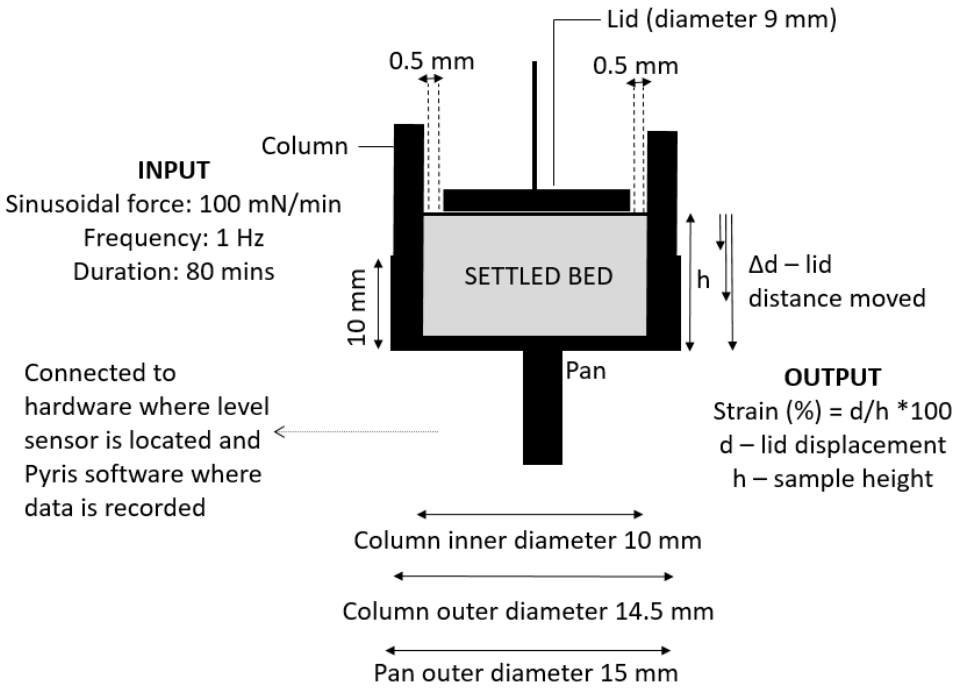

Figure11 – Schematic of DMA set up and dimensions. The lid has a diameter of 10mm and the column that sits inside the pan has an inner diameter of 11mm and an outer diameter of 14mm. A sinusoidal force of 100mN is applied at a frequency of 1Hz over a period of 80 minutes. The output is strain v time, where strain is the displacement of the lid relative to the sample height.

CHAPTER 2
MATERIALS AND METHODS

2. MATERIALS AND METHODS

This section outlines the experimental procedures used in different sections of this study as well as the materials used and where they were derived from.

All nine of the fresh resins used in this study – Capto Q (CQ), Capto Adhere (CA), MabSelect (MS), MabSelect Xtra (MSX), Q-Sepharose High Performance (Q-HP), Sepharose 6 Fast Flow (S6FF), Sepharose CL-6B (SCL6B), Sepharose 4 Fast Flow (S4FF), Sepharose CL-4B (SCL4B) – were from GE Healthcare, Uppsala, Sweden. Structural characterisation of these resins was performed using scanning electron microscopy (SEM). Pre-treatment procedures and the SEM technique itself are outlined in section 2.1. Pressure-flow characterisation and dynamic mechanical analysis are then used for mechanical characterisation of the fresh resins. The experimental procedures are outlined in sections 2.2 and 2.3 respectively. Four of the nine resins (CA, MS, Q-HP and MSX) were exposed to 2 bioprocessing conditions termed ‘CIP-exposed’ and ‘aged’ conditions. CIP-exposed conditions consist of buffers only and aim to assess the impact of clean-in-place conditions on structural and mechanical viability of the resins. The methods are outlined in section 2.4. Aged resins are resins that have been used for resin lifetime studies in the production of a monoclonal antibody or a fusion protein. Structural and mechanical characterisation of these resins was performed in-house. The methods of aging are outlined in section 2.5.

2.1.Scanning electron microscopy - preparation and experiments

Separate 1 ml slurries (75% slurry concentration in 20% ethanol) of the aforementioned fresh resins were used for this study.

2.1.1. Air drying

0.5 ml of each sample was syringed into a labelled petri dishes and left in a safety cabinet (Class 2 MSC Walker, Derbyshire) for 24 hours. In this time the ethanol evaporated to leave dry resin samples. These samples were then visually analysed under a scanning electron microscope.

2.1.2. Freeze drying

The protocol employed is as an adaptation of previously reported freeze drying methodologies (Tsinontides *et al.*, 2004; Jones, 2012; Nireesha *et al.*, 2013; Zeitvogel *et al.*, 2016). In this case, the time spent in the freezing and drying stages of the process is increased. A 0.5 ml aliquot of each sample was syringed into separate sterile polystyrene petri dishes (Fisher Scientific ™, 60mm x 15mm) and labelled accordingly. They were then placed on different shelves in the freeze dryer (Virtis Genesis 25EL, SP Scientific, US) to avoid cross-contamination. The samples were left in the freeze dryer for 30 hours. The freezing stage was held for 8.5 hours with a step-wise decrease in temperature, from 25˚C to -30˚C (a one degree decrease approximately every 9 minutes). The drying stage was held for 21.5 hours with a step-wise increase in temperature, from -40˚C to 25˚C (a one degree increase approximately every 20 minutes).

2.1.3. Critical point drying

The storage medium of our agarose beads is made up of 80% water, however water has an unfavourable critical point of +374˚C and 3212 p.s.i. which will cause heat damage to the beads (Bray, 2000). For this reason, the medium used for critical point drying is Carbon Dioxide (CO_2), with a critical point of 31˚C and 1072 p.s.i. (Pandithage, 2012). Water and CO_2 are not miscible however, and for this reason a transitional fluid is used. This fluid is miscible with both water and CO_2 and is usually an alcohol. As our chromatography media is stored in 20% ethanol, the

transitional fluid used in this case is ethanol.A 0.5 ml aliquot of each sample was syringed into a 1.5 ml Eppendorf tube and labelled accordingly. The beads were dehydrated in a graded ethanol-water series to 100% ethanol (20%, 50%, 70%, 90%, 100%) and put in critical point dryer (Polaron Critical point dryer, Quorum Technologies Ltd, Essex). In critical point dryer, the beads were flushed 3 times in CO_2 in a graded series for 30 minutes. The temperature was raised to above 32˚C for 60 minutes (figure 12).

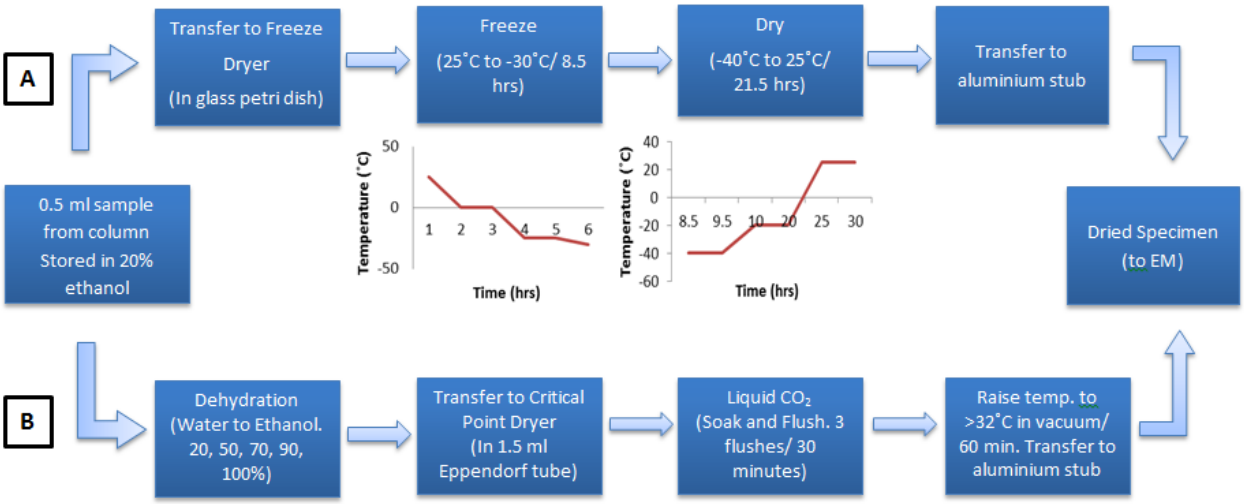

Figure 12 - (A) Selected freeze drying conditions. A 0.5 ml aliquot of sample is frozen over a period of 8.5 hours in a graded fashion from 25˚C to - 30˚C. The sample is transferred onto a sticky aluminium stub for SEM. (B) Selected critical point drying conditions. 0.5 ml of sample is dehydrated in graded fashion from 0-100% ethanol before transfer to critical point dryer where sample is flushed 3 times in liquid CO_2. The temperature is raised in a vacuum to above 32˚C for 60 minutes. The sample is transferred onto a sticky aluminium stub for SEM.

2.1.4. Sample coating preparation

A wooden spatula is used to remove the dried resin from the tubes onto the labelled 1x1 cm cylindrical aluminium specimen stub (Agar Scientific, UK) for sample coating. The surface of the specimen stub is sticky so that the sample is not removed during subsequent steps.

The sample is placed into the ion gun gas flow control where excess liquid is vacuumed out of the resin at 10^{-3} Pa. The Gatan, model 681 high resolution ion beam coater (Gatan, Inc., US) is then used to coat the samples in a gold/ palladium alloy (1-2 nm thickness of coating). SEM imaging requires the sample to be electrically conductive in order to prevent the build-up of electrostatic charge. It is for that reason that metal objects require little preparation for SEM imaging. However samples of resin beads and other non-conductive samples tend to charge when scanned by the electron beam, consequently causing scanning fault (Goldstein *et al.*, 2013). For this reason non-conductive samples are coated with conductive metals, most commonly gold or a gold/palladium alloy. The ion beam coater is operated at 5.8 ke V, angle 70˚.

2.1.5. SEM Imaging

After the coating process, the samples are then mounted onto an SEM carrier and inserted into the JEOL JSM-7401F field emission scanning electron microscope (JEOL USA, Inc., US) for imaging at 10.0µA and 2 keV accelerating voltage.

2.1.6. Quantitative analysis using ImageJ software

The scale was set by using the software by manually drawing a line of 0.6 cm (as this was the length of the scale bar measuring 100nm). The software then calculates the number of pixels equivalent to 0.6 cm and the user can then insert the actual length of the sample (100nm). The 'Smooth' filter is selected so that most projections are flattened (https://imagej.nih.gov/ij/docs/guide/146-29.html). The 'Invert' option is then selected to enhance the location of pores. The threshold limit is then set. The edges of each pore are then bordered using the 'Find edges' tool, to further facilitate pore sizing. The particle analyser function is selected to allow for the calculation of

pore sizes and related properties. Subsequently, a window appears numbering the location of each detected pore so that this can be corresponded with the results window. The user defines how the results are displayed. In this study results are displayed per unit area (nm^2). The software then displays two windows – a results window (containing raw data) and a summary window. The summary provides the user with the pore count information, average pore size and porosity. In this study, porosity is recorded as a percentage, for example, 15% porosity means that 15% of the image were pores and therefore 85% of the image is the fibrous network.

2.2.Pressure-flow characterisation

2.2.1. Equipment

A bench-scale column with adjustable column length and inner diameter of 1.6 cm (model XK16, GE Healthcare, Uppsala, Sweden) was used. This was operated on the AKTA Pure (GE Healthcare, Uppsala, Sweden). Column pressure drop (ΔP) was measured using the internal pressure measurement devices installed in the feed delivery system of the AKTA Pure and the volumetric flow rate was measured manually using the method employed by (Tran *et al.*, 2007).

2.2.2. Chromatography media

Sepharose CL-4B, Sepharose CL-6B, Sepharose 4 Fast Flow, Sepharose 6 Fast Flow, Q Sepharose High Performance, MabSelect Xtra, MabSelect, Capto Q and Capto Adhere (GE Healthcare, Uppsala, Sweden) were used in this study. These agarose-based chromatography resins have an average particle size of 80 µm, with a bead size distribution of between 24-165 µm. The mechanical differences between the seven resins lie in the agarose content and the extent of structural cross-linking present.

Sepharose 4 FF/ 6 FF, MabSelect Xtra, MabSelect, Capto Adhere and Capto Q are made of highly cross-linked agarose, whereas Sepharose CL-4B/CL-6B and Q Sepharose HP are structurally simpler in terms of their cross-linking. However Sepharose 6 FF, CL-6B, Q Sepharose HP and MabSelect all contain the same percentage of agarose in their matrices (6%), while Sepharose CL-4B and Sepharose 4 FF contain 4% and Capto Q 7%.

2.2.3. Characterisation procedure

Packing – All chromatography media was made up to 50% slurry concentration. The same procedure was repeated for all seven resins. 30 ml of slurry was poured into the column and allowed to gravity settle overnight. The adaptor was lowered into the supernatant to start the flow pack. All columns were packed at 15cm/hr for 60 minutes and subsequently at 30 cm/hr for 30 minutes. The columns shown in table 7

were further consolidated. The top adaptor was then lowered to the top of the bed. The packing medium used for all buffers was distilled H_2O (dH_2O) (as per resin manufacturer recommendations – see datasheets).

Table 7 – Packing flowrates for Sepharose 4FF, Sepharose 6FF, Q-Sepharose HP, MabSelect and Capto Q

Resin	**Packing flow rates**
Sepharose 4 FF, Sepharose 6 FF, Q Sepharose HP	400 cm/ hr – 2 minutes
MabSelect	500 cm/ hr – 2 minutes
Capto Q	600 cm/ hr – 2 minutes

Performance testing – 2% v/v of acetone was measured and added into 30 ml of dH_2O in a 50ml falcon tube (CELLSTAR®, UK). 1 ml of this solution was injected into a 600 µl loop and then loaded onto the column. The eluent used in this study was dH_2O at 30 cm/hr. A peak was then generated within 30 minutes. The asymmetry was calculated using the in-built function on the Unicorn 6.4 software. Pressure-flow method – The flow rate of the packing buffer was continually gradually increased until a 35 kPa increase in pressure drop was observed, as described by Tran et al. 2007. At this point, the flow rate and any changes in bed height were manually recorded. At a certain flow rate, the pressure began to increase exponentially with no further change to the flow velocity. At this point it was deemed that the critical velocity for the column had been reached.

2.3. Dynamic mechanical analysis

2.3.1. Column/ holder design

10 identical cylindrical blocks of transparent acrylic were drilled with an inner diameter of 11mm, an outer diameter of 14mm and a height of 15mm. The bottom was wrapped in a thin sheet of parafilm (0.1mm thickness) to contain the slurry.

2.3.2. Sample preparation

An aliquot of 10 ml of each resin was placed into a labelled 50 ml falcon tube and centrifuged for 5 minutes at 3000rpm (Eppendorf centrifuge 5810 R, Thermo Fisher Scientific, UK) and the slurry concentration was noted based on the volume ratio of liquid to slurry in the falcon tube. The storage buffer (20% ethanol) was decanted, replaced with their respective packing buffers and the slurry solution was made up to a 70% slurry concentration. The aliquots were resuspended and the procedure was repeated until the storage buffer had been completely removed. 1.42 ml of each aliquot was pipetted into their respectively labelled holder and left to settle overnight, such that their settled bed height was 1cm.

2.3.3. Characterisation procedure

DMA was carried out on the DMA 7e hardware, with a TAC 7/DX controller and Pyris Manager software (PerkinElmer, UK). In this procedure the force reading is zeroed, the weight of the probe is tared and the probe position is zeroed when the lid is lowered to the base of the pan. The lid is lifted and the holder containing the slurry is placed onto the pan. The lid is lowered to the top of the resin bed, the height is read and the methodology is started. In this methodology, the lid applies a force of 100mN/min at a frequency of 1 Hz for 80 minutes and a time-strain plot is generated simultaneously. Upon completion of the methodology, the slope of the line is manually fitted from the origin to the point before ultimate compression using the in-built slope function in the Pyris Manager software.

2.4. CIP cycling experiments (CIP-exposed conditions)

Four of the nine resins (CA, MS, Q-HP and MSX) were exposed to 2 bioprocessing conditions termed ‘CIP-exposed’ and ‘aged’ conditions. CIP-exposed conditions consist of buffers only and aim to assess the impact of clean-in-place conditions on structural and mechanical viability of the resins. This section outlines the procedure used to perform CIP cycling studies on MabSelect, MabSelect Xtra and Q-Sepharose High Performance. CIP cycling experiments on Capto Adhere were performed by Eli Lilly & Co. in a 45ml column, internal diameter 22mm, for 50 cycles and conditions are detailed subsequently. The CIP experiments using MS, MSX and Q-HP were performed in 1ml HiTrap columns (x5) on the AKTA Pure (GE Healthcare, Uppsala, Sweden) over a 50 cycle period. The experiments were initially designed to be as close to the buffers used for ‘aged’ resin conditions as possible. However, for confidentiality reasons, the exact conditions could not be disclosed. To address this, standard protocols used by GE Healthcare were used for MS, MSX and Q-HP instead. The protocols used for each resin is detailed below. Experiments were generally run at 1ml/min, however, elution steps were run at 0.5 ml/min to mimic standard process conditions. Certain less conventional conditions (such as the use of 0.5M NaOH for MS CIP protocol) were used after discussions with the sponsoring company.

2.4.1. MabSelect CIP cycling protocol

Mili Q wash (5CV)
Equilibration (3CV): 20 mM sodium phosphate, 0.15 M NaCl, pH 7.4
Blank load (no protein) (2CV): 20 mM sodium phosphate, 0.15 M NaCl, pH 7.4
Wash (5CV): 20 mM sodium phosphate, 0.15 M NaCl, pH 7.4
Elution (2CV): 0.1 M sodium citrate, pH 3.0
CIP (2CV): 0.5M NaOH
Regeneration (2CV): 20 mM sodium phosphate, 0.15 M NaCl, pH 7.4

2.4.2. MabSelect Xtra CIP cycling protocol

Every cycle

Mili Q wash 5 CV
Equilibration (3CV): 20 mM sodium phosphate, 0.15 M NaCl, pH 7.2
Blank load (no protein) (2CV): 20 mM sodium phosphate, 0.15 M NaCl, pH 7.2
Wash (5CV): 20 mM sodium phosphate, 0.15 M NaCl, pH 7.2
Elution (2CV): 0.1 M sodium citrate, pH 3.0–3.6
CIP1 (2CV): 0.5M acetic acid

Every 5th cycle

Mili Q wash 5 CV
Equilibration (3CV): 20 mM sodium phosphate, 0.15 M NaCl, pH 7.2
Blank load (no protein) (2CV): 20 mM sodium phosphate, 0.15 M NaCl, pH 7.2
Wash (5CV): 20 mM sodium phosphate, 0.15 M NaCl, pH 7.2
Elution (2CV): 0.1 M sodium citrate, pH 3.0–3.6
CIP1 (2CV): 0.5M acetic acid
Wash (2CV): 20 mM sodium phosphate, 0.15 M NaCl, pH 7.2
CIP2 (2CV): 0.1M NaOH
Regeneration (2CV): 20 mM sodium phosphate, 0.15 M NaCl, pH 7.2

2.4.3. Q-Sepharose High Performance CIP cycling protocol

Pre-equilibration (1CV): 1M NaCl
Equilibration (5CV): 20 mM Tris-HCl, 0.7 M NaCI, pH 8.0
Blank load (no protein) (2CV): 20 mM Tris-HCl, 0.7 M NaCI, pH 8.0
Wash (5CV): 20 mM Tris-HCl, 0.7 M NaCI, pH 8.0
Elution (2CV): 20 mM Tris-HCl, 1 M NaCI, pH 8.0
CIP (2CV): 1M NaOH
Regeneration (5CV): 20 mM Tris-HCl, 0.7 M NaCI, pH 8.0

2.4.4. Capto Adhere CIP cycling protocol

These experiments were conducted by Eli Lilly & Co. The disclosed process information is outlined below.

Wash: Tris buffer
Elution: 20mM Acetate buffer, 100 mM NaCl
Regeneration: Weak acid
Sanitisation: Strong base

The column pack is regenerated and sanitised after every run; the column is stored after every second run.

2.5. Aged conditions

All ‘aged’ resin experiments were conducted externally by Eli Lilly & Co. and other external partners. The resins used in this study were MabSelect, MabSelect Xtra, Q-Sepharose HP and Capto Adhere, 2 of which were used as a capture step and 2 of which were used as intermediate/polishing steps in 3 separate purification protocols. The experiments are resin lifetime studies which aim to somewhat mimic the process conditions used at large-scale manufacturing in the production of monoclonal antibodies and fusion proteins. MabSelect and Capto Adhere were used as capture and polishing steps respectively in the production of an IgG4. Q-Sepharose HP was used in the post-capture stages of fusion protein purification and MabSelect Xtra was used as a capture step in the purification of an IgG1 monoclonal antibody. The experimental conditions for each resin are outlined below.

2.5.1. MabSelect ‘aged’ conditions

MabSelect was used as the capture step in the purification of Ixekizumab (chinese hamster ovary (CHO) expression), an injectable drug used in the treatment of autoimmune diseases such as plaque psoriasis. The manufacturing process involved it being run over a 17 cycle period, in a 130 litre column (diameter 100cm, height 17cm). The buffer conditions are outlined below.

Wash: Tris buffers
Elution: Sodium Citrate, pH 3
Regeneration: 1% acetic acid, 1 % phosphoric acid.
Sanitisation: 50 mM NaOH, 1 M NaCl.
Storage: Sodium Acetate Buffer, pH 4

Sanitisation performed prior to the first cycle of two, and following the last cycle of two.

2.5.2. Capto Adhere ‘aged’ conditions

Capto Adhere was used as the polishing step in the purification of Ixekizumab. The manufacturing process involved it being run over a 17 cycle period, in a 145 litre column (diameter 80cm, height 29cm). The buffer conditions are the same as those outlined in section 2.4.4.

2.5.3. Q-Sepharose High Performance ‘aged’ conditions

Q-Sepharose HP was used in the post-capture stages in the purification of a fusion protein (CHO expression). The manufacturing process involved it being run over a 64 cycle period, in a 45 litre column (diameter 60cm, height 16cm). The buffer conditions are outlined below.
Wash and elution: Tris buffers.
Regeneration and Sanitisation: 1 N NaOH.
Storage: 0.1 N NaOH

Sanitisation performed prior to the first cycle of eight, and after every cycle.

2.5.4. MabSelect Xtra ‘aged’ conditions

MabSelect Xtra was used as the capture step in the purification of an IgG1 monoclonal antibody. The manufacturing process involved it being run over a 20 cycle period, in a 25ml column (bed height 20cm). The buffer conditions are outlined below.
Wash: phosphate based
Elution: acetate buffer
CIP: 0.5M acetic acid, every cycle. 0.1M NaOH, every 5 cycles

CHAPTER 3
THE STRUCTURAL CHARACTERISATION OF CHROMATOGRAPHY MEDIA USING SCANNING ELECTRON MICROSCOPY (SEM)

3. THE STRUCTURAL CHARACTERISATION OF CHROMATOGRAPHY MEDIA USING SEM

The performance of chromatography columns in large-scale manufacturing of biotherapeutics is intrinsically linked to cost of goods and quality control. Poor understanding of the events leading to column failure can make it difficult to ensure robust operation avoiding process failures. Close examination of the bead structure can aid in this understanding, particularly of the mechanical properties of the chromatography resin. While there are various approaches and imaging techniques that can be employed for the visualisation of chromatography resin, few techniques provide the level of resolution as well as the adequate representation of its three-dimensional structure required to analyse materials on the nanometre scale necessary for this.

Scanning Electron Microscopy (SEM) is a technique routinely used to generate high-resolution images. It is used widely in chemistry and biosciences to identify microstructures, spatial compositions and the general characterization of solid materials down to less than 50nm in size (Swapp, 2015). The benefits of SEM are that use the technique requires little sample preparation and is able to provide highly accurate information concerning the 3D morphology and the location of features relative to each other, whilst still providing sufficient resolution and magnification required for this particular application. Whilst there is arguably no other instrument with the breadth of applications in the study of solid micro-materials that compares with conventional SEM, the main limitation is that samples must be dry prior to imaging. This is particularly problematic with regards to agarose-based chromatography media, as water is a significant component in their structural composition.

Consequently, there is a need to determine the most suitable drying technique for the visualisation of agarose-based chromatography media. This chapter discusses the factors for consideration when choosing the most appropriate drying conditions by exploring three established drying techniques in the biosciences that have proven to preserve biological properties of proteins and retain structure, namely air drying, freeze drying and critical point drying. The selected drying technique is applied to

nine resins used in this study - Sepharose CL-4B (4% agarose content), Sepharose CL-6B (6% agarose), Sepharose 4 Fast Flow (4% agarose), Sepharose 6 Fast Flow (6% agarose), Q-Sepharose High Performance (6% agarose), MabSelect Xtra (6% agarose, highly cross-linked), MabSelect (6% agarose, highly cross-linked) Capto Adhere (7% agarose, highly cross-linked) and Capto Q (7% agarose, highly cross-linked), which are then subsequently imaged using SEM.

The micrographs are then analysed both qualitatively and quantitatively. Quantitative analysis is carried out using the Image J software in order to ascertain whether what can be seen can also be measured accurately, with particular focus on average pore size, apparent porosity, pore count and pore size distribution. Apparent porosity is termed as such as it is not a true value of 3-dimensional porosity. It is a value that is based on a 2-D image without account for the angle of the image. Differences in matrix fibre composition can also be inferred from this data. This information can then be used to characterise the structural properties of the resins, based on which mechanical characterisation will be investigated in subsequent chapters.

3.1.Choosing suitable drying conditions

Agarose beads can contain up to 16% moisture content in their composition, which means that water is an integral part of their structural make-up (Ghetie and Schell, 1971; Draveling, 2004). Furthermore, like most biological specimen, agarose-based chromatography resins favour an aqueous environment to remain viable and structurally intact (Joy and Pawley, 1992). Therefore, when choosing the most appropriate drying conditions, it is important to consider a technique that can be finely controlled. An uncontrolled dehydrating process can cause substantial changes in structure and functionality. These changes can include shrinkage, cracking, breakage, morphological alterations, contamination as well as other artefacts. It is therefore important to determine the drying process and the best set of controlled parameters (temperature and pressure) during this process that gives rise to the fewest artefacts in order that the images can be correctly interpreted to understand the structure (table 8).

Little has been reported on the drying technique best suited for the ultrastructural visualisation of agarose-based chromatography resin under scanning electron microscopy. There have been reports of the use of spray drying by Saito et al. 2013 as well as a non-parametric water-to-absolute ethanol dehydration technique by Amsterdam et al. 1975. However, each one of the aforementioned techniques does not provide a sufficient level of drying for the visualisation and characterization of an agarose bead on the nanometre scale. Furthermore, there have been reports that such methods do not perform well at lab-scale, in the case of spray drying or lead to collapse of the bead altogether (Schwartzbach, 2010).

Table 8 – Factors for consideration when choosing drying conditions for agarose-based chromatography resins under scanning electron microscopy (SEM)

Factors for consideration when choosing drying conditions under SEM
Resin composition
Resin stability
Desired imaging resolution (microstructural or nanostructural visualisation)

It is therefore important to investigate a range of drying techniques that have proven to preserve the properties and structure of biological specimen and can be adapted to meet the requirements of agarose beads. Three commonly reported methods used to dry biological material are air drying, freeze drying and critical point drying. There are few reports on the optimisation of these techniques for agarose-based chromatography resins. The subsequent chapters of this study investigate the application of these techniques in order to ascertain which technique and which sets of conditions are most preferable for the ultrastructural visualisation of agarose-based chromatography resins. Visualisation of the ultrastructural properties of the resins will allow for nanostructural characterisation, including pore sizing and matrix formation analysis.

3.1.1. Air drying – procedure development and results

Natural air drying is the process of drying with unheated air, taking advantage of a material's natural drying potential. When compared to vacuum-based drying techniques (such as freeze drying and critical point drying) it is considered to be a more straightforward method of drying as it the material generally requires little to no preparation and the procedure requires minimal technical expertise or machine operation.

In recent times, the procedure has been applied on agarose gels and agarose beads by Nursam et al. 2016 and Close et al. 2013 respectively, with the intention of obtaining structural information on the surface of the material using SEM. In both procedures the agarose was exposed to no more than 10 hours of air in an uncontrolled setting. Although microstructural information was obtained, it was difficult to view nanostructural detail, such as the fibrous network of the materials. Potential reasons for this could have been that the material was not sufficiently dried for higher resolution studies or possible artefact formation on the surface of the materials, which also limits the maximum resolution that can be achieved by SEM.

The air drying protocol used for this study was adapted to address the aforementioned issues. To encourage further drying, the agarose beads were exposed to air for an extended time period of 24 hours. To limit potential artefact formation on the surface of the beads, the resins were dried in a biosafety cabinet, meaning the beads were exposed to controlled air flow and sterile conditions. This technique was tested on Capto ™ Adhere and MabSelect ™ resins and subsequently imaged using SEM. Micrographs showing the 2 resins in different states were obtained. State 1 - individual beads (whole bead images) and state 2 - bead surface images. Whole bead micrographs intended to show any morphological effects of air drying on the resins, while bead surface images intended to show any potential ultrastructural alterations caused by the air drying technique. At least 3 micrographs of each state were acquired for each resin.

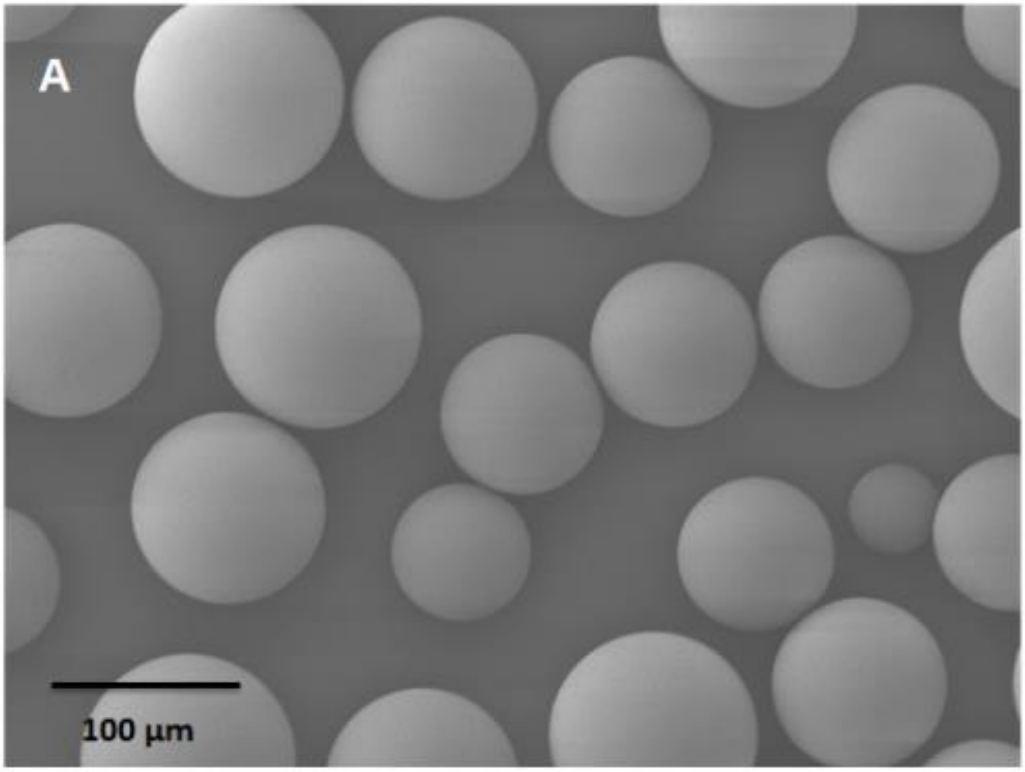

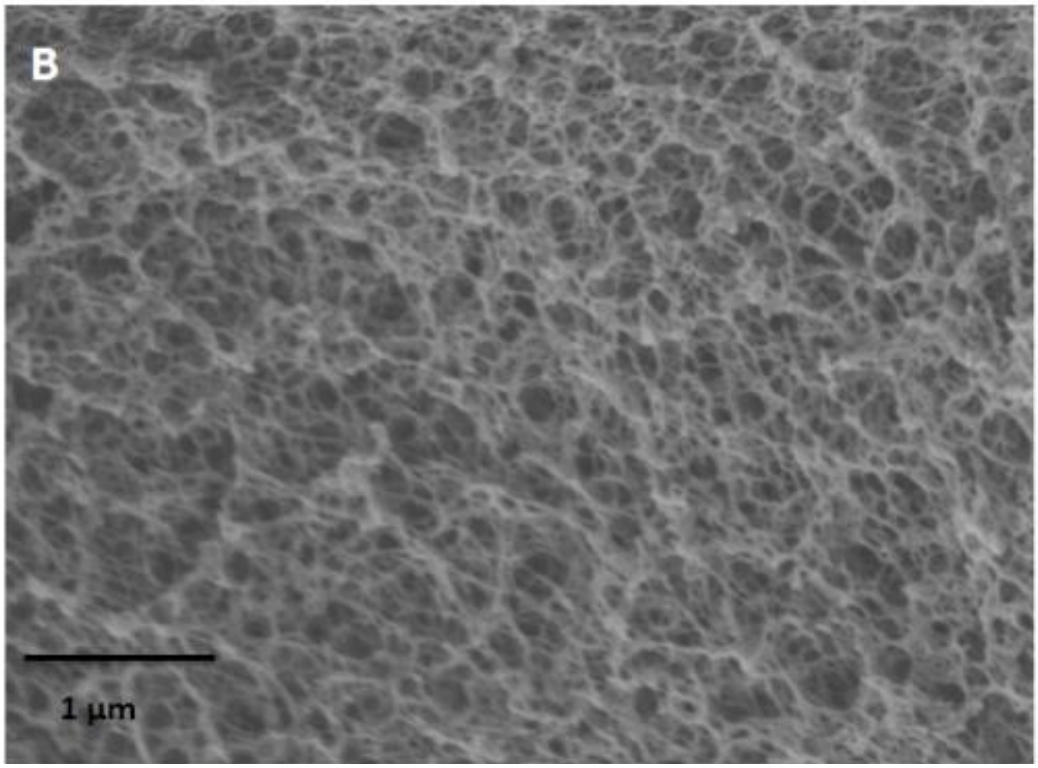

Figure 13 – (A) Scanning electron micrograph showing fresh Capto Adhere post-air drying. Whole bead image 2.0 kV accelerating voltage, x220 magnification, 3cm = 100 µm. (B) Scanning electron micrograph showing fresh Capto Adhere. Bead surface image 2.0 kV accelerating voltage, x25, 000 magnification, 3 cm = 1µm.

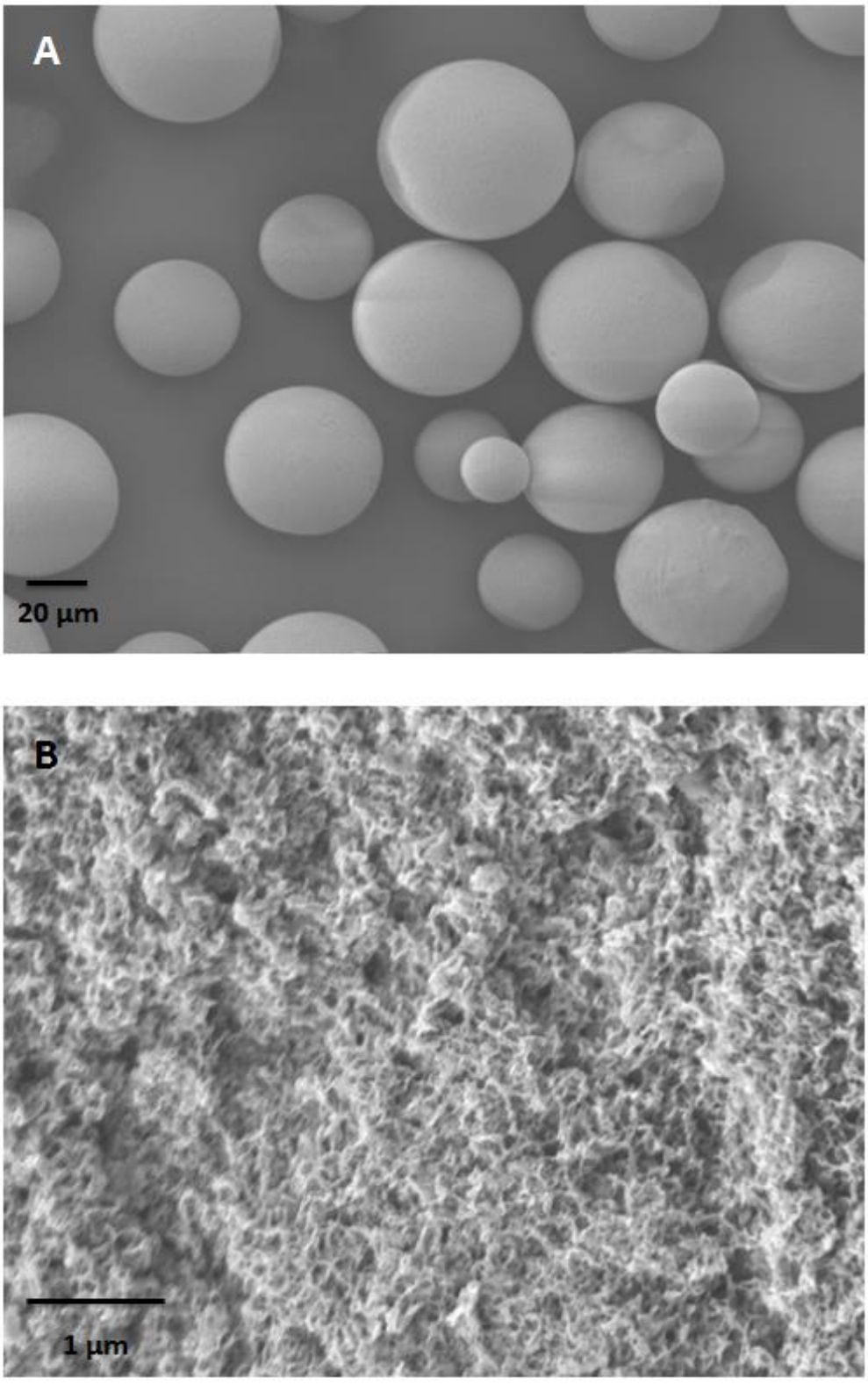

Figure 14– (A) Scanning electron micrograph showing fresh MabSelect post-air drying. Whole bead image 2.0 kV accelerating voltage, x350 magnification, 1cm = 20 µm. (B) Scanning electron micrograph showing fresh MabSelect. Bead surface image 2.0 kV accelerating voltage, x18, 000 magnification, 2.5 cm = 1µm.

The samples imaged post-air drying are represented by figures 13 and 14, fresh Capto Adhere (7% agarose content) and fresh MabSelect (6% agarose content) chromatography resins respectively. These resins are widely used resins for the intermediate and capture stages of monoclonal antibody purification respectively. They are made up of highly cross-linked agarose and it is this make up that helps in determining their structural and mechanical properties. The selected figures are representative of all the images obtained for this section of the study.

Figure 13(A) shows a randomly selected collection of Capto Adhere beads post-air drying. 1 cm of the micrograph represents 50 µm of the sample. The image shows that the individual beads are uniformly spherical in shape and clearly shows there to be a significant particle size distribution (~50-100µm) as specified by the manufacturer, GE Healthcare. This can also be observed in figure 14(A), showing a randomly selected region of MabSelect beads post-air drying (1 cm of the micrograph represents 20 µm of the sample). The beads are also homogeneously spherical with an observed pore size distribution (~40-100µm) as specified by the manufacturer, GE Healthcare. These results indicate that air drying can be used to characterise whole bead structures of chromatography media. It is important to note that imaging artefacts (such as the dark patches that appear in figure 14(A) are defects caused by the scanning speed as the image was captured as opposed to a sample-related defect (see section 3.2.4).

Figure 13(B) shows the surface of a Capto Adhere bead post-air drying selected at random. 3 cm of the micrograph represents 1µm of the sample. The image shows the heterogeneity of the matrix structure, a wide pore size distribution and diversity in pore morphology. The image also shows depth and some distinction can be made between the pores that are closer to the surface and those that extend inwards. However, moving towards the bottom of the micrograph, the image begins to drift. This distortion can occur when the microscope is operating at maximum magnification, meaning that a higher resolution image would be difficult to capture for that particular sample. A probable reason for this could be related to the extent of drying. Higher resolution images are more difficult to obtain if the sample is not sufficiently dried. An image with higher resolution would allow for further ultrastructural analysis and possible quantification of the nanostructure (Williams

and Clifford, 2000). It should be noted that due to the mixed mode properties of Capto Adhere, it has hydrophobic properties pertaining to its ligand characteristics. Further studies would need to be carried out to determine the impact of drying on the stability of these ligands.

Similarly figure 14(B) shows the surface of a MabSelect bead post-air drying selected at random. 2.5 cm of the micrograph represents 1µm of the sample. This image provides almost no ultrastructural information. Unlike figure 13(B), the surface appears to be homogeneously occluded and no observations can be made regarding the matrix structure, pore size distribution or pore morphology. The most likely cause of this could be related to the water retained in the sample due to insufficient drying (Dey *et al.*, 1989). Possible solutions to this issue may involve extending the drying time and increasing the air flow. However, air drying is highly susceptible to the effects of surface tension, as there are no controlled parameters (such as temperature or pressure) when going from liquid to vapour/gas phase (Reville and Cotter, 1991).

The results indicate that this air drying technique is sufficient enough to provide microstructural information and clearly shows the variations in particle size distribution and bead morphology under SEM. However, a drying technique that also allows for the analysis of the nanostructural properties of the resins is required for better characterisation. To address this, the subsequent section investigates the application of two other drying techniques, freeze drying and critical point drying.

3.1.2. Freeze drying vs critical point drying (CPD)

Freeze drying and critical point drying are two established drying procedures that have proven to preserve biological properties of proteins and retain structure. Unlike air drying, these techniques allow for temperature and pressure optimisation and therefore allow for a more controlled dehydration process. Furthermore, both processes avoid transitioning directly from liquid to gas phase, vastly minimising the effects of surface tension. However, there are a number of differences between the two techniques (table 9). Freeze drying works by freezing the sample and subsequently applying a vacuum. This allows for the removal of frozen water (solid phase) by sublimation, which in turn avoids the liquid phase and reduces the effects of surface tension (Tsinontides *et al.*, 2004). Additionally, freeze drying employs a wide range of temperatures when operating in the freezing and drying stages of the process.

The process of critical point drying relies on the continuity of state. Specifically, this occurs at a particular temperature and pressure at which liquid and vapour can co-exist, hence having the same density. The point at which this particular temperature and pressure occurs is termed the critical point. At this stage, there is no apparent difference between the liquid and vapour states in the solid material, reducing the surface tension to zero. This process takes place at a stable temperature range of 32-35˚C (Bray 2000).

There are limited sources that clearly outline the temperatures and pressures used at each stage of the freeze drying process when applied to agarose-based chromatography media. However, the technique has been applied widely to agarose gels and similar materials. The protocol employed in this study is an adaptation of previously reported freeze drying methodologies (Nordestgaard and Rostgaard, 1985; Bell, 1988; Tsinontides *et al.*, 2004; Wilson and Bacic, 2012; Nireesha *et al.*, 2013). In these methodologies, the solid materials are homogeneous in nature, meaning a consistent surface area. Chromatography resins display liquid-like behaviour as a slurry, which means that there is inconsistent exposure to the varying temperature and pressure conditions in the freeze dryer. For this reason, the the time spent in the freezing and drying stages of the process is increased.

The development of the critical point drying protocol used in this study took a number of factors into account. The storage medium of our agarose beads is made up of 80% water (and 20% ethanol), however water has an unfavourable critical point of +374˚C and 3212 p.s.i. which will cause heat damage to the beads (Bray, 2000). For this reason, the medium used for critical point drying is Carbon Dioxide (CO_2), with a critical point of 31˚C and 1072 p.s.i. (Pandithage, 2012). Water and CO_2 are not miscible however, and for this reason a transitional fluid is used. This fluid is miscible with both water and CO_2 and is usually an alcohol. As our chromatography media is stored in 20% ethanol, the transitional fluid used in this case is ethanol. The chromatography resins were then dehydrated in a graded ethanol-water series to 100% ethanol before being placed into the critical point dryer (see materials and methods).

Table 9 Factors for consideration when choosing critical point drying or freeze drying as a drying technique for agarose-based chromatography resin

*Optional; Sample can be fast-frozen in e.g. liquid nitrogen prior to freeze drying

**Selected conditions

***Can go down to as low as >-80˚for very delicate sample

Factors	CPD	Freeze drying
Preparation	Yes (water → ethanol)	None*
Media required	Ethanol, CO_2	Water
Phases	Liquid → Gas	Solid → Gas
Time	2-3 hours**	24-30 hours**
Working temperature	32-35˚C	-30/-40˚C***

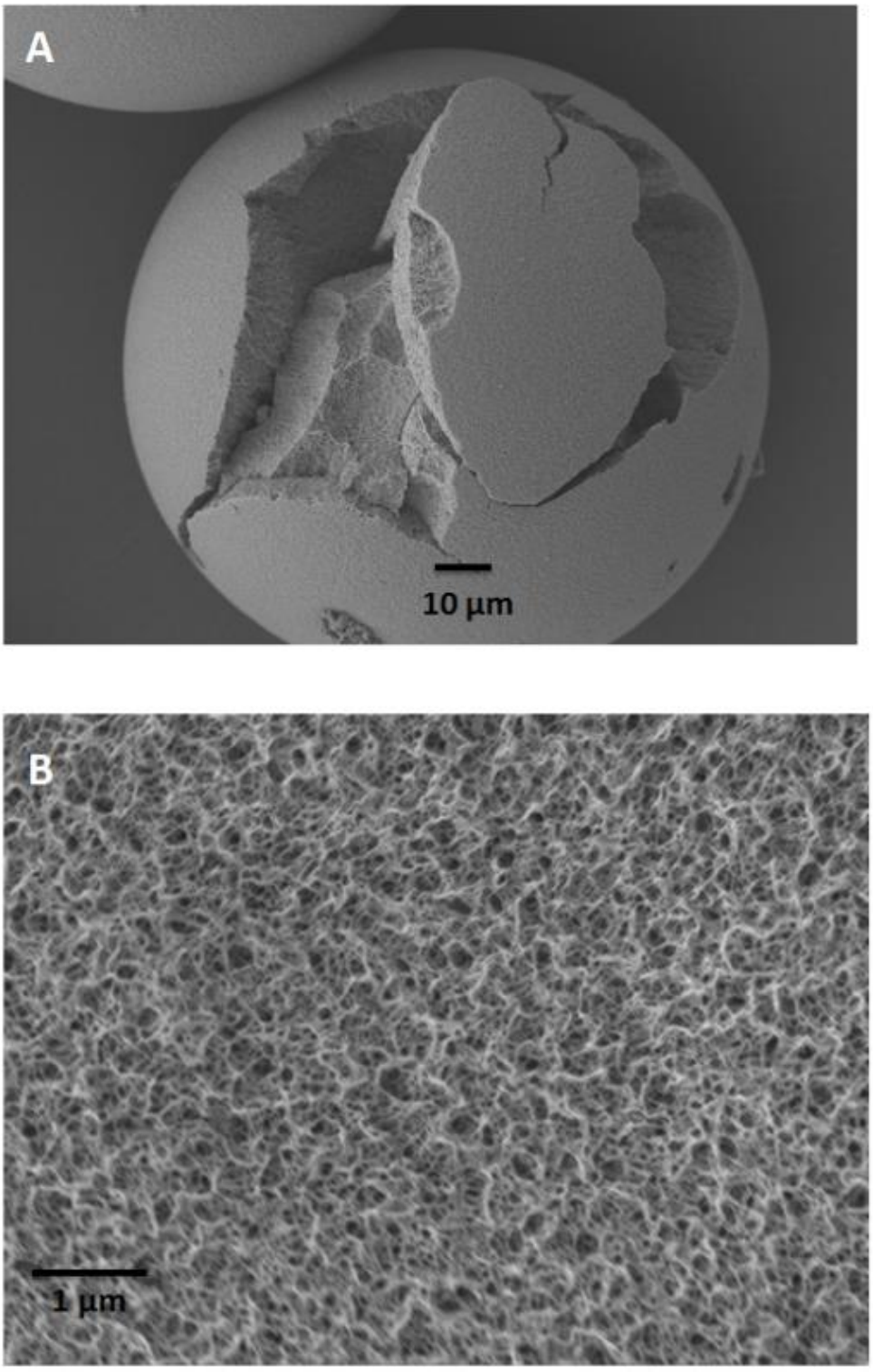

Figure 15 - (A) Scanning electron micrograph showing fresh Capto Adhere post-freeze drying. Whole bead image 2.0 kV accelerating voltage, x750 magnification, 1cm = 10 µm. (B) Scanning electron micrograph showing fresh Capto Adhere post-freeze drying. Bead surface image 2.0 kV accelerating voltage, x14, 000 magnification, 2 cm = 1µm.

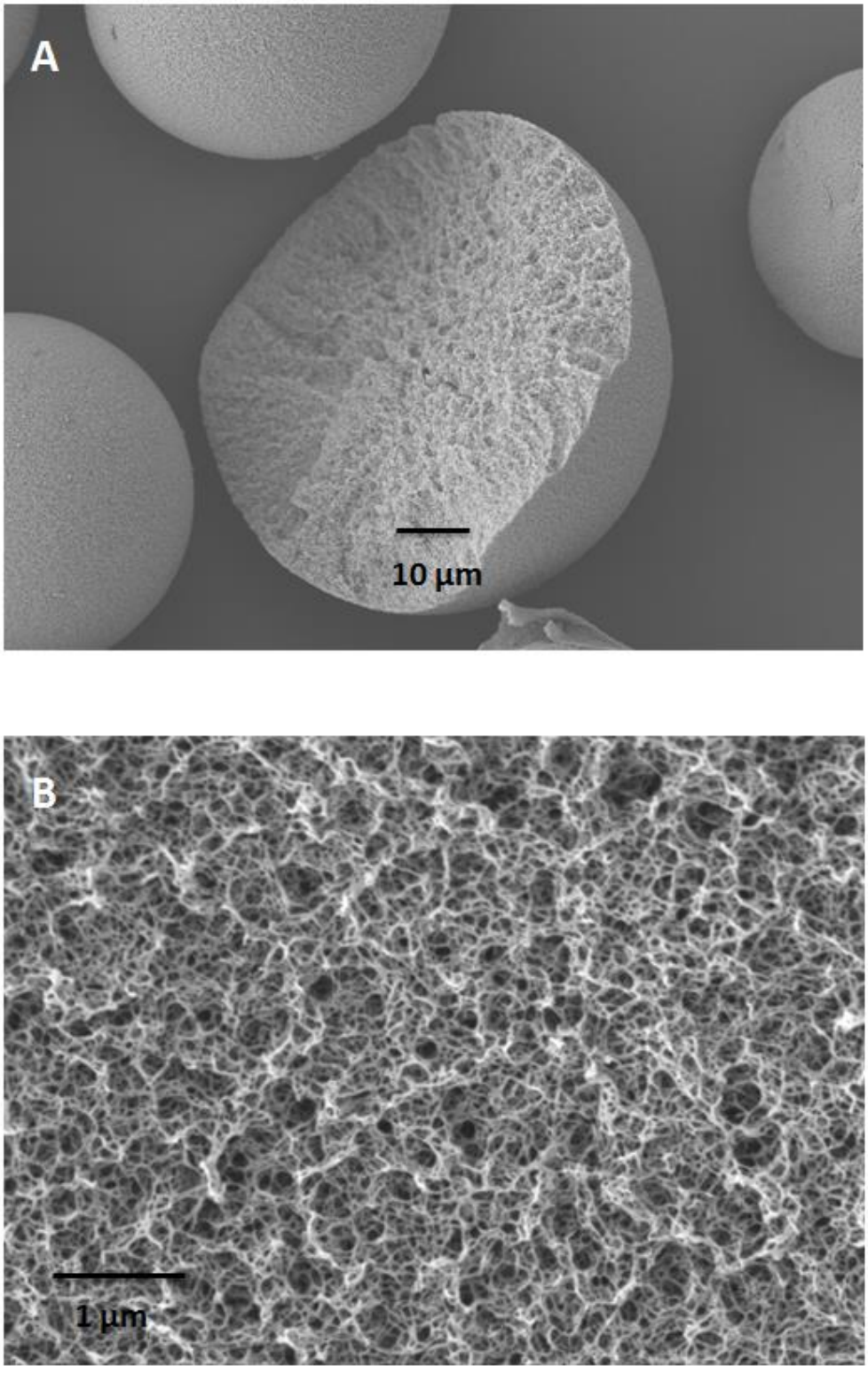

Figure 16 - (A) Scanning electron micrograph showing fresh MabSelect post-freeze drying. Whole bead image 3.0 kV accelerating voltage, x950 magnification, 1.5cm = 10 µm. (B) Scanning electron micrograph showing fresh MabSelect post freeze-drying. Bead surface image 2.0 kV accelerating voltage, x18, 000 magnification, 2.3 cm = 200nm.

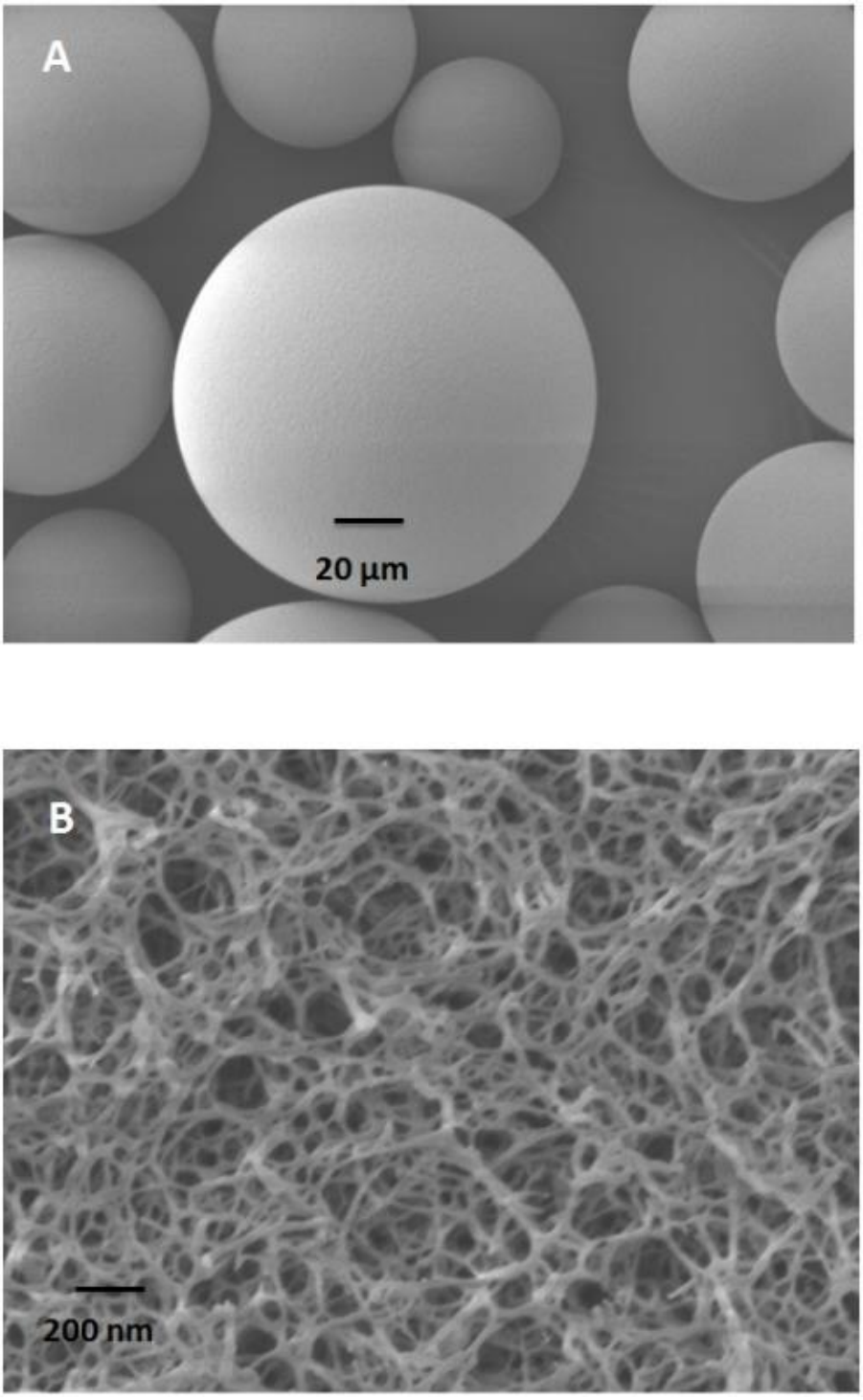

Figure 17 - (A) Scanning electron micrograph showing fresh Capto Adhere post-critical point drying. Whole bead image 2.0 kV accelerating voltage, x500 magnification, 1.2cm = 20 µm. (B) Scanning electron micrograph showing fresh Capto Adhere post-freeze drying. Bead surface image 2.0 kV accelerating voltage, x50, 000 magnification, 1.2 cm = 200nm.

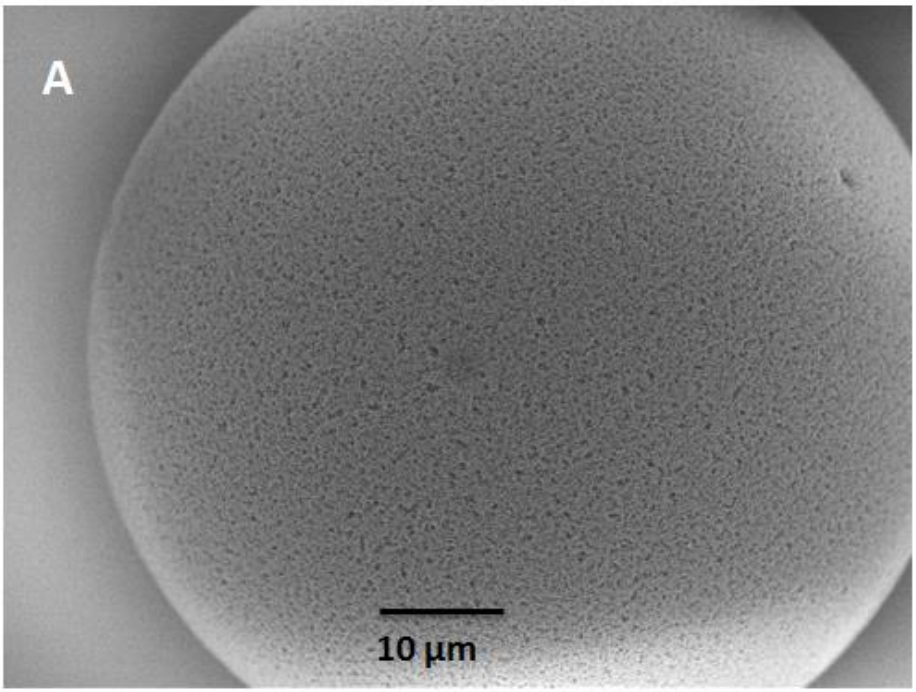

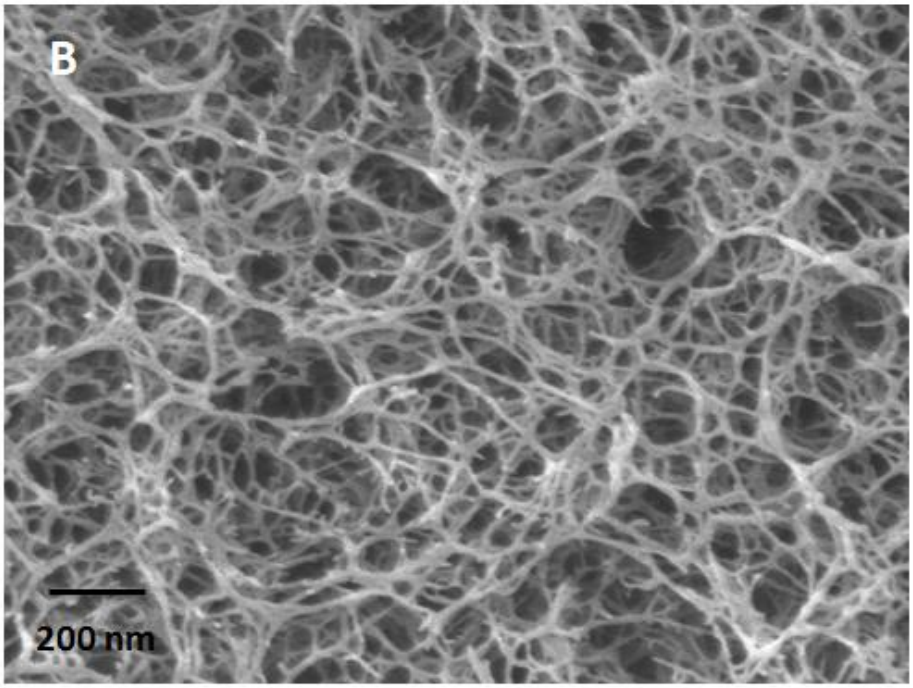

Figure 18- (A) Scanning electron micrograph showing fresh MabSelect post-critical point drying. Whole bead image 2.0 kV accelerating voltage, x1,500 magnification, 2 cm = 10 µm. (B) Scanning electron micrograph showing fresh MabSelect post-critical point drying. Bead surface image 2.0 kV accelerating voltage, x55, 000 magnification, 1.5 cm = 200 nm.

Both Capto Adhere and MabSelect were imaged after exposure to the selected freeze drying conditions. This is represented by figures 15 and 16 for Capto Adhere and MabSelect respectively. Figures 15(A) and 16(A) are whole bead images for both resins while figures 15(B) and 16(B) are bead surface images.

Figure 15(A) shows a Capto Adhere whole bead post-freeze drying. 1 cm of the micrograph represents 10 µm of the sample. The image shows partial fragmentation of the bead; the bead appears to be partially cracked, whilst still maintaining a semblance of its spherical structure. Similarly figure 16(A) (MabSelect whole bead image, 1.5 cm = 1µm) shows complete bead fragmentation – splitting of the bead into two parts – of which one can be seen in the image. It should be noted that most of the beads in both resin samples maintained their spherical structure and variations in particle size distribution could be observed clearly. However, the fragmentation of beads observed in figures 15(A) and 16A) represents a significant portion of the samples. In all images collected in this study, at least a third of the beads were disintegrated to some extent. What did differ, however, was the extent of fragmentation in both cases, as observed in similar studies that employ freeze drying on biological specimen (Polak and Pitombo, 2011). Figure 16(A) is completely fragmented, whereas figure 15(A) is partially fragmented. This could be due to the fact that Capto Adhere is a stronger resin type as it is made to have a higher percentage of cross-linking of agarose media than MabSelect, as specified by the manufacturer GE Healthcare. The results from this study indicate that freeze drying under these conditions can lead to severe morphological changes in bead structure (Draenert and Draenert, 1982).

Figure 15(B) shows the surface of a Capto Adhere bead post-freeze drying. 2 cm of the micrograph represents 1µm of the sample. Likewise figure 16(B) is a bead surface image of MabSelect post-freeze drying and 2.3 cm of the micrograph represents 1µm of the sample. In both cases, visualisation of the ultrastructure at high resolution proved difficult under these conditions. Similar to figure 13(B) obtained post-air drying, the images show the heterogeneity of the matrix structure, a wide pore size distribution and diversity in pore morphology. The images also show depth and some distinction can be made between the pores that are closer to the surface and those that extend inwards, albeit to a lesser extent than figure 13(B).

However, figures 15(B) and 16(B) show very little distinction in surface characteristics between the two resins, despite that they have different structural properties in their composition. This presents challenges when attempting to characterise the resins individually.

Furthermore, the images appear to drift somewhat, particularly figure 15(B), which can occur when the microscope is operating at maximum magnification, meaning that a higher resolution image would be difficult to capture for that particular sample. Unlike air drying, the temperature and pressure parameters were extensively controlled; therefore it is unlikely that the reason behind drifting in this case is related to the drying efficiency. Changes in morphology experienced by the beads under freeze drying meant that the surface topography was irregular, so the gold/palladium coating was not distributed evenly for clear imaging of the porous structure. An even distribution of the sputter coating is necessary to create a conductive layer on the sample. This inhibits charging, reduces thermal damage and also improves the secondary electron signal that is required for clear topographic observation. However, it should be noted that uneven distribution would not cause major distortions.

Figures 17 and 18 represent both Capto Adhere and MabSelect resins respectively after critical point drying. Figures 17(A) and 18(A) are whole bead images of the 2 resins and figures 17(B) and 18(B) are bead surface images.

Figure 17(A) shows a randomly selected collection of Capto Adhere beads post-CPD. 1.2 cm of the micrograph represents 20µm of the sample. The image shows that the individual beads are uniformly spherical in shape and clearly shows there to be a significant particle size distribution (~50-100µm) as specified by the manufacturer, GE Healthcare. This was also observed for all the whole bead images obtained post-CPD for MabSelect media (see appendix). Figure 18(A) shows a MabSelect whole bead image where 2 cm of the micrograph represents 10µm of the sample. In this image, the uniformity in sphericity is observed. A further observation is that, despite the relatively low magnification (x1500), the ultrastructure of the bead surface is still apparent. This allows for early stage bead surface characterisation comparisons between the two resins. Figure the surface topography

of figure18(A) appears to be more heterogeneous compared to figure 17(A). However, a higher image resolution is required for further analysis.

Figures 17(B) and 18(B) are higher resolution bead surface images for Capto Adhere and MabSelect respectively. In figure 17(B), 1.2 cm of the micrograph represents 200 nm of the sample and in figure 18(B) 1.5 cm represents 200 nm of sample. Both figures clearly show a heterogenous polymer fibre network structure and the pore size distribution and diversity in pore morphology can be clearly observed. However, the figures show that there are differences between the ultrastruture of the 2 resins. The matrix structure of MabSelect exhibits more discontinuity of fibres compared to Capto Adhere, which appears to be more homogeneous. This difference could affirm the aforementioned rationale that Capto Adhere is mechanically more robust than MabSelect.

The results observed in addition to the factors for consideration associated with both drying techniques (table 9) appear to favour critical point drying as the ideal approach for sufficient drying of agarose-based chromatography media for ultrastructural visualisation under SEM. This is corroborated by observations noted by Nordestgaard & Rostgaard, 1985 who investigated critical point drying versus freeze drying for studies on hepatocytes. From this, they were able to conclude that critical point drying under SEM resulted in fewer morphological changes and clearer ultrastructural visualisation. Whilst freeze drying requires next to no preparation or any necessary additional media, with regards to the handling of both techniques, critical point drying operates under less extreme temperature changes, which is quite critical in maintaining ultrastructure. Furthermore, critical point drying is also in the order of several hours less in time taken to carry out, which is important in the wider use of the technique and scalability. However, as indicated by the results, it must be noted that freeze drying can be applied to agarose-based chromatography media for a wide variety of applications not covered in the scope of this research. The extreme temperatures freeze drying is capable of achieving can be used to determine the effects of other physical and mechanical factors, such as stress testing or bead deformation testing and potentially used as a bead sectioning technique for observation of the bead’s interior mechanical properties using SEM.

3.2.Image analysis

The use of SEM for the visualisation agarose-based chromatography media allows for high resolution imaging upon the application of appropriate preparative techniques. Detailed analysis of the images obtained is an important aspect for improved understanding and characterisation of the properties of chromatography resins. There are two main analytical approaches that are employed for interpretation of images, namely qualitative analysis and quantitative analysis.

The use of qualitative analysis is of particular importance in this investigation as it allows for quick identification of the more distinct properties that characterise the resins used in this study. These properties include bead and pore sizing, size distribution and morphology. Additionally interpretations can be made on matrix structure differences and fibre sizing. Qualitative analysis also allows for quick distinctions to be made between imaging artefacts and sample artefacts. It forms the basis on which other analytical approaches are developed, hence highlighting the need for accurate and precise observation of structural detail.

The quantitative analysis approach used in this study aims to provide numerical information regarding the aforementioned properties. This approach cannot be directly applied to images obtained via SEM and hence requires the use of image processing software. The use of image processing software is ideal as it can be automated to reduce human error.

Image analysis is performed on all nine resins used in this study (post-CPD). Micrographs showing the all resins in different states were obtained. As previously stated, the first state captures individual beads (whole bead images) and the second are bead surface images. Whole bead micrographs intended to show any morphological differences between the resins, while bead surface images intended to show ultrastructural differences. At least 3 micrographs of each state were acquired for each resin (see appendix).

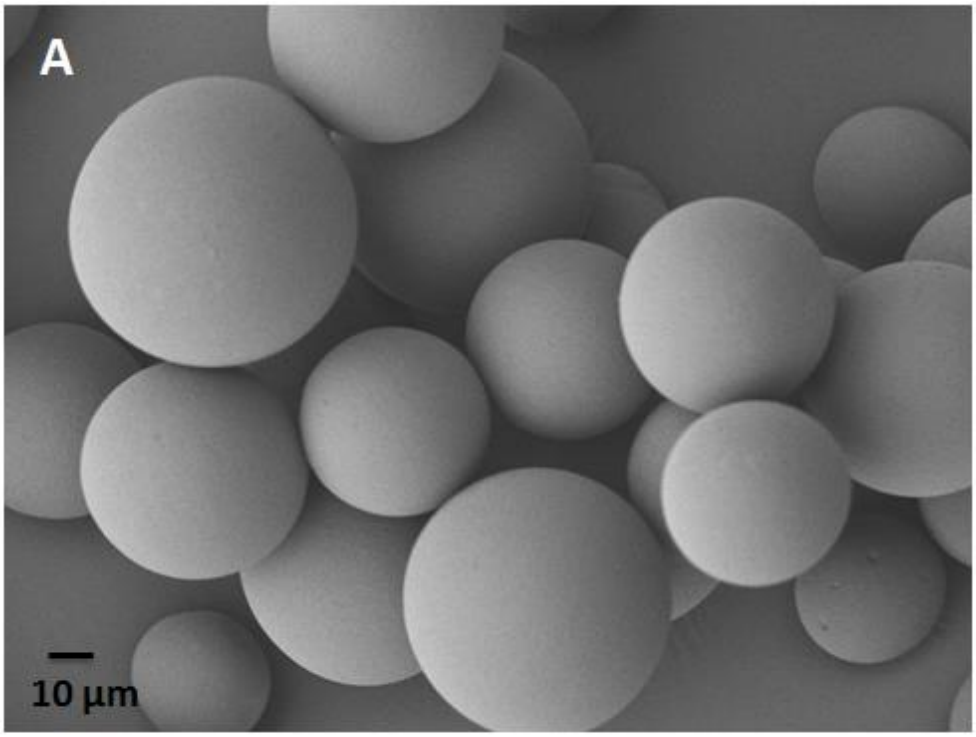

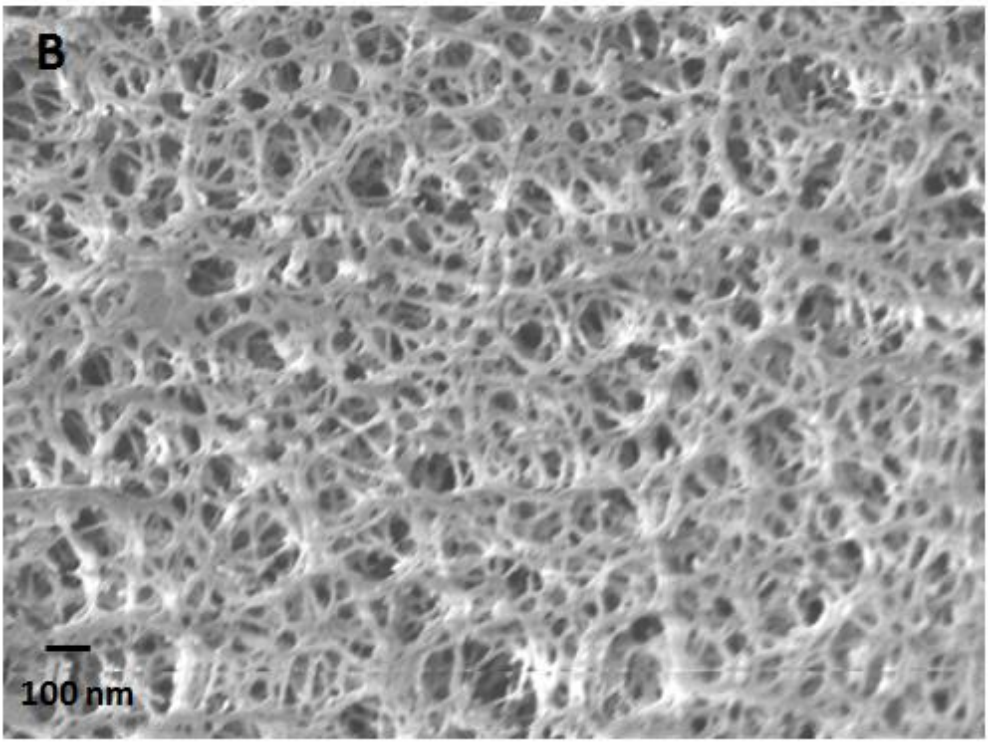

Figure 19 – (A) Scanning electron micrograph showing fresh Sepharose CL-4B post-critical point drying. Whole bead image, 2.0kV, magnification x450, 0.6 cm = 10 µm. (B) Scanning electron micrograph showing fresh Sepharose CL-4B post-critical point drying. Bead surface image, 2.0 kV, magnification x40,000, 0.6 cm = 100 nm.

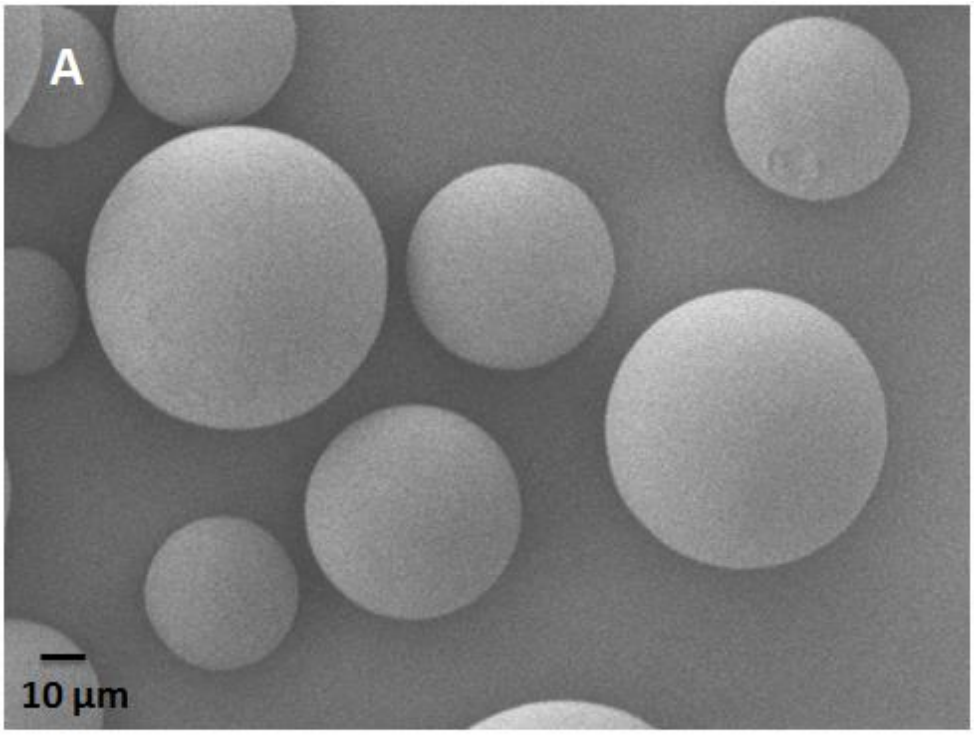

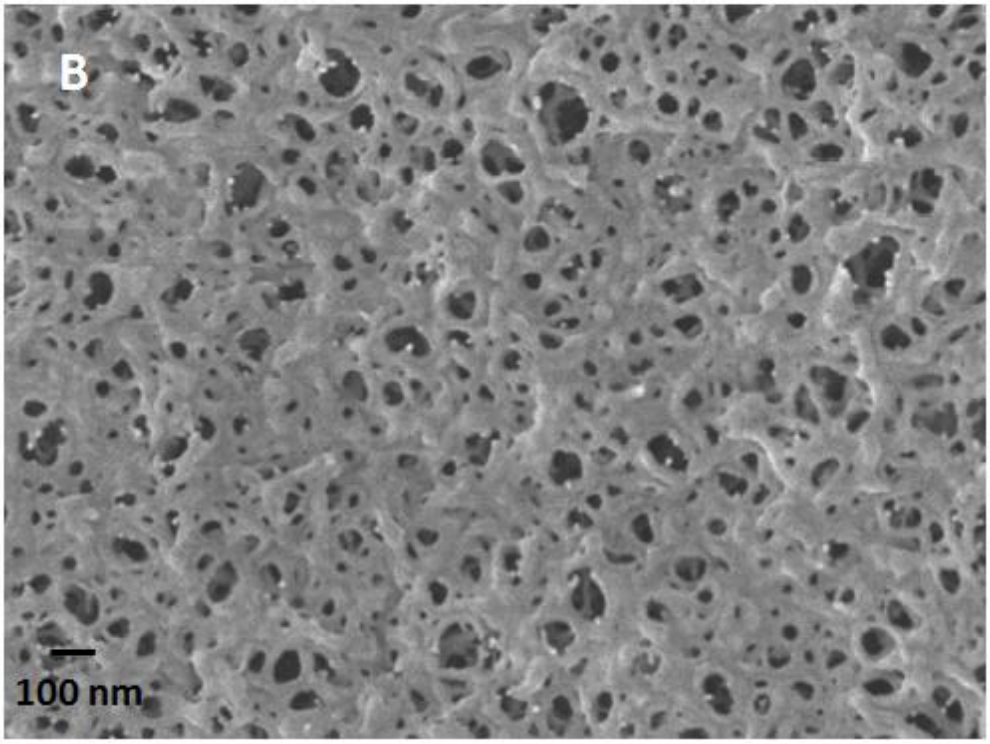

Figure 20 – (A) Scanning electron micrograph showing fresh Sepharose 4 Fast Flow post-critical point drying. Whole bead image, 2.0kV, magnification x500, 0.6 cm = 10 µm. (B) Scanning electron micrograph showing fresh Sepharose 4 Fast Flow post-critical point drying. Bead surface image, 2.0 kV, magnification x40,000, 0.6 cm = 100 nm.

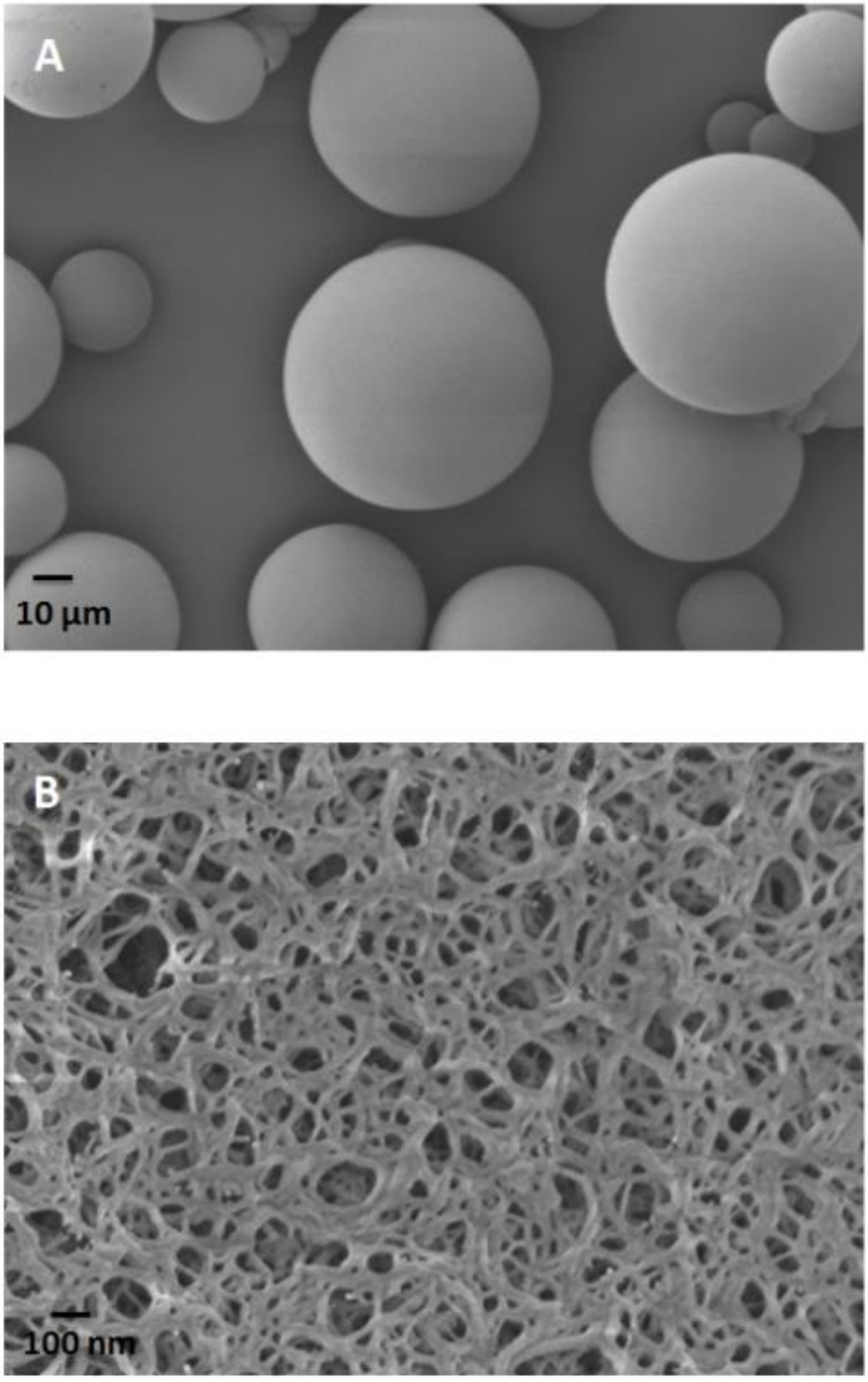

Figure 21 – (A) Scanning electron micrograph showing fresh Sepharose CL-6B post-critical point drying. Whole bead image, 2.0kV, magnification x400, 0.6 cm = 10 µm. (B) Scanning electron micrograph showing fresh Sepharose CL-6B post-critical point drying. Bead surface image, 2.0 kV, magnification x40,000, 0.6 cm = 100 nm.

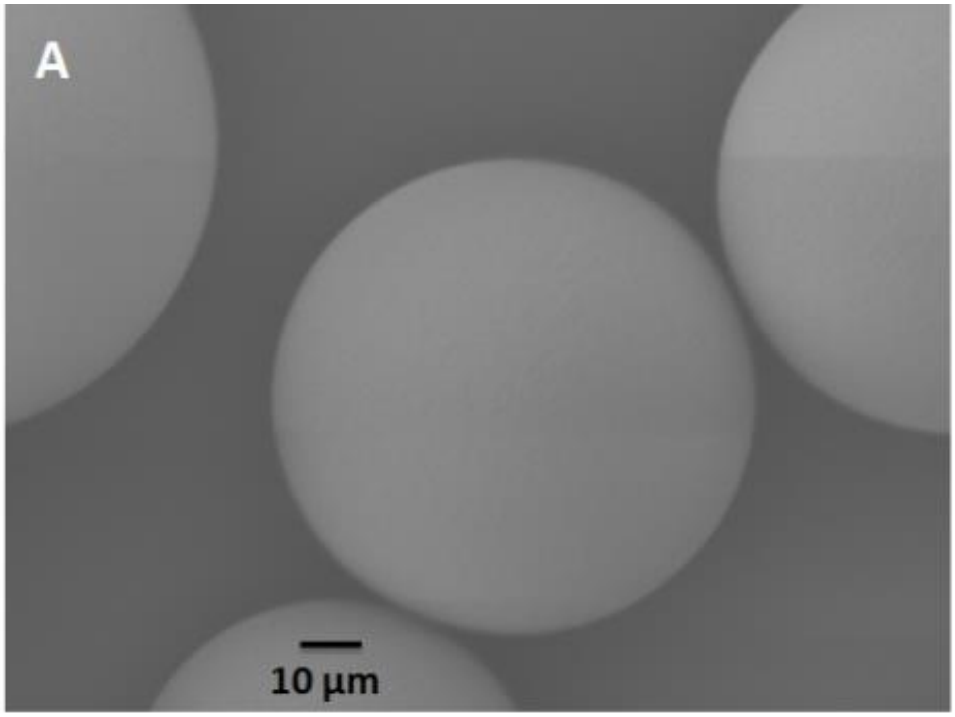

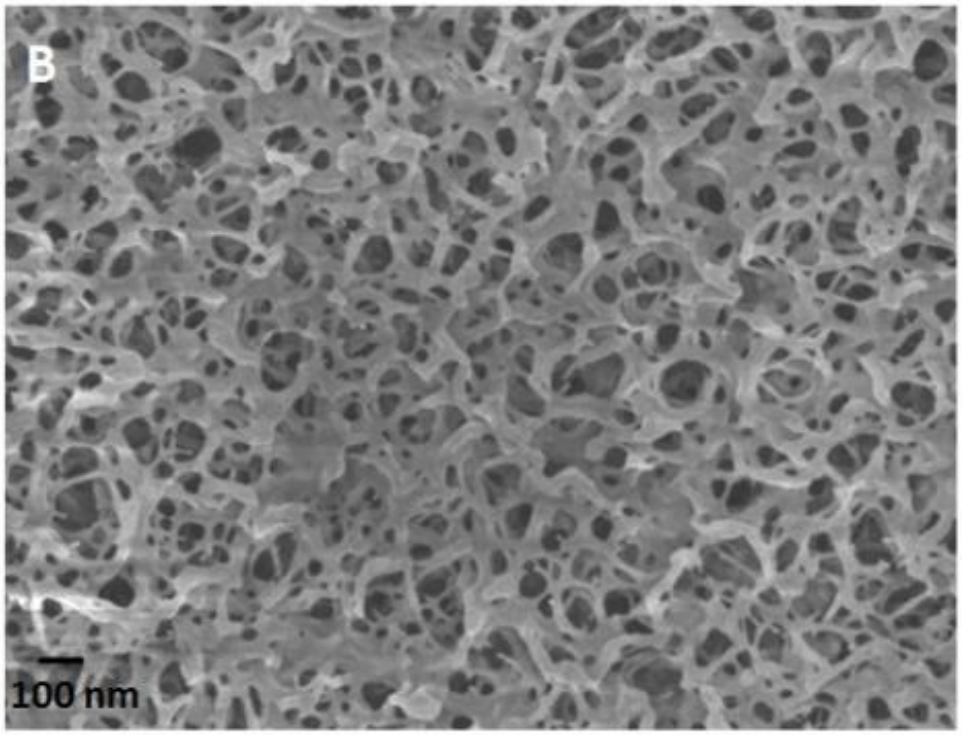

Figure 22 – (A) Scanning electron micrograph showing fresh Sepharose 6 Fast Flow post-critical point drying. Whole bead image, 2.0kV, magnification x700, 0.9 cm = 10 µm. (B) Scanning electron micrograph showing fresh Sepharose 6 Fast Flow post-critical point drying. Bead surface image, 2.0 kV, magnification x40,000, 0.6 cm = 100 nm.

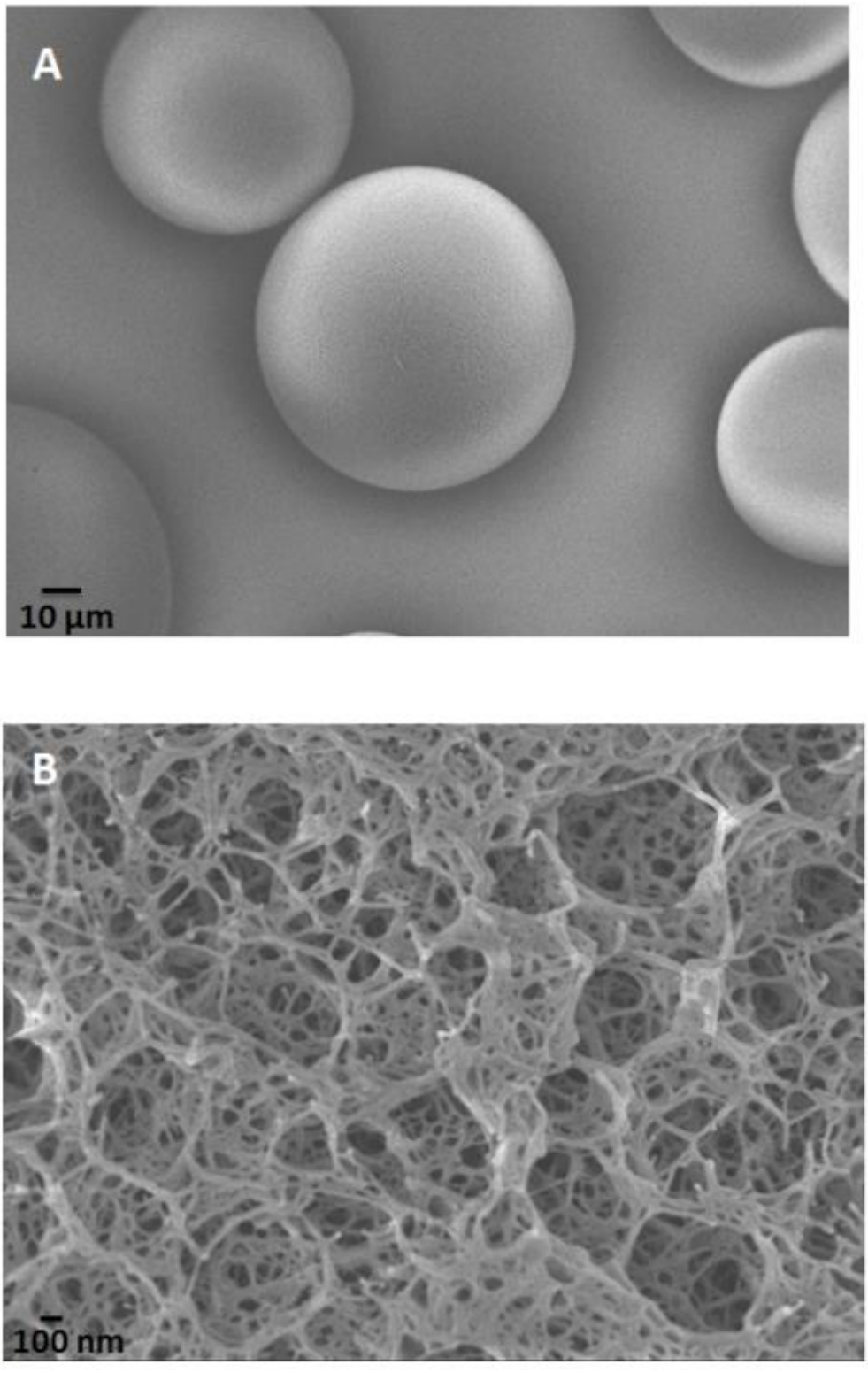

Figure 23 – (A) Scanning electron micrograph showing fresh Q-Sepharose High Performance post-critical point drying. Whole bead image, 2.0kV, magnification x430, 0.6 cm = 10 µm. (B) Scanning electron micrograph showing fresh Q-Sepharose High Performance post-critical point drying. Bead surface image, 2.0 kV, magnification x33,000, 0.4 cm = 100 nm.

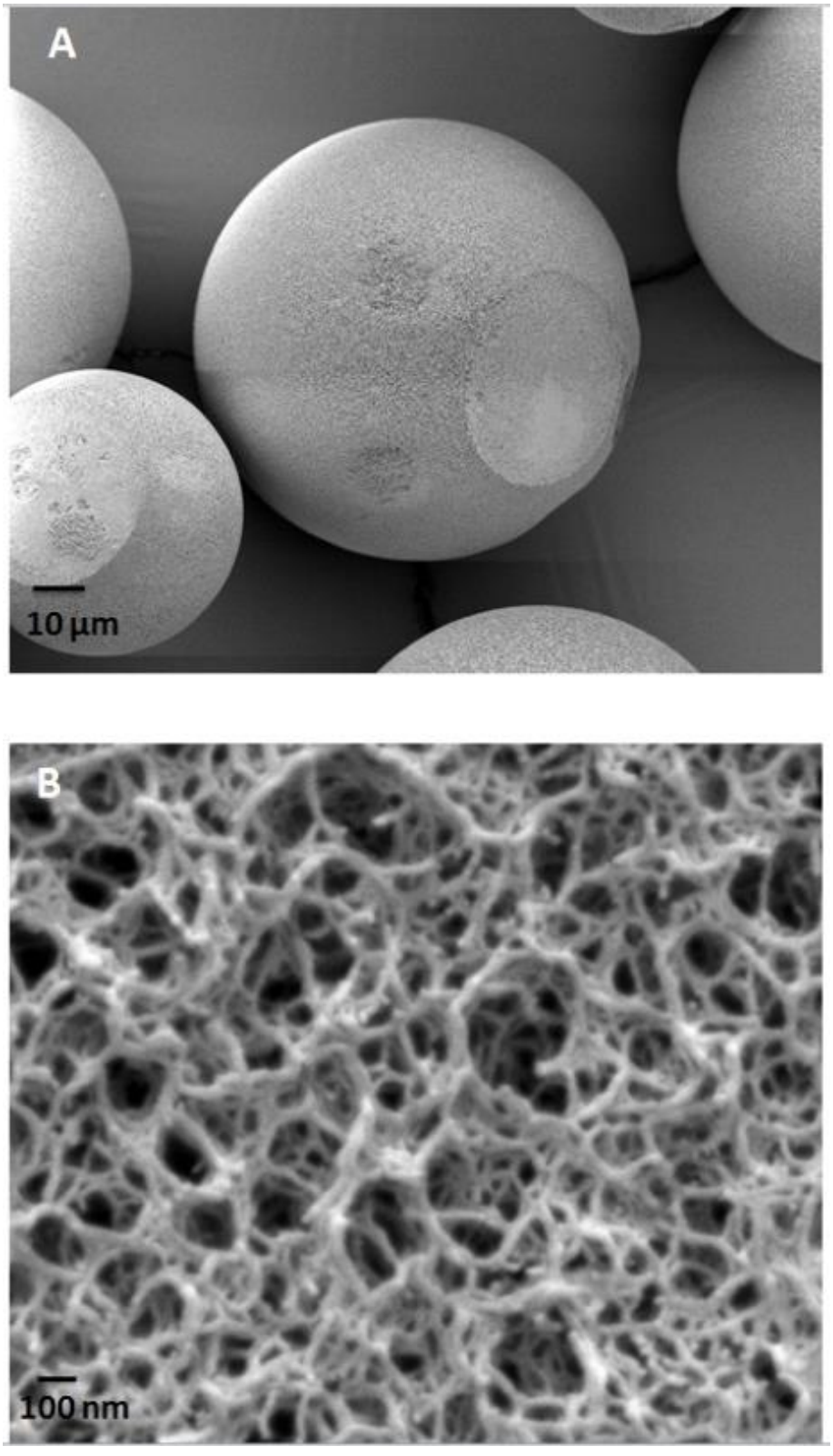

Figure 24 – (A) Scanning electron micrograph showing fresh MabSelect Xtra post-critical point drying. Whole bead image, 2.0kV, magnification x670, 1 cm = 10 µm. (B) Scanning electron micrograph showing fresh MabSelect Xtra post-critical point drying. Bead surface image, 2.0 kV, magnification x40,000, 0.6 cm = 100 nm.

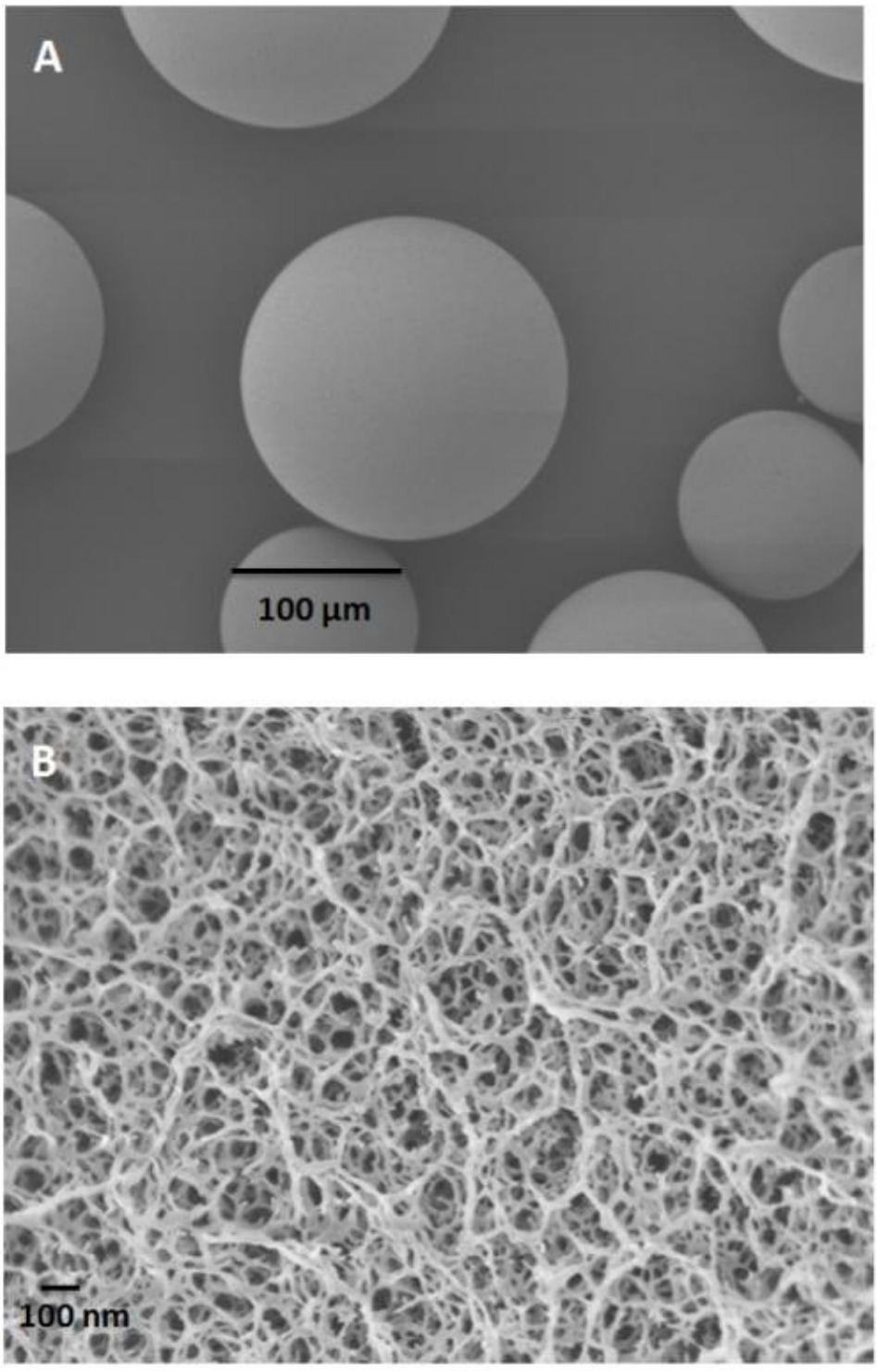

Figure 25 – (A) Scanning electron micrograph showing fresh Capto Q post-critical point drying. Whole bead image, 2.0kV, magnification x220, 3 cm = 100 µm. (B) Scanning electron micrograph showing fresh Capto Q post-critical point drying. Bead surface image, 2.0 kV, magnification x40,000, 0.6 cm = 100 nm.

3.2.1. Qualitative analysis

Figures 19-25 represent fresh Sepharose CL-4B, Sepharose 4 Fast Flow, Sepharose CL-6B, Sepharose 6 Fast Flow, Q-Sepharose High Performance, MabSelect Xtra and Capto Q respectively. Each figure labelled (A) show whole bead images and those labelled (B) show bead surface images for the respective resins.

Figure 19(A) shows a randomly selected collection of Sepharose CL-4B post-CPD. 0.6 cm of the micrograph represents 10µm of the sample. The image shows that the individual beads are uniformly spherical in shape and clearly shows a significant particle size distribution (~50-150µm), as specified by the manufacturer - GE Healthcare. These properties were generally observed for all whole beads images obtained post-CPD for all resins used in this study (figures 20(A) – 25(A)). However, figures 20(A) and 24(A) (Sepharose 4 Fast Flow and MabSelect Xtra whole bead images) appear to show a number of beads that have a small area displaying flat surfaces as opposed to spherical surfaces. This was observed in a significant number of MabSelect Xtra beads obtained but was far less apparent for Sepharose 4 Fast Flow. The flat surfaces could be associated with beads adhering to each other pre-drying due to the viscous nature of the samples. Upon the removal of water, the beads may have disjoined, resulting in the circular flat surfaces observed.

Figures 19(B)-25(B) are bead surface images for fresh Sepharose CL-4B (SCL4B), Sepharose 4 Fast Flow (S4FF), Sepharose CL-6B (SCL6B), Sepharose 6 Fast Flow (S6FF), Q-Sepharose High Performance (Q-HP), MabSelect Xtra (MSX) and Capto Q (CQ) respectively. A scale based on 100 nm is provided for each of these images. The results show structural similarities between groups of resins which can be compared and contrasted against one another. Sepharose CL-4B and -6B (figures 19(B) and 21(B)) share similar chemical and physical compositions in their manufacturing and are of the same subtype of resins. They both display a heterogenous polymer fibre network structure, pore size distribution and diversity in pore morphology. However, SCL6B appears to be more structurally stable as there is less discontinuity of fibres, so the matrix itself appears more robust. A similar observation can be seen between Sepharose 4 FF and 6 FF (figures 20(B) and 22(B)). Both resins display relatively thicker matrices but the extent of this is what

differs between the two. S4FF appears to be more ‘gel-like’ as it displays a much thicker, viscous matrix and smaller pores compared to S6FF, meaning that S6FF appears structurally more robust. Generally, the Cross-Linked Sepharose resin images display a finer fibrous network and larger pore sizes compared to their Fast Flow counterparts. S4FF and S6FF appear to have thicker fibres in the matrix structure and relatively smaller pores.

Figures 23(B) – 25(B) represent Q-HP, MSX and CQ surface images respectively. The three images display high heterogeneity in their matrices. They clearly show depth, and distinctions can be made between the pores that are closer to the surface and those that extend inwards. In each case, the pores closer to the surface appear to be larger compared to those beneath the surface. However, a number of differences can be observed between the three resins. The pore size distribution in shown in figure 23(B) appears greater than in figures 24(B) and 25(B). The size of the pores shown for MSX and CQ appear to be more uniform than that of Q-HP. Furthermore the three resins are distinct in their matrix composition. Figure 23(B) exhibits a more randomised matrix composition. Some regions in the image contain a high concentration of pores and others a high concentration of fibres, whereas figures 24(B) and 25(B) display a more consistent arrangement of pores and fibres.
The results show distinct structural differences between each of the nine resins used in this study. The main differences are observed in pore size distributions, fibre sizes, pore morphologies and differences between surface and sub-surface pores. Further differences are observed between the arrangement of pores and fibres in a matrix. Some of these properties are more straightforward to quantify than others, namely pore size distributions, apparent porosity (the ratio of pores-to-fibres), the total number of pores and average pore sizes. Quantification of these properties may serve as a more practical way to characterise the studied chromatography resins.

3.2.2. ImageJ method development and results

The software tool selected to numerically characterise the nine resins used in this study was ImageJ as it holds a number of advantages over other image processing software packages (e.g. Matlab) (table 10). It is a public domain open source software that is inexpensive. It requires no specific expertise and contains a vast array of plugins, some of which are particularly applicable for the quantification of the properties relevant to this study. Furthermore, it has been used widely in research to quantify the characteristics of many biological materials as reported by Jensen 2013, Helmy & Abdel Azim 2012 and Schneider et al. 2012.

Table 10 Advantages of using ImageJ software package.

Advantages of using ImageJ software package
Inexpensive
No specific expertise required
Open source (easily accessible)
Whole package: Image processing, analysis and display

The results obtained in section 3.2.1. show that the bead ultrastructure can be characterised based on features associated with their pores and their fibrosity. For this reason, a number of properties have been selected in order to adequately quantify what was readily observed in figures 17-25. The properties that are measured in this study are pore size distribution, average pore size, average pore count and apparent porosity.

These particular properties were selected for a number of reasons. Unlike average particle size and particle size distribution, information on average pore size and pore size distribution for each resin is not readily available by the manufacturer and there are challenges in characterising these properties by ocular examination alone. Pore count (the number of pores in an image) and apparent porosity may appear to

provide similar information, however the difference between the two is that apparent porosity supplies information about the non-porous portion of the image (i.e. the amount of the image that is composed of fibres). Furthermore, the two properties may not be correlative, as a high pore count may not necessarily indicate high apparent porosity, as observed in figure 20(B).

There were a number of steps involved in making the images suitable for image analysis. The first important step was setting the scale (figure 20(B) is used for illustrative purposes). This was done by using the software to draw a line of 0.6 cm. The software then calculates the number of pixels equivalent to 0.6 cm and the user can then insert the actual length of the sample (100nm). Subsequently, the image is 'smoothened out'. This filter replaces each pixel with the average of its 3 × 3 surrounding area, meaning that most projections are flattened (https://imagej.nih.gov/ij/docs/guide/146-29.html). The image is then inverted to create a reversed image (can be likened to a photographic negative) to enhance the location of pores. The user then decides on the threshold limit. This is done to filter out as much background information in the image as possible, such as sub-surface structures. The edges of each pore are then bordered using the 'Find edges' tool, to further facilitate pore sizing. The particle analyser function can then be selected to allow for the calculation of pore sizes and related properties.

Subsequently, a window appears numbering the location of each detected pore so that this can be corresponded with the results window. The user can define how the results are displayed. In this study results are displayed per unit area (nm^2) In the discussion section of this study, the pore diameter is approximated based on the area of a circle πr^2. The software then displays two windows – a results window (containing raw data) and a summary window. The summary provides the user with the pore count information, average pore size and apparent porosity. In this study, apparent porosity is recorded as a percentage, for example, 15% apparent porosity means that 15% of the image were pores and therefore 85% of the image is the fibrous network.

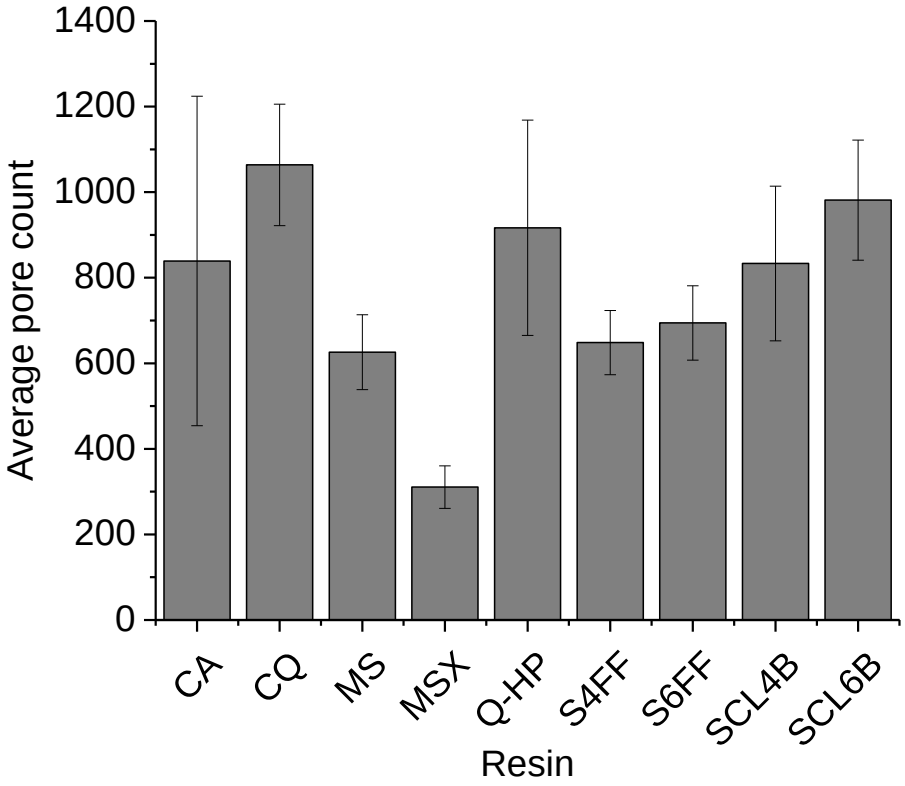

Figure 26 – Column graph showing average pore count for all nine resins – CA (Capto Adhere), CQ (Capto Q), MS (MabSelect), MSX (MabSelect Xtra), Q-HP (Q-Sepharose High Performance), S4FF (Sepharose 4 Fast Flow), S6FF (Sepharose 6 Fast Flow), SCL4B (Sepharose CL4B), SCL6B (Sepharose CL6B) - the total number of enclosed black pixels (pores) were calculated by the ImageJ software for 3 images of each resin. The averages are plotted with their standard deviations.

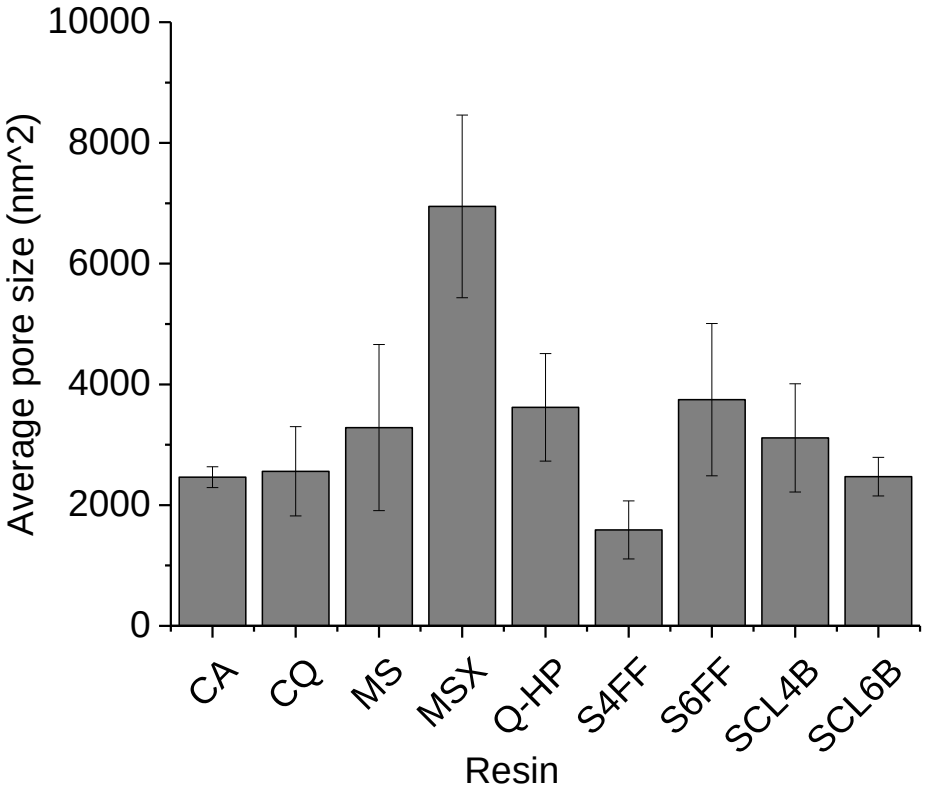

Figure 27 – Column graph showing average pore size in nm^2 for all nine resins – CA (Capto Adhere), CQ (Capto Q), MS (MabSelect), MSX (MabSelect Xtra), Q-HP (Q-Sepharose High Performance), S4FF (Sepharose 4 Fast Flow), S6FF (Sepharose 6 Fast Flow), SCL4B (Sepharose CL4B), SCL6B (Sepharose CL6B) - the areas of all enclosed black pixels (pores) were calculated by the ImageJ software for 3 images of each resin. The averages are plotted with their standard deviations. Pore diameters are calculated based on the area of a circle $\pi r^{2.}$

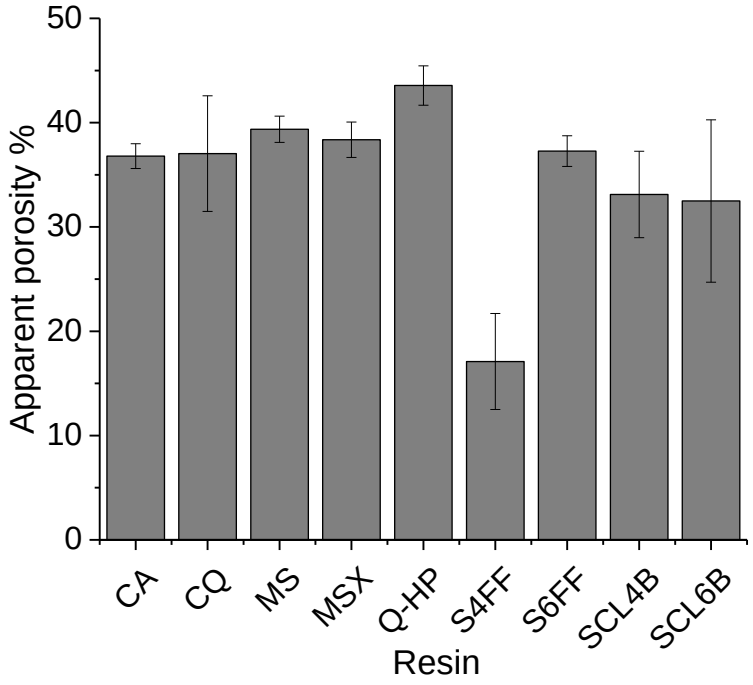

Figure 28 – Column graph showing average apparent porosity in % for all nine resins – CA (Capto Adhere), CQ (Capto Q), MS (MabSelect), MSX (MabSelect Xtra), Q-HP (Q-Sepharose High Performance), S4FF (Sepharose 4 Fast Flow), S6FF (Sepharose 6 Fast Flow), SCL4B (Sepharose CL4B), SCL6B (Sepharose CL6B) – ImageJ counts the total number of black pixels (pores) against the total number of pixels in the image and calculates this as a percentage. This was done on 3 images of each resin. The averages are plotted with their standard deviations.

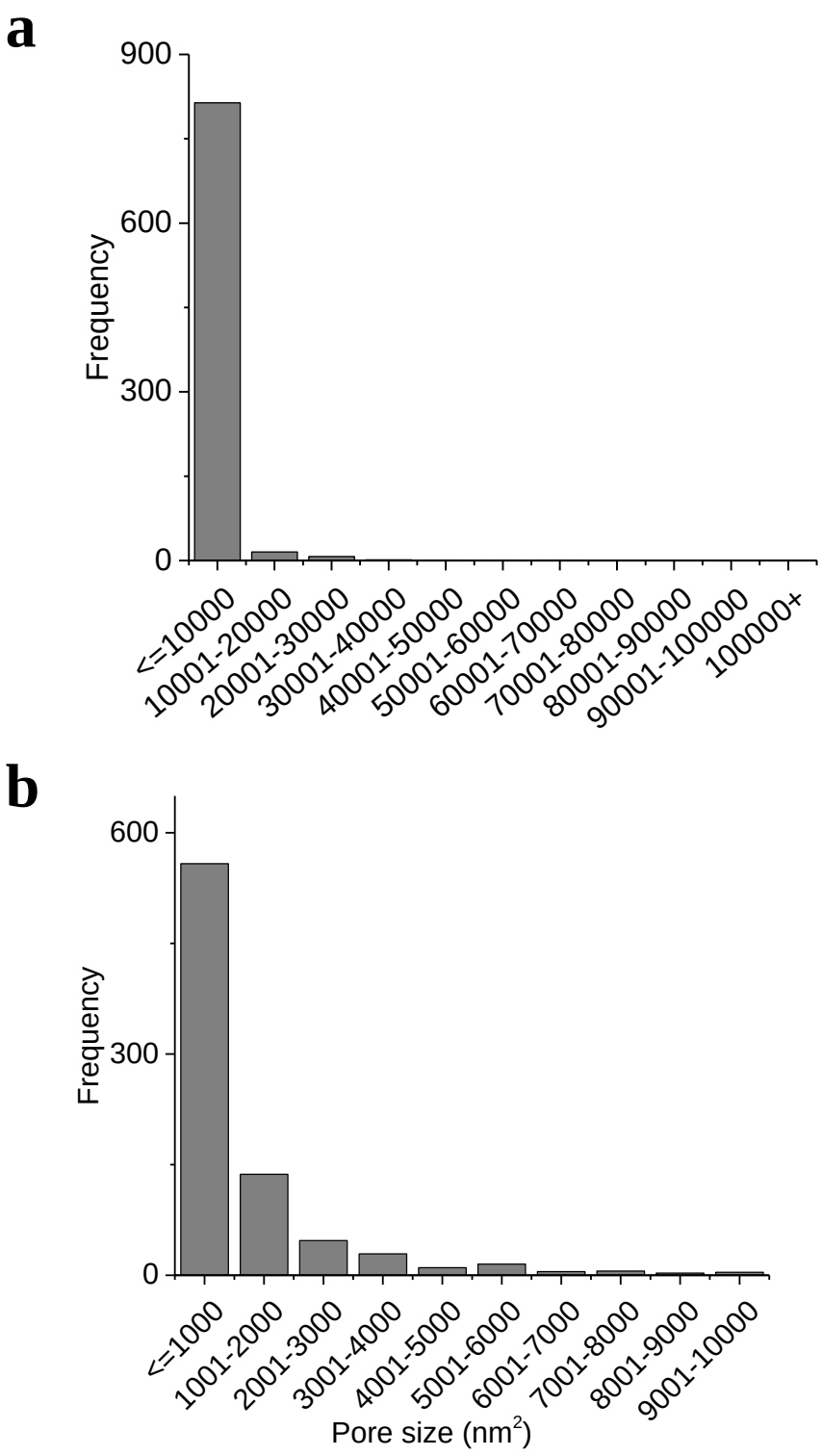

Figure 29 – Column graphs showing pore size distribution of Capto Adhere resin. (a) Graph showing the distribution of pores up to 1e05 nm^2. The graph shows that >97% of the pores are less than 10000 nm^2. (b) Graph showing the size distribution of pores up to 10000 nm^2. The graph shows that ~70% of the pores are less than 1000 nm^2 in size. 1000nm^2 ≈ 36nm (diameter) based on conversion πr^2.

Table 11 – Pore size distributions up to 100000nm^2 (≈d360nm based on area of a circle πr^2.) On average, 95% of all pores within 100000nm^2 are ≤10000nm^2 (≈d100nm).

	Resin Frequency								
Pore size range (nm^2)	**CA**	**CQ**	**MS**	**MSX**	**QHP**	**S6FF**	**SCL6B**	**S4FF**	**SCL4B**
≤10000	814	1010	589	273.3	862.3	642.3	942.6	638	824.6
10001-20000	15.3	44.6	18.6	12.3	29.3	34.3	27.3	9.3	8
20001-30000	7	6	8.3	9.6	6.6	7	5	1	0.6
30001-40000	1.3	1.6	4.3	4.3	5	5.6	2.6	0	0
40001-50000	0.3	1.3	1	2.3	2	2.3	1	0	0
50001-60000	0.3	0	1.6	2	2.3	1.3	1.3	0	0
60001-70000	0.3	0	0.6	1.6	4	1	1.3	0	0
70001-80000	0	0	0.3	0.6	1	0	0	0	0
80001-90000	0	0	0.6	2.3	1.3	0	0	0	0
90001-100000	0	0	0.3	0.3	0	0	0	0	0
100000+	0	0	1	1.6	2.6	0	0	0	0
Total	***838.6***	***1063.6***	***626***	***310.6***	***916.6***	***694.3***	***981.3***	***648.3***	***833.3***
%≤10000	***97%***	***95%***	***94%***	***88%***	***94%***	***93%***	***96%***	***98%***	***99%***

Table 12 – Pore size distributions up to 10000nm^2 (≈d100nm based on area of a circle πr^2.) On average, over 70% of all pores within 10000nm^2 are ≤1000nm^2 (≈d36nm).

	Resin Frequency								
Pore size range (nm^2)	**CA**	**CQ**	**MS**	**MSX**	**QHP**	**S6FF**	**SCL6B**	**S4FF**	**SCL4B**
≤1000	558	625	499.3	241.6	757.3	445.6	629.6	348	627
1001-2000	137	127	0	0	0	43.3	100.3	120.6	46.6
2001-3000	47	102.6	0	0	36.6	27.3	70.3	66.6	59.6
3001-4000	29	40	22.6	0	16	71.3	36	34	36
4001-5000	10.3	40.3	45	16.3	0	0	45.6	22.6	0
5001-6000	15	17.6	0	0	17.3	9	0	14	24.3
6001-7000	5	22.3	4.3	0	18.6	20.6	27	14.6	7
7001-8000	5.6	13.3	0	0	7	13.3	9	7.6	19
8001-9000	3	15.6	8	8.3	9.3	3.3	17.6	6	0
9001-10000	4	6	9.6	7	0	8.3	7	3.6	5
Total	***814***	***1010***	***589***	***273.3***	***862.3***	***642.3***	***942.6***	***638***	***824.6***
%<1000	***69%***	***62%***	***85%***	***88%***	***88%***	***69%***	***67%***	***55%***	***76%***

Table 13 – Pore size distributions up to 1000nm^2 (≈d36nm based on area of a circle πr^2.) On average, almost 100% of all pores within 1000nm^2 are ≤100nm^2

	Resin Frequency								
Pore size range (nm^2)	**CA**	**CQ**	**MS**	**MSX**	**QHP**	**S6FF**	**SCL6B**	**S4FF**	**SCL4B**
≤100	550	625	499.3	241.6	757.3	445.6	629.6	348	627
101-600	0	0	0	0	0	0	0	0	0
601-700	8	0	0	0	0	0	0	0	0
701-1000	0	0	0	0	0	0	0	0	0

3.2.3. Quantitative image analysis

Figures 26-28 are graphs showing the average pore count, pore size (nm^2), and apparent porosity (%) of all nine resins used in this study - CA (Capto Adhere), CQ (Capto Q), MS (MabSelect), MSX (MabSelect Xtra), Q-HP (Q-Sepharose High Performance), S4FF (Sepharose 4 Fast Flow), S6FF (Sepharose 6 Fast Flow), SCL4B (Sepharose CL4B), SCL6B (Sepharose CL6B) – based on 3 bead surface images. ImageJ calculates the total number of enclosed black pixels and converts this into nanometres, based on the scale set by the user (see section 3.2.2.). From this, the three aforementioned properties are determined. The total number of enclosed black pixels represents the pore count, the average area of all enclosed black pixels is the average pore size and the percentage of the image constituted by enclosed black pixels represents apparent porosity.

Figure 26 shows the average pore count of each resin used in this study. The results show Capto Q to have the highest pore count (>1000) and MabSelect Xtra to have the least number of pores (~300). Whilst this property is not so easily observed by ocular judgement of figures 17-25, it can quite clearly be observed that Capto Q does have a relatively high number of pores whilst MabSelect Xtra has a low pore count for the same surface area. In this case, both qualitative and quantitative analyses are in agreement. Capto Adhere and Q-Sepharose High Performance show a high degree of variability in their pore count, which is more readily observed in the images collected for Q-HP resin than Capto Adhere. Possible reasons for such variability not perceived by qualitative analysis could be due to differences during the thresholding stage of the quantitative analysis process, during which, some pores may not have been accounted for or/and many sub-surface pores were added to the total pore count, leading to high variability (Morse, 2000). The results also show that the Fast Flow resins - SF44 (~650) and S6FF (~700) - have lower pore counts compared to their Cross-linked (-CL) counterparts - SCL4B (~830) and SCL6B (~980). This can also be observed visually in figures 19-22, meaning that both qualitative and quantitative analyses are in agreement.

Figure 27 shows the average pore size (nm^2) of all nine resins used in this study. For simplicity, pore diameter information is calculated based on the assumption of a pore

having the shape of a circle. Therefore, to convert pore size in nm^2 to nm, the equation πr^2 is used. The results show that MabSelect Xtra has the highest average pore size (~7000nm^2 ≈ d95nm) whilst Sepharose 4 Fast Flow has the lowest (~1500nm^2 ≈ d44nm). This can be visually observed in figures 20 and 24 as MSX appears to have relatively larger pores whilst S4FF has uniformly smaller pores. Both qualitative and quantitative analyses are in agreement in this case. The remaining resins all display similar average pore sizes. Such similarities were not immediately visually observed for some resins, particularly for Q-HP. Q-HP appears to have relatively larger pores (see figure 23(B)). However, a possible reason for the discrepancies between qualitative and quantitative analysis in this case could be due to the observed irregularities in the matrix structure of Q-HP. There appear to be many large pores, however, there are many very small pores located randomly in clusters on the bead surface (as described in section 3.2.1) This may account for the reason why, on average, the pore size of Q-HP is similar to the other studied resins.

Figure 28 shows the average apparent porosity (%) of all nine resins used in this study. The results show Q-HP to have the highest porosity (44%) and S4FF to have the lowest (17%). The low apparent porosity of S4FF can be readily observed in figure 20, as S4FF appears to relatively be the most gel-like and therefore have higher fibrosity compared to the other studied resins, as figure 28 also clearly indicates. Figure 23(B) (Q-HP bead surface image) also shows relatively high apparent porosity, meaning that both qualitative and quantitative analyses are in agreement in this case. The remaining 7 resins also display very similar levels of apparent porosity. However, overall the results show that over 50% of the bead structure for all resins is composed of the fibrous network. This results cannot be directly compared with other studies that measure porosity such as Stickel & Fotopoulos 2001, as the 3-D nature of the pores is not accounted for in this study (hence the use of the term ‘apparent’ porosity), however similar studies have used 2-D pore measurements to provide comparative information to qualitative observations (Ioannidis, 2009).

Figure 29 and tables 11, 12 and 13 show the pore size distributions for all nine resins used in this study. Table 4 shows the pore size distributions every 10,000 nm^2 up to

1e5 nm^2 (≈d360nm). The results for all resins showed that on average 95% of the pores were less than 10,000 nm^2 (≈d100nm). Table 12 shows how the pore sizes were distributed for every 1000 nm^2 up to 10,000 nm^2. In this table, there appears to be more of a distribution observed in each band compared to table 11. Table 13 shows how the pores were distributed for every 100 nm^2 up to 1000 nm^2 (≈d36nm). Almost 100% of the pores within 1000 nm^2 were 100 nm^2 or less (≈d10nm).

The resin that showed the widest distribution of pore sizes was MabSelect Xtra. Over 12% of pores were larger than 10,000 nm^2, with pore sizes recorded in every band width. This could account for why the highest average pore size was measured for this resin. The resins that showed the narrowest distribution of pore sizes were Sepharose 4 Fast Flow and Sepharose CL-4B. This could account for why the lowest average pore size was recorded for Sepharose 4 Fast Flow. SCL4B had a mid-range average pore size, however, the narrow pore size distribution appears to be more in line with what is visually observed in figure 19(B). Resins that followed MabSelect Xtra with wide pore size distributions were MabSelect and Q-Sepharose High Performance. This could also be visually observed in figures 18(B) and 23(B) respectively. Capto Adhere and Capto Q showed similar distributions which could also be observed in figures 17(B) and 25(B). Both resins also had similar average pore sizes. Tables 11 and 12 also show that S6FF and SCL6B had similar distributions, however, S6FF has a slightly wider pore size distribution than SCL6B. Although this is not immediately obvious in figures 21(B) and 22(B), S6FF does report a slightly higher average pore size compared to its Cross-linked (-CL) counterpart. Direct comparison of these results to other similar studies conducted by Yao & Lenhoff 2004; Sepsey et al. 2014; Bacskay et al. 2014 cannot be made as these studies account for the 3-D nature of the pores. However, as previously alluded to, quantitative information gained by image analysis data can provide support to qualitative observations.

Overall the results show that the studied resins can be characterised according to the properties used in this study (table 14). The Capto family of resins have a greater number of pores whilst MabSelect Xtra has a low pore count, larger pores and a wide pore size distribution. Similarly, MabSelect and Q-HP also have a wide pore size distribution and relatively high apparent porosity values. The Sepharose Fast Flow

family (4 and 6) had lower pore sizes compared to their Cross-linked counterparts and S4FF in particular had the lowest recorded apparent porosity value. The results also show that general trends observed using qualitative analysis can be measured quantitatively. However, the results have also shown that there are challenges in attempting to quantify images displaying 3-D data.

Table 14 Summary table characterising the bead surface structure of the nine resins used in this study relative to each other, based on 4 properties – pore count, pore size, apparent porosity, pore size distribution. A green box represents relatively high values for the assigned category, yellow represents mid-range values and blue represents low values. The asterisk shows the resin that reported the highest/lowest value for the given property.

Resin	**Pore count**	**Pore size**	**Apparent porosity**	**Pore size distribution**
Capto Adhere	High	Low	High	Mid
Capto Q	High*	Low	High	Mid
MabSelect	High	Mid	High	High
MabSelect Xtra	Low*	High*	High	High*
Q-Sepharose HP	High	High	High*	High
Sepharose 6 FF	Mid	High	High	Mid
Sepharose CL-6B	High	Low	Mid	Mid
Sepharose 4 FF	Low	Low*	Low*	Low
Sepharose CL-4B	High	Mid	Mid	Low*

3.2.4. The challenges of using SEM for quantitative image analysis

Whilst SEM is one of the most widely used tools for structural analysis of biological materials (Kervrann *et al.*, 2016), there were a number of challenges faced in this study when using SEM to obtain a large number of high resolution images for quantitative analysis.

Due to the sensitivity of the fibrous polymer network that constitutes the agarose bead structure, the resins are particularly susceptible to damage due to the effects of irradiation by the focused beam of electrons. There are primary and secondary effects on the sample surface when the beam is focused on one area for a relatively short period of time. Primary effects involve polymer ionisation and damage to chemical bonds. Secondary effects are mainly heat generation, chain scission and charging-up of the sample, which affects the maximum resolution that can be achieved for that image (Michler, 2008).

A solution to this issue was to use a 'low-dose' technique when imaging. This involved adjustments to microscope parameters such as magnification, matching the electron dosage to the sensitivity of the bead sample and focusing on an area of the sample adjacent to the structure to be viewed (Buban *et al.*, 2010). However, there were still issues faced with this technique as, due to the spherical and heterogeneous nature of the bead and bead surface, focusing on an adjacent area still resulted in having to refocus the beam and readjust certain parameters when capturing images on the area of interest. The time spent making these adjustments on the area of interest created secondary effects, meaning that whilst some observations could be made using qualitative analysis, there would be further limitations when trying to use these images for quantitative analysis. Furthermore, each resin used in this study exhibited different levels of sensitivity when under the microscope. The softer gels, such as SCL4B and S4FF were much more difficult to image and exhibited higher levels of sensitivity, meaning even less contact time between the focused beam and the sample surface, resulting in fewer high resolution images being obtained.

A further challenge in using SEM for quantitative analysis was the use of 2-D imaging on 3-D specimen. As pores have 3 dimensions, using SEM for quantitative pore size analysis meant that the depth of pores could not be measured, resulting in imprecise values. However, these observations could be somewhat made out using qualitative analysis. Therefore, the values obtained using quantitative analysis cannot be used as 'true' characterisation values but the trends can be used to support what is visually observed (Ioannidis, 2009). A more general challenge faced during quantitative image analysis was the use of manual thresholding using ImageJ. Whilst the option to allow ImageJ to automatically threshold exists, this option was not feasible for the resins used in this study as each resin was structurally different and therefore each required a different amount of thresholding. Care was taken to neither over- nor under- threshold each image; however, due to the variability of this process, the quantitative values obtained maybe over or under representative of what can be observed qualitatively (https://imagej.net/Thresholding).

3.3.Conclusion

As previously outlined, scanning electron microscopy (SEM) is a imaging technique routinely used to generate high-resolution images and is used widely in chemistry and biosciences to identify microstructures, spatial compositions and the general characterization of solid materials down to less than 50nm in size (Swapp, 2015). Relatively little sample preparation is required and it provides accurate information regarding the 3D morphology and the location of features relative to each other, whilst still providing sufficient resolution and magnification required for this particular application. The main limitation however, is that samples must be dry prior to imaging.

This chapter explored three commonly applied drying techniques – air drying, freeze drying and critical point drying (CPD) – on two resins – Capto Adhere and MabSelect – to determine which drying technique was most suitable for the ultrastructural characterisation of the agarose-based chromatography media used in this study. The results showed that air drying was sufficient enough to provide microstructural information and clearly showed the variations in particle size distribution and bead morphology under SEM. However, no clear surface details could be identified using the air drying technique for both resins. Freeze drying resulted in changes to bead morphology. This meant that the surface topography was irregular, which created challenges in achieving clear topographic images. CPD however allowed for clearer microstructural and nanostructural imagining. This drying technique was applied to all resins used in this study for ultrastructural characterisation.

The images of all nine resins – Capto Adhere, Capto Q, MabSelect, MabSelect Xtra, Q-Sepharose High Performance, Sepharose 6 Fast Flow, Sepharose CL-6B, Sepharose 4 Fast Flow and Sepharose CL-4B were then qualitatively analysed based on differences in their structural make up, more precisely, apparent porosity and fibrosity differences. Based on this, four quantifiable properties were selected to better characterise the resins – pore count, average pore size, apparent porosity and pore size distribution. 3 images of each resin were analysed using ImageJ and the

results were used to determine whether they could support the characteristics observed qualitatively.

The values of the properties obtained for each resin using ImageJ analysis generally concurred with what could be observed by visual judgement and trends could be observed between sets of resins. The Capto family of resins had a greater pore count on average whilst MabSelect Xtra had the lowest pore count, larger pores and a wide pore size distribution. Similarly, MabSelect and Q-HP also had a wide pore size distribution and relatively high apparent porosity values. The Sepharose Fast Flow family (4 and 6) had lower pore sizes compared to their Cross-linked counterparts and S4FF in particular had the lowest recorded apparent porosity value. The results also show that general trends observed using qualitative analysis can be measured quantitatively. However, the results have also shown that there are challenges in using SEM for quantitative image analysis.

The main challenges faced when using SEM for quantitative image analysis involved obtaining a large number of images with consistently high enough resolution. This proved difficult due the high sensitivity of the polymers and their susceptibility to damage if exposed to the focused electron beam for too long. A further challenge was the use of 2-D imaging to characterise 3-dimensional properties. As a result, the values obtained can only be used to support visual observations.

CHAPTER 4
PRESSURE-FLOW CHARACTERISATION AND THE APPLICATION OF DYNAMIC MECHANICAL ANALYSIS (DMA)

4. PRESSURE-FLOW CHARACTERISATION AND THE APPLICATION OF DMA

In the previous chapter structural differences were observed across nine agarose-based chromatography resins – Sepharose CL-4B (4% agarose content), Sepharose CL-6B (6% agarose), Sepharose 4 Fast Flow (4% agarose), Sepharose 6 Fast Flow (6% agarose), Q-Sepharose High Performance (6% agarose), MabSelect Xtra (6% agarose, highly cross-linked), MabSelect (6% agarose, highly cross-linked) Capto Adhere (7% agarose, highly cross-linked) and Capto Q (7% agarose, highly cross-linked) - using scanning electron microscopy. The micrographs showed differences in matrix formation, pore size, pore size distribution, porosity and pore count. Capto Q had the highest pore count (>1000), MabSelect Xtra had the lowest pore count (~300), the highest pore size (7000nm^2) and the highest pore size distribution, while SCL4B had the lowest pore size distribution. S4FF had the smallest average pore size (1500nm^2) and the lowest porosity (17%), while Q-HP had the highest porosity at 44%.

This chapter looks to investigate whether the structural differences observed in chapter 3 are indicative of mechanical differences. The pressure-flow technique is an established method of mechanical characterisation and is used traditionally to determine the limit of the operating pressure drop and flow velocity. In order to obtain meaningful data, the column packing procedure is a critical step. The bed needs to be aligned such that the hydrodynamic pressure applied is evenly spread across the axial direction of the column. However, there are a number of issues associated with packing columns for the purpose of pressure-flow testing. This chapter reviews the importance of column packing and considers the challenges in achieving a well packed column.

The technique itself will be applied to the aforementioned nine resins for consistency. This method involves gradually increasing the flow rate until an infinite rise in the pressure drop is observed without further increase to the flow rate. The point at which an infinite rise in the pressure profile is observed without further increase to the flow rate is the point at which the column has ‘failed’ and is deemed

the critical velocity. The pressure-flow profiles of all nine resins and the limitations of the pressure-flow technique are discussed in this chapter.

A technique that addresses the limitations of pressure-flow characterisation and also allows for enhanced understanding of the mechanical behaviour of chromatography media is required. DMA is widely used to characterise a material's properties as a function of time, temperature, stress, strain, frequency, force, atmosphere or a combination of these parameters and provides information about the viscoelastic behaviour of the material. The choice of parameters to use for any given experiment is dependent on a number of factors such as sample consistency, morphology, size, among other factors. This chapter discusses the development of the DMA technique and parameter selection process for chromatography resins. The procedure is applied to the same nine resins and the results are presented and discussed. The application of this technique will need to be correlated with pressure-flow data to verify its validity. The DMA results are compared to pressure-flow data to observe any correlations.

4.1 The challenges of column packing

Column packing is central to chromatographic performance as it allows for maximum efficiency, high yield and purity. Because of this, regulatory authorities require that the packing process is robust and reproducible (Kennedy, 2003). The bed needs to be aligned such that the hydrodynamic pressure applied is evenly spread across the axial direction of the column and the density of the packed bed needs to be homogeneous with a controlled interstitial volume (Cheng, 2009). If this is not the case, channels may form in the bed resulting in loss of product yield and quality. Alternatively poor packing can also lead to cracking of the column and mechanical damage to the beads.

The most common packing method uses the flow packing technique, which was adopted in these investigations (Cheng, 2009). All the resins used in this study were packed with the same general technique in the sequence outlined below:

- Transfer the slurry to an empty column
- Slurry resuspension
- Lowering of the top adaptor
- Applying flow to the slurry to pack the rein
- Lowering the top adaptor to the final bed height

Despite the consistency in this technique, there were still challenges in achieving a well packed column in the first instance and in many cases, multiple attempts were required. The quality of the packing is known to be influenced by factors such as the chosen packing buffer, packing flow rates and the packing and compression factors specific to the resin type. For typical protein purification applications, the column asymmetry can range between 0.8-1.5. However a challenge faced when column packing for pressure-flow studies was that the asymmetry range was more stringent (0.8-1.2). Results in this study showed that when an asymmetry above 1.2 was obtained, the subsequent pressure-flow test led to no runaway rise to the pressure profile with increasing flow rate (table 15; figure 30).

Consequently various troubleshooting methods were employed (table 16) and the packing quality was re-evaluated (Bemberis, Noyes and Natarajan, 2003). More often than not, the troubleshooting techniques led to little improvement in the asymmetry value and the columns were repacked until an asymmetry of less than 1.2 was achieved. To ascertain whether the stringent asymmetry range was due to the apparatus used, the same experiment was performed on the AKTA Avant using Capto Q (3 tests were performed, results not shown). The outcome using the two systems (AKTA Pure and Avant) were the same (no pressure-flow profile was obtained when asymmetry was above 1.2). The critical velocity values obtained on the AKTA Avant were between 480 and 500 cm/hr (in agreement with AKTA Pure results, shown below).

A further challenge faced was that some matrices required more packing attempts than others. Although each resin required repacking on at least one occasion, the softer gels such as Sepharose CL-4B and Sepharose CL-6B in some instances required at least 3 attempts before an asymmetry of less than 1.2 was achieved. This was also the case with resins that had been exposed to aged and CIP conditions, Reasons for this could be that the softer gels have less cross-linking, lower agarose content and a wider particle size distribution compared to the Capto and MabSelect family of matrices, meaning that pressure fluctuations (either caused by flow or the lowering of the adaptor) were more likely to cause possible changes in bead morphology. The wider particle size distribution may have impacted the interstitial volume making it more difficult to control. The resins that had been exposed to aged/CIP conditions may have been mechanically compromised in this process, which may have made them more challenging to pack. It should be noted that automated packing systems e.g. AxiChrom can save both time and labour costs and achieve a more consistent pack compared with pack-in-place procedures however this was not an available resource during this study.

Table 15 Asymmetry results showing 3 repeats/runs for Capto Q, Sepharose CL-6B (SCL6B), Sepharose 4 Fast Flow (S4FF) and MabSelect in an XK16 column, bed height 15cm. N/A* indicates that no critical velocity value was recorded for the associated run. The flow rate was increased in a step-wise fashion until at least 50ml/min (~1500 cm/hr) before it was determined that there would be no critical velocity value recorded. The column consequently had to be repacked until an asymmetry below 1.2 was achieved.

Resin	**Run**	**Asymmetry**	**Critical velocity (cm/hr)**
Capto Q	1	1.07	477
	2	1.19	507
	3	1.23	N/A*
SCL6B	1	0.98	283
	2	1.21	N/A*
	3	1.30	N/A*
S4FF	1	1.41	N/A*
	2	1.08	194
	3	1.18	209
Mabselect	1	1.50	N/A*
	2	1.02	418
	3	1.04	418

Table 16 – Troubleshooting methods used in an attempt to achieve an asymmetry below 1.2. All methods resulted in a slight increase to the asymmetry value however a value below 1.2 was not obtained. A maximum of two troubleshooting methods were employed on each resin as to not cause any mechanical damage. All columns were repacked until an asymmetry of >1.2 was achieved.

Resin type	**Initial A_s**	**Troubleshooting method**	**New A_s**
Capto Q	1.23	Lower top adaptor	1.21
SCL6B	1.21	Reduce flow rate	1.21
S4FF	1.41	- Flow in reverse direction - Reduce flow rate	1.40
MabSelect	1.50	- Modify injection loop - Reduce flow rate	1.47

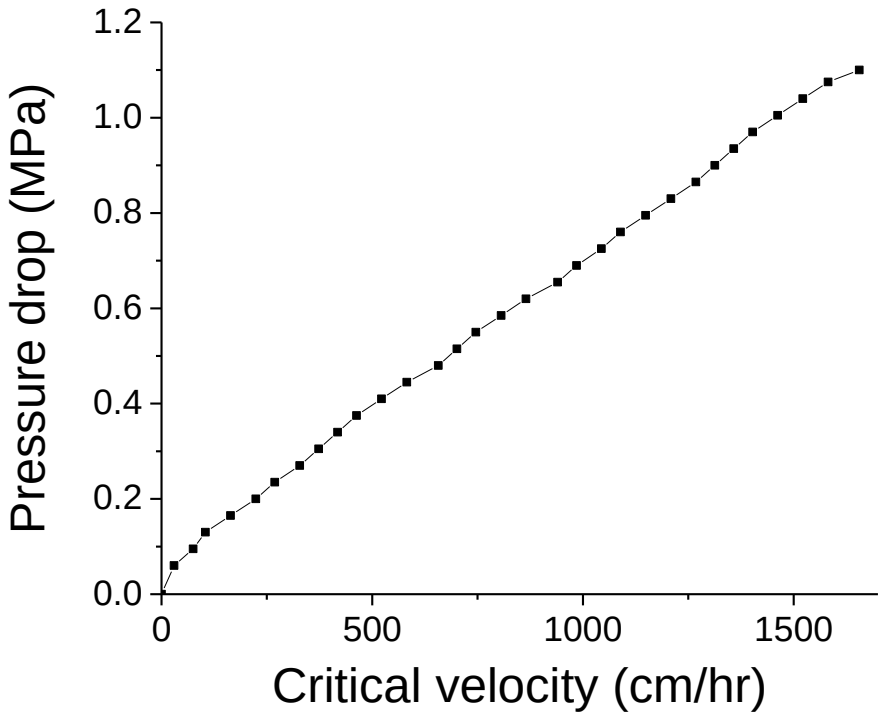

Figure 30 – Pressure-flow plot for Capto Q run 3 – asymmetry 1.23 (see table 15). The flow rate was gradually increased until a 35kPa increase in pressure drop was seen as described in Tran et al., 2007. This was continued until at least 50ml/min (~1500 cm/hr) before it was determined that there would be no critical velocity value recorded as no runaway pressure rise was observed. 1500 cm/hr was deemed to be a linear velocity that was more than sufficient to observe a runaway rise in pressure drop without compromise to the AKTA system which had a limit of 100 ml/min (~3000 cm/hr) and a maximum operating pressure of 20 MPa. (NB: a flow resistor was not used in this study.)

4.2.Pressure-flow characterisation

Pressure-flow characterisation is performed to obtain data that is representative of the pressure-flow relationship of the column during operation. This information is then used to predict the limit of the operating pressure drop and flow velocity. In contrast to open bed pressure-flow measurements, the top bed support is in contact with the bed, creating a compressed structure. Therefore, a compression factor (usually ranging from 1.15 to 1.20 for agarose-based resins) is applied during media packing. Packed bed pressure-flow information is mainly used to determine the pressure drop during column operation. The acquired data provides information regarding the flow velocity limit for the media in use. The limit denotes the point at which the bed will start to compress to such an extent that a gap is created between the top bed support and the bed (resin rigidity limit) (Jagschies, Sofer and Hagel, 2008).

In this technique, the flow rate of the packing buffer was increased until a 35 kPa increase in pressure drop was observed. This was achieved by applying gradual increments to the flow rate (usually a 0.5 ml/min increase each time). When each 35 kPa increase had been reached, the fluid flow rate measurements were taken. The procedure was conducted until the point at which the pressure proceeded to rise rapidly without further increase to the flow rate. The flow rate at which this occured was converted to linear velocity. This linear velocity value denoted the point at which the column had ‘failed’ and is generally termed the critical velocity (Tran *et al.*, 2007). In theory, the more rigid the resin is, the higher the critical velocity. This means that gels that are manufactured to be softer or more compressible will require lower pressures and fluid flow rates to ‘fail’ or reach critical velocity, while the more rigid resins will withstand higher pressures and fluid flow rates before critical velocity is reached. The analysis also gives an indication as to whether it is the resin or the column that sets the flow velocity and pressure limits (Stickel and Fotopoulos, 2001).

In this study an XK16 column (diameter 16mm) was used for all experiments and the bed was packed to a height of 15cm. This aspect ratio was chosen to avoid wall support issues that arise when using narrower columns, which can in turn lead to unexpectedly high pressures. Three repeats of the procedure were conducted for all nine resins and the averages were plotted. The standard deviations from the average (based on the repeats) are represented by the error bars (figure 31). The degree to which any individual repeat may vary is reliant mainly on column packing and the resulting asymmetry. The probability that a column will pack in exactly the same way, despite using the same procedure is low. This is represented by the asymmetry value obtained. Although the asymmetry differed for all repeats, it was maintained in the range of 0.8-1.2, which may have required multiple repacks to achieve (see section 4.1). A reduction in bed height during the changes to flow velocity may also be observed (Tran *et al.*, 2007).

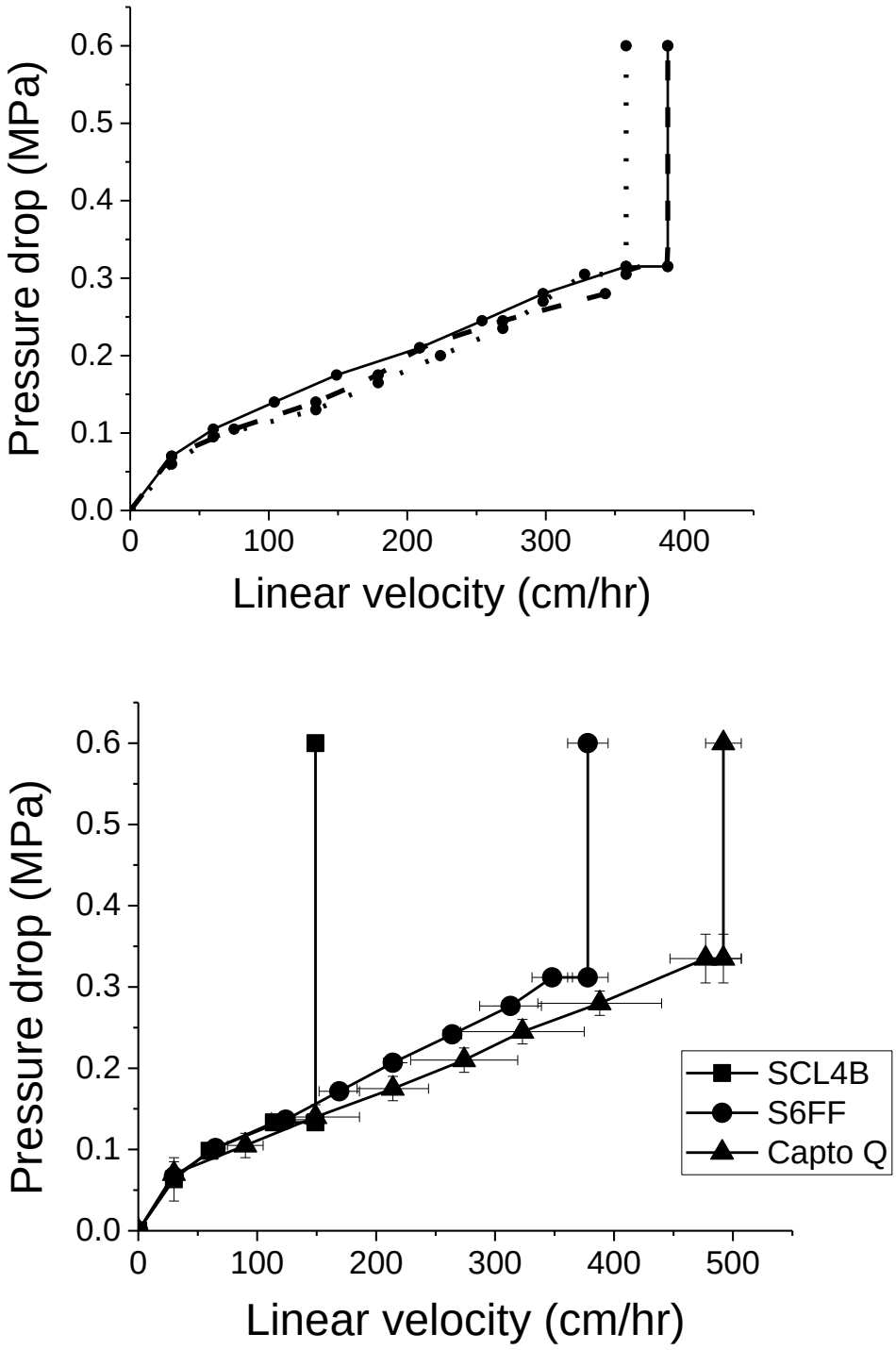

Figure 31 – (a) Pressure-flow plot showing 3 repeats for Sepharose 6FF (6% cross-linked agarose) (one solid line, one dashed line, one dotted line). (b) Pressure-flow plot showing averages of 3 out of the 9 resins – Sepharose CL-4B (4% cross-linked agarose) (squares), Sepharose 6FF (6% cross-linked agarose) (circles) and Capto Q (7% highly cross-linked agarose) (triangles). Error bars representing pressure and flow rate are +/- one standard deviation taken from the 3 repeats.

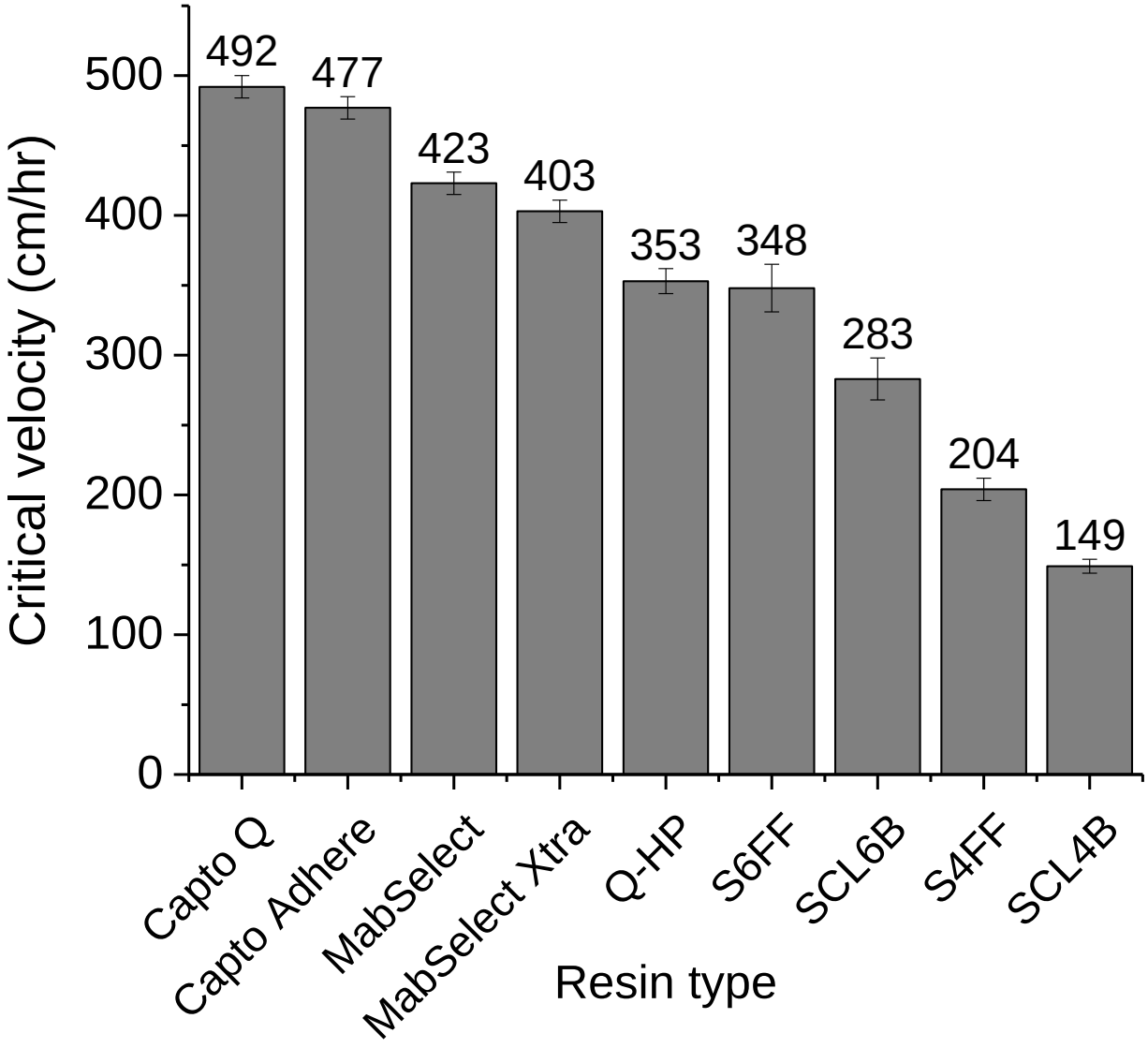

Figure 32 – Critical velocity for each resin obtained using the pressure-flow technique in an XK16 column, bed height 15cm. Each bar represents an average of the point before column failure. The error bars represent the standard deviation of 3 repeats of each resin. Capto Q - µcrit 492 cm/hr (7% highly cross-linked agarose), Capto Adhere - µcrit 477 cm/hr (7% highly cross-linked agarose), MabSelect - µcrit 423 cm/hr (6% highly cross-linked agarose), MabSelect Xtra - µcrit 403 cm/hr (6% highly cross-linked agarose), Q Sepharose HP - µcrit 353 cm/hr (6% cross-linked agarose), Sepharose 6FF - µcrit 348 cm/hr (6% cross-linked agarose), Sepharose CL-6B - µcrit 283 cm/hr (6% cross-linked agarose), Sepharose 4FF - µcrit 204 cm/hr (4% cross-linked agarose), Sepharose CL-4B - µcrit 149 cm/hr (4% cross-linked agarose)

Capto Q has the highest critical velocity at 492 cm/hr, followed by Capto Adhere – 477 cm/hr, MabSelect – 423 cm/hr, MabSelect Xtra – 403 cm/hr, Q-Sepharose HP – 353 cm/hr, Sepharose 6FF – 348 cm/hr, Sepharose CL-6B - 283 cm/hr, Sepharose 4FF – 204 cm/hr and Sepharose CL-4B – 149 cm/hr.

The results show that the Capto family (Capto Q and Adhere) are the least compressible of the resins, followed the MabSelect family. This is expected as both families are made of highly cross-linked agarose polymers and contain 7% and 6% agarose respectively. Q-HP and S6FF are cross-linked resins that contain 6% agarose. These two resins exhibit quasi-identical mechanical behaviour in the column. Their main structural differences are observed in their average bead size and their average pore size distributions (see chapter 3). S6FF resins are 2-3 times larger in size (d_p) compared to Q-HP, however the average pore size of S6FF (and Fast Flow resins in general) is approximately 2-3 times smaller than that of Q-HP (DePhillips and Lenhoff, 2000; Tarmann and Jungbauer, 2008; Hardin *et al.*, 2009). It has been established that both pore size distribution and bead size contribute to the mechanical properties of chromatography media (Zhou *et al.*, 2007; Yan *et al.*, 2009). The trade-off between these two parameters, as well as their identical mechanical traits, may explain why both resins mechanically perform almost identically in the column.

The results also show the differences in mechanical strength between SCL6B and S6FF, as well as SCL4B and S4FF. Both pairs of resins are cross-linked and contain 6% and 4% agarose in their matrices respectively, however both fast flow resins are mechanically stronger than their -CL counterparts. In both cases, the fast flow resins withstand much higher flow rates according to the manufacturer's specification, which may indicate that their cross-linking was more extensive. Furthermore, their electron micrographs show that they are structurally different (see chapter 3). SCL6B, for example, appears to be more fibrous and more discontinuous compared to its fast flow counterpart which has a more homogenous, continuous structure, which may indicate greater mechanical strength. A further consideration concerns the ligand chemistry. For example, the attachment of affinity chromatography ligands would alter the mechanical properties of the base matrix, which would differ for an ion exchange/hydrophobic ligand used as a polishing step.

4.2.1. The limitations of pressure-flow characterisation

There are advantages in using the pressure-flow technique to investigate the mechanical properties of resins. These include the ability to determine the behaviour of chromatography media in a packed bed and how mechanical properties vary with media viscosity, pH, ionic strength, among other properties. However, a drawback of this method is that it requires that the operator adheres to stringent packing criteria to obtain meaningful data. As described in section 4.1, packing of columns can be a time consuming and tedious process as several re-packs may be required to achieve the desired asymmetry and each resin, depending on its chemical and mechanical properties, has its own specific packing criteria. Furthermore, it is necessary to use a column of a suitable diameter, such that wall effects that support the resin in narrow columns do not dominate (Stickel and Fotopoulos, 2001). The bed height also needs to be representative, as pressure drop directly correlates to the height of the bed, meaning heights of 15cm or greater are typically used (Tran *et al.*, 2007). For these reasons, the pressure-flow technique consumes large quantities of chromatographic media and buffers, which is costly (Warner and Nochumson, 2003).

4.3. The development of the DMA technique

As previously outlined, DMA is a technique widely used to characterise a material's properties as a function of time, temperature, stress, strain, frequency, force, atmosphere or a combination of these parameters and provides information about the viscoelastic behaviour of the material. The choice of parameter to use for any given experiment is dictated by a number of factors including the sample's physical state, sample size, the difficulty in loading, the consistency of the sample and sample morphology (Menard and Menard, 2015). Generally, if the sample is irregularly shaped and/or difficult to mount (such as soft materials and gels) it is recommended to use DMA for compression studies, which involves using the stress, strain and time parameters in any suitable combination (Menard, 2008).

Traditionally, compression studies requiring the use of DMA measure stress (force per unit area) as a function of strain (proportional deformation/displacement). The stress-strain curve that is generated is used to calculate Young's modulus which is a

universal indicator of a material's stiffness (Moroni, De Wijn and Van Blitterswijk, 2006). However, in order to use Young's modulus, the material needs to be homogeneously solid, which is not the case for chromatography media. This means that a suitable combination of parameters in this case would involve the use of time. Given the physical properties of chromatography media and the liquid-like properties of a slurry, the application of consistent force to observe changes in shear seemed most ideal. Therefore in this study, a small deformation of constant force is applied to a 1ml sample of resin in a sinusoidal manner, allowing the media to respond to changes in strain over a period of time.

The DMA equipment itself is composed mainly of a pan and a lid, equipped with sensors. The lid is equipped with a sensor that allows it to stop just at the surface of the slurry once in descent, which allows the system to record the sample height. When the methodology is started, a sinusoidal force of 100mN is applied at a constant frequency of 1 Hz. As the lid descends, the slurry moves around the sides of the lid and this movement is recorded as a displacement percentage with time. Meanwhile, a time-strain profile is generated, where strain is the displacement of the lid through the resin bed recorded as a percentage. Once a strain threshold is exceeded, the rate of increase is vastly reduced or the plot begins to level out completely and at this point ultimate compression is reached. This is either when the lid has hit the bottom of the pan, or when little or no further deformation of the slurry can be achieved with constant force. For consistency, the slope of the line is taken before ultimate compression and this provides information about the movement of the lid through the slurry with constant force. The units are recorded as $\%min^{-1}$ (figure 33). The less viscous the media is, the quicker the lid will move through the slurry, therefore the higher the % strain per minute. The procedure is repeated 3 times for each resin (figure 34).

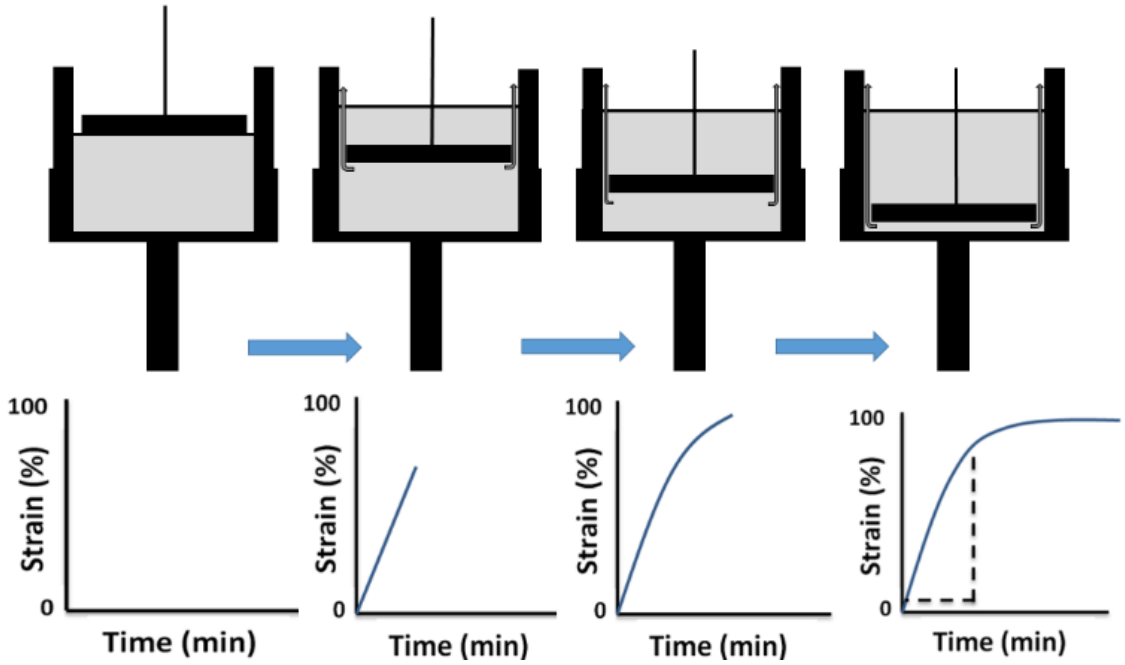

Figure 33 – Schematic of DMA methodology. The lid is equipped with a sensor that records the initial height of the sample. When the methodology is started the descending lid applies a sinusoidal force of 100 mN to the sample, causing the slurry to deform and move around the sides of the lid. Strain (slurry displacement) is recorded with time. A strain versus time plot is generated by the Pyris Manager software and the slope of the line before ultimate compression determines the slurry deformation rate.

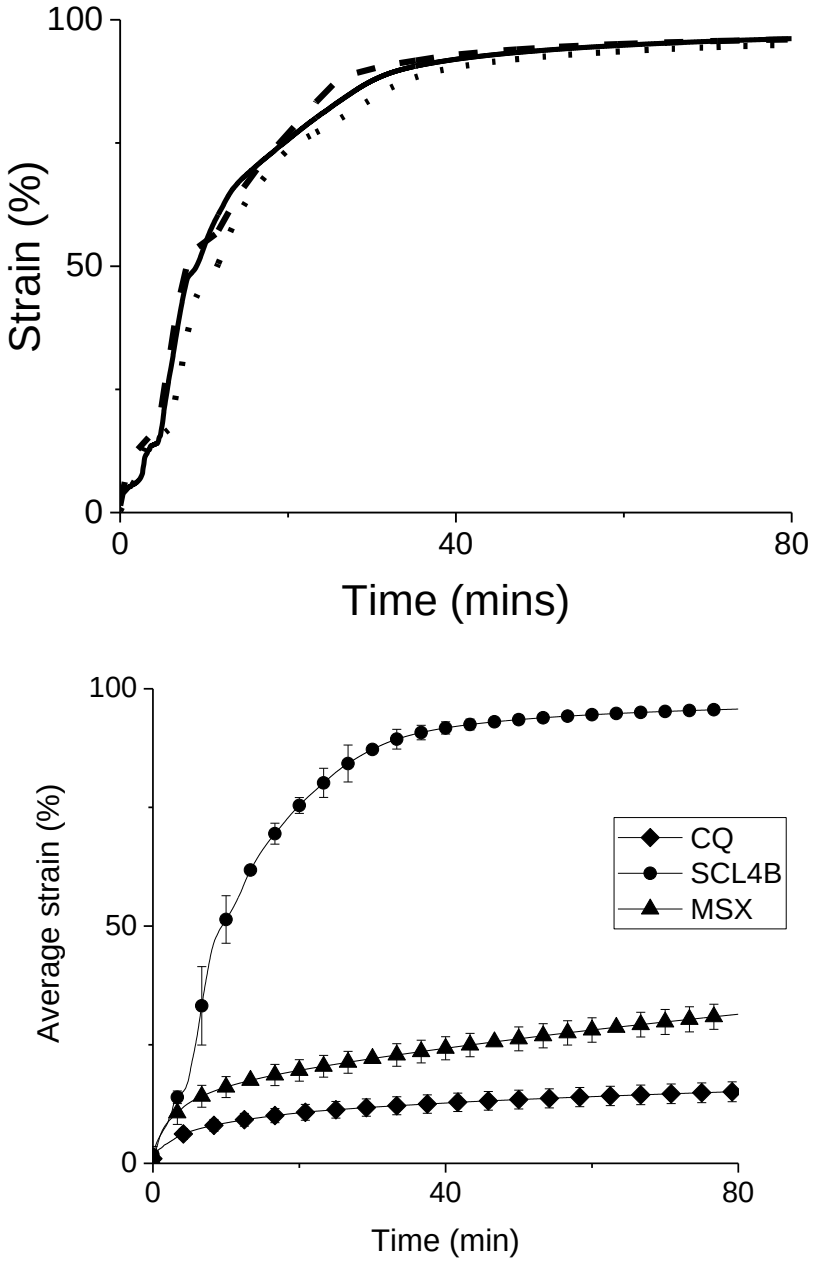

Figure 34 – (a) Strain v time plot for 3 repeats of Sepharose CL-4B (4% cross-linked agarose) (one solid line, one dashed line, one dotted line). (b) Averages for 3 out of 9 resins – Capto Q (7% highly cross-linked agarose) (diamonds), MabSelect Xtra (6% cross-linked agarose) (triangles) and Sepharose CL-4B (4% cross-linked agarose) (circles). Error bars representing strain are standard deviations taken from the 3 repeats of each resin. Shapes and error bars are plotted once every 250 data points

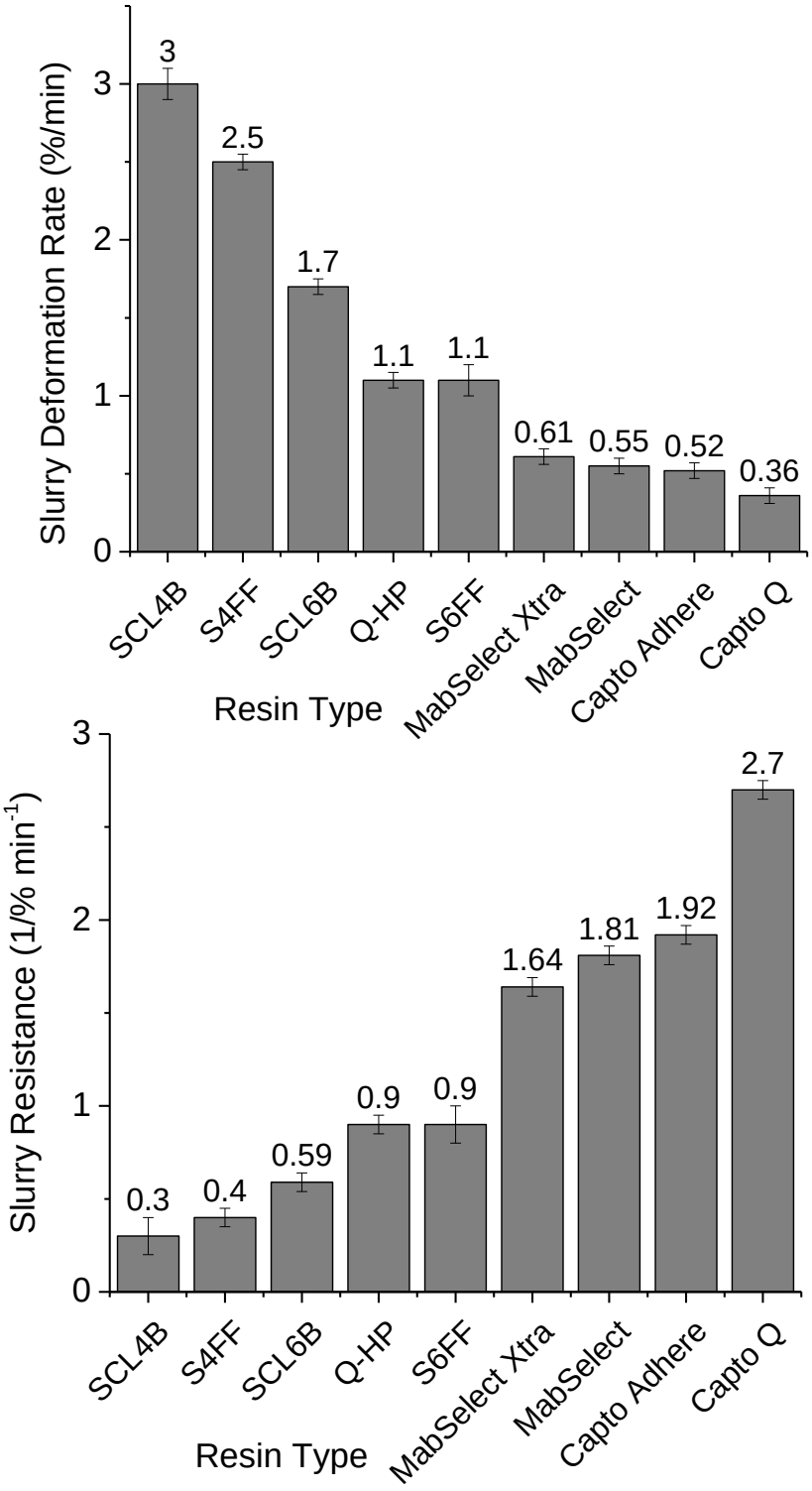

Figure 35 – (a) SDR for all 9 resins. For all resins, the gradient of the lines for all three repeats are taken and averaged. The bar represents the average value and the error bars are standard deviations based on the three repeats. (b) Parity plot – Slurry resistance. The values are obtained by calculating 1/SDR values obtained for all 9 resins. This can then be better compared to figure 32 as it also emphasises further the difference between the more rigid resins compared to the less rigid.

Figure 35a shows the slurry deformation rates for each resin using the DMA technique. Capto Q has the slowest slurry deformation rate at 0.36 %/min, followed by Capto Adhere – 0.52 %/min, MabSelect – 0.55 %/min, MabSelect Xtra – 0.61 %/min, Q-Sepharose HP and Sepharose 6FF – 1.1 %/min, Sepharose CL-6B – 1.7 %/min, Sepharose 4 FF – 2.5 %/min and Sepharose CL-4B – 3 %/min.

Figure 35b shows the graph obtained by plotting the reciprocal of the SDR values for each resin. The resulting parameter was termed 'slurry resistance ($1/\%min^{-1}$)'. This approach allowed for a positive correlation between the pressure-flow technique and the DMA technique and more clearly highlighted distinctions between the more mechanically robust resins and weaker resins. The results show Capto Q has the highest slurry resistance of 2.7, followed by Capto Adhere – 1.92, MabSelect - 1.81, MabSelect Xtra – 1.64, Q-Sepharose High Performance and Sepharose 6 Fast Flow - 0.90, Sepharose CL-6B - 0.59, Sepharose 4 Fast Flow - 0.4 and Sepharose CL-4B - 0.3.

The same trends observed in figure 32 are observed in figure 35b. The results from figure 35b show that Capto Q is most resistant to deformation, followed by Capto Adhere, MabSelect, MabSelect Xtra, Q-Sepharose High Performance and Sepharose 6 Fast Flow, Sepharose CL-6B, Sepharose 4 Fast Flow and Sepharose CL-4B. Similar to the trends observed in section 4.2, the results also show that Q-Sepharose High Performance and Sepharose 6 Fast Flow exhibit very similar viscoelastic properties. Both resins contain 6% agarose however there are differences in their average bead sizes and pore sizes. The results also show the differences in viscoelastic properties between SCL6B and S6FF, as well as SCL4B and S4FF. The possible reasons for the observed trends are further explained in section 4.2. The data from figures 32 and 35 are plotted for comparison (figure 36).

4.3.1. The advantages of DMA

The pressure-flow technique is useful for determining the mechanical behaviour of chromatography media within a packed bed as well as the effects of fluid viscosity, pH, ionic strength etc. However there are limitations associated with the stringent packing criteria, the potential of multiple repacks and the quantity of media and buffers consumed. DMA is a tool that allows for flexibility in the use of parameters and can be tailored according to the mechanical properties to be studied. It allows for the use of small quantities of sample (~1ml) and requires relatively little preparation. Furthermore, it measures mechanical behaviour based on changes in viscoelasticity as opposed to critical velocity, which allows for an enhanced understanding of the mechanical properties of chromatography media. The low force of 100 mN applied in a sinusoidal manner is non-destructive to the media over an extended period of time (80 minutes). Given these advantages, it can potentially be used to investigate the mechanical properties of other media types, e.g. non-agarose based resins. It may also be used in the development of new resins for rapid screening post-emulsification.

4.4. Data correlation – Pressure-flow vs Dynamic Mechanical analysis

The pressure-flow technique has proven to be a reproducible way of obtaining mechanical performance information of chromatography media. Despite this, the limitations of this technique indicate that further information about media mechanical performance is required. Therefore, additional techniques are necessary in order to further enhance the understanding of the mechanical behaviour of chromatography resins. However, the application of an additional technique will need to be correlated with pressure-flow data to verify its validity. This technique may then be applied as a combinatory technique together with pressure-flow for a more comprehensive understanding of the mechanical properties of chromatography media. The results from DMA are compared to that of pressure-flow to observe whether any correlations can be established.

Figure 36a shows a strong negative correlation between critical velocity and slurry deformation rate for all 9 resins used in this study. This means that the stronger resins such as MabSelect, Capto Adhere and Capto Q have low SDRs and high u_{crit} values and the opposite is true for mechanically weaker resins such as SCL4B and S4FF. The trend begins in a linear fashion with the first five resins but then tapers off when the more mechanically robust resins appear. This representation of results indicates that as the resins become mechanically more similar and the difference in their mechanical properties becomes less significant. However, as manufacturers and regulatory authorities favour the use mechanically robust resins for separation, there is an onus to better clarify the mechanical differences between the stronger resins.

Figure 36b shows a parity plot of figure 36a and the y-axis is represented as ‘slurry resistance’. The values are calculated based on 1/SDR for each resin. The trend observed is a positive polynomial trend for slurry resistance against critical velocity. The first 5 resins show a gradual increase in mechanical resistance, however, the difference in mechanical strength becomes more apparent when the more robust resins (MabSelect, Capto Adhere and Capto Q) are plotted. This plot better demonstrates the disparity in mechanical behaviour between each resin.

Both plots show strong correlations and can be used individually to either observe mechanical differences between mechanically weaker media (figure 36a) or to observe differences between more robust resins (figure 36b). The results therefore indicate that DMA can be used as a combinatory technique to pressure-flow for the characterisation of chromatography media.

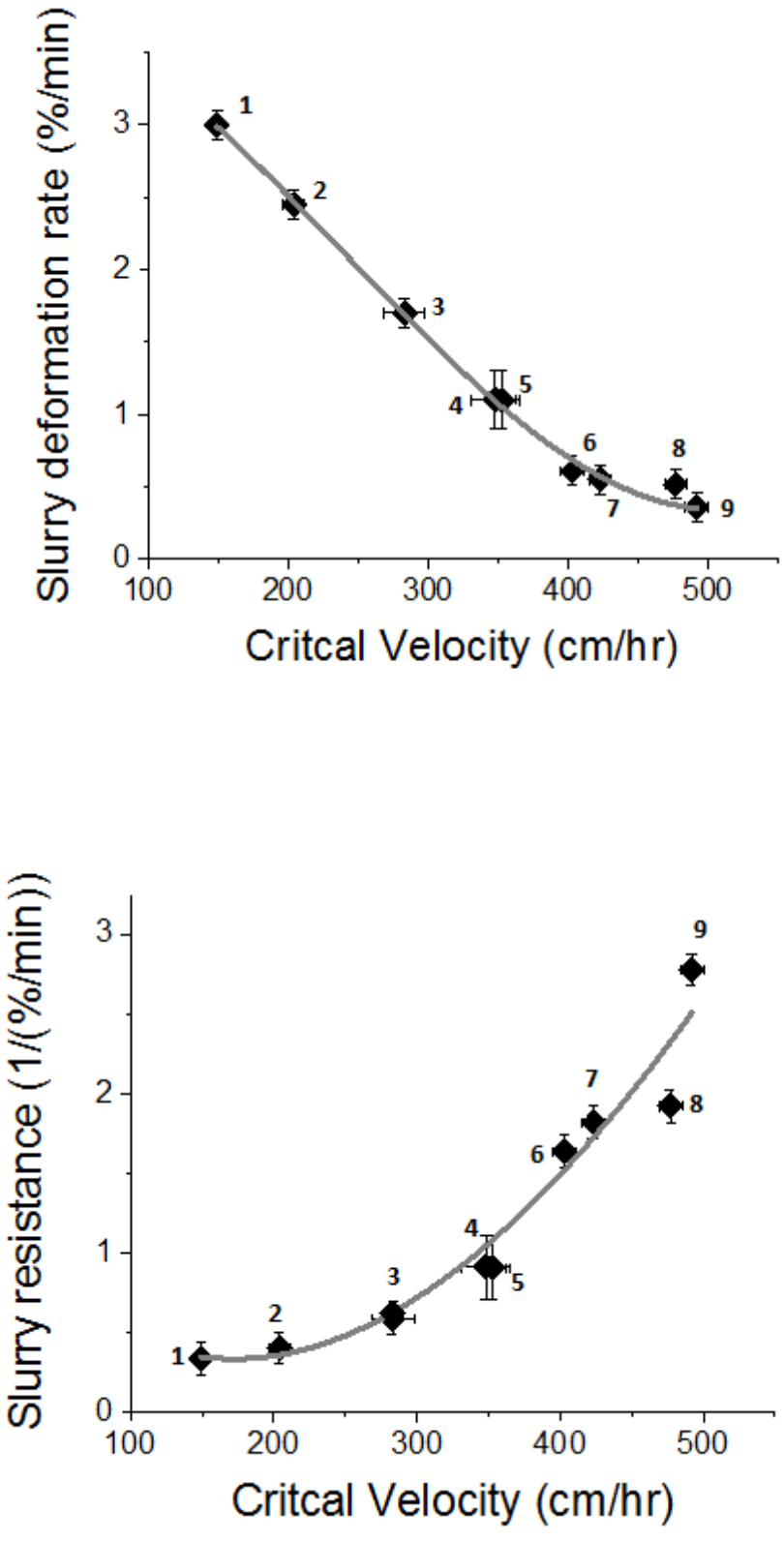

Figure 36 – (a) SDR values shown in figure 35(a) plotted against ucrit values shown in figure 32. Plot shows strong negative trend (b) Parity plot showing slurry resistance. Slurry resistance values are calculated as 1/SDR. Plot shows strong positive trend. Key: 1 – Sepharose CL-4B, 2 – Sepharose 4 Fast Flow, 3 – Sepharose CL-6B, 4 – Sepharose 6 Fast Flow, 5 – Q-Sepharose High Performance, 6 – MabSelect Xtra, 7 – MabSelect, 8 – Capto Adhere, 9 – Capto Q

4.5. Conclusion

Two important characteristics in determining mechanical strength of resins are their percentage agarose content and their extent of cross-linking. Currently, chromatography resin manufacturers use the pressure-flow characterisation technique to determine the limit of the operating pressure drop and flow velocity that resins can withstand. It is an established technique and allows for the behaviour of chromatography media in a packed bed to be determined. Furthermore, the pressure-flow technique can be used to investigate how mechanical properties of resins vary with changes to media viscosity, pH, ionic strength, among other properties. In this procedure, the fluid flow rate is manually increased until a runaway rise in the pressure profile is observed. This is the point at which the column has 'failed' and is termed the critical velocity. There are however, disadvantages in the use of this method, including stringent column packing criteria and packing columns potentially up to many litres in size. These processes can be both costly and time-consuming, requiring a number of buffers to be used.

This chapter discussed the development of a DMA technique that does not require the use of multiple buffers and uses a much reduced quantity of resin (~1ml). The technique was tested on nine resins with varying mechanical properties and compared to their pressure-flow characteristics. The results show a strong correlation between both techniques and show the most mechanically robust resins to be Capto Q, Capto Adhere, MabSelect and MabSelect Xtra. Both techniques also show that Sepharose 6 Fast Flow and Q-Sepharose High Performance are mechanically similar. The main differences in the techniques are observed in the quantitative values obtained. Using the pressure-flow method, the most robust resin (Capto Q) had a critical velocity 3 times higher than Sepharose CL-4B, whilst the DMA technique showed Capto Q to have a slurry deformation rate 9 times higher than Sepharose CL-4B. This could be due to increased sensitivity of mechanical changes as the sample volume used for DMA is much smaller than that of pressure-flow. Notwithstanding, the results do indicate that DMA can be used as a combinatory technique with pressure-flow for determining mechanical performance of a given resin. However, DMA alone does exhibit additional benefits over the pressure-flow technique. It could be applied to non-agarose resins to determine mechanical

performance. The technique may also be useful for rapid testing of a range of resins post-emulsification and during the development of new resins. It may also be considered as a test to investigate mechanical differences in different parts of the column during bioprocessing. These points are further discussed in Chapter 7 – Future Work. Furthermore, it may also be used to test resins at different stages of its lifetime during bioprocessing and also to test resins exposed to different conditions in the column. This final point is investigated in the next chapter.

General correlations between the studied parameters in chapters 3 and 4 can be drawn as to ascertain whether there is a link between the observed structural and mechanical properties. The mechanically stronger resins (CQ, CA, MS) generally had a higher pore count, higher apparent porosity and relatively smaller pore sizes compared to the mechanically weaker resins. The pore size distribution was relatively lower for older generation resins, compared to newer resins.

CHAPTER 5
THE STRUCTURAL AND MECHANICAL CHARACTERISATION OF CYCLED RESINS

5. THE STRUCTURAL AND MECHANICAL CHARACTERISATION OF CYCLED RESINS

Previous chapters explored the structural and mechanical characterisation of nine fresh chromatography resins – Capto Adhere, Capto Q, MabSelect, MabSelect Xtra, Q-Sepharose High Performance, Sepharose 6 Fast Flow, Sepharose CL-6B, Sepharose 4 Fast Flow and Sepharose CL-4B - using scanning electron microscopy and pressure-flow/dynamic mechanical analysis respectively. The resins were structurally characterised based on pore count, apparent porosity, average pore size and pore size distribution. Each resin exhibited different structural characteristics when viewed under the electron microscope. Q-Sepharose HP had relatively high values in all elements characterised, reporting the highest level of apparent porosity at 44% whilst Sepharose 4FF had relatively low values in all elements characterised, including the lowest level of apparent porosity at 17%. This indicates that the bead structure is highly fibrous, which was also observed qualitatively (see chapter 3).

Pressure-flow analysis was then used to determine whether the structural properties were indicative of mechanical strength. The results showed that the Capto family had the highest critical velocities, followed by the MabSelect family. Q-HP and S6FF exhibited quasi-identical behaviour in the column whilst SCL6B, S4FF and SCL4B had the lowest critical velocity values (chapter 4). However, there were practical limitations in using the pressure-flow technique alone to for mechanical characterisation, including the large quantity of chromatography media required and buffers, the stringent criteria required to pack a column, among others. The use of DMA as a technique allowed for further mechanical characterisation based on the viscoelastic properties of the resin using 1ml of resin. It also gives the user flexibility in choice of parameters to be measured. The technique was also applied to the nine studied resins and correlated with the results obtained using the pressure-flow technique. The same trends were observed – The Capto family showed the highest resistance to deformation, followed by the MabSelect family. Q-HP and S6FF showed similar resistance and SCL6B, S4FF and SCL4B had the lowest slurry resistance values.

These techniques are applied in this chapter to characterise the structural and mechanical changes observed in resins that had undergone use in a bioprocess. The resins used in this study were MabSelect, MabSelect Xtra, Q-Sepharose HP and Capto Adhere and each resin has been exposed to two conditions – CIP and aged. This chapter discusses the reasoning behind the selection of these conditions. Subsequently, these resins are structurally characterised to determine whether there are differences between resins exposed to buffers only (CIP) and resins used for lifetime studies in the production of biopharmaceuticals (aged), namely monoclonal antibodies and fusion proteins. ImageJ is used to quantify the structural properties observed. Pressure-flow and DMA are then used to investigate the mechanical differences between CIP and aged resins, which is then compared to the characteristics observed in their fresh counterparts. Statistical analysis using one-way ANOVA is carried out to determine whether the relationships between pressure-flow and DMA data is significant and if so, to what extent. Further understanding of the changes in structural and mechanical properties of resins over their lifetime may facilitate timely and improved decisions in large-scale chromatographic operations, potentially maximising resin lifetime.

5.1.Selecting bioprocessing conditions

MabSelect, Q-Sepharose High Peformance and Capto Adhere are resins widely used in the biopharmaceutical industry as elements in platform type processes for the purification of monoclonal antibodies and in this case, were used by Eli Lilly & Co. in the purification of two biopharmaceutical products, a monoclonal antibody and a fusion protein. In this study, the resins used form capture and polishing steps. These resins were supplied by the company in their fresh and aged states as part of laboratory-scale resin lifetime studies. Figure37 shows the process flow of unit operations used to obtain the aged sample in the production of monoclonal antibodies (table 17). MabSelect and Capto Adhere were used for lifetime studies studies of an IgG4 product and make up the two chromatography operations in this process (figure 37), whereas Q-HP was used in the latter stages of the separation process in the production of a fusion protein. MabSelect Xtra was supplied by another manufacturing company and is used as a capture step for monoclonal antibody IgG1. This company had noticed severe back pressure increase as a function of cycle number and therefore wanted to understand how the changing structural and mechanical properties of aging MabSelect Xtra contributed to this phenomenon.

The resins were also exposed to buffer-only conditions, termed CIP conditions (table 18). The purpose of this was to observe any changes in structural and mechanical properties post-exposure to buffers only, i.e. without loading any biological material onto the columns, with key focus on the effects of CIP reagents, which is likely to be the most damaging element of the process cycle in absence of any biological material. These experiments were designed to determine the impact of buffers and CIP reagents on the structural and mechanical integrity of the resins compared to their fresh and aged counterparts. These studies may also provide insight into the effects of biological material on the columns as they can be used as a negative control in studies of the bioprocess lifetime.

The CIP experiments were performed in-house on MabSelect, Q-HP and MabSelect Xtra resins and Eli Lilly & Co. conducted CIP experiments on Capto Adhere resin. All were conducted for 50 cycles. Due to the vast quantities of buffers that would

have to be used on larger columns, the experiments were conducted on smaller columns. They were carried out five times for each resin on 5 separate 1ml HiTrap columns supplied by GE Healthcare (Uppsala, Sweden). One column was used for SEM studies and the remaining columns were used for DMA studies. The Capto Adhere CIP material supplied by Eli Lilly & Co. was large enough to perform SEM, pressure-flow and DMA studies (45ml column). The CIP conditions to which the columns were exposed, aimed to be as closely matched as possible to the buffer conditions used to generate the aged resins supplied by the aforementioned companies. For confidentiality reasons, not all the information could be supplied by both Eli Lilly & Co. and the second company. Where there were gaps in information, process conditions on freely accessible data sheets reported by GE Healthcare were substituted.

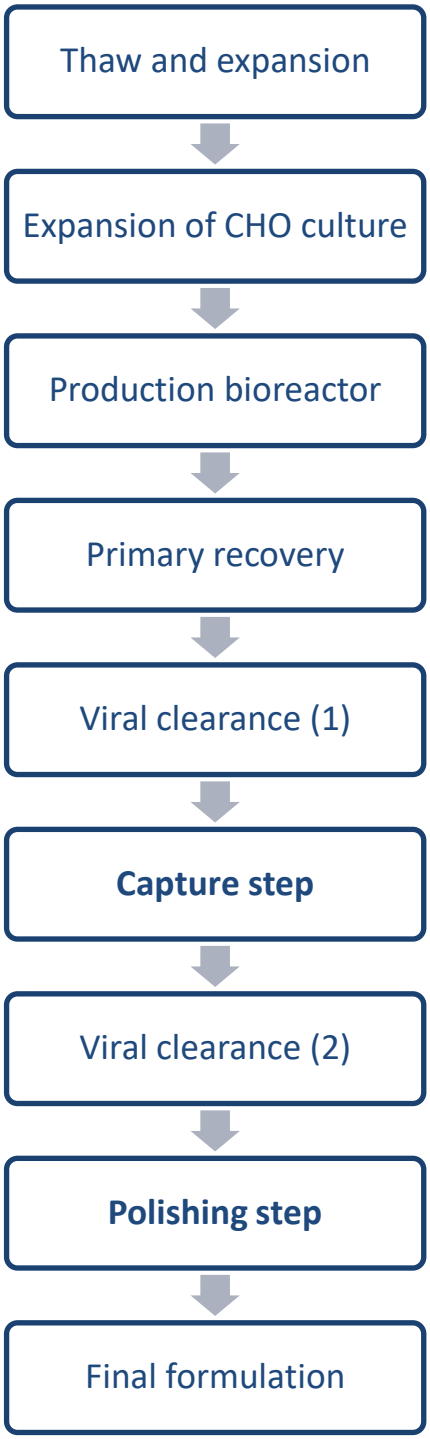

Figure 37 – Eli Lilly & Co. process flow chart showing unit operations for the creation of an IgG4 product. Where the capture and polishing steps feature in the process is highlighted.

Table 17 Process conditions for aged resins – MabSelect & Capto Adhere, Q-Sepharose High Performance and MabSelect Xtra. The table provides information on the number of cycles, the column size used, buffer/CIP conditions, the product and mode of expression.

Resin type	**Condition**	**No. of cycles**	**Column size**	**Buffers**	**Application**
MabSelect	Aged	17	100 cm diameter, 17 cm bed height (~130L)	Wash: Tris buffers Elution: Sodium Citrate, pH 3 CIP: Regeneration: 1% acetic acid, 1 % phosphoric acid. Sanitisation: 50 mM NaOH, 1 M NaCl. Sanitisation performed prior to the first cycle of two, and following the last cycle of two. Storage: Sodium Acetate Buffer, pH 4	IgG4, CHO expression
Capto Adhere	Aged	17	80 cm diameter, 29 cm bed height (~145L)	Wash: Tris buffer Elution: 20mM Acetate buffer 100 mM NaCl CIP: Regeneration → weak acid. Sanitisation → strong base. The column pack is regenerated and sanitised after every run; the column is stored after every second run.	IgG4, CHO expression
Q-Sepharose HP	Aged	64	60 cm diameter, 16 cm bed height (~45L)	Wash and elution: Tris buffers. Regeneration and Sanitisation: 1 N NaOH. Sanitisation performed prior to the first cycle of eight, and after every cycle. Storage: 0.1 N NaOH	Fusion protein, CHO expression
MabSelect Xtra	Aged	20	25ml column, bed height 20 cm	Wash: phosphate based Elution: acetate buffer CIP: 0.5M acetic acid, every cycle. 0.1M NaOH, every 5 cycles	In-house developed IgG1 (hydrodynamic radius 8-12 nm)

Table 18 – Process conditions for resins exposed to buffers only (CIP conditions) - MabSelect & Capto Adhere, Q-Sepharose High Performance and MabSelect Xtra. All experiments were carried out for 50 cycles. 1ml HiTrap columns from GE Healthcare (Uppsala, Sweden) were used for MS, MSX and Q-HP and 45ml of CA material was supplied by Eli Lilly & Co.

Resin type	**Condition**	**No. of cycles**	**Column size**	**Buffers**
MabSelect	CIP	50	1ml Hi Trap	*Mili Q wash* *Equilibration*: 20 mM sodium phosphate, 0.15 M NaCl *Blank load* (no protein): 20 mM sodium phosphate, 0.15 M NaCl *Wash*: 20 mM sodium phosphate, 0.15 M NaCl *Elution*: 0.1 M sodium citrate, pH 3.0 *CIP*: 0.5M NaOH *Regeneration*: 20 mM sodium phosphate, 0.15 M NaCl
MabSelect Xtra	CIP	50	1ml Hi Trap	Same as MabSelect. *CIP*: 0.5M acetic acid, every cycle. 0.1M NaOH, every 5 cycles
Q-HP	CIP	50	1ml Hi Trap	*Equilibration*: 20 mM Tris, 60 mM NaCl *Blank load*: 20 mM Tris, 60 mM NaCl *Wash*: 50mM Tris, 1M NaCl *Elution*: 20 mM Tris, 300mM NaCl, *CIP/regeneration*: 1N NaOH
Capto Adhere	CIP	50	45ml column (internal diameter 22mm) Bed height 12 cm	Same as table 17

5.2.SEM image analysis

The images obtained show whole bead and surface structures under CIP and aged conditions for the four resins used in this study – MabSelect, MabSelect Xtra, Q-Sepharose High Performance and Capto Adhere post-critical point drying. Qualitative analysis is used to characterise morphological differences observed in whole bead and bead surface images. Structural properties are compared and contrasted between the resins under each condition. The images are also compared to their fresh counterparts (chapter 3 also see figure 38 – summary image). Quantitative analysis is carried out using ImageJ software. Pore count, average pore size, pore size distribution and apparent porosity values are calculated and compared to observations made qualitatively.

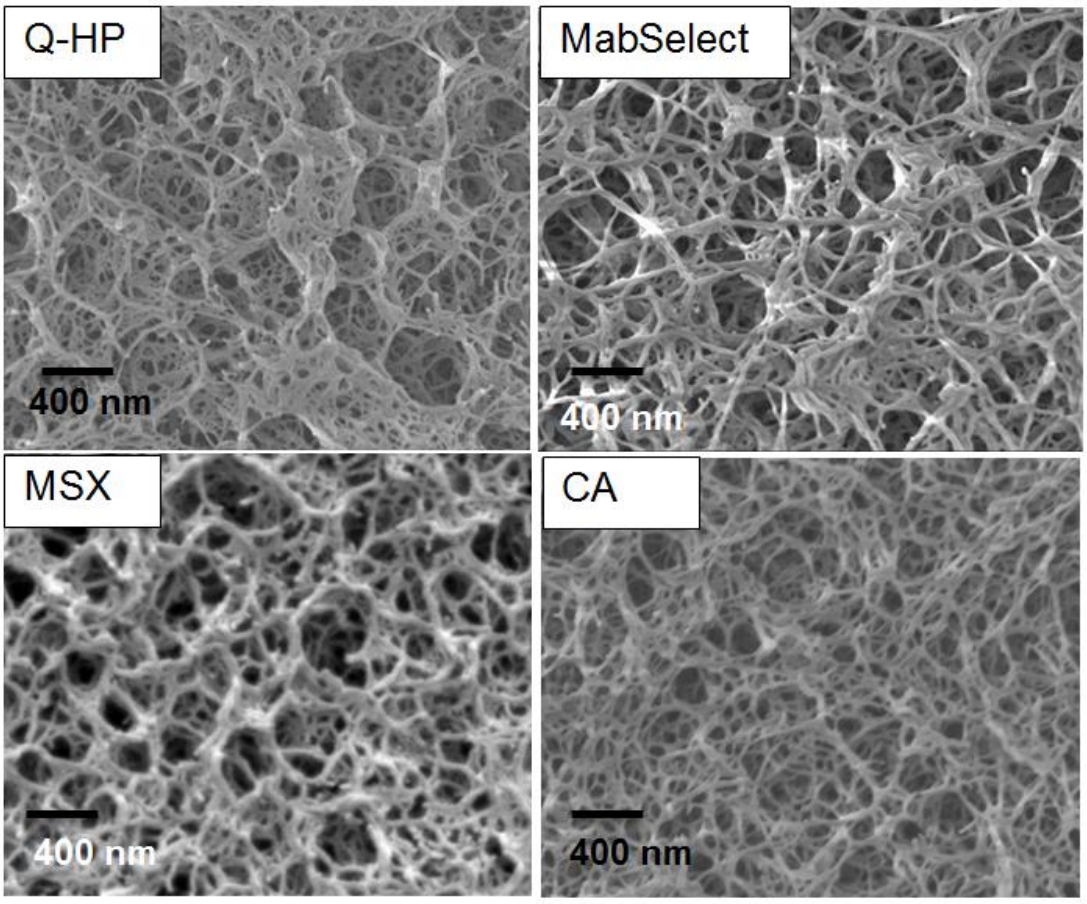

Figure 38 – summary of SEM surface images from chapter 3 of fresh resins for comparative purposes. Q-HP – Q-Sepharose HP, MSX – MabSelect Xtra, CA – Capto Adhere. 1cm = 400nm

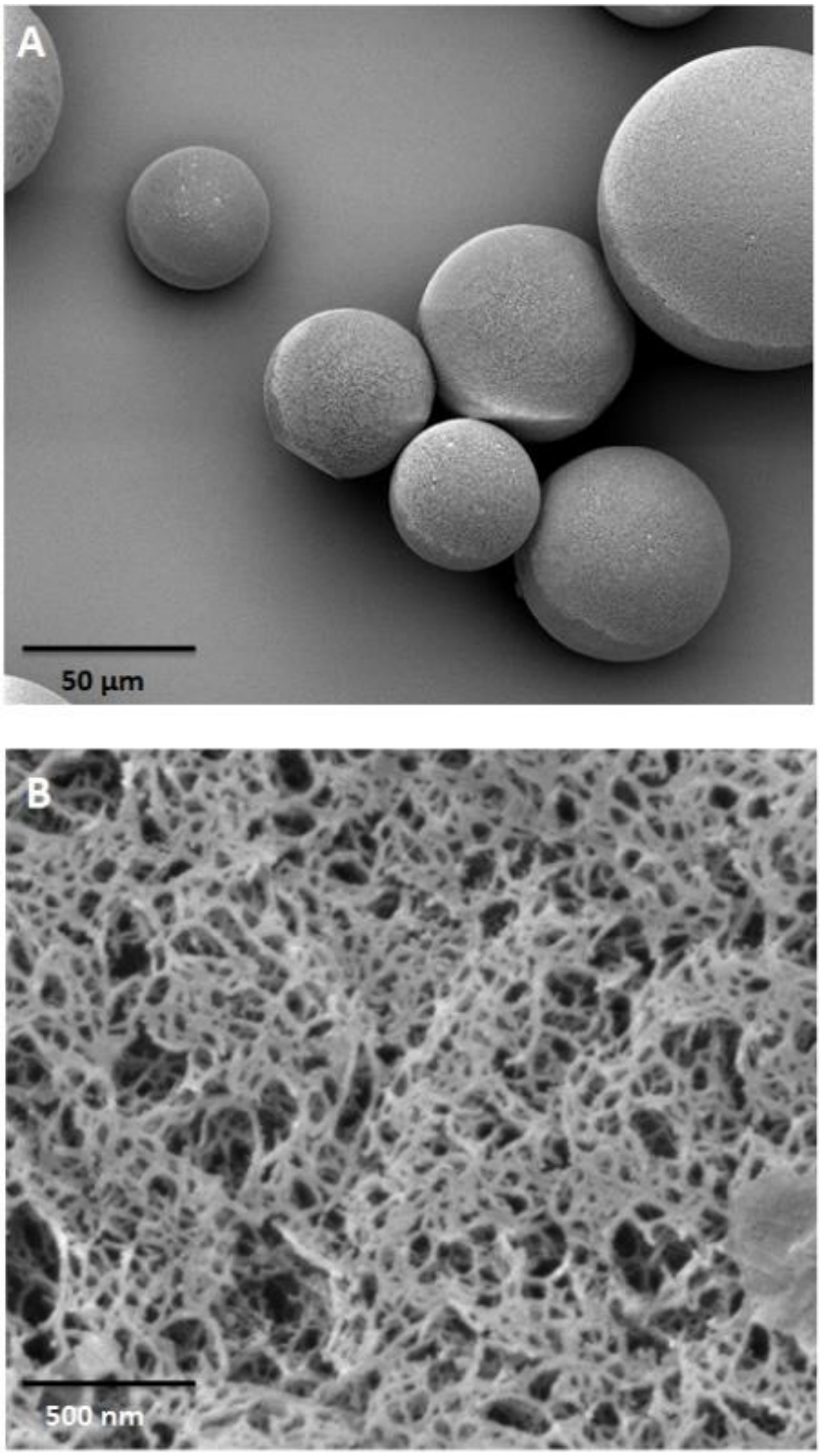

Figure 39 – (A) Scanning electron micrograph showing CIP-exposed MabSelect (0.5M NaOH). Whole bead image 2.0 kV accelerating voltage, x400 magnification, 3 cm = 50 µm. (B) Scanning electron micrograph showing CIP-exposed MabSelect. Bead surface image 5.0 kV accelerating voltage, x40, 000 magnification, 3 cm = 500 nm.

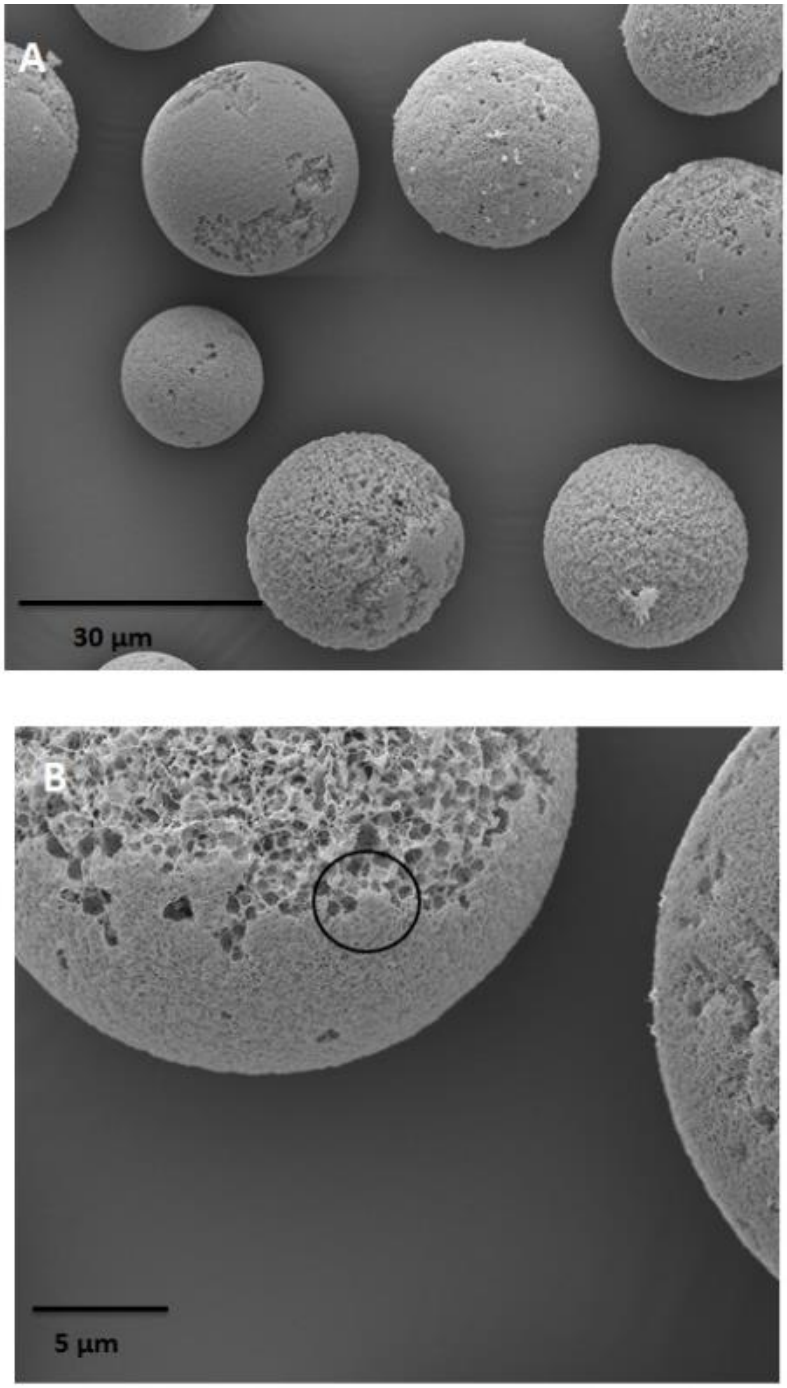

Figure 40 – (A) Scanning electron micrograph showing CIP-exposed MabSelect Xtra (0.5M acetic acid, 0.1M NaOH). Whole bead image 5.0 kV accelerating voltage, x1000 magnification, 4.5 cm = 30 µm. (B) Scanning electron micrograph showing CIP-exposed MabSelect Xtra. Whole bead image close-up 5.0 kV accelerating voltage, x3600 magnification, 2.5 cm = 5 µm. Circled section clearly shows surface distinctions.

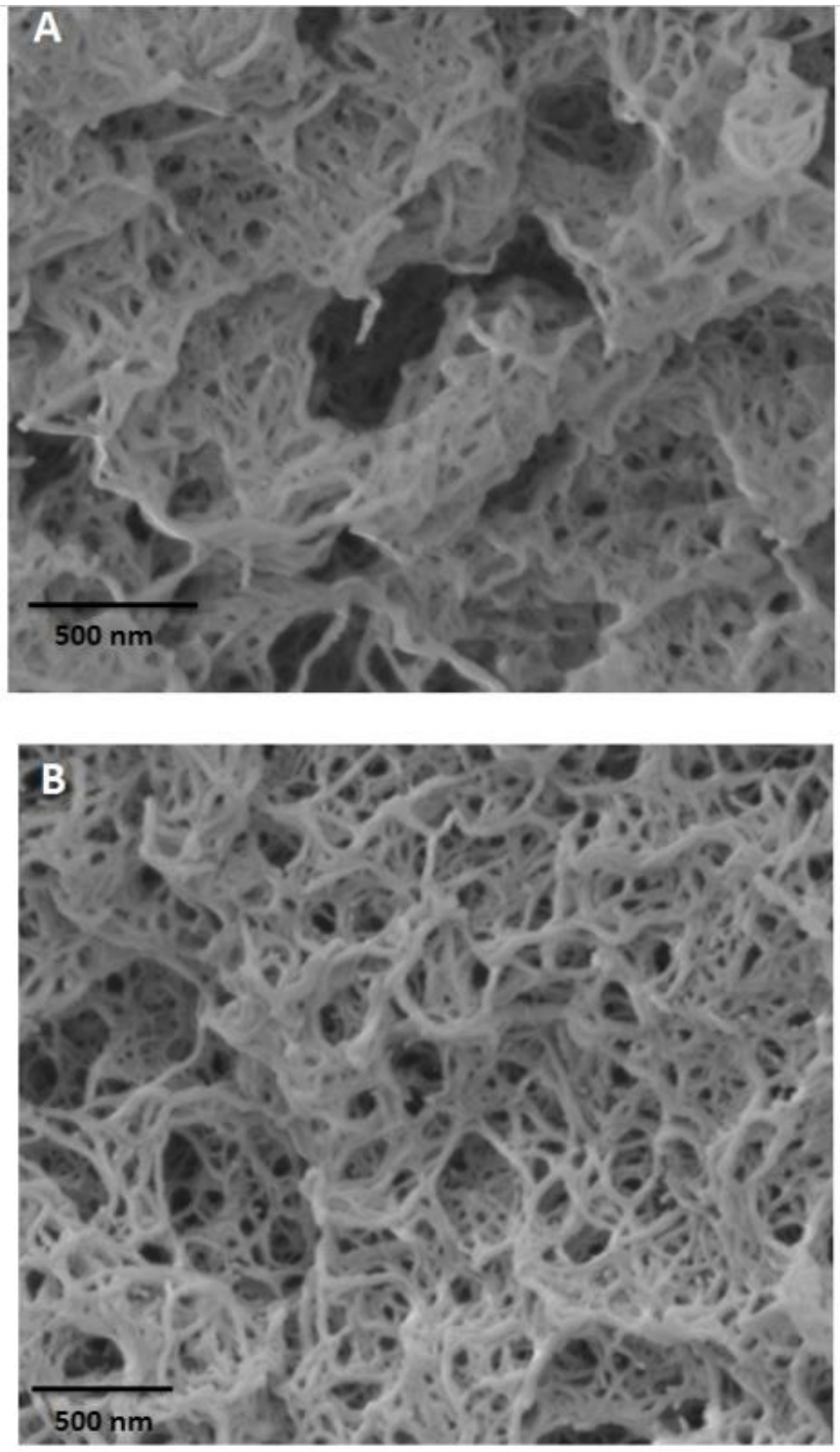

Figure 41 – (A) Scanning electron micrograph showing CIP-exposed MabSelect Xtra (0.5M acetic acid, 0.1M NaOH). 'Inner' bead surface image 5.0 kV accelerating voltage, x40,000 magnification, 3 cm = 500 nm. (B) Scanning electron micrograph showing CIP-exposed MabSelect Xtra. 'Outer' bead surface image 5.0 kV accelerating voltage, x40, 000 magnification, 3 cm = 500 nm.

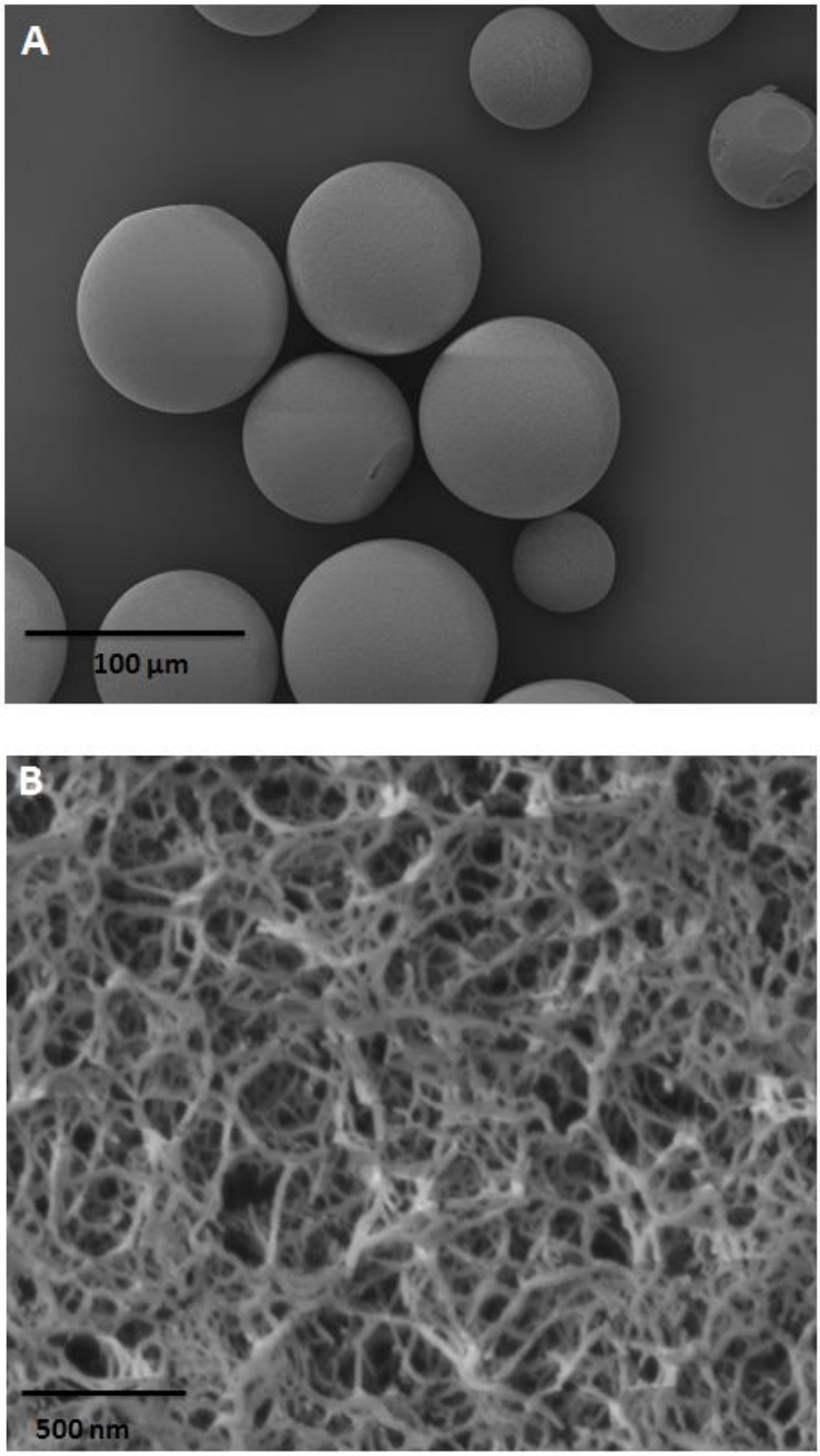

Figure 42 – (A) Scanning electron micrograph showing CIP-exposed Q-HP (1N NaOH). Whole bead image 5.0 kV accelerating voltage, x270 magnification, 4 cm = 100 µm. (B) Scanning electron micrograph showing CIP-exposed Q-HP. Bead surface image 5.0 kV accelerating voltage, x40, 000 magnification, 3 cm = 500 nm.

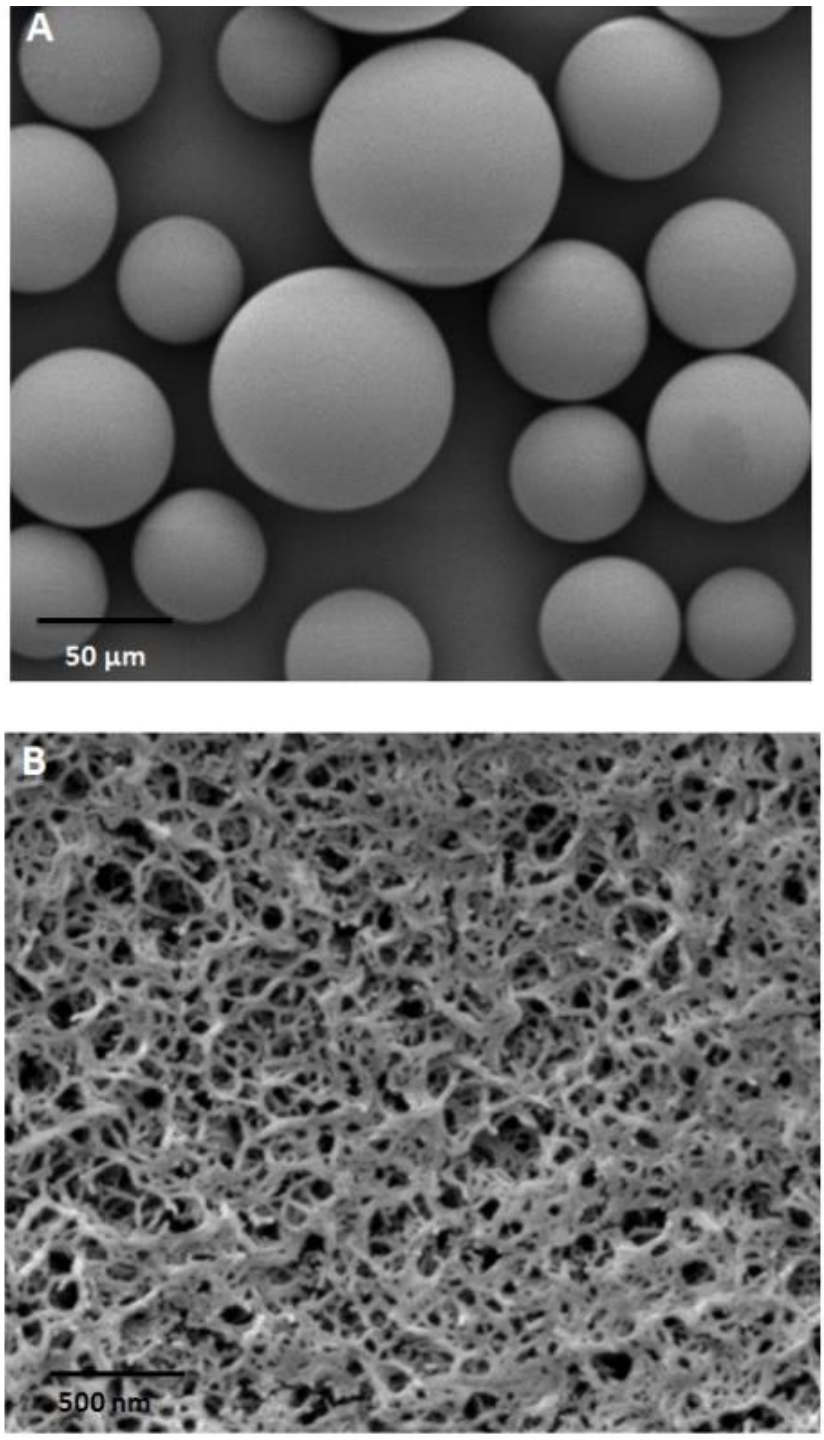

Figure 43 – (A) Scanning electron micrograph showing CIP-exposed Capto Adhere (weak acid, strong base). Whole bead image 5.0 kV accelerating voltage, x330 magnification, 2.5 cm = 50 µm. (B) Scanning electron micrograph showing CIP-exposed Capto Adhere. Bead surface image 5.0 kV accelerating voltage, x33, 000 magnification, 2.5 cm = 500 nm.

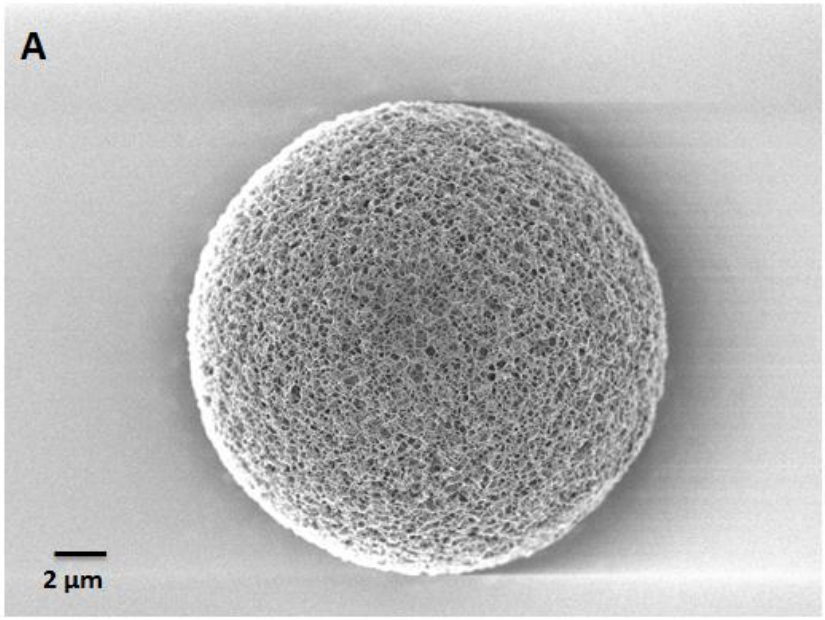

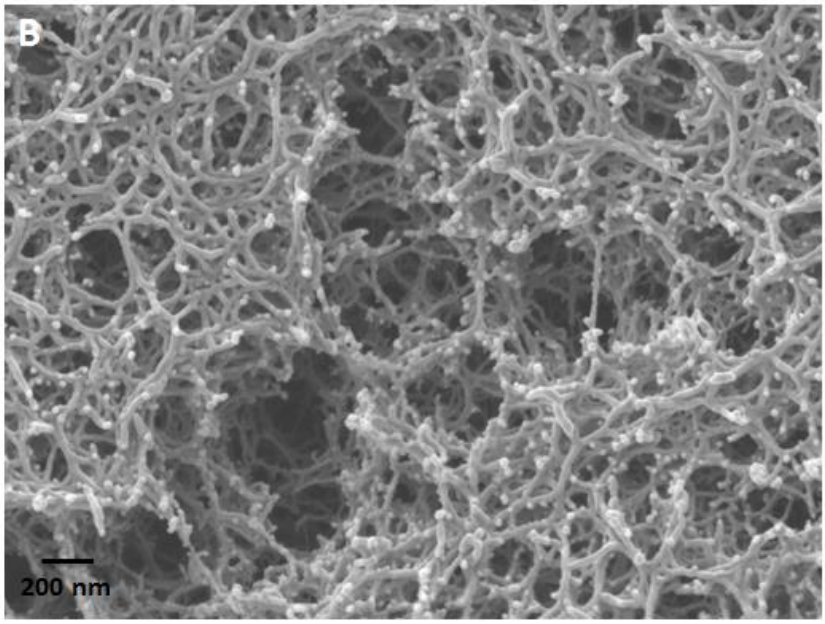

Figure 44– (A) Scanning electron micrograph showing aged MabSelect (17 cycles, IgG4, CHO expression). Whole bead image 2.0 kV accelerating voltage, x3700 magnification, 1 cm = 2 µm. (B) Scanning electron micrograph showing aged MabSelect. Bead surface image 2.0 kV accelerating voltage, x40, 000 magnification, 1 cm = 200 nm.

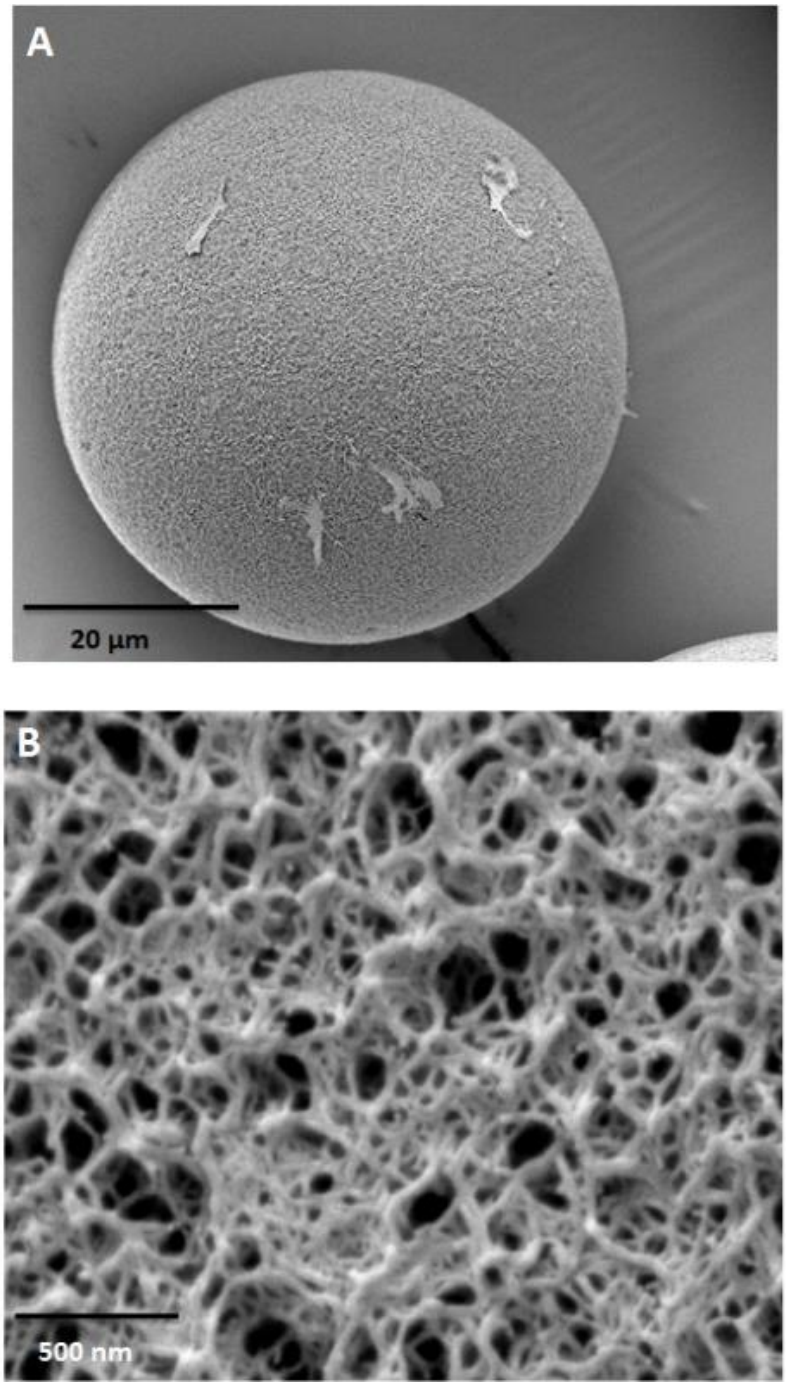

Figure 45 – (A) Scanning electron micrograph showing aged MabSelect Xtra (20 cycles, IgG1). Whole bead image 2.0 kV accelerating voltage, x1000 magnification, 4 cm = 20 µm. (B) Scanning electron micrograph showing aged MabSelect Xtra. Bead surface image 2.0 kV accelerating voltage, x40, 000 magnification, 3 cm = 500 nm.

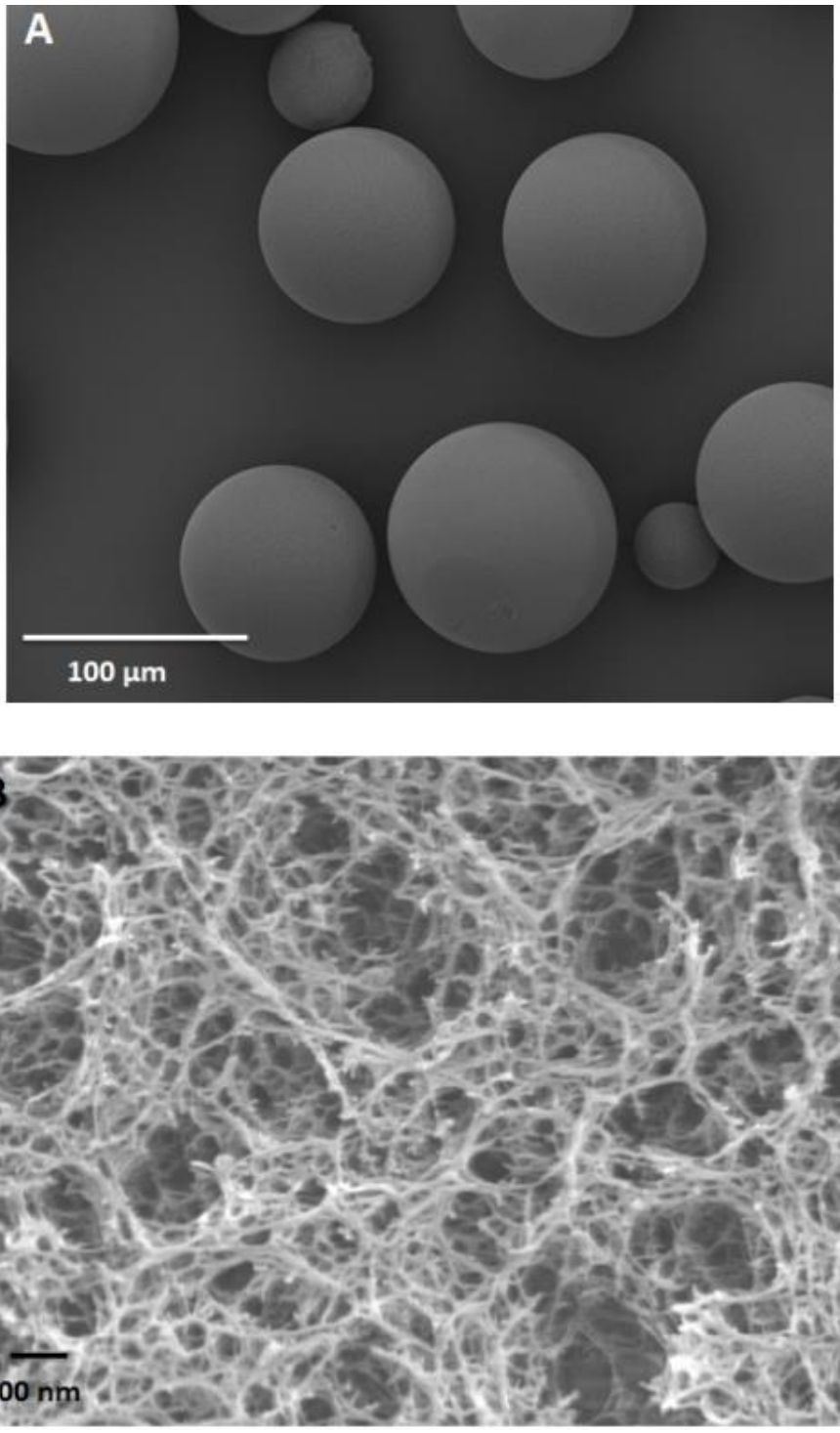

Figure 46 – (A) Scanning electron micrograph showing aged Q-HP (64 cycles, fusion protein, CHO expression). Whole bead image 5.0 kV accelerating voltage, x270 magnification, 4 cm = 100 µm. (B) Scanning electron micrograph showing aged Q-HP. Bead surface image 2.0 kV accelerating voltage, x40, 000 magnification, 1 cm = 200 nm.

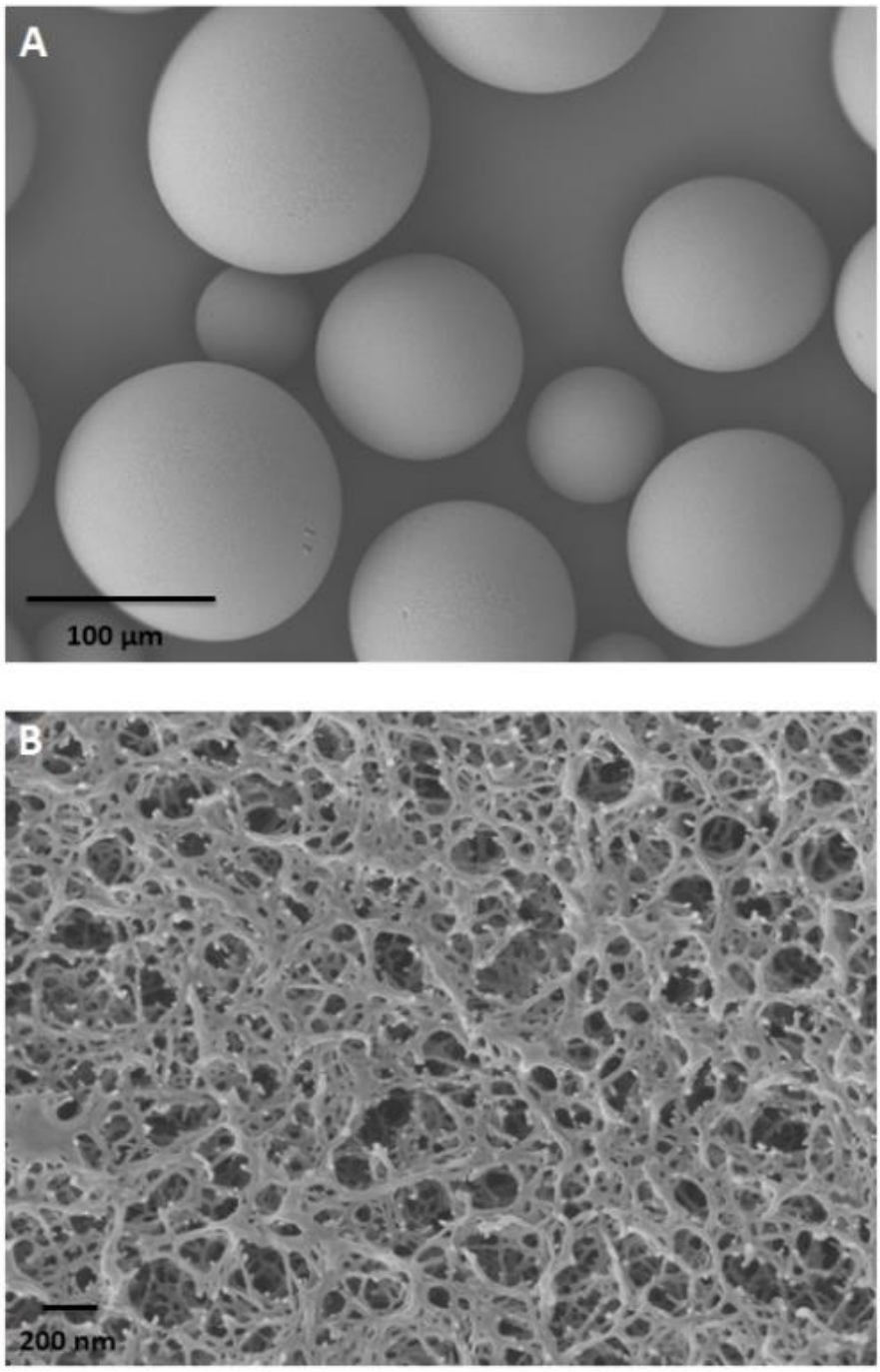

Figure 47– (A) Scanning electron micrograph showing aged Capto Adhere (17 cycles IgG4 CHO expression). Whole bead image 3.0 kV accelerating voltage, x270 magnification, 3.5 cm = 100 µm. (B) Scanning electron micrograph showing aged Capto Adhere. Bead surface image 2.0 kV accelerating voltage, x40, 000 magnification, 1 cm = 200 nm.

5.2.1. Qualitative analysis

The aim of this section is to describe the changes to the bead ultrastructural properties under CIP and aged conditions and compare any changes to their fresh counterparts. From this, the significance of these structural changes is discussed. Figures 39-43 are SEM micrographs of MabSelect, MabSelect Xtra, Q-Sepharose HP and Capto Adhere post-exposure to CIP conditions and figures 44-47 are micrographs of the same resins post-exposure to aged conditions. All resins underwent the same drying process – critical point drying – as outlined in materials & methods and chapter 3. Figures 39(A), 40(A) and 42(A)-47(A) show whole bead images whilst figures 39(B), 41 and 42(B)-47(B) show bead surface images. 3 images of each state were taken (see appendix).

5.2.1.1.CIP-exposed resins

Figure 39(A) shows a randomly selected collection of MabSelect beads post-CIP. 3 cm of the micrograph represents 500µm of the sample. The image shows that most of the beads are consistently spherical, with a wide particle size distribution (approx. 30-60µm) consistent with the range of sizes specified on GE Healthcare's product data sheet for this resin. However 2 of the beads on display appear to have flat surfaces, something which was not observed with fresh MabSelect. The reason for this could be as a result of beads sticking to each other in the column under flow conditions. Figure 39(B) is a bead surface image of MabSelect after exposure to CIP conditions. 3 cm of the micrograph represents 500nm of the sample surface. When compared to its fresh counterpart (figure 38) the pores appear more occluded and the fibres appear to be thicker, indicating a reduction in apparent porosity. Because of this, the pores also appear to be smaller on average and the pore size distribution appears to be narrower. The contrast between the fresh and CIP-exposed MabSelect resins is apparent. The exposure to CIP conditions appears to have significantly altered the surface ultrastructure. This could have occurred due to chemical interactions between the matrix fibres and the sodium hydroxide and build-up and depositing of salts and caustic reagents on the surface of the bead, causing an apparent increase in fibrosity (see section 5.2.1.3).

Figure 40(A) shows a randomly selected collection of MabSelect Xtra beads post-CIP. 4.5 cm of the micrograph represents 30µm of the sample. The figure shows the average particle size to be much smaller than MabSelect (figure 39(A)), as specified by the manufacturer GE Healthcare. This was observed in all images obtained for the 2 resins. Figure 40(A) also shows the beads to be uniformly spherical. However, the image reveals distinct differences between what appears to be an 'outer' surface structure and an 'inner' surface structure. The reason for this could be that prolonged exposure to CIP conditions may have caused erosion of the outer layer, exposing the inner layer and creating resin fines, which can also be observed in figure 40(A) (see section 5.2.1.3). Figure 40(B) shows a close up of this phenomenon, circling the abrupt change in surface characteristics shown in figure 40. Figures 41(A) and 41(B) show the 'inner' and 'outer' surface of the bead respectively. The vast majority of the pores shown on the 'inner' surface appear to be more occluded than that of the outer surface and the structure appears more fibrous, however, there are also large pores located randomly in the surface structure. The pores and distribution of pores shown on the 'outer' surface appear to be more homogeneous. Both the 'outer' and 'inner' surface structures differ greatly compared to their fresh counterpart, which indicates that exposure to CIP conditions (0.5M acetic acid, 0.1M NaOH) creates significant changes in the ultrastructural properties of MabSelect Xtra resins.

Figure 42(A) shows a randomly selected collection of Q-HP beads post-CIP. 4 cm of the micrograph represents 100µm of the sample. The figure shows the beads to be mostly spherical in shape however, as was seen in figure 39(A), there are a number of beads with flat surfaces. Again, this could be associated with beads adhering to each other. Figure 42(B) shows the bead surface. 3 cm of the micrograph represents 500nm of the sample surface. Compared to its fresh counterpart (figure 38) the pores appear more homogeneous in size and distribution, however the fibrosity appears reduced. This could be because exposure to CIP conditions (1N NaOH) may have caused a thinning of the fibres. Surprisingly however, the effects of CIP exposure on Q-HP do not appear to be as significant as what has been observed in MabSelect (0.5M NaOH) and MabSelect Xtra (0.1M NaOH), despite that it had been exposed to much higher concentrations of sodium hydroxide (see section 5.3.1).

Figure 43(A) shows a randomly selected collection of Capto Adhere beads post-CIP. 2.5 cm of the micrograph represent 50µm of the sample. The beads appear to be homogeneously spherical, with a similar particle size and distribution as their fresh counterpart (chapter 3). Figure 43(B) shows the bead surface (2.5 cm = 500nm). The surface shows more occlusion of the pores compared to its fresh counterpart (figure 38). Many pores appear smaller and the matrix appears to be thicker. Similar to observations in figure 39(B), this could be due to chemical interactions of CIP reagents with the bead surface and chemical or biological depositions on the matrix, causing the fibres to appear to be thicker; indicating that exposure to CIP conditions creates significant changes in the surface properties of Capto Adhere resins.

5.2.1.2.Aged resins

Figure 44(A) shows a whole bead image of aged MabSelect after 17 cycles of exposure to the conditions highlighted in table 17. In this image, uniform sphericity is observed. A further observation is that, despite the relatively low magnification (x3700), the ultrastructure of the bead surface is still apparent, allowing for early stage topological characterisation of the sample surface. From this magnification, the bead surface structure appears to be more porous compared to its CIP-exposed and fresh counterparts. This can be seen in more detail in figure 44(B). The image shows gaping holes in the ultrastructure and a greater discontinuity of fibres, indicating damage to the matrix. This could have resulted due to the combined interaction of process feed material and CIP reagents with the matrix. Repeated exposure may have caused degradation of the fibres over time, resulting in large disparities in pore size and an increase in apparent porosity. The results show that the ultrastructure of MabSelect exposed to CIP conditions differ from the effects seen after the aging process.

Figure 45(A) shows a whole bead image of aged MabSelect Xtra after 20 cycles of exposure to the conditions in table 17. The image shows a uniformly spherical bead, which was observed for all images obtained for this sample. There also appears to be deposits on the surface of the bead, occluding the ultrastructure. These deposits may contribute to the increase in back pressure observed by the second company, as they inhibit the flow of process media through the column, causing blockages resulting in build-up of back pressure, however mechanical testing may further corroborate this (section 5.3.). Figure 45(B) shows the bead surface image of aged MabSelect Xtra (3 cm = 500nm). This image displays distinct surface characteristics compared to figure 41 (CIP counterpart). However, there are ultrastructural similarities between this figure and its fresh counterpart figure 38. The matrix structure in both images are similar, however the more pores appear to be occluded in figure 45(B) compared to fresh resin, which may be as a result of matrix interaction with process feed material and chemical reagents in CIP buffers.

Figure 46(A) shows a whole bead image of aged Q-HP after 64 cycles of exposure to the conditions in table 17. The vast majority of the beads are uniformly spherical,

with a relatively wide particle size distribution. Figure 46(B) shows a bead surface image of aged Q-HP (1 cm = 200nm). Similar to aged MabSelect, the mechanism of aging appears to be associated with the breakdown of the matrix structure. More discontinuous fibres can be observed and as a result, large pores and reduced fibrosity compared to its fresh and CIP-exposed counterparts. As with MabSelect, this could be due to repeated exposure causing degradation of the fibres over time. Overall, results do indicate surface structure differences between fresh, CIP-exposed and aged Q-HP resins.

Figure 47(A) shows a whole bead image of aged Capto Adhere after 17 cycles of exposure to the conditions in table 17. There is a difference in bead morphology compared to its fresh and CIP-exposed counterparts, appearing more oval in shape. This could be due to a number of possible reasons associated with in-process conditions such as high flow rates, packing procedures and column properties. Another possible reason for the change in morphology could be unforeseen effects of the critical point drying process on aged Capto Adhere resin. The critical point drying procedure used in this study has not previously contributed to any observed morphological changes to the beads, however, investigations to further optimise the CPD process could be carried out to definitively determine its impact on bead morphology. Figure 47(B) shows the bead surface of aged Capto Adhere (1 cm = 200 nm). The bead surface shows similar characteristics to what was observed in the CIP-exposed image for this resin (figure 43(B)). However, the pores appear to be even more occluded and there are more occurrences of gel-like depositions on the matrix structure, resulting in a reduction in apparent porosity. The mechanism of aging appears to be associated with the adherence of process feed material to the fibres and the chemical interaction of CIP reagents with the matrix, all contributing to a build-up of depositions on the bead surface. The results have shown surface structure differences between fresh, CIP-exposed and aged Capto Adhere resins.

5.2.1.3.Qualitative analysis – discussion

The four resins used in this study have all shown vast ultrastructural differences under fresh, CIP-exposed and aged conditions. The greatest structural differences were observed for 2 resins, MabSelect Xtra under CIP conditions and Capto Adhere

under aged conditions. Micrographs for MSX showed that exposure to the CIP conditions in table 17, resulted in the formation of two surface layers with distinct properties and the creation of resin fines. Aged MSX, however, appeared to age via pore occlusion (fouling), suggesting that the interaction of CIP reagents, protein and feed material can change the mechanism of aging. Similar studies corroborate this and also report that the mechanism of aging of protein A resin is associated with fouling and the adhesion of product/feed material to bead fibres (Jiang *et al.*, 2009; Zhang, Daniels, *et al.*, 2015; Zhang, Xu, *et al.*, 2015; Lintern *et al.*, 2016; Pathak and Rathore, 2016). Resins used post-capture, such as ion exchange resins and multimodal resins have also been reported to age similarly to protein A resins, which was observed in micrographs for Capto Adhere (figure 47 (A)) (Siu and Boushaba, 2006; Siu *et al.*, 2006, 2007; Jin *et al.*, 2009). However, CIP results for Capto Adhere (figure 43(A)) indicate that chemical deposits from CIP conditions contribute more greatly to the fouling mechanism by which Capto Adhere appears to age, as opposed to biological deposits, as has been reported with protein A resins. In this case, this could be because CA is a latter-stage purification step and is therefore exposed to smaller quantities of biological material but stronger CIP conditions than the preceding protein A step.

Contrastingly, MabSelect and Q-HP displayed similar mechanisms of aging, not widely reported in literature for both media types. Both resins showed a breakdown of matrix fibres and consequently larger pores. There have been a number of studies on the stability of matrices under strong CIP conditions (Tengliden, 2008; Grönberg *et al.*, 2011). Whilst many studies indicate high levels of matrix stability under varying CIP and sanitization conditions, a number of studies indicate structural changes to resins as a result of repeated exposure to high concentrations of NaOH combined with process feed material, such as the conditions reported in this study for Q-Sepharose High Performance (1N NaOH) (Carter-Franklin *et al.*, 2007; Thillaivinayagalingam *et al.*, 2007; Zhang, Xu, *et al.*, 2015). As MabSelect was exposed to relatively mild CIP conditions, its mechanism of aging was unexpected. However, it is important to note that other factors, such as physical stresses of process conditions e.g. flow rate or mobile phase viscosity can contribute towards a decline in aging Further consideration include the fact that different expression systems (e.g. mammalian vs microbial) will result in the expression of different

foulants and may therefore impact the aging process. However mechanical/structural characterization studies will need to be carried out to determine any differences.

5.2.2. Quantitative analysis - results

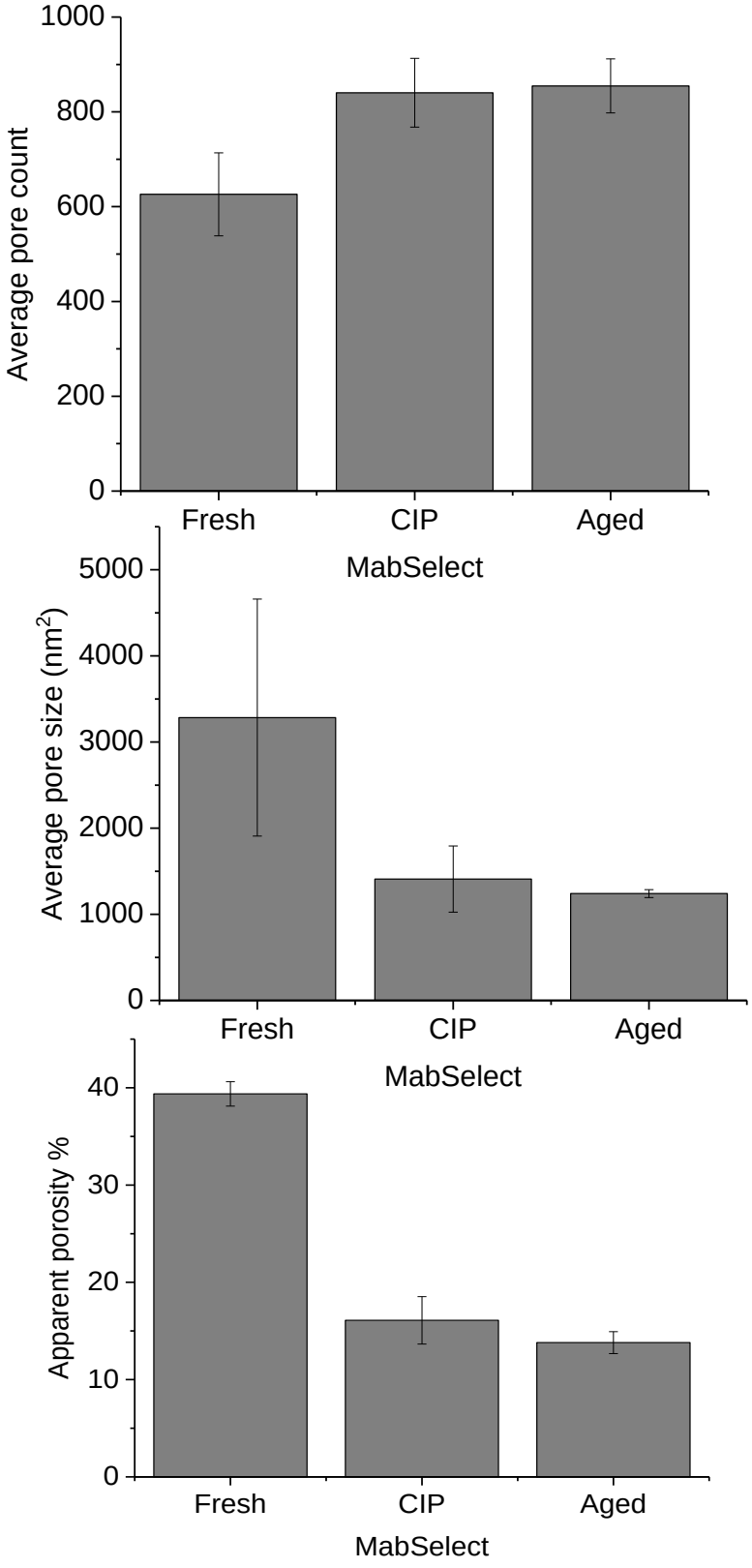

Figure 48 – Column graphs showing surface properties of MabSelect under fresh, CIP-exposed and aged conditions. The averages for 3 images were plotted with their standard deviations. (a) Column graph showing average pore count. (b) Column graph showing average pore size in nm^2. (c) Column graph showing average apparent porosity in %.

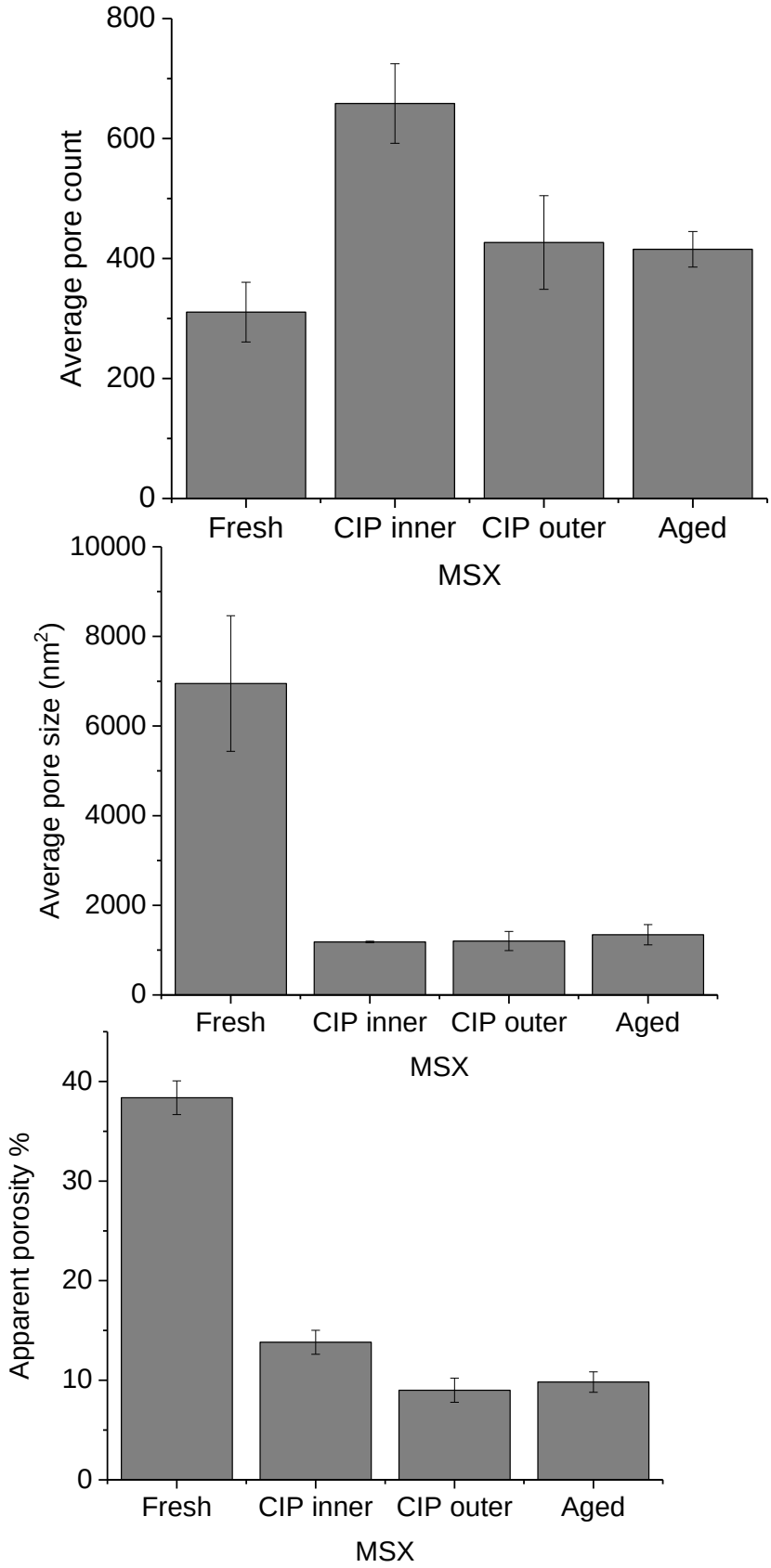

Figure 49 – Column graphs showing surface properties of MabSelect Xtra under fresh, CIP-exposed and aged conditions. The averages for 3 images were plotted with their standard deviations. (a) Column graph showing average pore count. (b) Column graph showing average pore size in nm^2. (c) Column graph showing average apparent porosity in %.

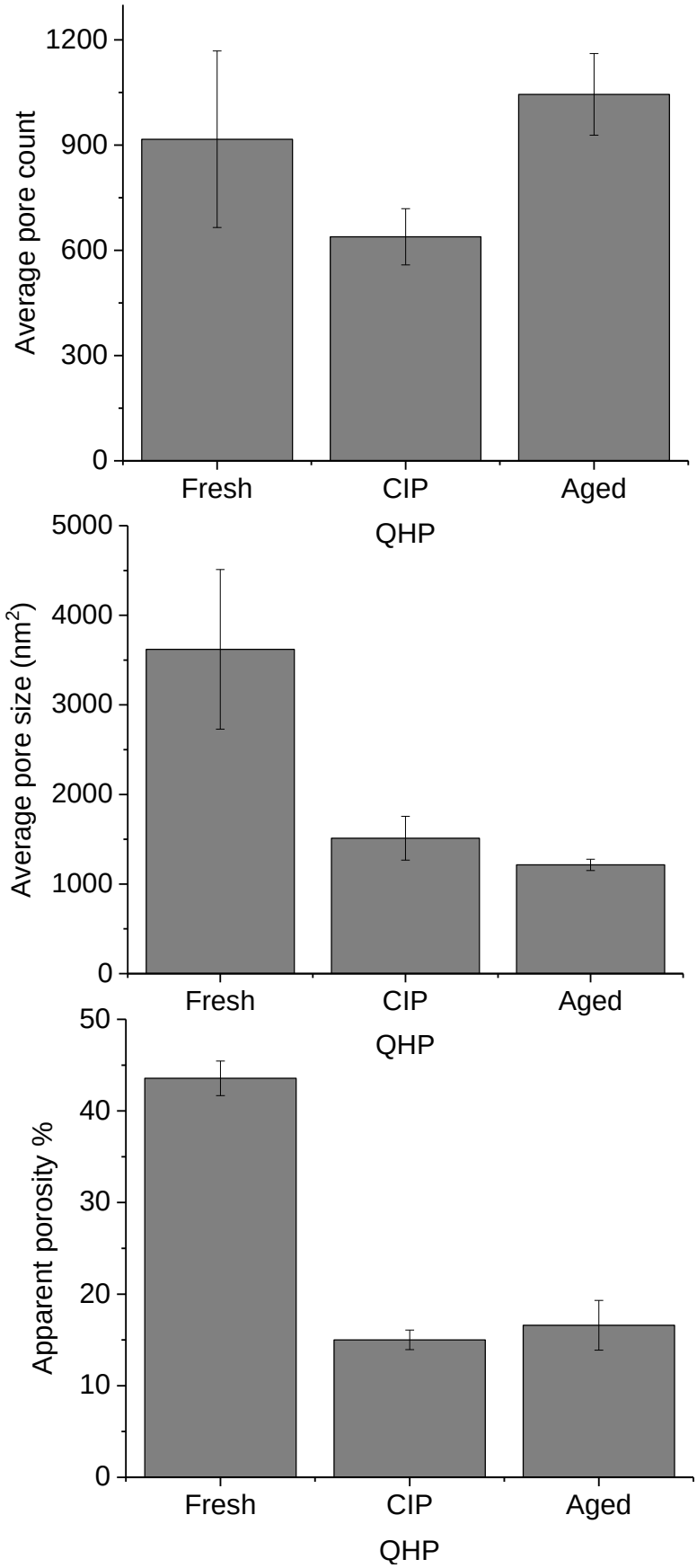

Figure 50 – Column graphs showing surface properties of Q-HP under fresh, CIP-exposed and aged conditions. The averages for 3 images were plotted with their standard deviations. (a) Column graph showing average pore count. (b) Column graph showing average pore size in nm^2. (c) Column graph showing average apparent porosity in %.

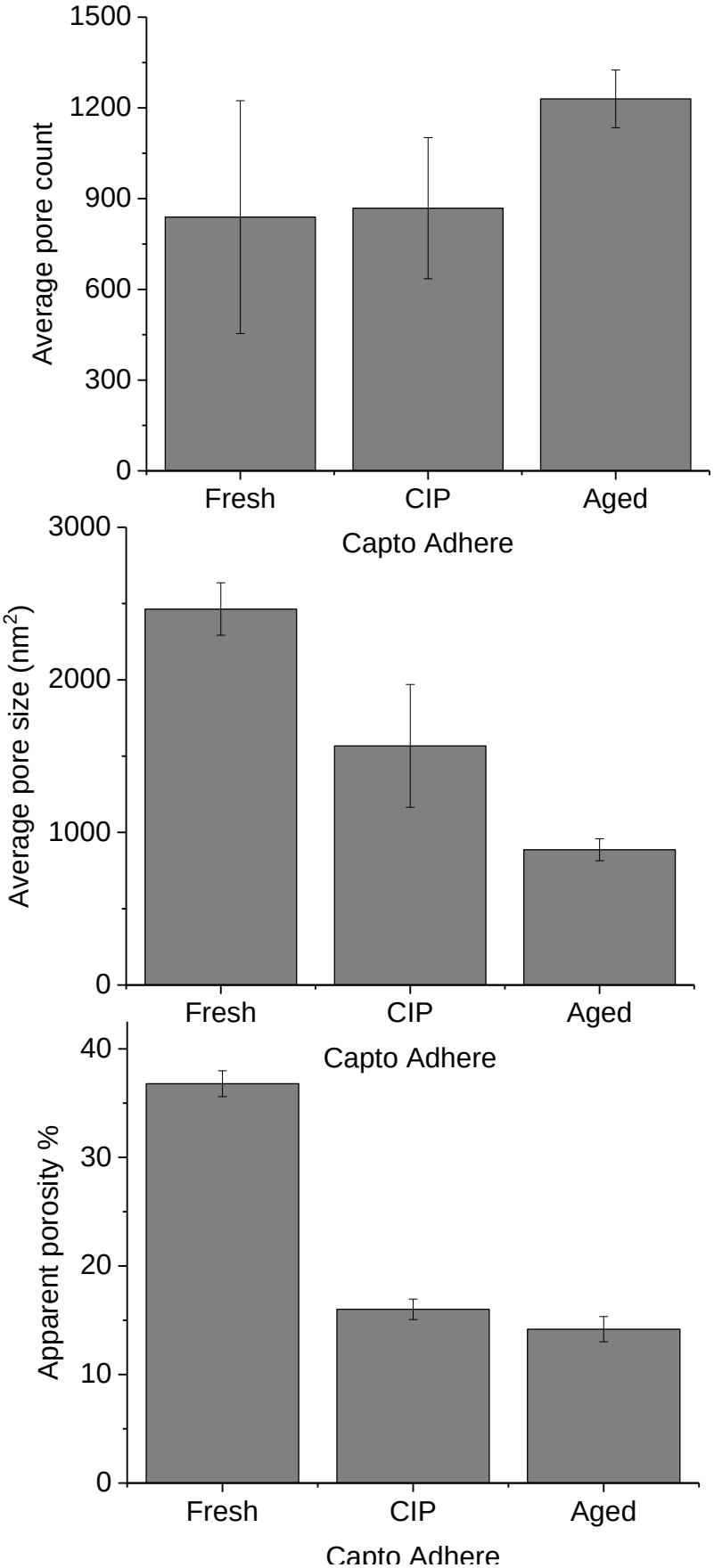

Figure 51– Column graphs showing surface properties of Capto Adhere under fresh, CIP-exposed and aged conditions. The averages for 3 images were plotted with their standard deviations. (a) Column graph showing average pore count. (b) Column graph showing average pore size in nm^2. (c) Column graph showing average apparent porosity in %.

Table 19 Pore size distributions of CIP –exposed resins up to 100000nm^2 (≈d360nm based on area of a circle πr^2.) On average, 99% of all pores within 100000nm^2 are ≤10000nm^2 (≈d100nm).

	Resin Frequency				
Pore size range (nm^2)	**CA**	**MS**	**MSX$_{inner}$**	**MSX$_{outer}$**	**QHP**
≤10000	857.3̇	830	655.6̇	419.3̇	634.3̇
10001-20000	10.3̇	8	2	5.3̇	3.6̇
20001-30000	0.6̇	1.6̇	0.3̇	2	0.6̇
30001-40000	0	0.6̇	0.3̇	0	0.3̇
40001- 100000	0	0	0	0	0
Total	***868.3***	***840.3***	***658.3***	***426.6***	***639***
%≤10000	***99%***	***99%***	***99%***	***98%***	***99%***

Table 20 Pore size distributions of CIP-exposed resins up to 10000nm^2 (≈d100nm based on area of a circle πr^2.) On average, over 70 % of all pores within 10000nm^2 are ≤1000nm^2 (≈d36nm).

	Resin Frequency				
Pore size range (nm^2)	**CA**	**MS**	**MSX$_{inner}$**	**MSX$_{outer}$**	**QHP**
≤1000	574	593.6̇	468	358	462.3̇
1001-2000	142	122.6̇	112.6̇	35	77.3̇
2001-3000	68	48.3̇	31	5.6̇	39.6̇
3001-4000	28.3̇	24.6̇	19.6̇	8	18.6̇
4001-5000	20.6̇	14.3̇	9	4.3̇	11.3̇
5001-6000	4	6	7.6̇	2.6̇	9.3̇
6001-7000	2.6̇	7.3̇	3.6̇	1.6̇	4.3̇
7001-8000	5.6̇	6.3̇	2	0.6̇	6.6̇
8001-9000	5.3̇	4.3̇	1.3̇	3	2.6̇
9001-10000	2.6̇	2.6̇	0.6̇	0.3̇	2
Total	***853.3̇***	***830***	***655.6̇***	***419.3̇***	***634.3̇***
%≤1000	***67%***	***72%***	***71%***	***85%***	***73%***

Table 21 Pore size distributions of CIP-exposed resins up to 1000nm^2 (≈d36nm based on area of a circle πr^2.) On average, about 80% of all pores within 1000nm^2 are ≤100nm^2 (≈d10nm). Note: pores smaller than approx. 7nm were not detected by the ImageJ software.

	Resin Frequency				
Pore size range (nm^2)	**CA**	**MS**	**MSX$_{inner}$**	**MSX$_{outer}$**	**QHP**
≤100	421.3	459	337	331	366
101-500	0	0	0	0	0
501-600	86	72	0	0	0
601-700	0	0	131	0	0
701-800	0	0	0	0	0
801-900	66.6	0	0	0	96
901-1000	0	62	0	72	0
%≤100	***73%***	***77%***	***72%***	***92%***	***79%***

Table 22 - Pore size distributions of aged resins up to 100000nm^2 (≈d360nm based on area of a circle πr^2.) On average, 99% of all pores within 100000nm^2 are ≤10000nm^2 (≈d100nm).

	Resin Frequency			
Pore size range (nm^2)	**CA**	**MS**	**MSX**	**QHP**
≤10000	1227.6̇	846.6̇	414.3̇	1030.3̇
10001-20000	1.6̇	3.6̇	1	10.3̇
20001-30000	0.3̇	1.6̇	0	2.3̇
30001-40000	0	0.6̇	0	1.3̇
40001-50000	0	1	0	0.3̇
50001-60000	0	0	0	0
60001-70000	0	0.3̇	0	0
70001-80000	0	0.3̇	0	0
80001-100000	0	0	0	0
100000+	0	0.3̇	0	0
Total	***1229.6***	***854.6***	***415.3***	***1044.6***
%≤10000	***99%***	***99%***	***99%***	***99%***

Table 23 Pore size distributions of aged resins up to 10000nm^2 (≈d100nm based on area of a circle πr^2.) On average, over 75 % of all pores within 10000nm^2 are ≤1000nm^2 (≈d36nm).

	Resin Frequency			
Pore size range (nm^2)	**CA**	**MS**	**MSX**	**QHP**
≤1000	995.3̇	685.3̇	255.6̇	838.6̇
1001-2000	133	97.3̇	103	92.3̇
2001-3000	48.6̇	23	25.3̇	39
3001-4000	19.6̇	23.6̇	15.3̇	24
4001-5000	14.3̇	2.6̇	5	11
5001-6000	8	8.6̇	3.3̇	10
6001-7000	4	1	3	6
7001-8000	3.3̇	2.6̇	1.6̇	4
8001-9000	1	0	0.6̇	2.6̇
9001-10000	0.3̇	2.3̇	1.3̇	2.6̇
Total	***1227.6̇***	***846.6̇***	***414.3̇***	***1030.3̇***
%≤1000	***81%***	***81%***	***62%***	***81%***

Table 24 Pore size distributions of CIP-exposed resins up to 1000nm^2 (≈d36nm based on area of a circle πr^2.) On average, over 75% of all pores within 1000nm^2 are ≤100nm^2 (≈d10nm). Note: pores smaller than approx. 7nm were not detected by the ImageJ software.

	Resin Frequency			
Pore size range (nm^2)	**CA**	**MS**	**MSX**	**QHP**
≤100	473	685.3	175	721
101-300	0	0	0	0
301-400	113	0	0	0
401-500	278	0	0	0
501-600	0	0	41	0
601-700	0	0	40	0
701-800	47	0	0	0
801-900	44	0	0	61
901-1000	41	0	0	57
%≤100	***48%***	***100%***	***68%***	***86%***

5.2.3. Quantitative analysis - discussion

The purpose of this section is to determine whether the quantitative results obtained corroborate qualitative analysis findings in section 5.2.1. If this is the case, the obtained values can be used to characterise the ultrastructure of the studied resins. However, inconsistencies in quantitative results would suggest the values may not be true indicators of the structural properties. Figures 48-51 and tables 19-24 show pore count, average pore size, apparent porosity and pore size distributions for MabSelect, MabSelect Xtra, Q-Sepharose High Performance and Capto Adhere under CIP-exposed and aged conditions. 3 images of each resin under each condition were quantitatively analysed using ImageJ software and average values are plotted with their standard deviations.

5.2.3.1.MabSelect

Figure 48 (a-c) shows average pore count, average pore size (nm^2) and apparent porosity (%) information respectively for fresh, CIP-exposed and aged MabSelect resin. All 3 graphs show that the values obtained for CIP-exposed and aged conditions are quasi-identical. Figure 48(a) shows that the average pore count of CIP-exposed is higher (840) than its fresh counterpart (626). Figure 39(b) corroborates this, as there appears to be more pores on the surface of CIP-exposed MabSelect resin compared to its fresh counterpart. The same trends are observed in figures 48(b) and 48(c). Average pore size and apparent porosity is lower in CIP-exposed MabSelect compared to fresh resin. Qualitative analysis showed that aged MabSelect (figure 44(b)) had a higher number of discontinuous fibres, creating larger pores and as a result, what would likely be a fewer number of surface pores, a larger average pore size and higher apparent porosity compared to its fresh and CIP-exposed counterparts. However, the opposite is observed in figures 48 a, b and c. This could be as a result of manual thresholding during ImageJ software analysis. SEM images showed that aged MabSelect images had the least surface homogeneity, i.e. a higher amount of surface protrusions compared to fresh and aged images, which meant that differentiating between the top surface and subsurface pores during thresholding was more challenging. As a result, the values calculated by the software for each property were not in agreement with what could be observed qualitatively.

Tables 19-21 and 22-24 show pore size distributions for CIP-exposed and aged MabSelect resin respectively. Under both conditions, at least 99% of the pores are less than 10000nm^2 (which is ~100nm in diameter, based on the area of a circle.) Both CIP-exposed and aged MabSelect data show similar distributions, however, there are fewer pores between 5000-10000nm^2 under aged conditions. This corroborates figure 48(b) which shows aged MabSelect to have the lowest average pore size. However this is contradictory to what can be observed in the SEM micrograph - figure 44(b). As previously mentioned, this could be as a result of thresholding due to high surface heterogeneity.

5.2.3.2.MabSelect Xtra

Figure 49 shows average pore count, average pore size (nm^2) and apparent porosity (%) information respectively for fresh, CIP-exposed and aged MabSelect Xtra resin. The figures also compare the properties of the 'inner' and 'outer' surfaces of MabSelect Xtra post-CIP-exposed conditions and show distinct characteristics between fresh resin and processed resin. Figure 49(a) provides average pore count information. It shows that fresh resin has far fewer pores (310) compared to its processed counterparts. The 'inner' surface (CIP-exposed) has the highest pore count (658) whilst the 'outer' CIP-exposed surface and aged resin surface have a similar number of pores (427 and 415 respectively). This is not necessarily apparent at first glance of the SEM images (figures 41 and 45(b)) however, upon close observation, figure 41(a) (CIP-exposed, 'inner' surface) is made up of a large number of very small pores and randomly dispersed bigger ones, whilst CIP-exposed 'outer' surface image (figure 41(b)) and aged MabSelect Xtra (figure 45(b)) have more occluded pores. Figures 49(b) and (c) compare the average pore size and apparent porosity of fresh MabSelect Xtra to its processed counterparts. The figures show that both the average pore size and apparent porosity of CIP-exposed and aged MabSelect Xtra is less than half that of fresh resin. This can also be seen in the electron micrographs gathered for each condition.

Tables 19-21 and 22-24 shows pore size distributions for CIP-exposed and aged MabSelect Xtra resin.Under both conditions, at least 98% of the pores are less than 10000nm^2 (which is ~100nm in diameter, based on the area of a circle.) Both CIP-

exposed and aged MabSelect Xtra data show similar distributions percentage-wise, with pores in every bandwidth. This is corroborated by figure 49(b) that shows MabSelect Xtra resin under CIP-exposed and aged conditions with similar average pore sizes.

5.2.3.3.Q-Sepharose High Performance

Figure 50 shows average pore count, average pore size (nm^2) and apparent porosity (%) information respectively for fresh, CIP-exposed and aged Q-Sepharose High Performance resin. Qualitative analysis showed that aged Q-HP (figure 46(b)) had a higher number of discontinuous fibres, creating larger pores and as a result, what would likely be a fewer number of surface pores, a larger average pore size and higher apparent porosity compared to its fresh and CIP-exposed counterparts. However, the opposite is observed in figures 50 a, b and c. Similar to the case of MabSelect, this could be associated with difficulties in manual thresholding in ImageJ due to a highly heterogeneous bead surface. Large differences in average pore size and apparent porosity between fresh and CIP-exposed Q-HP were not apparent when analysed quantitatively. However, figures 50(b) and (c) show CIP-exposed Q-HP resin to have a significantly lower average pore size and apparent porosity compared to fresh Q-HP. Similarly, the pore size distribution information (tables 19-24) show that the pore size distributions of CIP-exposed and aged Q-HP are very similar, although the opposite is observed in their electron micrographs (figures 42(b) and 46(b)).

5.2.3.4.Capto Adhere

Figure 51 shows average pore count, average pore size (nm^2) and apparent porosity (%) information respectively for fresh, CIP-exposed and aged Capto Adhere resin. The average pore count (figure 51(a)) shows aged Capto Adhere to have the highest pore count (1230), whilst fresh and CIP-exposed CA have a similar number of pores (839 and 868 respectively). It should be noted however, that there is large pore count variability, as represented by the standard deviations, indicating that the pore count may not vary greatly under any given condition. However, more images would need to be quantitatively analysed to ascertain this. Figure 51(b) shows that the average

pore size is highest under fresh conditions (2464 nm^2) followed by CIP-exposed conditions (1567 nm^2), whilst aged CA had the lowest average pore size (886 nm^2). Figure 51(c) shows that fresh CA is more than two times more porous than CIP-exposed and aged CA, which show similar apparent porosity levels. These properties can also be observed in the electron micrographs obtained for each condition (figure 43(b) and 47(b)). Under CIP-exposed and aged conditions, the pores appear occluded and as a result, vastly smaller compared to their fresh counterpart. Similarly, the pore size distribution information corroborates average pore size results and qualitative results. Table 19 shows that ~99% of pores are less than 10000nm^2 in size (which is ~100nm in diameter, based on the area of a circle.) Table 23 shows a higher frequency of smaller pores (<1000nm^2) compared to table 20, which supports a smaller average pore size.

The use of the term apparent porosity accounts for the fact that the porosity measurements in this study are based on 2-D images that do not account for the angle at which the micrographs were attained. For this reason, the values obtained in this study for average pore size, apparent porosity and pore size distribution differ from studies that account for the 3-D nature of the pores (Yao and Lenhoff, 2004; Bacskay, Sepsey and Felinger, 2014; Sepsey, Bacskay and Felinger, 2014). However, some studies have made use of 2-D pore information as a general guide (Ioannidis, 2009). The results of this study have shown that while some of the values obtained using quantitative analysis corroborate some of the observed properties in section 5.2.1, overall, the results vary substantially with each resin. However, a trend can be observed based on the values obtained. Table 25 shows a summary table characterising the resins under each condition relative to their fresh counterparts. As the values cannot be directly used, the resins are characterised on the basis of high-mid-low ranging.

Table 25 Summary table characterising the bead surface structure of the 4 resins used in this study – MabSelect, MabSelect Xtra, Q-Sepharose HP and Capto Adhere under 3 conditions – fresh, CIP-exposed and aged. The surfaces are characterised based on 4 properties – pore count, pore size, apparent porosity, pore size distribution. A green box represents relatively high values for the assigned category, yellow represents mid-range values and blue represents low values. The asterisk shows the resin that reported the highest/lowest value for the given property.

Resin	**Condition**	**Pore count**	**Pore size**	**Apparent porosity**	**Pore size distribution**
MabSelect	Fresh	Mid	High	High	High
	CIP-exposed	High	Low	Mid	Mid
	Aged	High	Low	Low	Low*
MabSelect Xtra	Fresh	Low*	High*	High	High*
	CIP-exposed (inner)	Mid	Low	Low	Mid
	CIP-exposed (outer)	Low	Low	Low*	Mid
	Aged	Low	Low	Low	Mid
Q-Sepharose HP	Fresh	High	High	High*	High
	CIP-exposed	Mid	Low	Mid	Mid
	Aged	High	Low	Mid	Mid
Capto Adhere	Fresh	High	Mid	High	Mid
	CIP-exposed	High	Low	Mid	Mid
	Aged	High*	Low*	Low	Mid

5.3.Pressure-flow and DMA characterisation – results

There were a number of structural differences observed between the four resins under fresh, CIP-exposed and aged conditions. Pressure-flow and dynamic mechanical analysis are used to determine whether there are differences in mechanical behaviour of the same studied resins exposed to the aforementioned conditions and to compare the two techniques. The same pressure-flow and DMA techniques as described in chapter 4 are used in this study. The results are presented below.

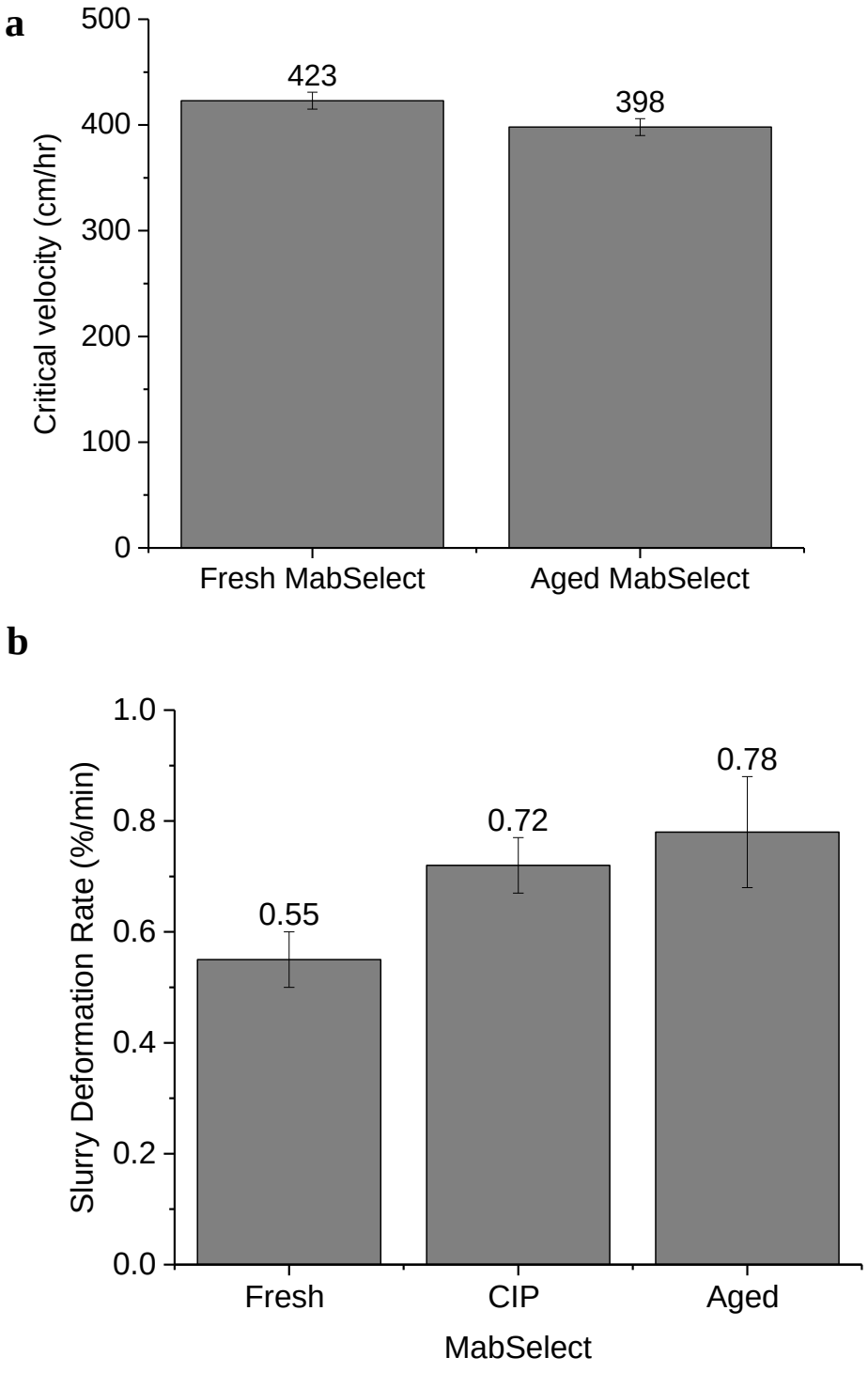

Figure 52– (a) column graph showing critical velocity values of fresh and aged MabSelect resin (423 and 398 cm/hr respectively). Error bars based on 3 runs. (b) column graph showing Slurry deformation rate values (SDR) for MabSelect resin under fresh, CIP-exposed and aged conditions (0.55, 0.72 and 0.78 $\%min^{-1}$.) Error bars based on 3 runs.

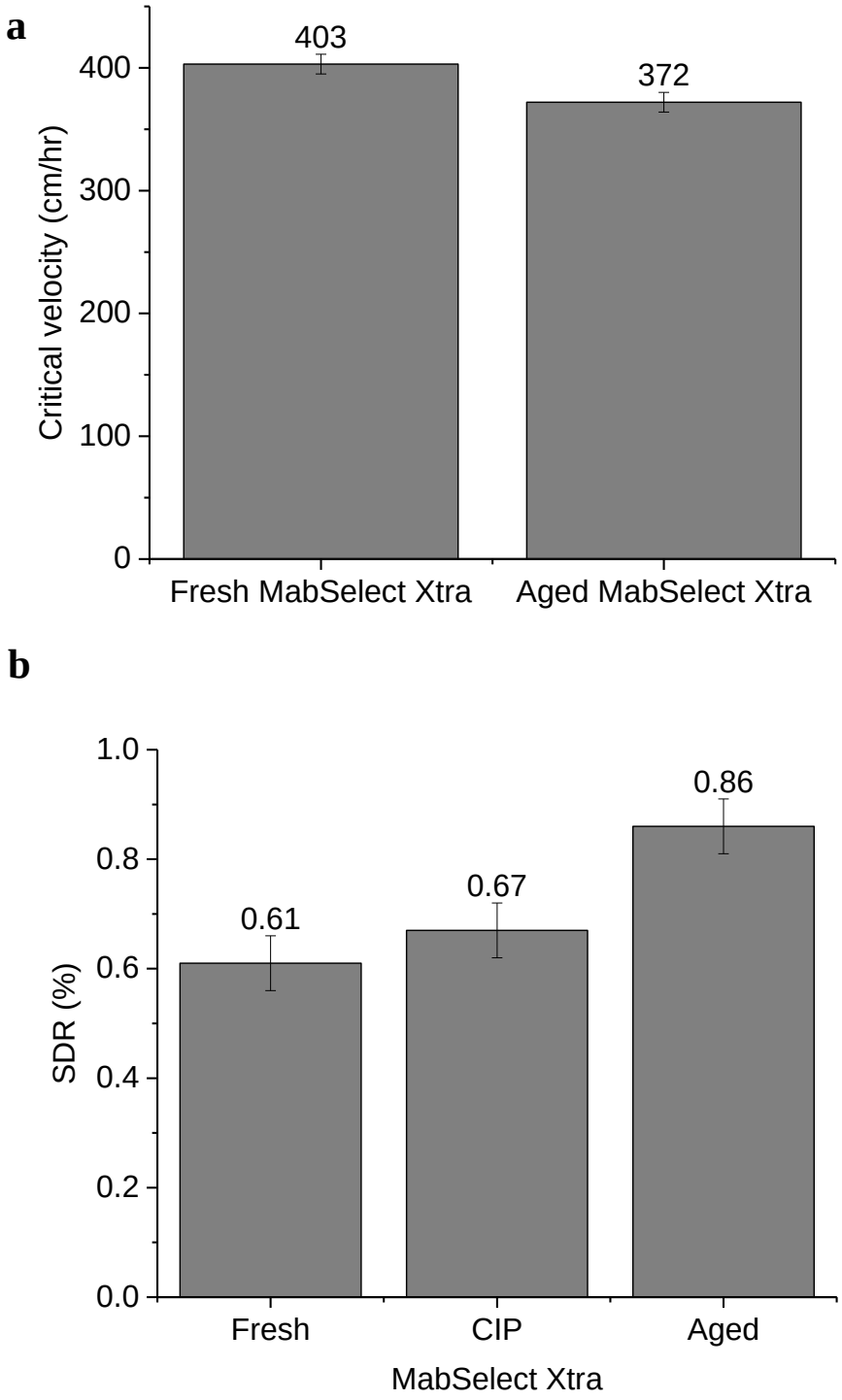

Figure 53- (a) column graph showing critical velocity values of fresh and aged MabSelect Xtra resin (403 and 372 cm/hr respectively). Error bars based on 3 runs. (b) column graph showing Slurry deformation rate values (SDR) for MabSelect Xtra resin under fresh, CIP-exposed and aged conditions (0.61, 0.67 and 0.86 $\%min^{-1}$.) Error bars based on 3 runs.

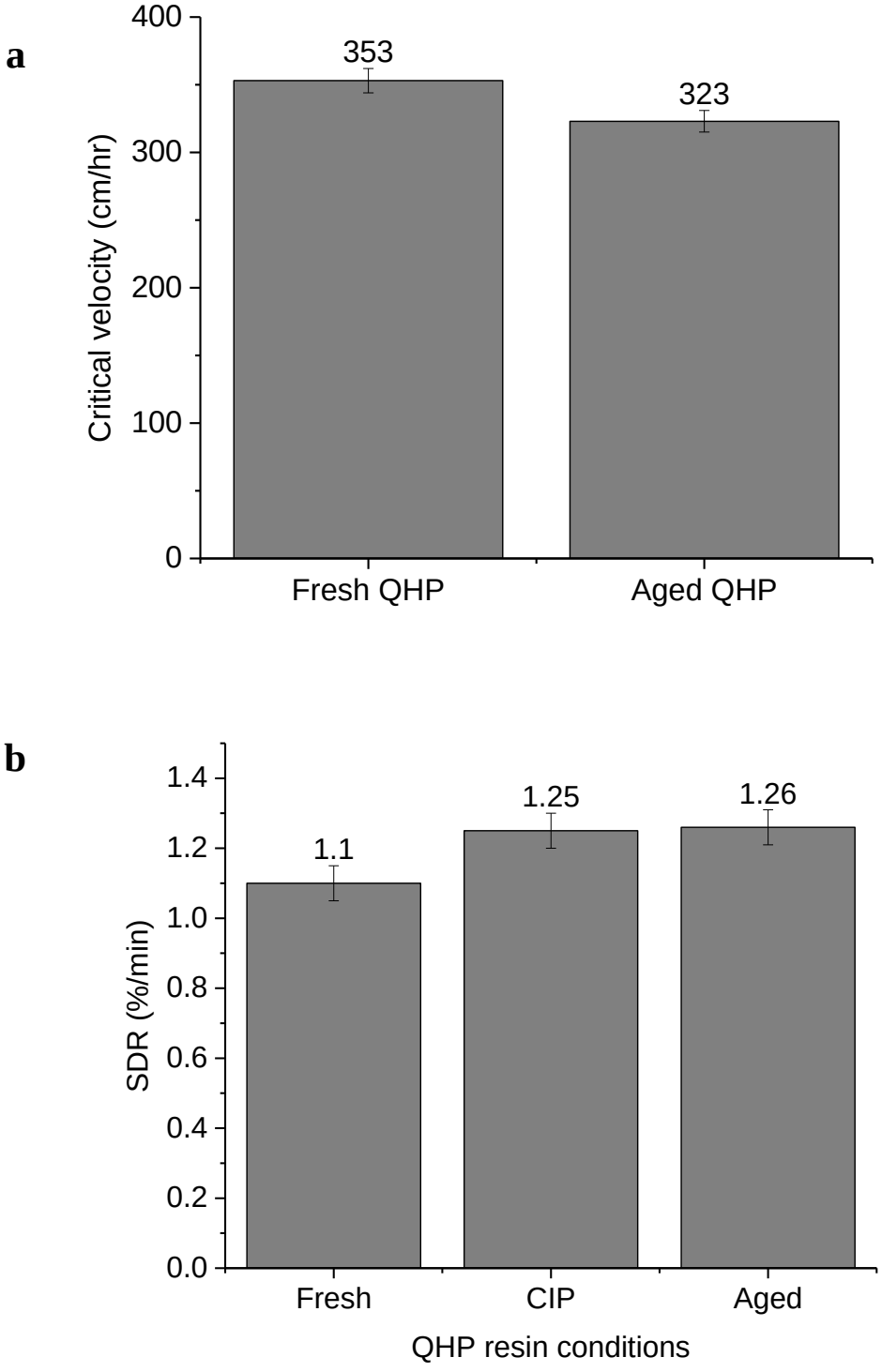

Figure 54 - (a) column graph showing critical velocity values of fresh and aged Q-Sepharose HP resin (353 and 323 cm/hr respectively). Error bars based on 3 runs. (b) column graph showing Slurry deformation rate values (SDR) for MabSelect resin under fresh, CIP-exposed and aged conditions (1.1, 1.25 and 1.26 $\%min^{-1}$.) Error bars based on 3 runs.

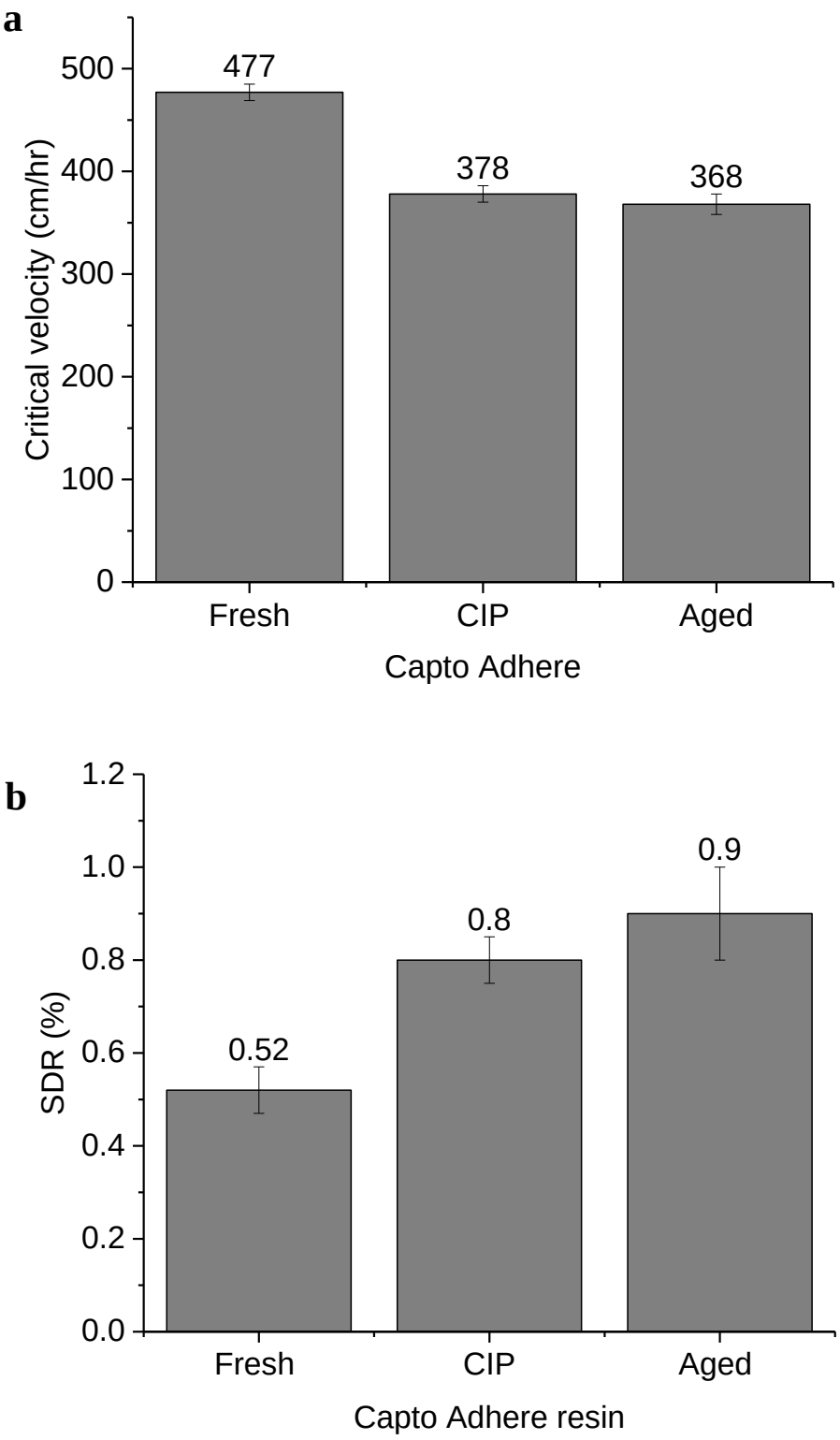

Figure 55 - (a) column graph showing critical velocity values of fresh, CIP-exposed and aged Capto Adhere resin (477, 378 and 368 cm/hr respectively). Error bars based on 3 runs. (b) column graph showing Slurry deformation rate values (SDR) for Capto Adhere resin under fresh, CIP-exposed and aged conditions (0.52, 0.8 and 0.9 $\%min^{-1}$.) Error bars based on 3 runs.

Table 26 – Slurry resistance values for MabSelect, MabSelect Xtra, Q-Sepharose HP and Capto Adhere under fresh, CIP-exposed and aged conditions. The slurry resistance value is the inverse of the SDR value, 1/SDR. *The standard deviation is 0.05 for all apart from aged MabSelect and aged Capto Adhere (+/- 0.1).

Resin	**MabSelect**			**MabSelect Xtra**			**Q-Sepharose HP**			**Capto Adhere**		
Condition	Fresh	CIP	Aged	Fresh	CIP	Aged	Fresh	CIP	Aged	Fresh	CIP	Aged
Slurry resistance (1/SDR) (+/- 0.05 STD)*	1.81	1.38	1.23 (+/- 0.1)	1.64	1.49	1.16	0.90	0.8	0.79	1.92	1.25	1.1 (+/- 0.1)

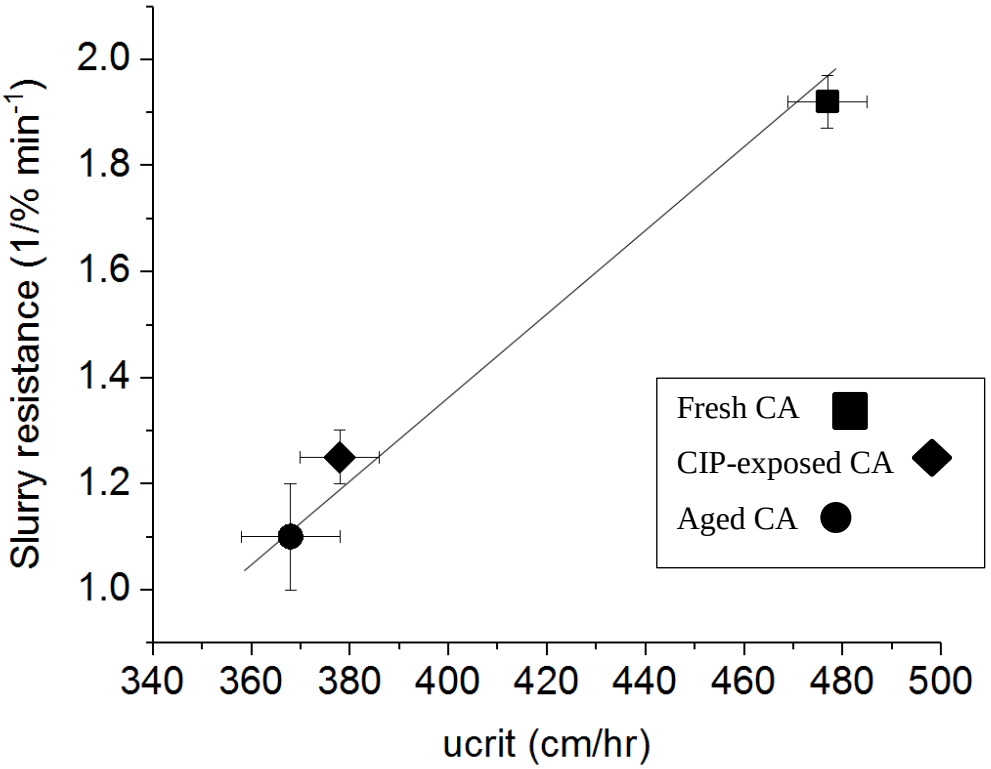

Figure 56 – Parity plot - Slurry resistance vs critical velocity for Capto Adhere. The square represents fresh resin, the diamond represents CIP-exposed resin and the circle represents aged resin.

5.3.1. Comparison of results from pressure-flow characterisation and DMA

Figures 52(a)-55(a) show pressure-flow characterisation results for 4 resins - MabSelect, MabSelect Xtra, Q-Sepharose High Performance and Capto Adhere - under fresh and aged conditions, while figures 52(b) - 55(b) show DMA results for the 4 resins under fresh, CIP-exposed and aged conditions. Figure 55(a) also includes pressure-flow characterisation data for CIP-exposed Capto Adhere resin. Table 26 shows slurry resistance data for all resins under all conditions, which is calculated by inversing the slurry deformation values provided in figures 52(b)-55(b). These sets of data can be compared to analyse mechanical differences between resins under different bioprocessing conditions.

The results for each resin using both techniques all show that fresh resin is more mechanically robust than its bioprocessed counterparts and that CIP-exposed resin is mechanically more robust than aged resin. However, what does differ between each technique is the extent to which the means vary. For example, Figure 52 shows pressure-flow characterisation of MabSelect (a) and dynamic mechanical analysis (b). In figure 52(b) there is approximately a 40% increase between the mean values for fresh and aged MabSelect, whereas in figure 52(a) the percentage change is far less significant (~6%). This is also the case for MabSelect Xtra. Figure 53(b) shows a difference of approximately 40% between fresh and aged resin, whereas in figure 53(a), the difference is far less significant (~8%). Furthermore, Capto Adhere also shows similar differences. The percentage reduction in mechanical strength shown in figure 55(b) between fresh and aged CA is over 70%, which is almost 2.5 times higher than the percentage reduction in mechanical strength shown in figure 55(a) (<30%). These results could indicate that due to the reduced volumes used for DMA, the sensitivity is increased, allowing for differences in mechanical behaviour to be more readily detected.

Contrastingly figure 54 (Q-HP) shows that the percentage difference of the mean values for fresh and aged resins using both techniques is much closer, meaning mechanical differences between fresh and aged Q-HP resin were less apparent using both techniques. This could indicate that Q-HP is the more robust resin as it is most

resistant to mechanical changes regardless of process conditions, which would corroborate findings observed in section 5.2.1.1. It is important to note however, that each resin used for this study has been exposed to different process conditions and/or lies in different stages of 3 individual separation processes. MabSelect and MabSelect Xtra are traditionally used in the same stages of mAb separation processes (capture). The similarities in their mechanical behaviour could be explained by that they were both exposed to a similar number of cycles.

However their observed differences (section 5.2) could be explained by the fact that they were both exposed to varying process conditions and the separation of different products. Another important thing to note is the vast difference in column sizes used in both cases (130L MabSelect vs 25ml MabSelect Xtra). Capto Adhere and Q-Sepharose HP are both used in latter stages of 2 separate purification process however, both display different mechanical behaviours. Whilst Capto Adhere has shown to be the more mechanically robust pre-bioprocessing, the results have indicated that Q-HP is the most resistant to mechanical change despite that it had undergone almost 4 times more in the number of cycles and repeated exposure to 1N NaOH. What is unknown however, are the process titres, levels of impurities that each resin was exposed to and how many purification steps there were in the process involving Q-HP. The use of statistical analysis will allow for the quantification of the significance of these results and the determination as to whether DMA can be used independently as a tool to test for mechanical differences with varying process conditions.

Figure 56 shows a plot of slurry resistance versus critical velocity for the fresh, CIP-exposed and aged conditions of Capto Adhere. The plot correlates with previously discussed trends – Fresh resin is the most mechanically robust followed by CIP-exposed and aged CA resin. Similar to SEM structural analysis for CA, the mechanical performance of CIP-exposed resin is more closely matched to its aged counterpart than its fresh counterpart, which may indicate that structural analysis is somewhat indicative of mechanical performance. It is important to note that Capto Adhere is the only resin for which pressure-flow and DMA data were collected under all 3 conditions and is therefore the only media that has 3 points that can be

plotted on a graph. However the collated information for fresh and aged pressure-flow and DMA data for other studied resins can be found in the appendix.

5.4.Statistical analysis - results

In order to ascertain whether there is a significant difference in the mechanical behaviour of fresh, CIP-exposed and aged resins, statistical analysis needs to be performed. This will account for areas of uncertainty between standard deviations. If the statistical results for both pressure-flow and DMA data are in agreement, it would indicate that DMA could be used as a small volume, high throughput technique to analyse mechanical differences in the studied agarose-based chromatography media independent of pressure-flow characterisation data. However, there are a number of factors to consider when choosing the most appropriate method with which to carry out statistical analysis.

ANOVA (analysis of variance) holds many advantages over other conventional statistical methods, such as t-tests. T-tests only allow for the comparison of means between 2 samples. However, if more than 2 conditions are used in an experiment, ANOVA is required. Furthermore, the larger the number of hypotheses tested using the t-test, the higher the Type I error and the less powerful the statistical results become (Boslaugh, 2012). This study will use one-way ANOVA (or ANOVA: single-factor) as significant differences between 3 conditions will be tested. ANOVA works by either rejecting or failing to reject a null hypothesis. A null hypothesis assumes that the means in all populations in all conditions are the same and is expressed as:

$$H_0: \mu_{fresh} = \mu_{CIP\text{-}exposed} = \mu_{aged}$$

meaning that there is no difference between the mean mechanical strength values for fresh, CIP-exposed or aged resins. If the null hypothesis is rejected then it can be concluded that at least one population mean is different to the others. In that case the alternative hypothesis (H_a) would be true (Seltman, 2007).

$$H_a: \exists \text{ fresh, CIP-exposed, aged: } \mu_{fresh} \neq \mu_{CIP\text{-}exposed} \neq \mu_{aged}$$

In order to ascertain whether this is the case, a comparison of F ratios are made. If the F value is higher than the F_{crit} value, then the null hypothesis rejected, meaning that there is a statistical difference between the populations. The F-statistics can be automatically computed in many packages including Microsoft Excel and is

calculated based on a number of sums of squares and degrees of freedom (Mendenhall and Sincich, 2006). It should be noted that the F_{crit} value is calculated based the number of samples and the number of conditions. As this is the same in both pressure-flow and DMA experiments, the calculated F_{crit} value will be the same in all cases.

Table 27- Statistical analysis showing whether there is significance between results for fresh and aged resin using the pressure-flow and DMA techniques. Blue indicates that both techniques show agreed significance of results and therefore prove the same hypothesis. Red indicates the opposite.

Technique	**Resin (fresh - aged conditions)**	**F**	**F_{crit} (to 1dp)**	**Proven hypothesis**
Pressure-flow	MabSelect	12.5	7.7	H_a
DMA	MabSelect	12.7	7.7	H_a
Pressure-flow	MabSelect Xtra	6.1	7.7	H_0
DMA	MabSelect Xtra	9.4	7.7	H_a
Pressure-flow	Q-Sepharose HP	4.5	7.7	H_0
DMA	Q-Sepharose HP	3.1	7.7	H_0
Pressure-flow	Capto Adhere	125	7.7	H_a
DMA	Capto Adhere	17.8	7.7	H_a

Table 28- Statistical analysis of results for Capto Adhere. The table shows the significance values for the results comparing fresh to CIP-exposed CA and CIP-exposed CA to aged for both pressure-flow and DMA. Blue indicates that both techniques show agreed significance and therefore prove the same hypothesis.

Technique	**Capto Adhere conditions**	**F**	**F_{crit} (to 1dp)**	**Proven hypothesis**
Pressure-flow	Fresh- CIP-exposed	104	7.7	H_a
DMA	Fresh- CIP-exposed	16	7.7	H_a
Pressure-flow	CIP-exposed-Aged	2	7.7	H_0
DMA	CIP-exposed-Aged	1	7.7	H_0

Table 29- Statistical analysis of DMA results for MabSelect, MabSelect Xtra and Q-Sepharose HP comparing fresh- CIP-exposed conditions and CIP-exposed- aged conditions for each resin.

Resin	**Conditions**	**F**	**F_{crit}**	**Proven hypothesis**
MabSelect	Fresh- CIP-exposed	33	7.7	H_a
	CIP-exposed - Aged	1	7.7	H_0
MabSelect Xtra	Fresh- CIP-exposed	0.6	7.7	H_0
	CIP-exposed - Aged	5	7.7	H_0
Q-Sepharose HP	Fresh- CIP-exposed	2.5	7.7	H_0
	CIP-exposed - Aged	0.08	7.7	H_0

5.4.1. Statistical analysis - discussion

The results from table 27 show whether there are statistical differences between the fresh and aged resins used in this study using both pressure-flow characterisation and dynamic mechanical analysis techniques. When the F value is greater than the F_{crit} value, the null hypothesis (H_0) is rejected, meaning that there is a significant difference between fresh and aged resin, making the alternative hypothesis true (H_a). If this is shown for both pressure-flow and DMA, it is an indication that DMA can be used independent of pressure-flow characterisation to characterise changes to mechanical integrity over the lifetime of chromatography media. The boxes highlighted in blue indicate that both pressure-flow and DMA prove the same hypothesis. This is the case for 3 out of the 4 studied resins - MabSelect, Q-Sepharose and Capto Adhere. The results show that there is a significant difference between fresh and aged MabSelect resin as well as fresh and aged Capto Adhere resin. This was also observed structurally in their corresponding SEM micrographs (chapter 3 and section 5.2.) The results indicate that there are no statistical differences between fresh and aged Q-HP. This corroborates aforementioned findings that the mechanical differences between fresh and aged Q-HP resin were less apparent using both techniques (section 5.3.) Furthermore, structural characterisation studies in section 5.2 and chapter 3 indicated that the structural changes observed in Q-HP were not as distinct and other studied resins such as Capto Adhere and MabSelect.

Contrastingly, statistical analysis using the DMA technique for MabSelect Xtra showed H_a to be true, i.e. that there is a significant difference between fresh and aged MabSelect Xtra, however, the opposite was proven using pressure-flow characterisation (highlighted in red). Reasons for this could be associated with increased sensitivity of the DMA technique, given that it uses a much reduced volume of resin, mechanical changes that were otherwise undetectable using pressure-flow could have been detected with DMA. Furthermore, the expectation of substantial changes to mechanical integrity of MabSelect Xtra is not completely surprising given the structural changes observed in section 5.2. Substantial mechanical changes would also corroborate with the aforementioned problem of severe back pressure increases observed by the second company after a relatively

low number of cycles. It is also important to note however, that more experimental repeats (*n*) would increase the statistical power to get an enhanced understanding of what these results truly indicate and increase confidence in these results as a whole.

Table 28 shows the statistical differences for Capto Adhere under CIP-exposed conditions and aged conditions using both the pressure-flow and DMA techniques. Both techniques corroborated the same hypotheses, hence why the table is highlighted in blue. The results show that there is a significant difference between fresh and CIP-exposed Capto Adhere however there is no significant difference between CIP-exposed and aged Capto Adhere. This would indicate that the addition of protein feed material would not have a significant effect on the mechanical robustness of the resin and that CIP-exposed conditions contribute the most to the mechanical aging of Capto Adhere. However, this could be due to the fact that the CIP-exposed conditions ran for 50 cycles compared to 17 cycles under aged conditions. Furthermore, as Capto Adhere is used as the last chromatography step in the production of an IgG4 product, it is exposed to far fewer impurities than MabSelect. Therefore the impact of foulants on the bead structure and mechanical integrity may be much reduced.

Table 29 shows statistical analysis of DMA results for MabSelect, MabSelect Xtra and Q-Sepharose High Performance comparing the significance of fresh to CIP-exposed conditions and CIP-exposed to aged conditions. The results show that there is a significant difference between fresh and CIP-exposed MabSelect but no statistical significance going from CIP-exposed to aged conditions. This also appears to be shown quite clearly in figure 52(b) as the error bars overlap. This is contrary to what was observed in the structural analysis of MabSelect under CIP-exposed and aged conditions. Aged MabSelect appeared to have a higher amount of fibre breakage and more evident damage to the matrix structure (figure 44(b)). It may suggest that a higher number of DMA experimental repeats may be necessary to determine whether these structural findings bear any impact on mechanical integrity. The results also show that there is no statistical difference between fresh and CIP-exposed MabSelect Xtra resin, as well as CIP-exposed and aged MabSelect Xtra resin. It should be noted that the CIP-exposed data used in this analysis was the ‘outer’ surface data. The SEM images in section 5.2. figure 41(b) show that the outer

surface has similar surface characteristics to its aged counterpart (figure 45(b)). This could explain why statistical analysis would show no significance between the two conditions. But, as previously alluded to, a higher number of DMA experimental repeats would increase confidence in these statistical findings.

The results also show that there are no statistical differences between fresh and CIP-exposed Q-HP resin, as well as CIP-exposed and aged Q-HP resin. This is corroborated by the structural analysis results that indicate that whilst there are observed structural differences in fresh, CIP-exposed and aged Q-HP, these differences, relative to the other studied resins, appear to be the least distinct. This would also aid in validating an aforementioned supposition that based on similar results, Q-HP would appear to be the most resilient to mechanical changes in spite of varied process conditions. The results also indicate that structural changes observed in the micrographs between fresh, CIP and aged resins, are indicative of mechanical changes, which is in agreement with similar studies comparing structural changes to other chromatographic performance parameters (Ioannidis, 2009; Jiang *et al.*, 2009; Close *et al.*, 2013; Gavara *et al.*, 2015). For example, the fibre degradation observed in aged MabSelect micrographs, resulted in reduced mechanical robustness compared to its fresh counterpart under both pressure-flow and DMA studies. What structural analysis does not indicate is the extent of reduction in mechanical strength. Despite Q-HP and MabSelect appearing to show similar amounts of fibre degradation, they display different levels of mechanical strength, as pressure-flow and DMA showed Q-HP to be far more mechanically robust than what the SEM micrographs would suggest. From this, it can be concluded that SEM can be used as an early stage indicator of mechanical robustness; however, mechanical testing would still have to be conducted to determine the extent of loss in mechanical strength.

5.5.Conclusion

Four resins were analysed – MabSelect, MabSelect Xtra, Q-Sepharose High Performance and Capto Adhere - to determine whether there were any structural and/or mechanical changes to the resins once exposed to typical process conditions (see tables 17 and 18). The experimental design compared "CIP-exposed" and "aged" to their fresh counterparts. CIP-exposed conditions involved exposing the resins to 50 cycles of buffer-only conditions to assess the impact of CIP reagents on structural and mechanical integrity, whilst aged resins were generated by two manufacturing companies who had conducted lifetime studies for the purification of two monoclonal antibodies (IgG 1 and 4) and a fusion protein under separate processes. The structural analysis studies were conducted using scanning electron microscopy imaging, while the mechanical integrity studies were conducted using pressure-flow characterisation studies and dynamic mechanical analysis.

The results from the structural analysis of the studied resins under different conditions show that there are structural differences under fresh, CIP-exposed and aged conditions for all 4 resins. The results indicate that each resin ages differently. MabSelect and Q-HP show matrix fibre degradation characteristics with aging, whilst Capto Adhere and MabSelect Xtra show matrix occlusion – possibly foulants adhering to the surfaces, causing reduced pore sizes. In the case of MabSelect Xtra, this aging mechanism may be a large contributor towards overpressuring of the column observed by the second company, as pore diffusion has been reported to be a rate limiting step in recent studies of protein A mass transfer characteristics, which can lead to back pressure issues (Bemberis, Noyes and Natarajan, 2003; Pathak and Rathore, 2016). The impact of CIP-exposed conditions appeared to have little visual effect on most resins; however Capto Adhere observed the biggest visual structural change under these conditions. The surface properties appeared to resemble Capto Adhere under aged conditions. This could indicate that impact of process feed material on the structural integrity of Capto Adhere is relatively minimal; however, more tests would need to be conducted to verify this. Subsequently mechanical testing was conducted on these resins to ascertain whether the observed structural changes were indicative of mechanical differences.

The results from the mechanical analysis of the studied resins under different conditions show that there were mechanical differences under fresh, CIP-exposed and aged conditions for all 4 resins. Mechanical tests were carried out using pressure-flow and dynamic mechanical analysis techniques. Both techniques showed that fresh resins were mechanically more robust than their processed counterparts and resins exposed to CIP conditions were more robust than their aged counterparts. In order to determine the significance of these results, ANOVA: single-factor statistical analysis was conducted. This showed that the results from DMA experiments corroborated that of pressure-flow experiments on 5/6 occasions, which is a strong indication that DMA can be used independently of pressure-flow to test the mechanical integrity bioprocessed resin throughout its lifetime. The statistical results also showed that there were significant differences between fresh and aged MabSelect, Q-HP and Capto Adhere as well as fresh and CIP-exposed Capto Adhere, which is supported by observations in the corresponding SEM micrographs. In the case of MabSelect Xtra, while pressure-flow characterisation suggested that there was no significant difference between fresh and aged resin, DMA suggested the opposite to be true, which would corroborate the findings of the structural analysis data.

The results indicate that while repeated exposure of buffers and CIP reagents can affect the structural and mechanical integrity of chromatography resins to a large extent, the interaction of product/feed material does have a different and more significant impact on the way in which the resins age. In order to possibly extend resin lifetime, these results would indicate the need for two things: a review of the clarification strategy used and ways to lower burdens on downstream processing or that more studies would need to be conducted in order to determine ideal CIP-process feed interactions that would result in the least damage to chromatography media whilst still maintaining acceptable column performance.

CHAPTER 6
FINAL CONCLUSIONS

6. FINAL CONCLUSIONS

The work presented in this thesis has made use of structural and mechanical testing tools (SEM, pressure-flow characterisation and DMA) to further enhance the understanding of the changes that occur when chromatography media is exposed to different bioprocessing conditions. This chapter reviews each results chapter in order to determine whether the initial objectives have been addressed.

The objectives of the first results chapter involved visualising a range of resins and quantifying associated structural properties. Using scanning electron microscopy (SEM), the properties of nine commercially available resins were observed and quantified using ImageJ software (section 6.1 for results).

The objective of the second results chapter was to quantify mechanical differences between the nine resins. To fulfil this, mechanical properties of these resins were investigated using pressure-flow characterisation. The limitations of this technique led to the development of a novel technique to this field – dynamic mechanical analysis. The results reported in section 6.1 of this chapter show pressure-flow and DMA to display the same trends and indicate that DMA can be used as a small volume, high-throughput technique for mechanical characterisation of resins.

The objective of the final results chapter involved the use of SEM, pressure-flow and DMA in order to characterise four resins that had been exposed to varying bioprocess conditions - buffer conditions (CIP-exposed) as well as protein purification conditions (aged) over repeated cycle. The results reported in section 6.1 have shown that the 4 resins used in this study age via matrix degradation or fouling when exposed to certain conditions and suggest that the interaction of CIP reagents and foulants have the biggest impact on resin integrity.

6.1.Conclusions – Review of objectives

The objectives addressed in the first results chapter (chapter 3) are outlined below:

- Ultrastructural visualisation and qualification of a range of commercially available agarose-based chromatography media
- Quantification of the observed ultrastructural properties

The first results chapter used scanning electron microscopy (SEM) to observe the structural properties of nine agarose-based chromatography media - Sepharose CL-4B (SCL4B), Sepharose CL-6B (SCL6B), Sepharose 4 Fast Flow (S4FF), Sepharose 6 Fast Flow (S6FF), Q-Sepharose High Performance (Q-HP), MabSelect Xtra (MSX), MabSelect (MS), Capto Adhere (CA) and Capto Q (CQ). The samples require a drying step as a pre-treatment procedure that can impact the quality of images produced using SEM. This chapter investigated 3 commonly used drying techniques – air drying, freeze drying and critical point drying (CPD). Air drying did not provide sufficient drying for clear ultrastructural visualisation, whilst freeze drying caused bead breakage. It was found that CPD was the most suitable drying procedure as it best preserved the ultrastructural properties of the resins and allowed for high resolution imaging of surface properties.

The micrographs were then analysed both qualitatively and quantitatively. Quantitative analysis was carried out using Image J software in order to ascertain whether what was assessed qualitatively could also be measured accurately, with particular focus on average pore size, apparent porosity, pore count and pore size distribution. Certain properties, such as pore size and pore size distribution were difficult to assess by sight only. It should be noted that the use of terms such as ‘apparent porosity’ accounts for the fact that the porosity measurements in this study are based on 2-D images that do not account for the angle at which the micrographs were attained. For this reason, the values obtained in this study for average pore size, apparent porosity and pore size distribution differ from studies that account for the 3-D nature of the pores (Yao and Lenhoff, 2004; Bacskay, Sepsey and Felinger, 2014; Sepsey, Bacskay and Felinger, 2014). Some studies have however made use of

2-D pore information as a general guide (Ioannidis, 2009). However, a trend can be observed based on the values obtained. The results showed that Capto Q had the highest pore count (>1000), MabSelect Xtra had the lowest pore count (~300), the highest pore size (~d95nm) and the highest pore size distribution, while SCL4B had the lowest pore size distribution. S4FF had the smallest average pore size (~d45nm) and the lowest apparent porosity (17%), while Q-HP had the highest apparent porosity at 44%.

The main challenges faced when using SEM for quantitative image analysis involved obtaining a large number of images with consistently high enough resolution. This proved difficult due the high sensitivity of the polymers and their susceptibility to damage if exposed to the focused electron beam for too long. A further challenge was the use of 2-D imaging to characterise 3-dimensional properties. As a result, the values obtained can only be used as a general guide to support visual observations.

The objective addressed in the second results chapter (chapter 4) is outlined below:

- Quantification of the mechanical properties of the resins

Pressure-flow analysis was used to determine whether the differences in the observed structural properties were in any way indicative of mechanical strength. This was carried out to determine the mechanical limits of each resin, operated in an XK16 column, ~30ml. The results showed that the Capto family had the highest critical velocities (CA- 492, CQ- 477 cm/hr), followed by the MabSelect family (MS- 423, MSX- 403 cm/hr). Q-HP (353 cm/hr) and S6FF (348 cm/hr) exhibited quasi-identical behaviour in the column whilst SCL6B, S4FF and SCL4B had the lowest critical velocity values (283, 204, 149 cm/hr respectively).

There were practical limitations in using the pressure-flow technique alone for mechanical characterisation, including the large quantity of chromatography media and buffers required, as well as the stringent criteria required to pack a column. The development of a low volume, high throughput technique – dynamic mechanical analysis (DMA) - that aimed to address the challenges associated with the pressure-

flow characterisation was also presented in this chapter. The DMA technique allowed for further mechanical characterisation based on the viscoelastic properties using 1ml of resin. The technique was applied to the nine studied resins and correlated with the results obtained using the pressure-flow technique. The same trends were observed – The Capto family showed the highest resistance to deformation (CA- 2.7, CQ- 1.92 $1/\%min^{-1}$), followed by the MabSelect family (MS- 1.81, MSX- 1.64 $1/\%min^{-1}$). Q-HP and S6FF showed similar resistance and SCL6B, S4FF and SCL4B had the lowest slurry resistance values (0.59, 0.4, 0.3 $1/\%min^{-1}$ respectively). These results indicate that DMA can be used as a small volume, high-throughput technique for the mechanical characterisation of chromatography media.

The objective addressed in the third results chapter (chapter 5) is outlined below:

- The use of these tools (SEM, pressure-flow characterisation and DMA) to investigate structural and mechanical properties of a selection of these resins exposed to varying bioprocessing conditions.

The final results chapter utilises all three structural and mechanical testing tools – SEM, pressure-flow characterisation and DMA – to assess the structural and mechanical changes observed in resins exposed to different bioprocessing conditions. The four selected resins used in this chapter were MabSelect, MSX, Q-HP and Capto Adhere. Each resin had been exposed to two different conditions termed CIP-exposed and aged. CIP conditions involved exposing each resin to 50 cycles of buffer conditions only (i.e. no protein product exposure), in order to gain an understanding into how these conditions contribute to the structural and mechanical integrity of the resins. Regarding the second condition, aged, each resin had been used for resin lifetime studies in the production a monoclonal antibody (or a fusion protein, in the case of Q-HP) and had therefore been exposed to repeated cycles of process feed, including impurities as well as buffer and CIP reagents. The impact of this condition on the structural and mechanical properties of the resins was compared with its fresh and CIP-exposed counterparts to observe how the properties of the resins had changed.

MS and Q-HP appeared to show similar mechanisms of aging. Their matrices degraded with increased exposure, leading to the formation of larger pores, whilst the opposite was true for CA and MSX. In these cases, there appeared to be foulants adhering to the surface fibres, leading to a reduction in pore size. The results from mechanical analysis were consistent in all cases. Fresh resins showed higher mechanical resistance compared to their bioprocessed counterparts, while CIP-exposed resins were mechanically more robust than their aged counterparts, but to different extents. Statistical analysis was performed with one way ANOVA to determine whether DMA alone could be used to assess the impact of process conditions on the mechanical properties of chromatography media and the results show a >80% certainty that DMA can be employed for this purpose. To increase this value, it is likely that more experimental repeats would need to be carried out.

The results indicate that while repeated exposure of buffers and CIP reagents can affect the structural and mechanical integrity of chromatography resins to a large extent, the interaction of CIP reagents with foulants does have a different and more significant impact on the way in which the resins age. In order to possibly extend resin lifetime, these results would indicate the need for two things: a review of the clarification strategy used and ways to lower burdens on downstream processing or that more studies would need to be conducted in order to determine ideal CIP-process feed interactions that would result in the least damage to chromatography media whilst still maintaining acceptable column performance.

6.2.Overall aim

The results from these studies have shown that a combination of structural and mechanical testing tools can provide a more rounded picture of the contrasting properties of different resins, as well as resins exposed to different bioprocessing conditions. The use of these tools can be employed to investigate a number of emerging concerns for process validation and manufacturing companies. Concerns over batch-to-batch variation, how to evaluate these studies and the frequency of these studies have become areas of scrutiny, as regulatory authorities tighten up process criteria requirements as a means of making safety enhancements (Hentschel, 2013). Further drug manufacturing concerns relate to the lack of understanding

surrounding mass transfer through certain sections of the column. A combination of the structural and mechanical techniques presented in this thesis, along with work that has shown potential to be applied in further understanding the aging mechanisms of chromatography resins can contribute greatly to addressing some of the aforementioned concerns. DMA in particular could be used to test for mechanical variations between batches of resins. It also has the potential to test resins post-emulsification, aid in the development of new resins and be applied to resins of non-agarose based material.

6.3. Study bottlenecks

As outlined above, a number of primary objectives were met in this study. However, with the provision of information pertaining to certain aspects of this study, a range of secondary objectives could have been explored (further outlined in chapter 7 – Future Work). Use of the structural and mechanical tools developed in this study on non-agarose based beads may have contributed to a deeper understanding on the effectivity of this tools, however this could be studied in future work (see chapter 7). Disclosure of certain information such as the position of the column from which samples were sent by the sponsoring company, any changes in DBC/HETP observed as a result of mechanical degradation and structural/mechanical information from the resin vendors (all of which were deemed confidential) may have also aided in the understanding of the resin aging process. Although there are many advantages in using a small volume of sample for DMA studies, tests could be carried out to determine whether there are mechanical differences in different sections of the column in order to get a more representative mechanical characterization profile of a large-scale column. Finally, as well as the application of tools developed in this study to non-agarose beads, the flexibility of the DMA technique, as described in chapter 4 means it can be adapted to test non-beaded chromatography formats. The information collected could then be linked/correlated to other chromatography performance characteristics such as DBC, yield etc. (see chapter 7).

CHAPTER 7
FUTURE WORK

7. FUTURE WORK

With chromatography being the workhorse of the biopharmaceutical purification train, it is responsible for producing over 500 tons of biopharmaceutical products, such as monoclonal antibodies (mAbs) per year (Jagschies, Sofer and Hagel, 2008). It is also considered to be the most expensive part of downstream processing. It has been estimated that in a typical mAb process, 60% of downstream costs come from chromatography alone and the cost of a typical Protein A resin is 50% higher than the cost of other types of chromatographic media, such as ion exchangers (Rathore *et al.*, 2015; Hernandez, 2016). Aside from economic implications, the increased product titres achieved within the last few years have led to a heavier burden on downstream processing, which in turn, has led to regulatory authorities calling for manufacturers to better define their processes to deal with the increased load (Hentschel, 2013). The Quality by Design (QbD) and Process Analytical Technology (PAT) initiatives call for increased process and product understanding to ensure each process consistently meets precisely defined quality attributes. This has led to increased research in factors that define the critical quality attributes (CQAs) of resin aging and linking them to their corresponding critical process parameters (CPPs), meaning a thorough and systematic approach to characterise the process parameter space (Hanke and Ottens, 2014).

Due to these pressures, there is a need to identify procedures that can be implemented to contribute to an increase in resin lifetime. As previously alluded to, a number of approaches could be taken. Improvements to clarification strategies as well as alterations to process feed material and process conditions, such as flow rate and mobile phase viscosity, can act as troubleshooting techniques for the extension of resin lifetime. Bracewell et al. 2008 reported that more poorly clarified suspensions required proportionally larger filters, however increased clarification led to greater column capacity. They also reported that the use of centrifugation followed by filtration left lipids in their soluble state, meaning that they were not removed. Similarly, Jin et al. 2009 found that the presence of lipids in the purification of virus-like particles (VLPs) greatly reduced recovery by almost 70% over 40 cycles. However improvements to CIP conditions caused a 20% rise in recovery but only when higher degrees of lipid fouling had occurred. Revisions to

clean-in-place (CIP) and regeneration conditions can also extend resin lifetime (Sofer and Yourkin, 2007). In 2008, Tengliden investigated a number of CIP procedures optimised for protein A chromatography using design of experiments (DoE) approach. The study showed that after exposure to 0.55 M NaOH for 24 hours, MabSelect Sure had retained 90% of its original capacity and the addition of sodium chloride provided a stabilizing effect on the resin. More recently, Grönberg et al. 2011 developed a high-throughput method for screening for CIP conditions on MabSelect Sure and had found similar results, also with the addition of sodium chloride acting as a stabilizing agent.

Choosing the adsorbent most suitable for the specific protein to be purified is important. The degree of agarose-based resin cross-linking has been reported to contribute towards both the chemical and mechanical stability of the resin (Andersson, Ramberg and Johansson, 1998; Hardin *et al.*, 2009). Langer 2013 found that too high a degree of cross-linking caused mass transfer limitations leading to a decrease in resin functionality. A further property is resin bead size. Masters 2012 reported on the impact of using smaller vs. larger resins on chromatographic performance. Smaller beads tend to encourage faster mass transfer than larger beads, higher efficiency and better resolution. However they exhibit greater tendencies for high back pressure issues and equipment and economic implications. Larger resins provide higher capacity, fewer back pressure issues and better economics. However, achievable resolution and efficiency is lower than that of smaller beads.
The following sections briefly describe a number of experimental procedures that can be employed to enhance the results of this study and contribute towards further understanding of the aging of chromatography resins.

7.1.Resin fines studies

The results from chapter 5 have indicated that 2 of the 4 studied resins show matrix fibre degradation characteristics (MabSelect and Q-HP). This indicates that beads may have disintegrated during column operation that has led to the observed breakdown of the matrix structure, creating small particles or fines. This build-up may contribute to back pressure build-up and mechanical instability of the column. In order to ascertain whether this is the case, studies could be carried out intended to

collect resin fines with the use of sieves. Particle size analysis could then be conducted on the resin fines to further understand the effects of these particulates on column stability.

7.2.Cryo-microtoming of bioprocessed samples

In order to gain an enhanced understanding of the mechanical stability of the column during operation, it is important to investigate the beads in their entirety and not solely surface characteristics. One way of potentially achieving this would be to visualise the interior of the beads to observe whether the surface characteristics are distinct from the sub-surface characteristics. Pathak et al. 2017 recently used an ultramicrotoming device to view the interior of fouled MabSelect resin using transmission electron microscopy (TEM). Limitations to the employed techniques are that ultramicrotoming does not allow for controlled temperatures within the microtoming chamber and the use of TEM requires extensive sample preparation. Furthermore, a wider range of resins under different bioprocessing conditions would need to be investigated for enhanced understanding. A tool that could potentially be used to address one of these limitations is cryo-microtoming. This tool can be used to slice thin sections (50nm-100µm) of the bead at a suitable temperature and potentially without the need for further pre-treatment prior to visualisation. Subsequently, SEM can be used for clearer ultrastructural visualisation of the sections. The flatness of the sections will allow for better quantitative analysis of the sub-surface properties.

7.3.Column sectioning studies

Samples from different sections of the column could also be structurally and mechanically analysed during and post-column operation by combining tools presented in this work and work from recent studies, particularly Johnson et al. 2017 and Pathak et al. 2017. With this understanding, the effects of mechanical stability could be correlated with other performance parameters such as DBC, yield, etc. A combination of these studies will lead to improved process understanding and the maximisation of resin lifetime and performance.

7.4.Potential uses of DMA

Chapter 4 showed that DMA has the potential to be used as a small volume, high-throughput technique for the mechanical characterisation of chromatography media. Based on this, DMA could be used by resin manufacturers and researchers to test for mechanical variations between batches of resins. It also has the potential to test resins post-emulsification, aid in the development of new resins and be applied to resins of non-agarose based material, e.g. ceramic, cellulose, etc. The versatility of the DMA technique means it can be adapted depending on the nature of the material's mechanical properties. Mechanical testing for non-beaded chromatographic materials such as filters can be carried out using DMA in its more traditional mode of operation, as described in section 4.3. DMA may also be applied in more recently developed chromatographic technologies such as simulated moving bed chromatography (SMB). Further studies on how DMA correlates to each parameter used during structural analysis could be studied. The use of mercury intrusion for 3D pore size evaluation, porosity and pore size distribution could have been compared.

7.5.Implementing resin aging analytical tools to satisfy QbD initiatives

Whilst research continues in this area, it should be noted that most of these techniques are yet to be employed during industrial-scale separations due to the high cost of some of the equipment. A number of strategies have been presented for optimising process economics in purification, such as using less expensive sanitization buffers and moving towards single use filters, prepacked columns and membrane adsobers (Hernandez, 2016). The employment of more economically optimised processes, as well as the regulatory pressures for better process characterisation, a shift towards the implementation of these diagnostic techniques based on the understanding of column aging mechanisms, needs to be something of the not-too-distant future. Table 6b highlights the maturity of certain resin aging analytical tools (i.e. their extent of use within research) and the specific QbD properties they would meet.

REFERENCES

Amsterdam, A., Er-El, Z. and Shaltiel, S. (1975) 'Ultrastructure of beaded agarose', *Archives of biochemistry and biophysics*. 171(2) pp.673-677

Andersson, M. (2014) *Characterisation of Chromatography Media Aimed for Purification of Biomolecules*. PhD thesis - Uppsala Universitet.

Andersson, M., Ramberg, M. and Johansson, B.-L. (1998) 'The influence of the degree of cross-linking, type of ligand and support on the chemical stability of chromatography media intended for protein purification', *Process Biochemistry*, 33(1), pp. 47–55.

Attwood, T., Nelmes, B. and Sellen, D. (1988) 'Electron microscopy of beaded agarose gels', *Biopolymers*, 27(2), pp. 201–212.

Bacskay, I., Sepsey, A. and Felinger, A. (2014) 'The pore size distribution of the first and second generation of silica monolithic stationary phases', *Journal of Chromatography A*, 1359, pp. 112–116.

Bahme, H. -J, P. Hedman, E. H. (2002) 'Advances in Biochemical Engineering/Biotechnology', *Springer*. Edited by R. Freitag, 76, p. 273.

Bell, B. (1988) 'Comparison of the effects of critical point-drying and freeze-drying on cytoskeletons and microtubules', *Journal of Microscopy*, 151(August), pp. 103–114.

Bemberis, I., Noyes, A. and Natarajan, V. (2003) 'Column Packing for Process-Scale Chromatography: Guidelines for Reproducibility', *BioPharm International Guide*, (July), pp. 23–30.

Bio-Rad Laboratories (2014) *Process-Scale Chromatography Columns*. Available at: http://www.bio-rad.com/en-uk/category/process-scale-chromatography-columns.

Blewett, J. M. (2000) *Micromanipulation of plant cell mechanical properties*. University of Birmingham, UK.

Boslaugh, S. (2012) *Statistics in a Nutshell*. 2nd Editio. O'Reilly Media, Inc.

Bracewell, D. G. *et al.* (2008) 'Impact of clarification strategy on chromatographic separations: Pre-processing of cell homogenates.', *Biotechnology and bioengineering*, 100(5), pp. 941–9.

Bray, D. (2000) 'Critical point drying of biological specimens for scanning electron microscopy', *Supercritical Fluid Methods and Protocols*, 13, pp. 235–243.

Buban, J. P. *et al.* (2010) 'High-resolution low-dose scanning transmission electron

microscopy', *Journal of Electron Microscopy*, 59(2), pp. 103–112.
Carter-Franklin, J. N. *et al.* (2007) 'Fragments of protein A eluted during protein A affinity chromatography', *Journal of Chromatography A*, 1163(1–2), pp. 105–111.
Cheng, J. H. (2009) *Packing and Quality Control of a Chromatography Column*.
Chochois, H. *et al.* (2011) 'Industrial-Scale Biochromatography Columns Address Challenging Purification Needs', *BioProcess International*.
Close, E. J. *et al.* (2013) 'Fouling of an anion exchange chromatography operation in a monoclonal antibody process: Visualization and kinetic studies.', *Biotechnology and bioengineering*, 110(9), pp. 2425–35.
Close, E. J. (2015) *The derivation of bioprocess understanding from mechanistic models of chromatography*. University College London.
DePhillips, P. and Lenhoff, A. (2000) 'Pore size distributions of cation-exchange adsorbents determined by inverse size-exclusion chromatography', *Journal of Chromatography A*, 883, pp. 39–54.
Dey, S. *et al.* (1989) 'A new rapid method of air-drying for scanning electron microscopy using tetramethylsilane', *Journal of Microscopy*, 156(2), pp. 259–261.
Ding, P. *et al.* (2007) 'Mechanical properties of gelatin – rich microparticles', *Journal of Food Engineering*, 86, pp. 307–314.
Dorn, M. *et al.* (2017) 'Influence of different packing methods on the hydrodynamic stability of chromatography columns', *Journal of Chromatography A*. Elsevier B.V.
Draenert, Y. and Draenert, K. (1982) 'Ice crystal damage in freeze-dried articular cartilage studied by scanning electron microscopy', *Scan Electron Microsc*, (4), pp. 1799–1804.
Fatin-Rouge, N., Konstantin, S. and Jacques, B. (2004) 'Size effects on diffusion processes within agarose gels', *Biophysical Journal*, 86, pp. 2710–2719.
Gavara, P. *et al.* (2015) 'Chromatographic Characterization and Process Performance of Column-Packed Anion Exchange Fibrous Adsorbents for High Throughput and High Capacity Bioseparations', *Processes*, 3(1), pp. 204–221.
Gerstein, A. (2004) *Molecular Biology Problem Solver: A Laboratory Guide*. 2nd edn. Edited by A. Gerstein. Wiley.
Ghetie, V. and Schell, H. D. (1971) *Cellular and Molecular Life Sciences*. Springer. doi: 10.1007/BF02154242.
Goldstein, J. *et al.* (2013) *Scanning Electron Microscopy and X-Ray Microanalysis*. 3rd edn. Springer US.

Grier, S. and Yakubu, S. (2016) ‘Prepacked chromatography columns: evaluation for use in pilot and large-scale bioprocessing’, *BioProcess International*.
Griess, G., Guiseley, K. and Serwer, P. (1993) ‘The relationship of agarose gel structure to the sieving of spheres during agarose gel electrophoresis’, *Biophysical Journal*, 65(1), pp. 138–148.
Grimaud, E. *et al.* (1978) ‘Comparison of gels for molecular sieving of proteins by electron microscopy and pore parameters determination’, *Journal of Chromatography A*, 166(1), pp. 1–348.
Grönberg, A. *et al.* (2011) ‘A tool for increasing the lifetime of chromatography resins’, *mAbs*, 3(2), pp. 192–202.
Gu, T. *et al.* (1990) ‘Displacement effect in multicomponent chromatography’, *AIChE Journal*, 36, pp. 1156–1162.
Guélat, B. *et al.* (2012) ‘Simulation model for overloaded monoclonal antibody variants separations in ion-exchange chromatography’, *Journal of Chromatography A*, 1253, pp. 32–43.
Guichon, G., A, F. and Shirazi, D. (2006) *Fundamentals of preparative and nonlinear chromatography*. 2nd Editio. Academic Press.
Hagel, L., Ostberg, M. and Andersson, T. (1996) ‘Apparent pore size distributions of chromatography media’, *Journal of Chromatography A*, 743(1), pp. 33–42.
Hahn, T. *et al.* (2015) ‘Simulating and Optimizing Preparative Protein Chromatography with ChromX’, *Journal of Chem. Educ*, 92(9), pp. 1497–1502.
Hanke, A. T. and Ottens, M. (2014) ‘Purifying biopharmaceuticals: knowledge-based chromatographic process development’, *Trends in Biotechnology*. Elsevier Ltd, 32(4), pp. 210–220.
Hardin, A. M. *et al.* (2009) ‘Ion exchange chromatography of monoclonal antibodies: Effect of resin ligand density on dymanic binding capacity’, *Journal of Chromatography A*, 20(1216), pp. 4366–4371. doi:
Helmy, I. M. and Abdel Azim, A. M. (2012) ‘Efficacy of ImageJ in the assessment of apoptosis’, *Diagnostic Pathology*, 7(1), p. 15.
Hemph, R. *et al.* (2007) ‘Discrete eluent simulations and experimental validation of particle packing in a 5mm chromatography column’, in *International conference for multiphase flow*. Leipzig.
Hentschel, N. (2013) ‘EMA Expert Workshop on Validation of Manufacturing for Biological Medicinal Products’,

Hernandez, R. (2016) ‘Achieving Cost-Effective Bioprocesses’, *BioPharm International*, 29(3), pp. 14–19.
Hubbuch, J. and Kula, M. R. (2008) ‘Confocal laser scanning microscopy as an analytical tool in chromatographic research.’, *Bioprocess and biosystems engineering*, 31(3), pp. 241–59.
Ioannidis, N. (2009) *Manufacturing of agarose-based chromatographic media with controlled pore and particle size*. University of Birmingham.
Ioannidis, N. *et al.* (2012) ‘Manufacturing of agarose-based chromatographic adsorbents - Effect of ionic strength and cooling conditions on particle structure and mechanical strength’, *Journal of Colloid and Interface Science*. Elsevier Inc., 367(1), pp. 153–160.
Jagschies, G., Sofer, G. and Hagel, L. (2008) *Handbook of Process Chromatography - Development, Manufacturing, Validation and Economics*. 2nd edn. Elsevier.
Jensen, E. C. (2013) ‘Quantitative Analysis of Histological Staining and Fluorescence Using ImageJ’, *Anatomical Record*, 296(3), pp. 378–381.
Jiang, C. *et al.* (2009) ‘A mechanistic study of Protein A chromatography resin lifetime’, *Journal of Chromatography A*, 1216(31), pp. 5849–5855.
Jin, J. *et al.* (2009) ‘Evaluation of the impact of lipid fouling during the chromatographic purification of virus-like particles from Saccharomyces cerevisiae’, *Journal of Chemical Technology & Biotechnology*, (June 2009),
Johnson, T. F. *et al.* (2017) ‘X-ray computed tomography of packed bed chromatography columns for three dimensional imaging and analysis’, *Journal of Chromatography A*. Elsevier B.V., 1487, pp. 108–115.
Jones, C. G. (2012) ‘Scanning Electron Microscopy: Preparation and Imaging for SEM’, *Methods in Molecular Biology Springer Protocols*. Edited by L. S. Bell. Totowa, NJ: Humana Press (Methods in Molecular Biology), 915, pp. 1–20.
Joy, D. and Pawley, J. (1992) ‘High-resolution scanning electron microscopy’, *Ultramicroscopy*, 47(I 992), pp. 80–100.
Jungbauer, A. (2005) ‘Chromatographic media for bioseparation’, *Journal of Chromatography A*, 1065(1), pp. 3–12.
Keener, R., Maneval, J. and Fernandez, E. (2004) ‘Toward a Robust Model of Packing and Scale-Up for Chromatographic Beds. 1. Mechanical Compression’, *Biotechnology progress*, 20, pp. 1146–1158.
Keller, K., Friedmann, T. and Boxman, A. (2001) ‘The bioseparation needs for

tomorrow', *Trends in Biotechnology*, 19(11), pp. 438–441.
Kennedy, R. (2003) 'Qualification of a Chromatographic Column', *BioPharm International*, (March).
Kervrann, C. *et al.* (2016) 'A Guided Tour of Selected Image Processing and Analysis Methods for Fluorescence and Electron Microscopy', *IEEE Journal of Selected Topics in Signal Processing*, 10(1), pp. 6–30.
Knox, J. and Ritchie, H. (1987) 'Determination of pore size distribution curves by size-exclusion chromatography', *Journal of Chromatography A*, 387, pp. 65–84.
Kong, D. *et al.* (2017) 'Effects of Bed Compression on Protein Separation on Gel Filtration Chromatography at Bench and Pilot Scale', *Journal of Chemical Technology & Biotechnology*.
Laas, T. (1998) *Protein Purification: Principles, High Resolution Methods and Applications*. 2nd editio. Wiley-VCH.
Langer, E. (2013) 'Influence of conditions of chromatographic analysis and cross-linking process on Flory-Huggins parameters and solubility parameters of selected epoxy resins', *Chemik International Edition*, 64(4), pp. 301–308.
Laursen, K., Justesen, U. and Rasmussen, M. (2011) 'Enhanced monitoring of biopharmaceutical product purity using liquid chromatography mass spectrometry', *Journal of Chromatography A*, 1218(28), pp. 4340–4348.
Lienqueo, E. ., Shene, C. and Asenjo, J. (2009) 'Optimization of hydrophobic interaction chromatography using a mathematical model of elution curves of a protein mixture', *J. Mol. Recognit*, 22, pp. 110–120.
von Lieres, E. *et al.* (2014) 'Chromatography Analysis and Design Toolkit (CADET)', *Chemie Ingenieur Technik*, 86(9), p. 1629.
von Lieres, E. and Andersson, J. (2010) 'A fast and accurate solver for the general rate model of column liquid chromatography', *Comput. Chem. Eng.*, 34(8), pp. 1180–1191.
Linden, T. *et al.* (1999) 'Visualizing two-component protein diffusion in porous adsorbents by confocal scanning laser microscopy.', *Biotechnology and bioengineering*, 65(6), pp. 622–30.
Linden, T. *et al.* (2002) 'Visualizing patterns of protein uptake to porous media using confocal scanning laser microscopy', *Separation Science and Technology*, 37(1), pp. 1–32.
Lintern, K. *et al.* (2016) 'Residual on column host cell protein analysis during

lifetime studies of protein A chromatography', *Journal of Chromatography A*, 1461, pp. 70–77.
Liu, T., Donald, A. and Zhang, Z. (2005) 'Novel manipulation in Environmental SEM for measuring the mechanical properties of single nano-particles', *Materials Science and Technology*, 21(3), pp. 289–294.
Luo, X. *et al.* (2002) 'Simulation of packed bed formation in chromatography columns', in *Proceedings of the WCPT World Congress of Particle Technology*. Sedney.
Maaloum, M., Pernodet, N. and Tinland, B. (1998) 'Agarose gel structure using atomic force microscopy: gel concentration and ionic strength effects', *Electrophoresis*, 19(10), pp. 1606–1610.
Mashmoushy, H., Zhang, Z. and Thomas, C. (1998) 'Micromanipulation of the mechanical properties of baker's yeast cells', *Biotechnology Techniques*, 12, pp. 925–929.
Masters, A. (2012) *Types of Ion Exchange Chromatography Media*.
Medin, A. (1995) *Studies on Structure and Properties of Agarose*. Uppsala: Acta Universitatis Upsaliensis.
Menard, K. (2008) *Dynamic Mechanical Analysis: A Practical Introduction*.
Menard, K. and Menard, N. (2015) *Dynamic Mechanical Analysis in the Analysis of Polymers and Rubbers*.
Mendenhall, W. and Sincich, T. (2006) *Statistics for Engineering and the Sciences*. 5th editio. Pearsons.
Meyvis, T. and Stubbe, B. (2002) 'A comparison between the use of dynamic mechanical analysis and oscillatory shear rheometry for the characterisation of hydrogels', *International Journal of Pharmaceutics*, 244, pp. 163–168.
Michler, G. H. (2008) '8 Problems Associated with the Electron Microscopy', *Electron Microscopy of Polymers*, p. 473.
Mollerup, J. M. (2008) 'A review of the thermodynamics of protein association to ligands, protein adsorption, and adsorption isotherms', *Chemical Engineering and Technology*, 31(6), pp. 864–874.
Moroni, L., De Wijn, J. R. and Van Blitterswijk, C. A. (2006) '3D fiber-deposited scaffolds for tissue engineering: Influence of pores geometry and architecture on dynamic mechanical properties', *Biomaterials*, 27(7), pp. 974–985. Morse, B. S. (2000) 'Thresholding', in *Bringham Young University*, pp. 1–5.

Mu, Y., Lyddiatt, A. and Pacek, A. W. (2005) 'Manufacture by water/oil emulsification of porous agarose beads: Effect of processing conditions on mean particle size, size distribution and mechanical properties', *Chemical Engineering and Processing: Process Intensification*, 44(10), pp. 1157–1166.

Müller-Späth, T. *et al.* (2011) 'Model simulation and experimental verification of a cation-exchange IgG capture step in batch and continuous chromatography', *Journal of Chromatography A*, 1218, pp. 5195– 5204.

Muller, E., Chung, T. and Zhang, Z. (2005) 'Characterization of mechanical properties of polymeric chromatographic particles', *Journal of Chromatography A*, 1097, pp. 116–123.

Nireesha, G. R. *et al.* (2013) 'Lyophilization / Freeze Drying - An Review', *IJNTPS*, 3(4), pp. 87–98.

Nordestgaard, B. and Rostgaard, J. (1985) 'Critical-point drying versus freeze drying for scanning electron microscopy: a quantitative and qualitative study on isolated hepatocytes', *Journal of Microscopy*, 137(October 1984), pp. 189–207.

Nursam, N. M. *et al.* (2016) 'Probing the Effects of Templating on the UV and Visible Light Photocatalytic Activity of Porous Nitrogen-Modified Titania Monoliths for Dye Removal', *ACS Applied Materials and Interfaces*, 8(27), pp. 17194–17204.

Nweke, M. C. *et al.* (2016) 'Drying techniques for the visualisation of agarose-based chromatography media by scanning electron microscopy', *Biotechnology Journal*, (12), p. 1600583.

Pandithage, R. (2012) *Brief Introduction to Critical Point Drying*. Available at: http://www.leica-microsystems.com/science-lab/brief-introduction-to-critical-point-drying/.

Pathak, M. *et al.* (2017) 'Fluorescence based real time monitoring of fouling in process chromatography.', *Scientific reports*. Nature Publishing Group, 7(October 2016), p. 45640.

Pathak, M. and Rathore, A. S. (2016) 'Mechanistic understanding of fouling of protein A chromatography resin', *Journal of Chromatography A*. Elsevier B.V., 1459, pp. 78–88.

Pernodet, N., Maaloum, M. and Tinland, B. (1997) 'Pore size of agarose gels by atomic force microscopy', *Electrophoresis*, 18, pp. 55–58.

Pluen, A. *et al.* (1999) 'Diffusion of macromolecules into agarose gels: Comparison

of linear vs. globular configurations', *Biophysical Journal*, 77, pp. 542 – 552.
Polak, R. and Pitombo, R. (2011) 'Care during freeze-drying of bovine pericardium tissue to be used as a biomaterial: A comparative study', *Cryobiology*, 63(2), pp. 61–66.
Rabe, M., Verdes, D. and Seeger, S. (2011) 'Understanding protein adsorption phenomena at solid surfaces', *Advances in Colloid and Interface Science*. Elsevier B.V., 162(1–2), pp. 87–106.
Rathore, A. *et al.* (2015) 'Re-use of Protein A Resin: Fouling and Economics', *BioPharm International*, 28(3).
Rathore, A. S. (2009) 'Roadmap for implementation of quality by design (QbD) for biotechnology products', *Trends in Biotechnology*, 27(9).
Rathore, A. S. and Kapoor, G. (2016) 'Implementation of Quality by Design for processing of food products and biotherapeutics', *Food and Bioproducts Processing*. Institution of Chemical Engineers, 99, pp. 231–243.
Rathore, A. S. and Kumar, V. (2017) 'Mechanistic modeling of preparative ion-exchange chromatography', *BioPharm International*, 30(4).
Reville, W. and Cotter, M. (1991) 'An evaluation of the usefulness of air-drying biological samples from tetramethylsilane in preparation for scanning electron microscopy', *J Electron Microsc*, 40(3), pp. 198–202.
Saito, M., Kurosawa, Y. and Okuyama, T. (2013) 'Scanning electron microscopy-based approach to understand the mechanism underlying the adhesion of dengue viruses on ceramic hydroxyapatite columns.', *PloS one*, 8(1), p. e53893.
Scharl, T. *et al.* (2016) 'Trend analysis of performance parameters of pre-packed columns for protein chromatography over a time span of ten years', *Journal of Chromatography A*, 1465, pp. 63–70.
Schneider, C. A., Rasband, W. S. and Eliceiri, K. W. (2012) 'NIH Image to ImageJ: 25 years of image analysis', *Nature Methods*. Nature Publishing Group, 9(7), pp. 671–675.
Schwartzbach, H. (2010) 'The possibilities and challenges of spray drying', *Pharm. Technol. Europe*.
Seltman, H. (2007) *Experimental design and analysis*. Available at: http://www.stat.cmu.edu/~hseltman/309/Book/chapter7.pdf.
Sepsey, A., Bacskay, I. and Felinger, A. (2014) 'Molecular theory of size exclusion chromatography for wide pore size distributions', *Journal of Chromatography A*,

1331, pp. 52–60.
Siu, S. and Boushaba, R. (2006) ‘Visualising fouling of a chromatographic matrix using confocal scanning laser microscopy’, *Biotechnology and …*. doi: 10.1002/bit.
Siu, S. C. *et al.* (2006) ‘Effect of fouling on the capacity and breakthrough characteristics of a packed bed ion exchange chromatography column.’, *Bioprocess and biosystems engineering*, 28(6), pp. 405–14.
Siu, S. C. *et al.* (2007) ‘Confocal imaging of chromatographic fouling under flow conditions’, *Journal of Chemical Technology & Biotechnology*, 82, pp. 871–881.
Sofer, G. and Yourkin, J. (2007) ‘Cleaning and Cleaning Validation in Process Chromatography’, *Bioprocess international*, (November), pp. 72–82.
Srinorakutara, T. (1997) *Mechanical Strength of Yeasts*. University of Birmingham, UK.
Stenekes, R. *et al.* (2000) ‘Pore sizes in hydrated dextran microspheres’, *Biomacromolecules*, 1, pp. 696–703.
Stickel, J. J. and Fotopoulos, A. (2001) ‘Pressure-flow relationships for packed beds of compressible chromatography media at laboratory and production scale’, *Biotechnology Progress*, 17(4), pp. 744–751.
Sun, Y. and Yang, K. (2008) ‘Analysis of mass transport models based on Maxwell–Stefan theory and Fick’s law for protein uptake to porous anion exchanger’, *Separation and Purification Technology*, 60, pp. 180–189.
Susanto, A. *et al.* (2006) ‘Developing a chromatographic column model for bovine serum albumin on strong anion-exchanger Source30Q using data from confocal laser scanning microscopy.’, *Journal of chromatography. A*, 1137(1), pp. 63–75.
Swapp, S. (2015) *Scanning Electron Microscopy*. Available at: http://serc.carleton.edu/research_education/geochemsheets/techniques/SEM.html
Tarmann, C. and Jungbauer, A. (2008) ‘Adsorption of plasmid DNA on anion exchange chromatography media’, *Journal of Separation Science*, 31(14), pp. 2605–2618.
Tengliden, H. (2008) *Development of cleaning-in-place procedures for protein A chromatography resins using design of experiments and high throughput screening technologies*. Linkoping University.
Thillaivinayagalingam, P. *et al.* (2007) ‘Detection and quantification of affinity ligand leaching and specific antibody fragment concentration within chromatographic fractions using surface plasmon resonance’, *Biotechnology and*

Applied Biochemistry, 48(4), p. 179.
Tran, R. *et al.* (2007) 'A framework for the prediction of scale-up when using compressible chromatographic packings.', *Biotechnology progress*, 23(2), pp. 413–22.
Tran, R. (2011) *Evaluation of Challenges to the Ubiquitous Nature of Chromatography, UCL Doctoral Thesis*. University College London.
Tsinontides, S. C. *et al.* (2004) 'Freeze drying--principles and practice for successful scale-up to manufacturing.', *International journal of pharmaceutics*, 280(1–2), pp. 1–16.
Tugcu, N., Roush, D. and Goklen, K. (2007) 'Maximizing productivity of chromatography steps for purification of monoclonal antibodies', *Biotechnology and bioengineering*, 99(3), pp. 599–613.
Waki, S., Harvey, J. and Bellamy, A. (1982) 'Study of agarose gels by electron microscopy of freeze-fractured surfaces', *Biopolymers*, 21(9), pp. 1909–1926.
Wang, C., Wang, L. and Thomas, C. (2003) 'Modelling the mechanical properties of single suspension – cultured tomato cells', *Annals of Botany*, 93, pp. 443–453.
Warner, T. and Nochumson, S. (2003) 'Rethinking the Economics of Pensions', *BioPharm International*, 22(3), pp. 15–39.
Williams, J. R. and Clifford, A. A. (2000) *Supercritical Fluid Methods and Protocols*. Methods in Biotechnology.
Wilson, S. M. and Bacic, A. (2012) 'Preparation of plant cells for transmission electron microscopy to optimize immunogold labeling of carbohydrate and protein epitopes', *Nature Protocols*, 7(9), pp. 1716–1727.
Yan, Y. *et al.* (2009) 'Mechanical characterization of agarose micro-particles with a narrow size distribution', *Powder Technology*. Elsevier B.V., 192(1), pp. 122–130.
Yang, K., Shi, Q.-H. and Sun, Y. (2006) 'Modeling and simulation of protein uptake in cation exchanger visualized by confocal laser scanning microscopy.', *Journal of chromatography. A*, 1136(1), pp. 19–28.
Yao, Y. and Lenhoff, A. (2004) 'Determination of pore size distributions of porous chromatographic adsorbents by inverse size-exclusion chromatography', *Journal of Chromatography A*, 1037(28), pp. 273–282.
Zeitvogel, F. *et al.* (2016) 'Comparison of Preparation Methods of Bacterial Cell-Mineral Aggregates for SEM Imaging and Analysis Using the Model System of Acidovorax sp. BoFeN1', *Geomicrobiology Journal*. Taylor & Francis, 34(4), pp. 1–

11.
Zhang, S., Daniels, W., *et al.* (2015) ‘Nature of foulants and fouling mechanism in the Protein A MabSelect resin cycled in a monoclonal antibody purification process.’, *Biotechnology and bioengineering*, pp. 1–28.
Zhang, S., Xu, K., *et al.* (2015) ‘Structural and functional characteristics of virgin and fouled Protein A MabSelect resin cycled in a monoclonal antibody purification process.’, *Biotechnology and bioengineering*, pp. 1–29.
Zhang, Z. *et al.* (1991) ‘A novel micromanipulation technique for measuring the bursting strength of single mammalian cells’, *Applied Microbiology and Biotechnology*, 36, pp. 208–210.
Zhou, Q.-Z. *et al.* (2007) ‘Preparation of uniform-sized agarose beads by microporous membrane emulsification technique’, *Journal of Colloid and Interface Science*, 311(1), pp. 118–127.
Zhou, Q.-Z. *et al.* (2008) ‘Multi-stage premix membrane emulsification for preparation of agarose microbeads with uniform size’, *Journal of Membrane Science*, 322(1), pp. 98–104.
Zhou, Q.-Z., Ma, G.-H. and Su, Z.-G. (2009) ‘Effect of membrane parameters on the size and uniformity in preparing agarose beads by premix membrane emulsification’, *Journal of Membrane Science*, 326(2), pp. 694–700.

APPENDIX

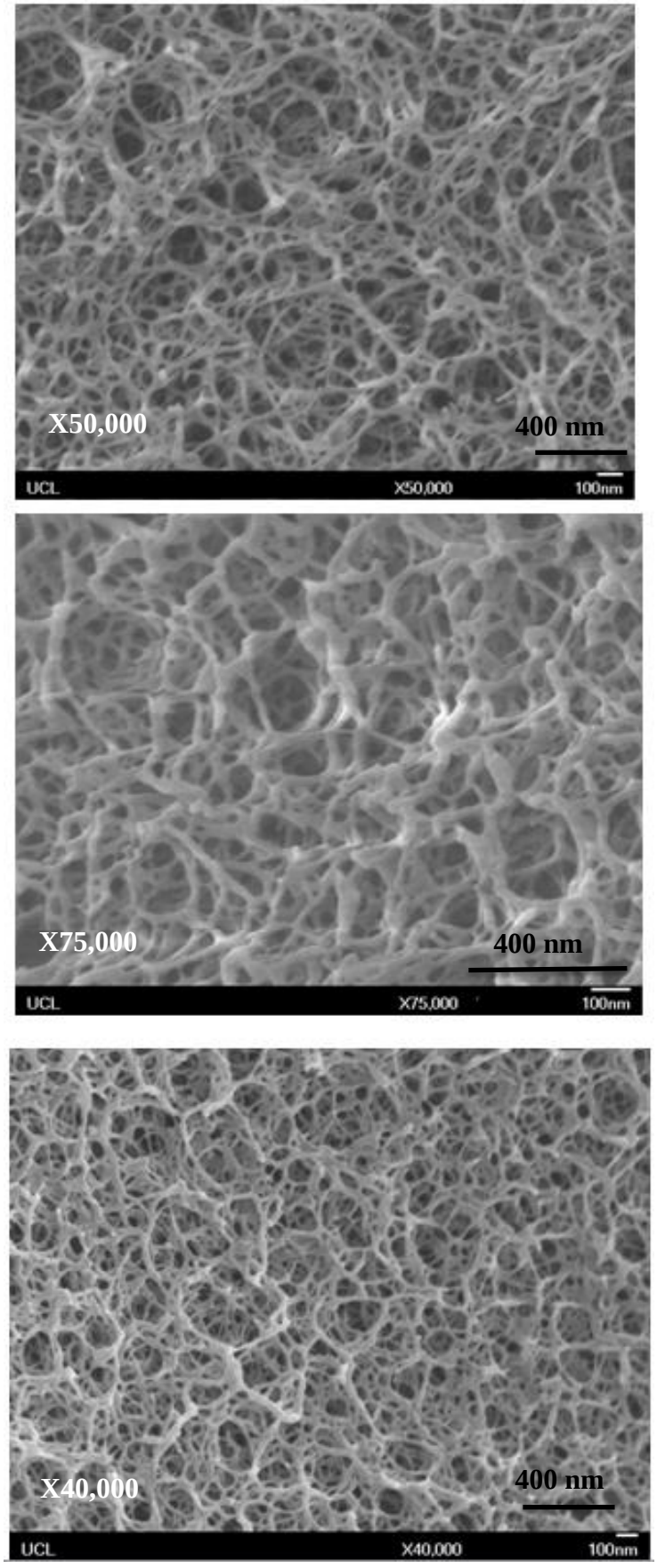

Figure 57 – SEM micrographs of fresh Capto Adhere post- critical point drying used for quantitative analysis

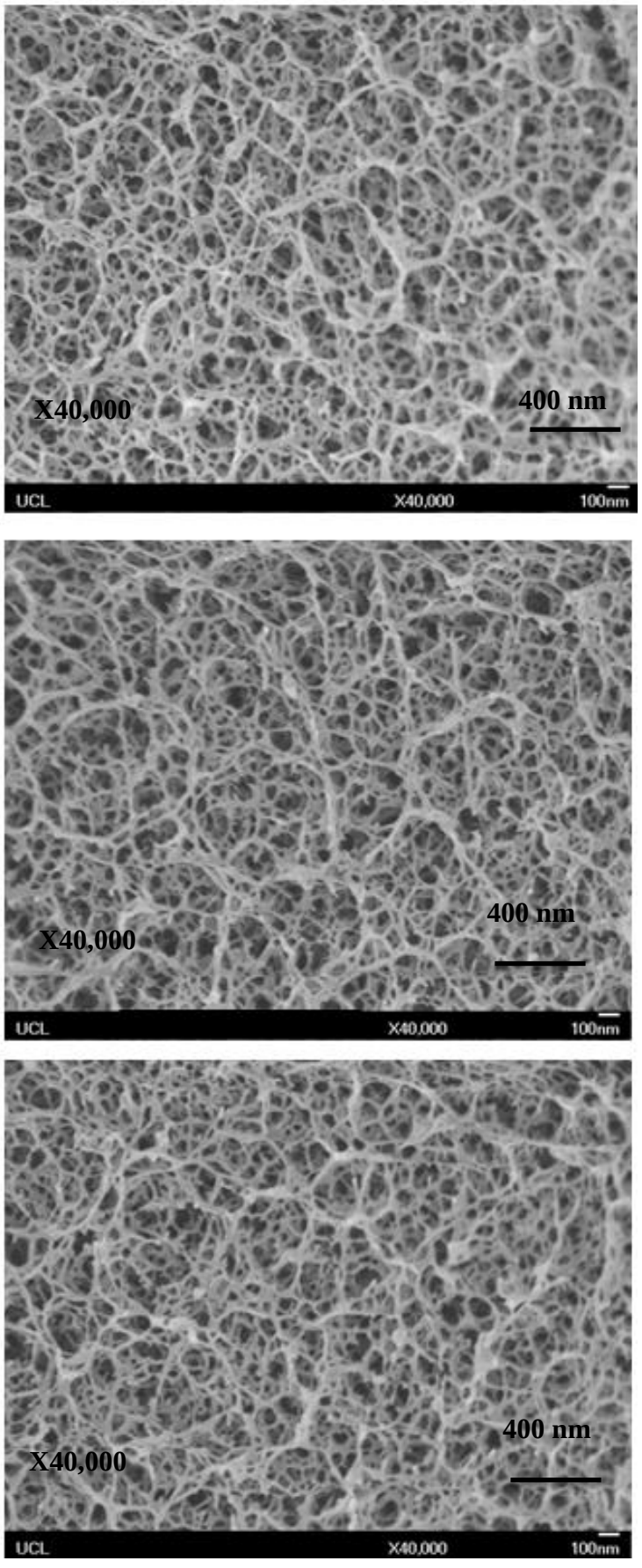

Figure 58 – SEM micrographs of fresh Capto Q post- critical point drying used for quantitative analysis

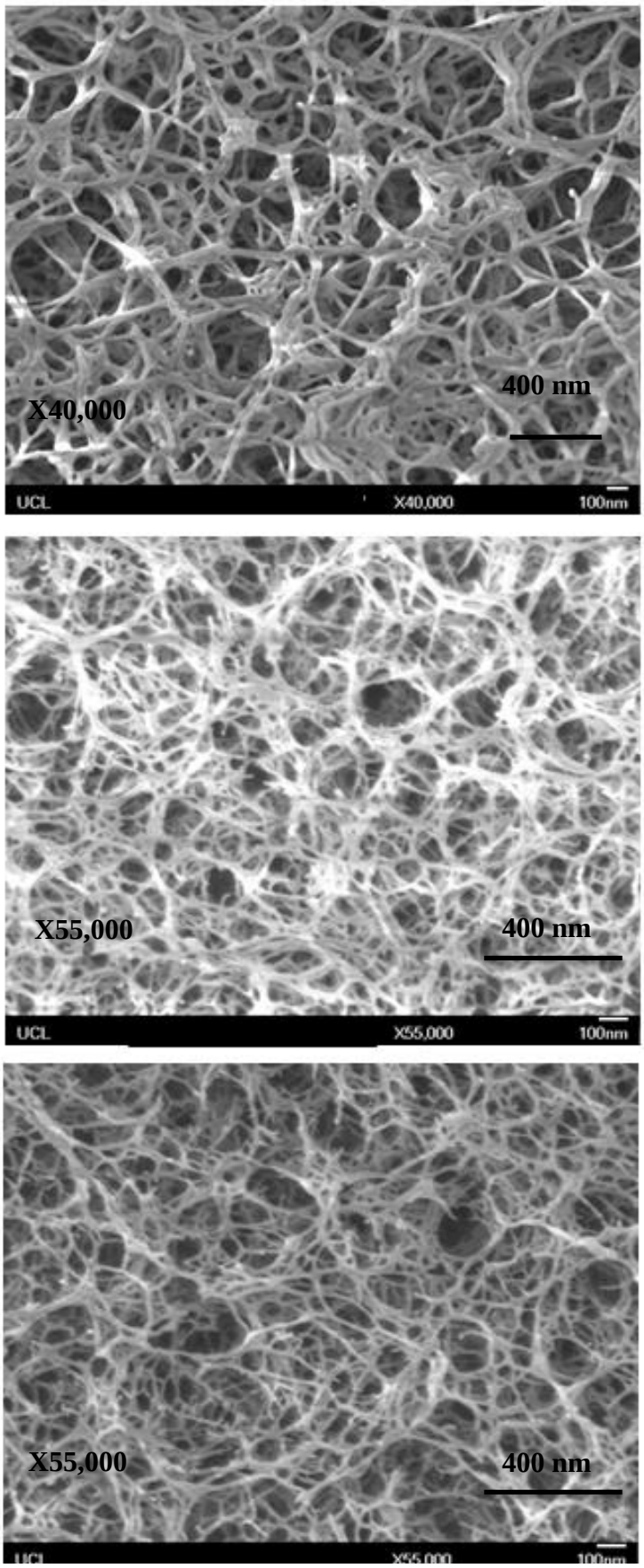

Figure 59– SEM micrographs of fresh MabSelect post- critical point drying used for quantitative analysis

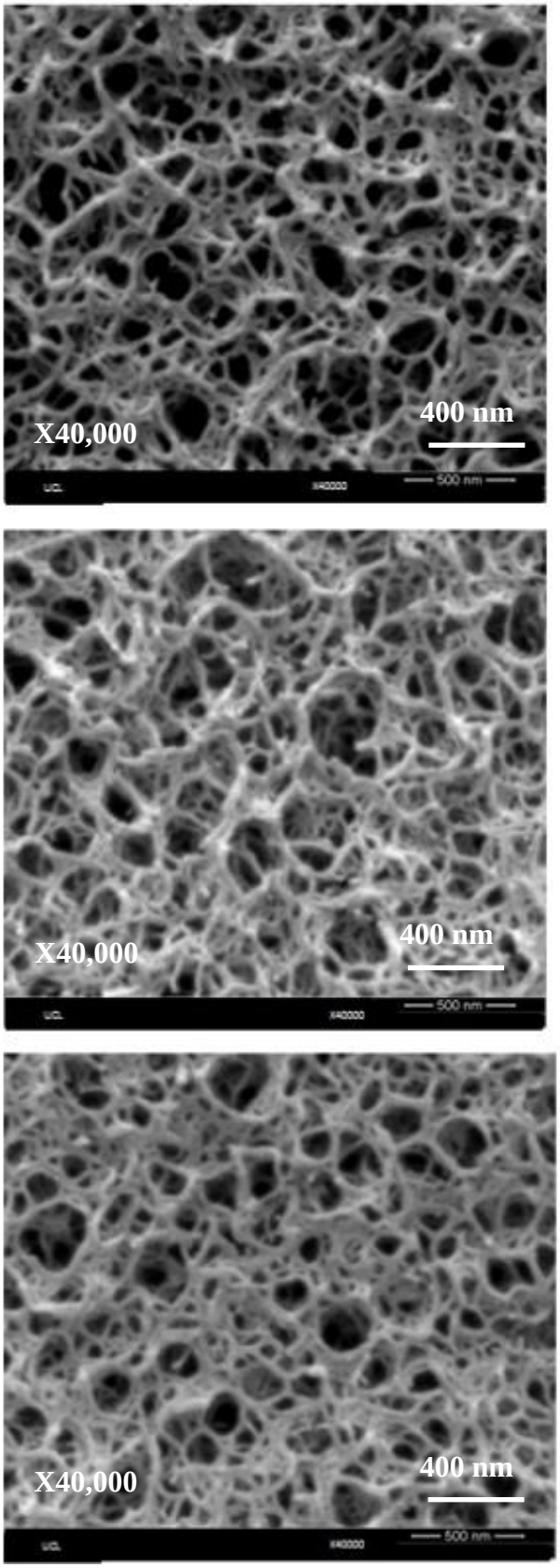

Figure 60 – SEM micrographs of fresh MabSelect Xtra post- critical point drying used for quantitative analysis

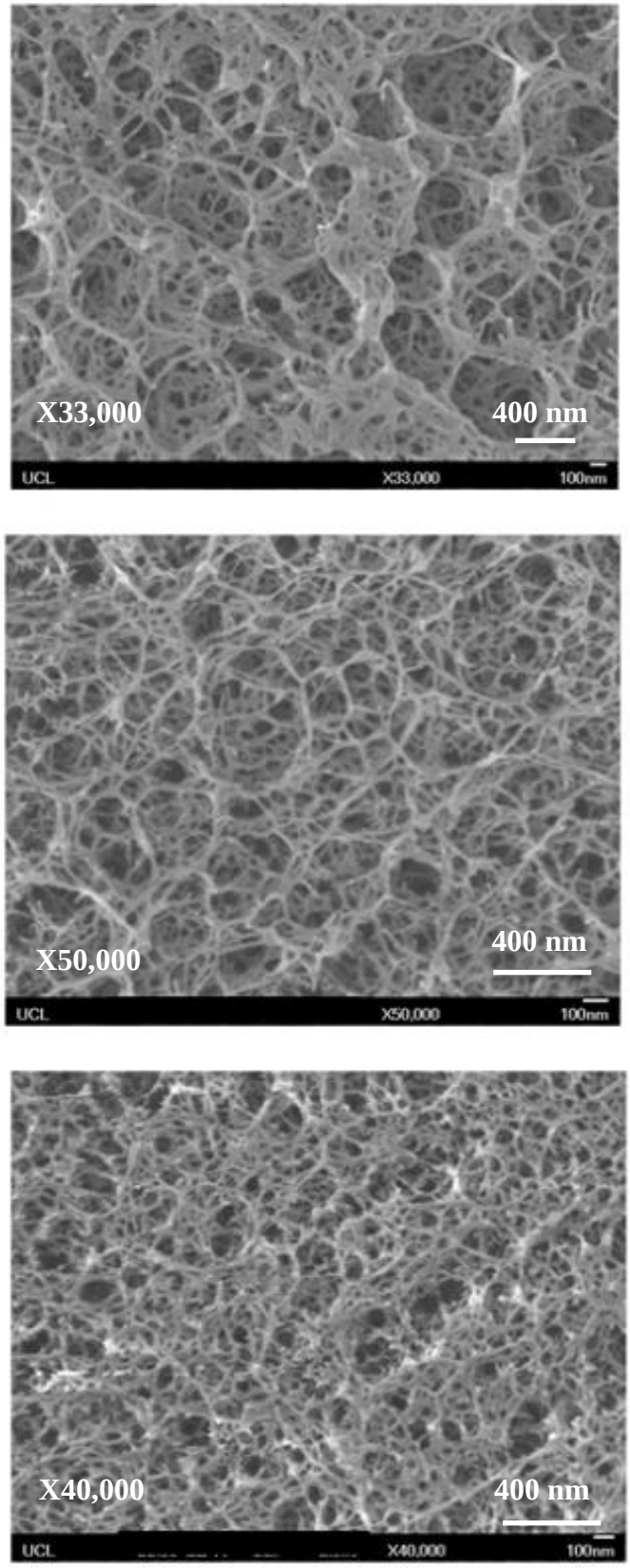

Figure 61 – SEM micrographs of fresh Q-Sepharose High Performance post- critical point drying used for quantitative analysis

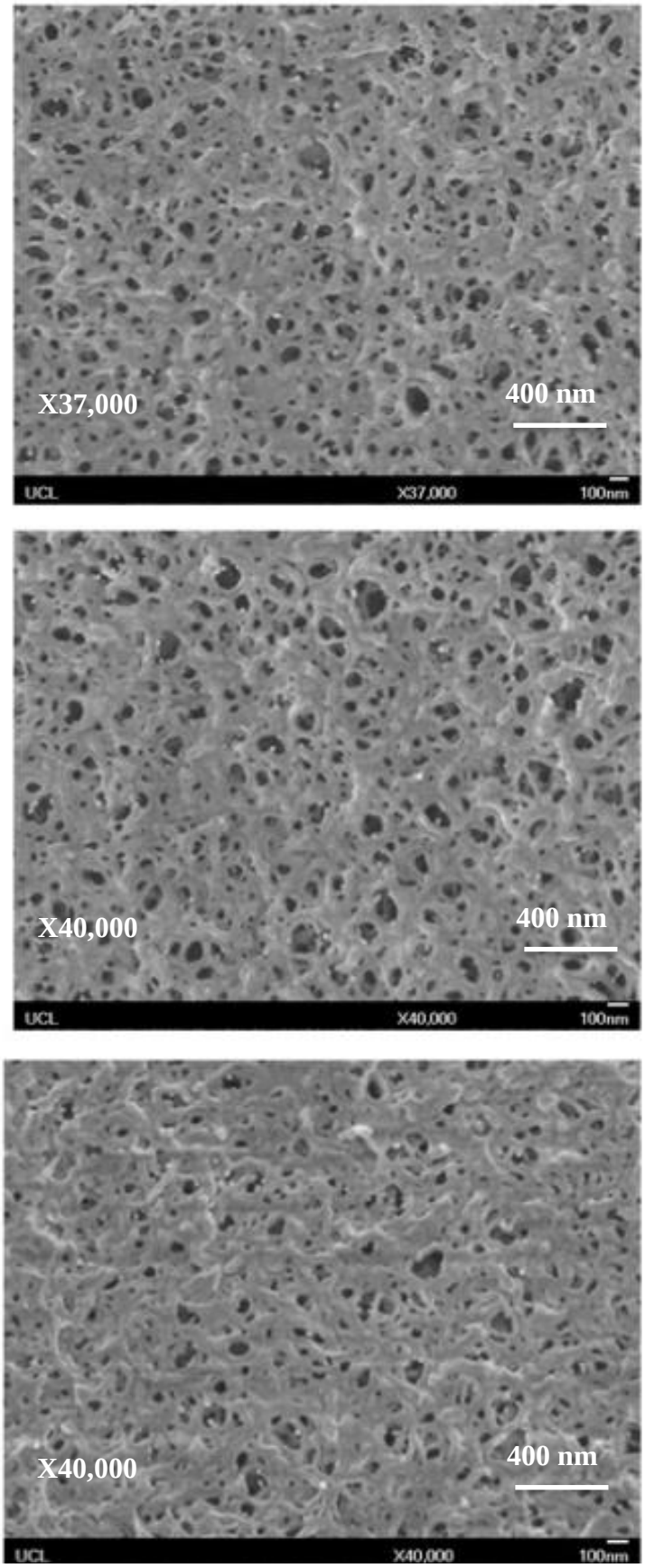

Figure 62 – SEM micrographs of fresh Sepharose 4 Fast Flow post-critical point drying used for quantitative analysis

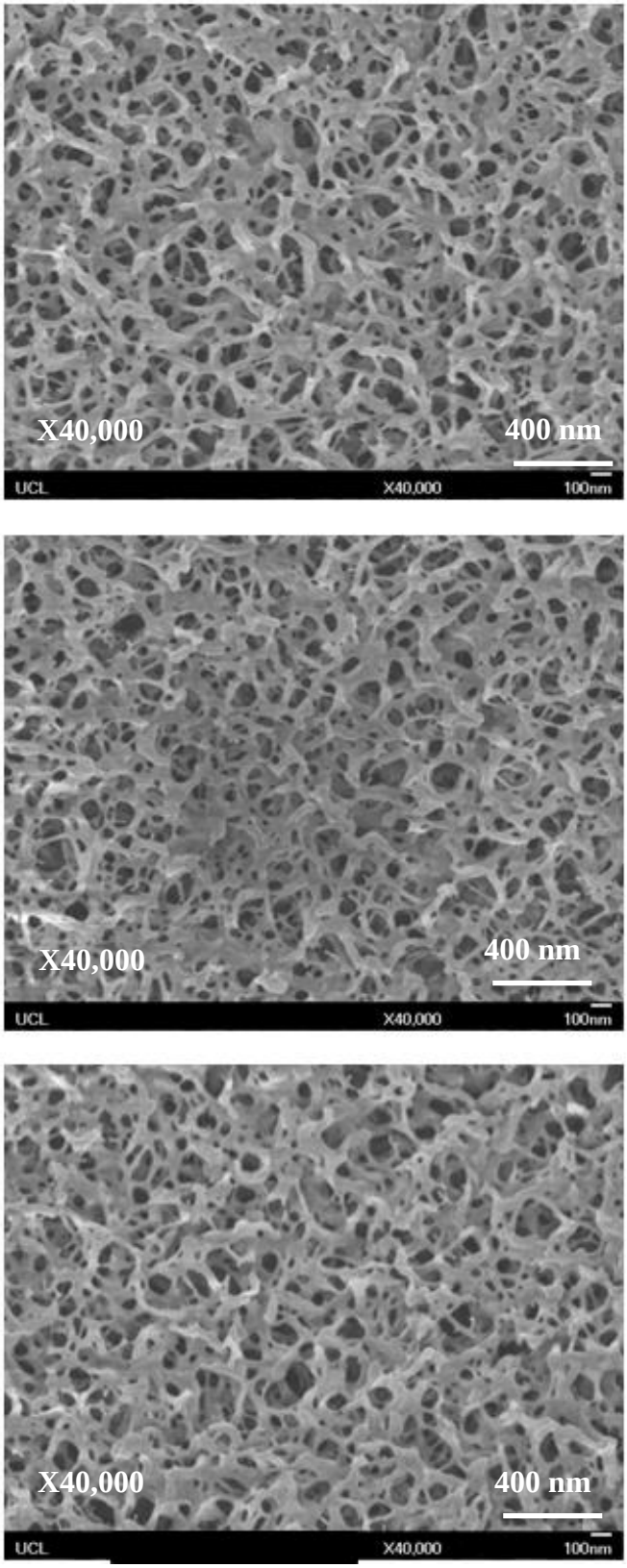

Figure 63 – SEM micrographs of fresh Sepharose 6 Fast Flow post- critical point drying used for quantitative analysis

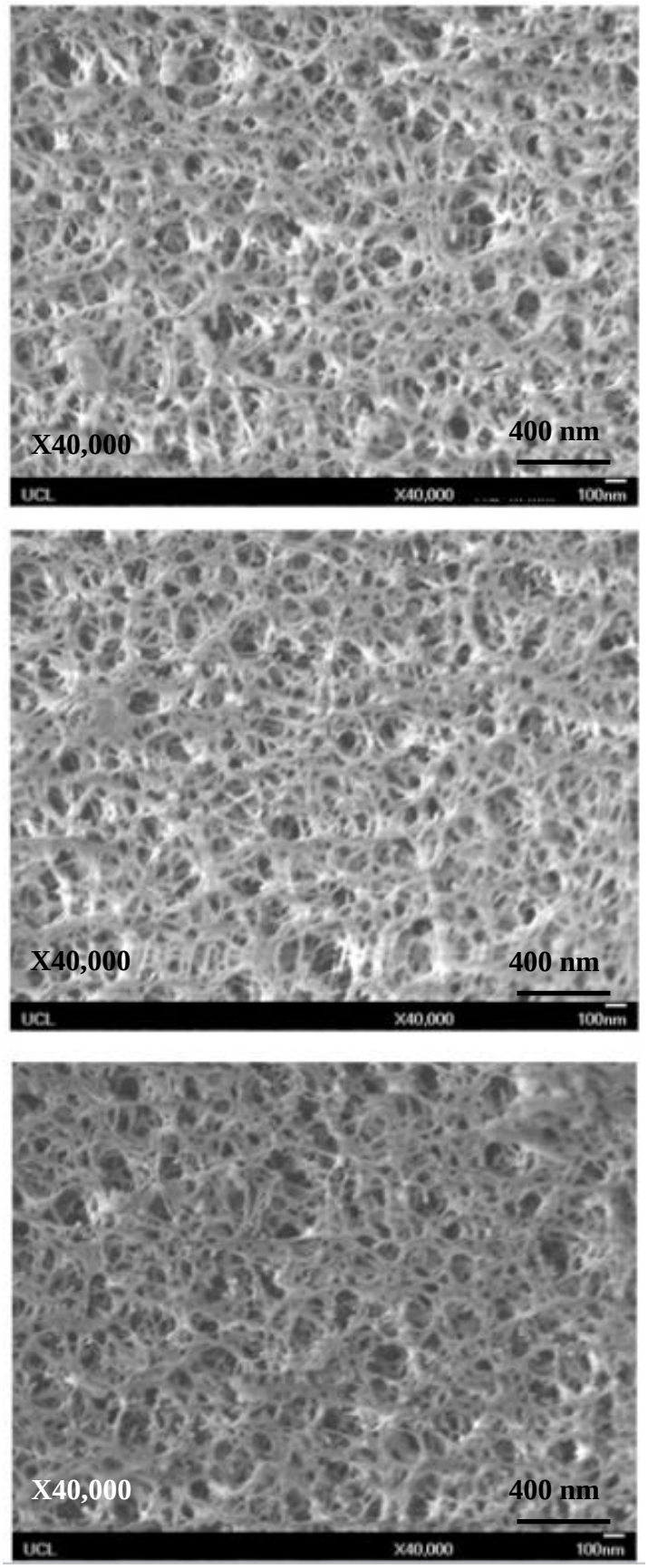

Figure 64 – SEM micrographs of fresh Sepharose CL-4B post- critical point drying used for quantitative analysis

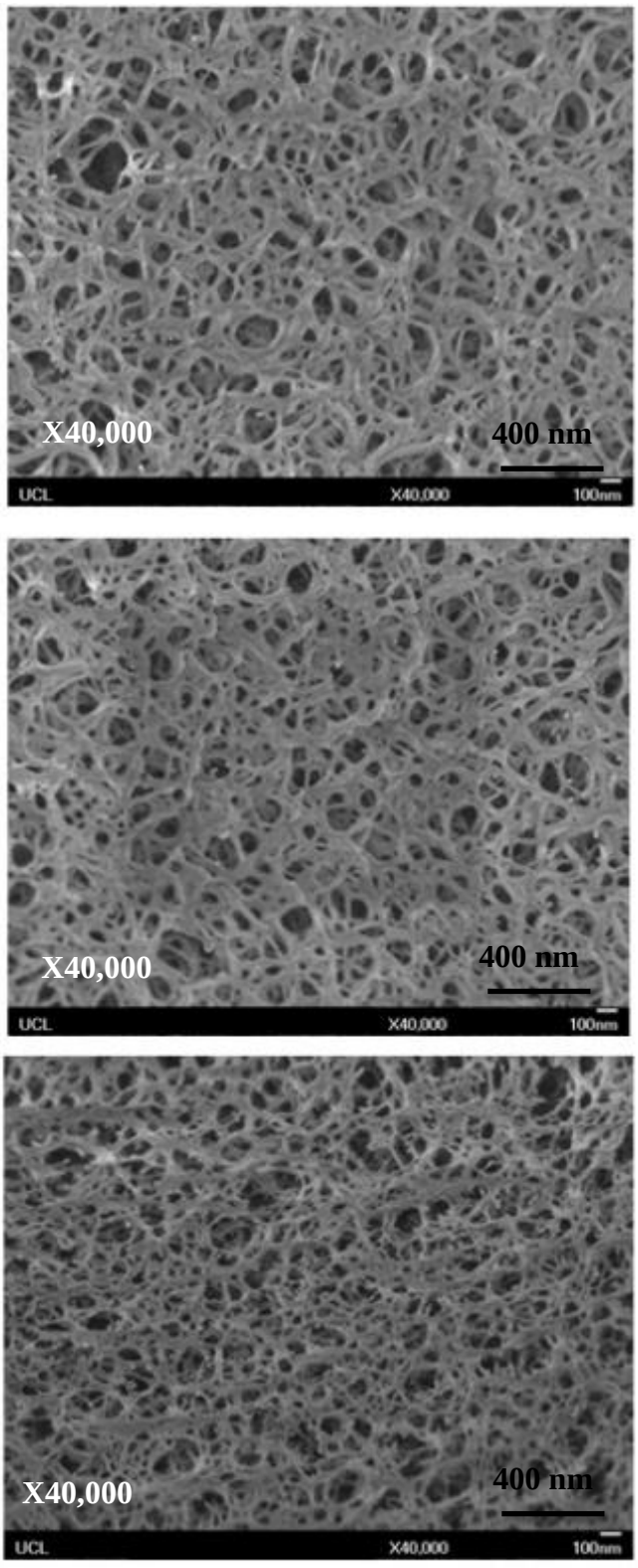

Figure 65 – SEM micrographs of fresh Sepharose CL-6B post- critical point drying used for quantitative analysis

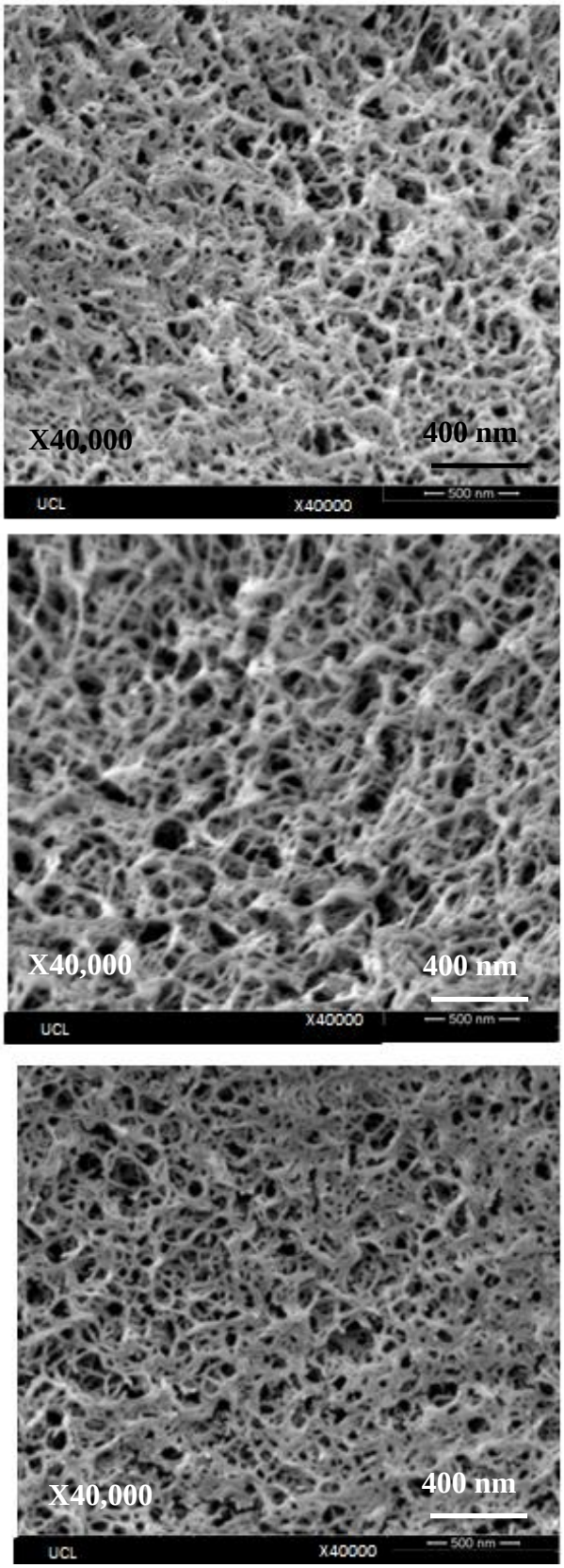

Figure 66 – SEM micrographs of CIP-exposed Capto Adhere used for quantitative analysis

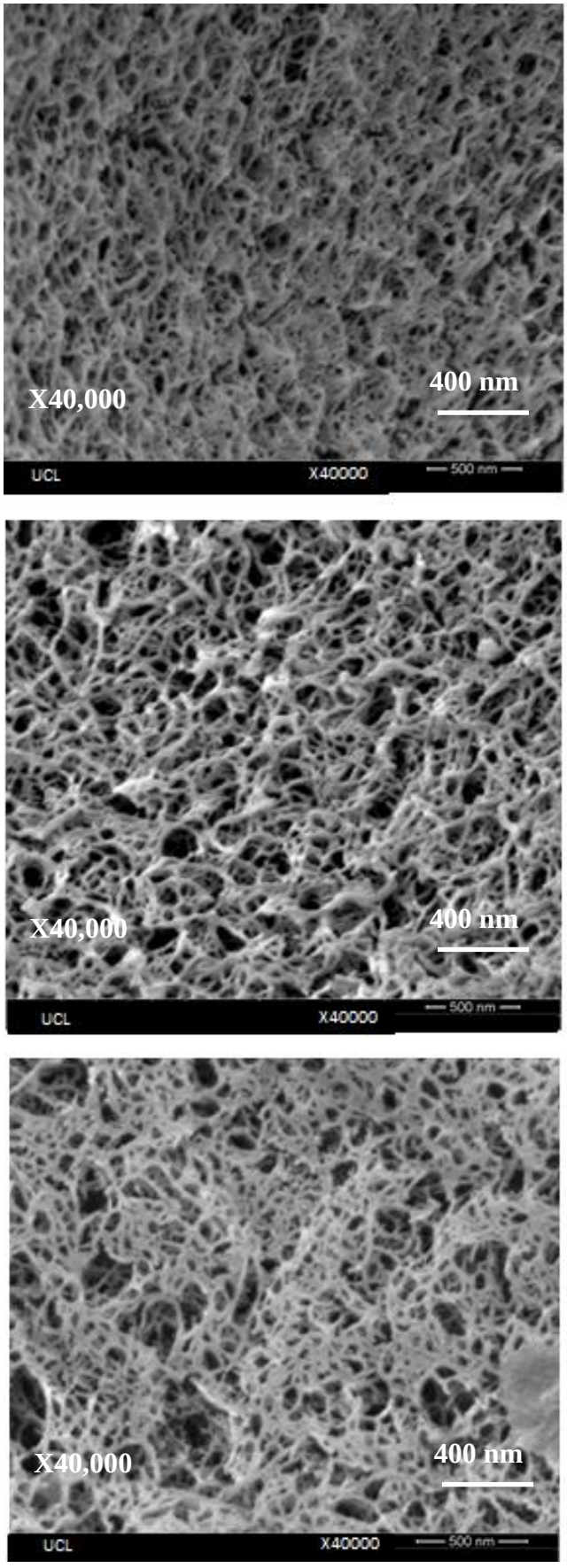

Figure 67 – SEM micrographs of CIP-exposed MabSelect used for quantitative analysis

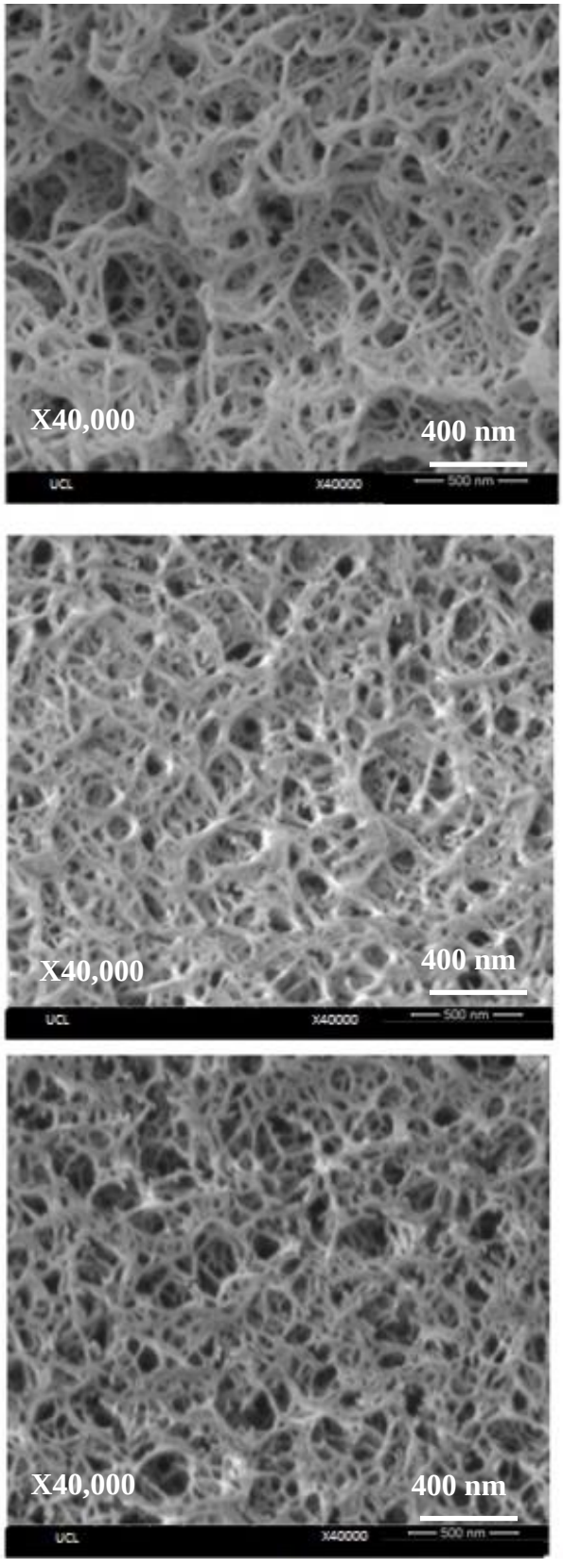

Figure 68 – SEM micrographs of CIP-exposed MabSelect Xtra (inner surface) used for quantitative analysis

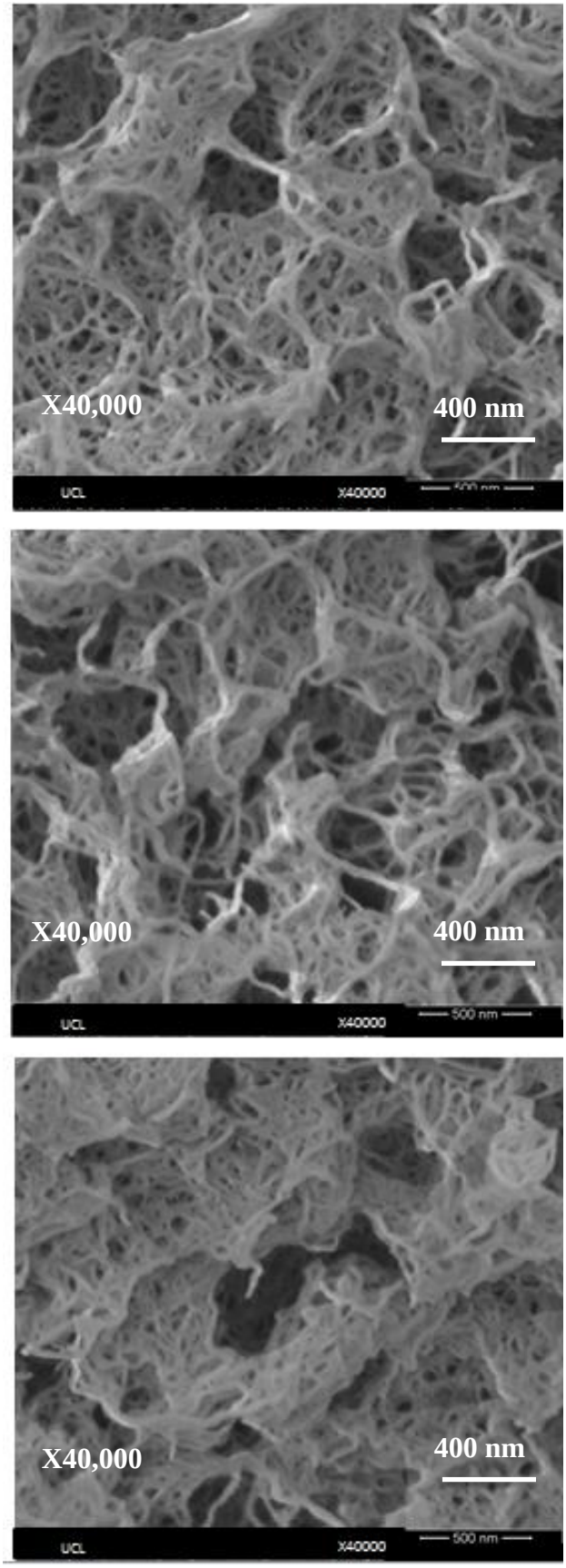

Figure 69 – SEM micrographs of CIP-exposed MabSelect Xtra (outer surface) used for quantitative analysis

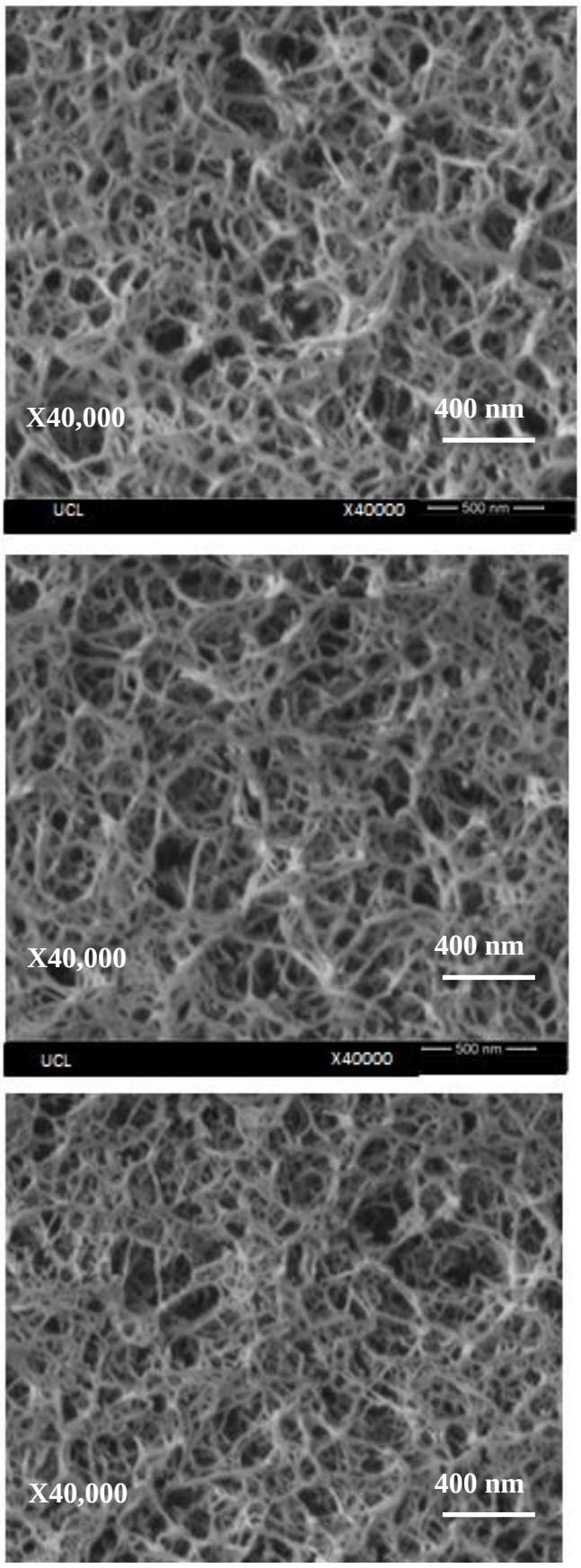

Figure 70 – SEM micrographs of CIP-exposed Q-Sepharose High Performance used for quantitative analysis

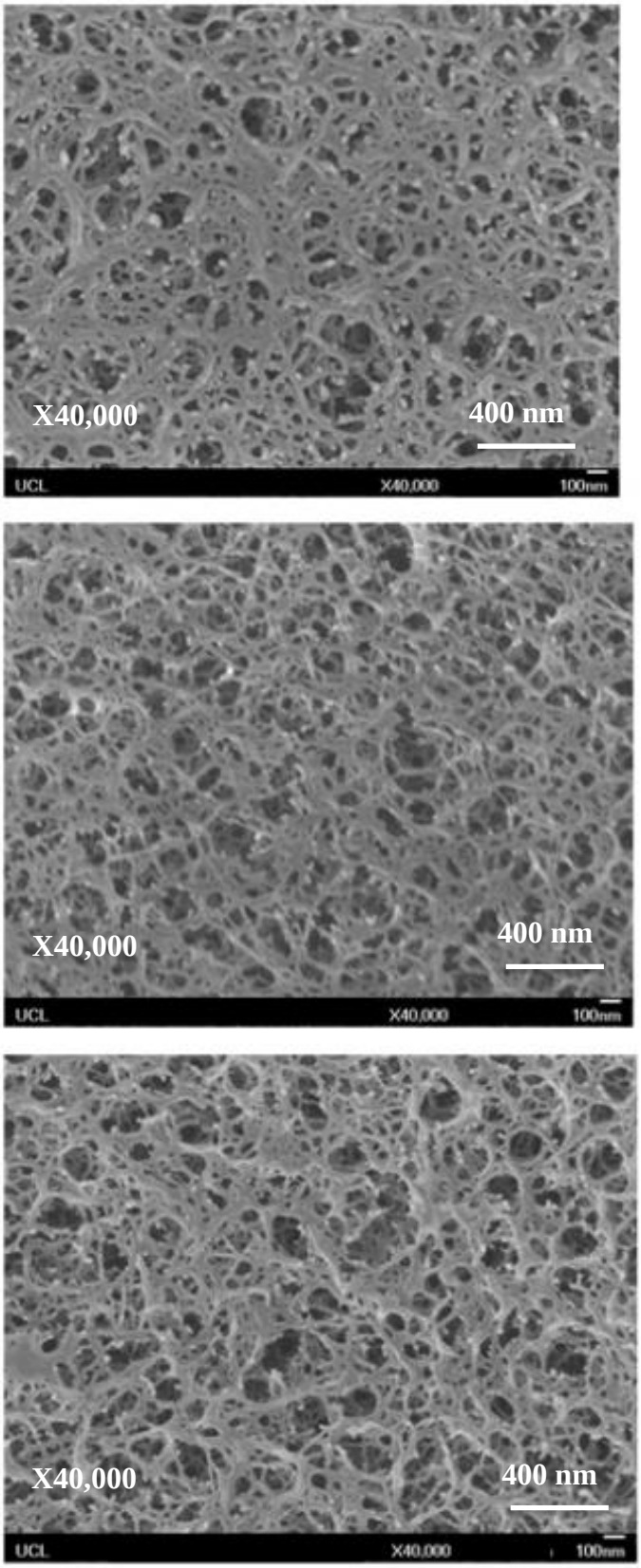

Figure 71 – SEM micrographs of aged Capto Adhere used for quantitative analysis

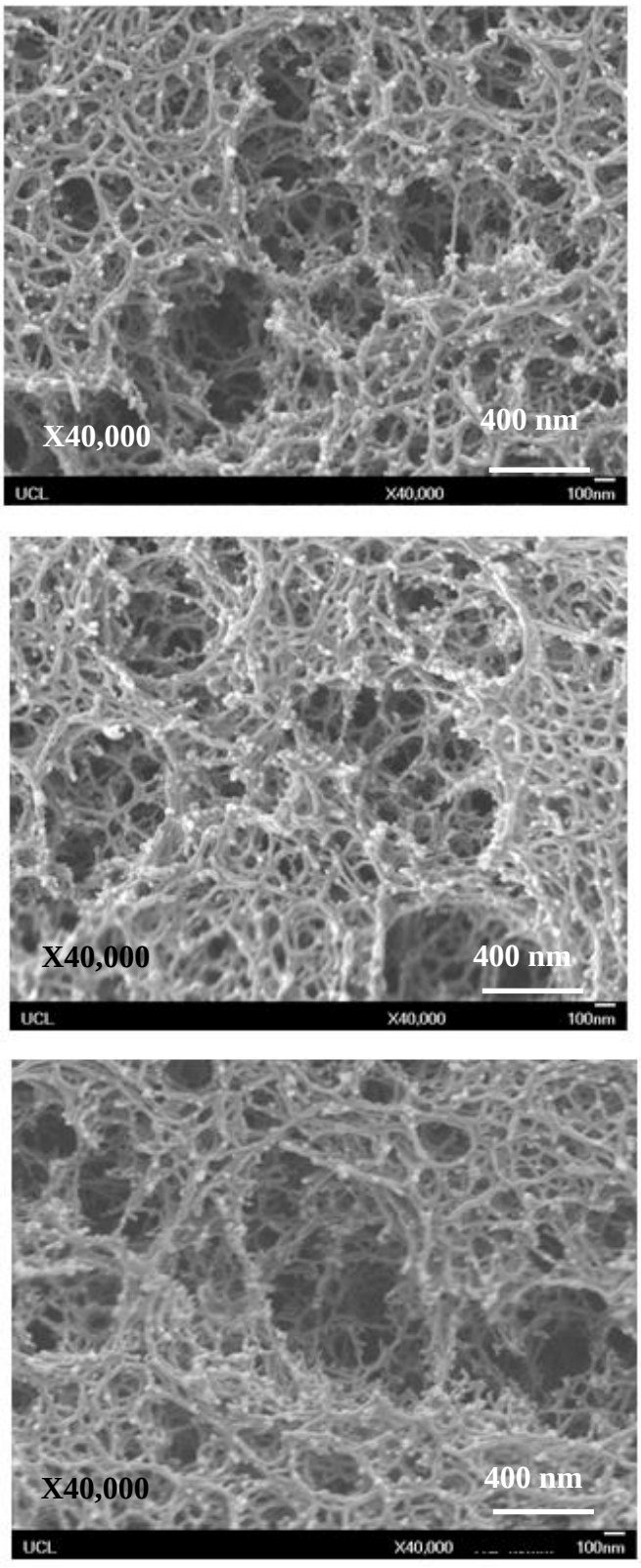

Figure 72 – SEM micrographs of aged MabSelect used for quantitative analysis

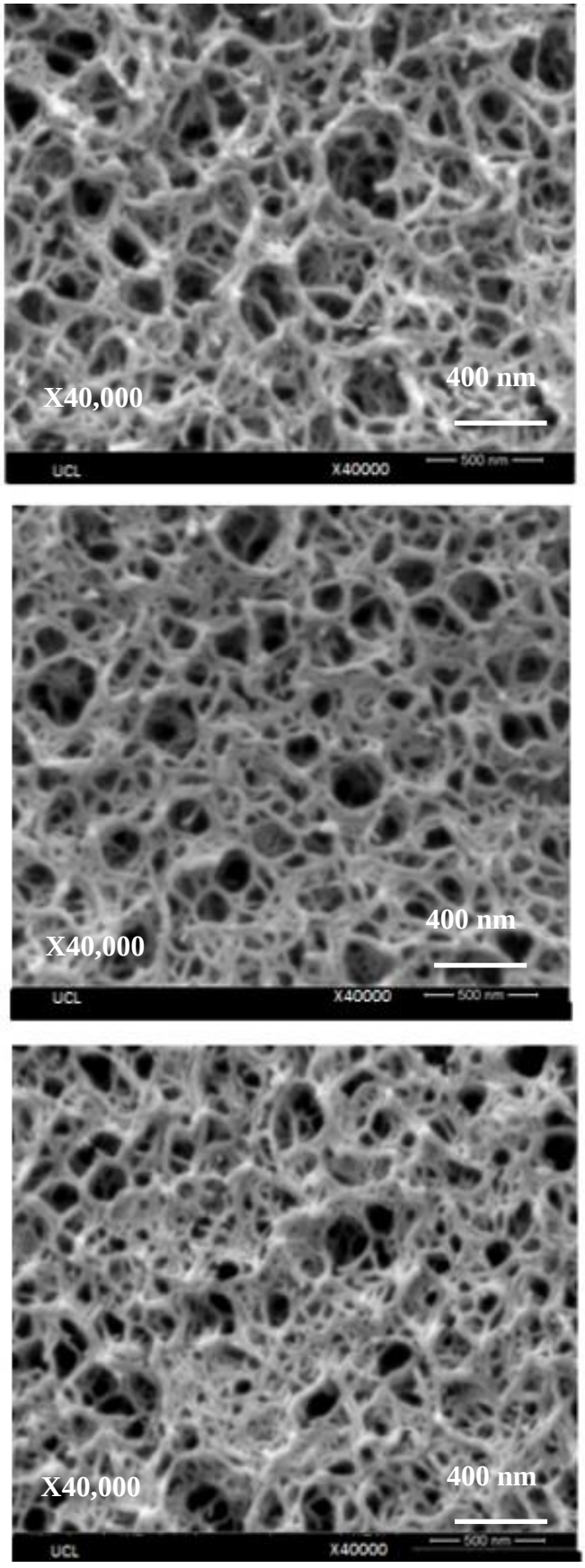

Figure 73 – SEM micrographs of aged MabSelect Xtra used for quantitative analysis

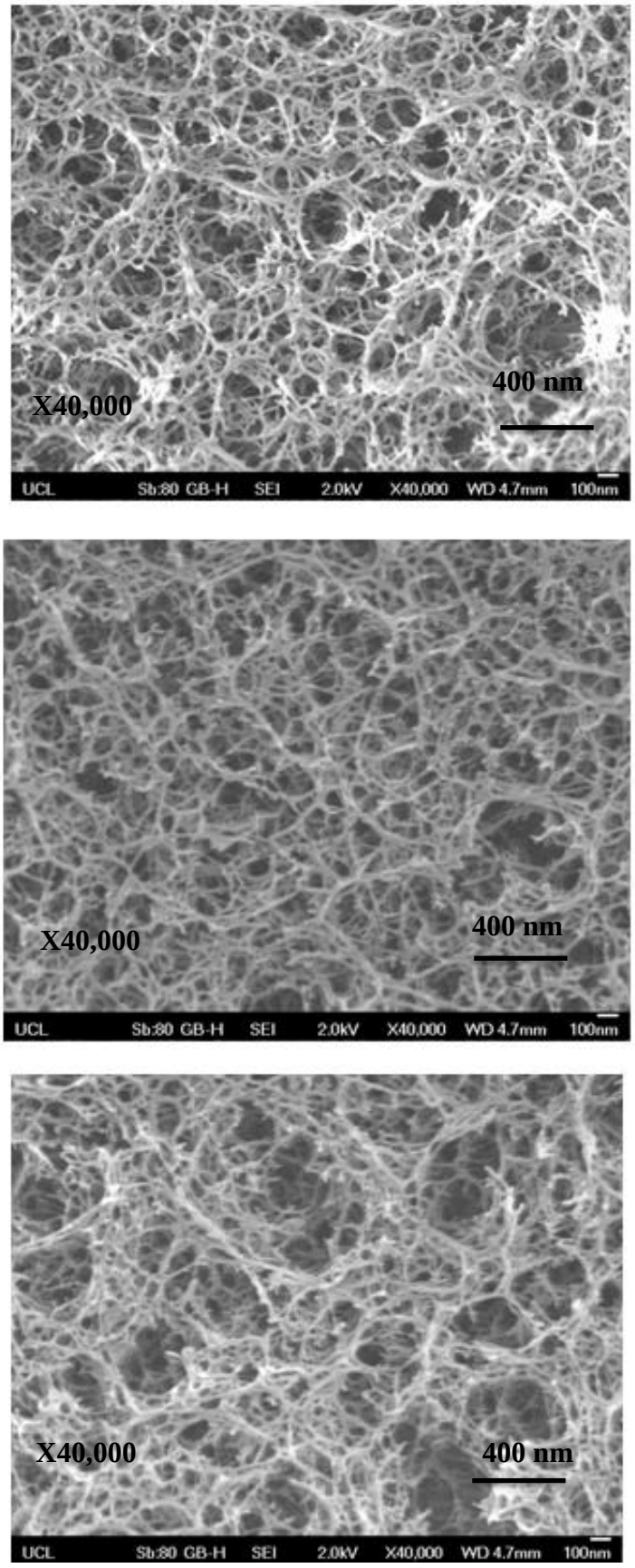

Figure 74 – SEM micrographs of aged Q-Sepharose High Performance used for quantitative analysis

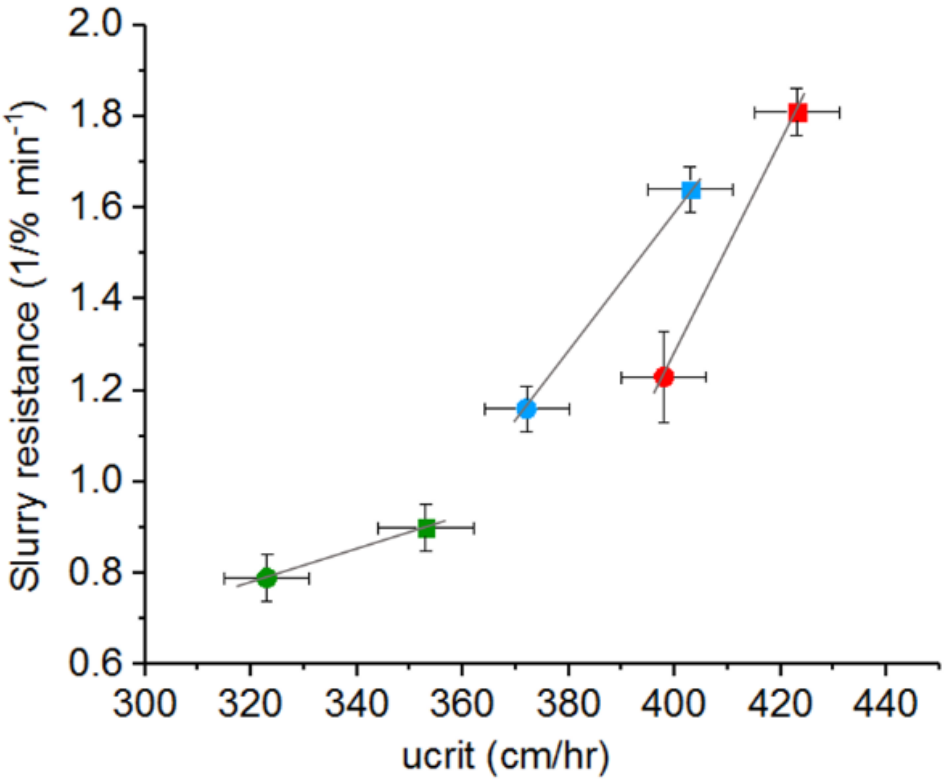

Figure 75 – Slurry resistance vs critical velocity for MS (red), MSX (blue) and QHP (green). The squares represent fresh resin data and the circles represent aged resin data